KAUNAS UNIVERSITY OF TECHNOLOGY

MALEK MAHMOUDI SHARABIANI

DEVELOPMENT OF ORGANIC LIGHT-EMITTING DIODES BASED ON NEW WIDE-BAND-GAP SEMICONDUCTORS

Doctoral dissertation
Technological Sciences, Materials Engineering (T 008)

2024, Kaunas

Dissertation Defense Board of Materials Engineering Science Field:
Prof. Dr. Hab. Sigitas TAMULEVIČIUS (Kaunas University of Technology, Technological Sciences, Materials Engineering, T 008) – **chairperson**;
Prof. Dr. Vladimir DYAKONOV (Julius Maximilians University of Würzburg, Germany, Natural Sciences, Physics, N 002);
Chief Researcher Dr. Marius FRANCKEVIČIUS (Center for Physical Sciences and Technology, Natural Sciences, Physics, N 002);
Prof. Dr. Hab. Arvaidas GALDIKAS (Kaunas University of Technology, Technological Sciences, Materials Engineering, T 008);
Prof. Dr. Saulius GRIGALEVIČIUS (Kaunas University of Technology, Technological Sciences, Materials Engineering, T 008).

The public defense of the dissertation will be held at 11 a.m. on 29 January, 2024 at the public meeting of Dissertation Defense Board of Materials Engineering Science Field in Rectorate Hall at Kaunas University of Technology.

Address: K. Donelaičio 73-402, Kaunas, LT-44249, Lithuania
Phone: (+370) 608 28 527; e-mail doktorantura@ktu.lt

The doctoral dissertation was sent out on 22 December, 2023.
The doctoral dissertation is available on the internet http://ktu.edu and at the library of Kaunas University of Technology (Gedimino 50, LT-44239, Kaunas, Lithuania).

KAUNO TECHNOLOGIJOS UNIVERSITETAS

MALEK MAHMOUDI SHARABIANI

ORGANINIŲ ŠVIESOS DIODŲ TOBULINIMAS TAIKANT NAUJUS ORGANINIUS PUSLAIDININKIUS, PASIŽYMINČIUS DIDELIU ENERGETINIŲ LYGMENŲ SKIRTUMU

Daktaro disertacija
Technologijos mokslai, medžiagų inžinerija (T 008)

2024, Kaunas

Disertacija rengta 2019 – 2023 metais Kauno technologijos universiteto Cheminės technologijos fakultete, Polimerų chemijos ir technologijos katedroje. Mokslinius tyrimus rėmė Lietuvos mokslo taryba.

Mokslinis vadovas:
vyr. m. d., dr. Dmytro VOLYNIUK (Kauno technologijos universitetas, technologijos mokslai, medžiagų inžinerija, T 008).

Disertaciją redagavo: anglų kalbos redaktorė Brigita Brasienė (leidykla „Technologija"), lietuvių kalbos redaktorė Aurelija Gražina Rukšaitė (leidykla „Technologija").

Medžiagų inžinerijos mokslo krypties disertacijos gynimo taryba:
prof. habil. dr. Sigitas TAMULEVIČIUS (Kauno technologijos universitetas, technologijos mokslai, medžiagų inžinerija, T 008) – **pirmininkas**;
prof. dr. Vladimir DYAKONOV (Julius Maximilians universitetas Viurcburge, Vokietija, gamtos mokslai, fizika, N 002);
vyr. m. d., dr. Marius FRANCKEVIČIUS (Fizinių ir technologijos mokslų centras, gamtos mokslai, fizika, N 002);
prof. habil. dr. Arvaidas GALDIKAS (Kauno technologijos universitetas, technologijos mokslai, medžiagų inžinerija, T 008);
prof. dr. Saulius GRIGALEVIČIUS (Kauno technologijos universitetas, technologijos mokslai, medžiagų inžinerija, T 008).

Disertacija bus ginama viešame Medžiagų inžinerijos mokslo krypties disertacijos gynimo tarybos posėdyje 2024 m. sausio 29 d. 11 val. Kauno technologijos universiteto Rektorato salėje.

Adresas: K. Donelaičio g. 73-402, Kaunas, LT-44249, Lietuva
Tel. (+370) 608 28 527; el. paštas doktorantura@ktu.lt

Disertacija išsiųsta 2023 m. gruodžio 22 d.
Su disertacija galima susipažinti interneto svetainėje http://ktu.edu ir Kauno technologijos universiteto bibliotekoje (Gedimino g. 50, LT-44239, Kaunas, Lietuva).

TABLE OF CONTENTS

LIST OF ABBREVIATIONS

1 – 9,9'-bis(4-fluorophenyl)-3,3'-bicarbazole
2 – 9,9'-bis(4-trifluoromethylphenyl)-3,3'-bicarbazole
3 – 4,4'-bis[*N*-(1-naphthyl)-*N*-phenylamino]benzophenone
4 – 4,4'-bis[*N*-(2-naphthyl)-*N*-phenylamino]benzophenone
5 – 2',3',5',6'-Tetrakis(3,6-di-tert-butyl-9H-carbazol-9-yl)-[1,1'-biphenyl]-2,4'-dicarbonitrile
6 – 4-(2H-benzo[d][1,2,3]triazol-2-yl)-2,3,5,6-tetrakis(3,6-di-tert-butyl-9H-carbazol-9-yl)benzonitrile
7 – 2,3,5,6-tetrakis(3,6-di-tert-butyl-9H-carbazol-9-yl)-2'-(trifluoromethyl)-[1,1'-biphenyl]-4-carbonitrile
8 – methyl 4'-cyano-2',3',5',6'-tetrakis(3,6-di-tert-butyl-9H-carbazol-9-yl)-[1,1'-biphenyl]-2-carboxylate
9 – methyl 4'-cyano-2',3',5',6'-tetrakis(3,6-di-tert-butyl-9H-carbazol-9-yl)-2-methyl-[1,1'-biphenyl]-4-carboxylate
10 – 9,9′,9″,9‴-[3-(pyrimidin-5-yl)-6-(trifluoromethyl)-benzene-1,2,4,5-tetrayl]tetrakis(3,6-di-tert-butyl-9H-carbazole)
11 – 9,9′,9″,9‴-[3-(pyrimidin-2-yl)-6-(trifluoromethyl)benzene-1,2,4,5-tetrayl]tetrakis(3,6-di-tert-butyl-9H-carbazole)
12 – 9,9′,9″,9‴-[3-bromo-6-(trifluoromethyl)benzne-1,2,4,5-tetrayl]-tetrakis(3,6-di-tert-butyl-9H-carbazole)
13 – 2′,3′,5′,6′-Tetrakis(3,6-di-tert-butyl-9H-carbazol-9-yl)-2-methyl-4′-(trifluoromethyl)-[1,1′-biphenyl]-4-carbonitrile
14 – 9,9′,9″,9‴-[3-(pyridin-2-yl)-6-(trifluoromethyl)benzene-1,2,4,5-tetrayl]tetrakis(3,6-di-tert-butyl-9H-carbazole)
4CzTPN – 2,3,5,6-tetrakis(carbazol-9-yl)-1,4-dicyanobenzene
ACQ – aggregation-caused quenching
AIE – aggregation-induced emission
AIEE – aggregation-induced emission enhancement
CE – current efficiency
CIE – Comission Internationale de I'Eclairage
CT – charge transfer
CV – cyclic voltammetry
DCM – dichloromethane
DF – delayed fluorescence
DFT – density functional theory
DMF – dimethylformamide
DMSO – dimethyl sulfoxide
DSC – differential scanning calorimetry
E_a – activation energy
EA_{CV} – electron affinity measured by CV
EBL – electron blocking layer
E_g^{opt} – optical band gap
EIL – electron injection layer

EL – electroluminescent
EML – emissive layer
E_{ox} – oxidation potential
EQE – external quantum efficiency
E_{S1} – energy of first singlet state
ETL – electron transport layer
ETM – electron-transporting material
E_{T1} – energy of first triplet state
ExBL – exciton blocking layer
Fc – ferrocene
FL – fluorescence
FTO – fluorine doped tin oxide
F_w –water fractions
HIL – hole injection layer
HOMO – highest occupied molecular orbital
HTL – hole transport layer
HTM – hole transporting material
IC – internal conversion
ICT – intermolecular charge transfer
IP_{CV} – ionization potential measured by CV
IP_{PE} – ionization potential measured by photoelectron spectroscopy
IQE – internal quantum efficiency
$Ir(piq)_2(acac)$ – bis(1-phenylisoquinoline)(acetylacetonate)iridium(III)
ISC – intersystem crossing
ITO – indium tin oxide
J-V – current density-voltage
L_{max} – maximum brightness
LUMO – lowest unoccupied molecular orbital
mCP – 1,3-bis(N-carbazolyl)benzene
MoO_3 – molybdenum trioxide
NPB – N,N'-Di(1-naphthyl)-N,N'-diphenyl-(1,1'-biphenyl)-4,4'-diamine
OLED – organic light emitting diode
OPVs – organic photovoltaic cells
PE – power efficiency
PEDOT:PSS – poly(3,4-ethylenedioxythiophene) polystyrene sulfonate
PFBP-2b – 10,10'-(perfluoro-[1,1'-biphenyl]-4,4'-diyl)bis(2,7-di-tert-butyl-9,9-dimethyl-9,10-dihydro-acridine)
PhOLEDs – phosphorescent organic light-emitting diodes
PL – photoluminescence
PLQY – photoluminescence quantum yield
PVD – physical vacuum deposition
RISC – reversed intersystem crossing
TADF – thermally activated delayed fluorescence
TAPC – 1,1-bis[(di-4-tolylamino)phenyl]cyclohexane
$T_{de-5\%}$ – 5% weight loss temperature

T_d^{onset} – temperature of onset of thermal degradation

TFB – poly(9,9-dioctylfluorene-alt-N-(4-sec-butylphenyl)-diphenylamine)

T_g – glass transition temperature

TGA – thermogravimetric analysis

THF – tetrahydrofuran

TICT – twisted intermolecular charge transfer

T_m – melting temperature

ToF – time-of-flight

TPBi – 2,2',2''-(1,3,5-benzinetriyl)-tris(1-phenyl-1-H-benzimidazole)

TSPO1 – diphenyl[4-(triphenylsilyl)phenyl]phosphine oxide

TTA – triplet-triplet annihilation

UV-VIS – ultraviolet-visible

V_{on} – turn-on voltage

ΔE_{S1T1} – first singlet-triplet energy gap

k_{DF} – radiate rates of delayed fluorescence

k_{ISC} – intersystem crossing rate

k_{nr}^s – non-radiative rates of the singlet state

k_{nr}^T – non-radiative rates of the triplet state

k_{PF}^r – radiative rates of prompt fluorescence

k_{RISC} – reverse intersystem crossing rate

λ_{abs} – wavelength of absorption maximum

λ_{PL} – wavelength of emission maximum

μ_0 – hole drift mobility value at 0 V cm^{-1} field strength

μ_{holes} – hole drift mobility

η_{DF} – delayed fluorescence quantum yield

η_{ISC} – intersystem crossing quantum yield

η_{PF} – prompt fluorescence quantum yield

η_{RISC} – reverse intersystem crossing quantum yield

τ – excited-state lifetime

τ_{DF} – lifetime of delayed fluorescence

τ_{PF} – lifetime of prompt fluorescence

τ_{PF}^{nr} – non-radiative decay of prompt fluorescence

τ_{PF}^r – radiative decay of prompt fluorescence

1. INTRODUCTION

Organic semiconductors attract an outstanding attention due to their astonishing optoelectronics properties having numerous potentialities[1–3]. Due to their tunable properties, organic materials have the potential to be used in different devices, such as photovoltaics (PVs), field-effect transistors (FETs), and specifically, light-emitting diodes (LEDs)[4,5]. Additionally, organic materials are widely adaptable with different fabrication methods (for instance, vacuum deposition, spin-coating method, roll-to-toll coating as well as ink-jet printing), which provide all possibilities for commercialization[6,7]. Since the publication of the research article by Tang and VanSlyke in 1987[8], reporting the world's first working organic light-emitting diodes (OLEDs) by embedding the two layers of organic thin films between two electrodes, these diodes have attracted strong interest from both industrial researchers as well as academic scientists, and OLEDs have become a well-established and mature display technology. Almost half of the sold mobile phones during the year 2021 were made up of OLED displays[9]. OLED fabrication needs lower temperatures[10] and less hazardous substances in comparison to the inorganic materials. Instead of the narrow viewing angle provided by the liquid-crystal displays (LCDs), OLEDs usually feature a Lambertian emission distribution and require less active components compared to an LCD[11,12]. It is more practical to fabricate micro-OLED displays for the eye-friendly screens by minimizing the OLED pixel size to only a few micrometers[13]. The breakthrough in the development of efficient high quality sources of light that can be utilized for artificial lighting was the introducing of blue-colored LEDs, which was rewarded with the Physics Nobel Prize in 2014[14]. In addition to the white organic light emitting diodes (WOLEDs), which are high potential candidates for industrial scale solid state light sources, monochrome OLEDs can be utilized as light sources in automotive industries[15,16]. Two main practical applications of Organic LEDs as solid-state lighting and display are enabled by two core properties of derived device layouts and organic semiconductor materials. The OLEDs, which are made from thin films, are area light sources, and they can provide new opportunities for different applications. Associated with the quite low rigidity of the organic materials, the nanoscale films grant the fabrication of OLEDs on foldable and flexible substrates as well[17,18]. Additionally, the color and the broadening of the emission spectrum from organic semiconductors can be tuned by the synthesis of organic compounds. Using more than one emitter in the emissive layer allows eye-friendly natural light to be made most efficiently[19,20]. New fabricated efficient OLEDs have reached efficiencies, which are on a par with fluorescent tubes[21,22]. At the same time, the device lifetime becomes compatible with other commercial light sources, and OLEDs that are reaching more than 100,000 hours have already been reported[23]. However, still suitable material combinations that obtain long lifetime and high efficiency together with good color rendering in OLEDs are hard to find. One of the main explanations for widespread market of OLED in display technology and not in lighting area, is the efficiency roll-off, which is a quite fast efficiency loss at high current density or luminance[24,25]. Fig. 1.1 a shows this efficiency roll-off and illustrates two different OLED applications, which are separated according to their brightness regime. The

required brightness for the display market and industry is between 100 to 500 cd/m^2, and in the case of solid state lighting, it is between 1,000 and 10,000 cd/m^2 [26–28]. Therefore, high brightness is one of the most important challenges to be addressed in order to enable the use of OLEDs in the solid state lighting. Along with stability and efficiency of OLEDs, the color quality and purity of the lights are highly demanded, especially in the display market. In 2012, the International Telecommunication Union (ITU) introduced the new color gamut standard called the BT 2020 or Rec. 2020 for ultra-high-definition TV (UHDTV), and in comparison with the previously reported standards, such as National Television Standards Committee (NTSC), the color gamut became wider (Fig. 1.1 b)[29].
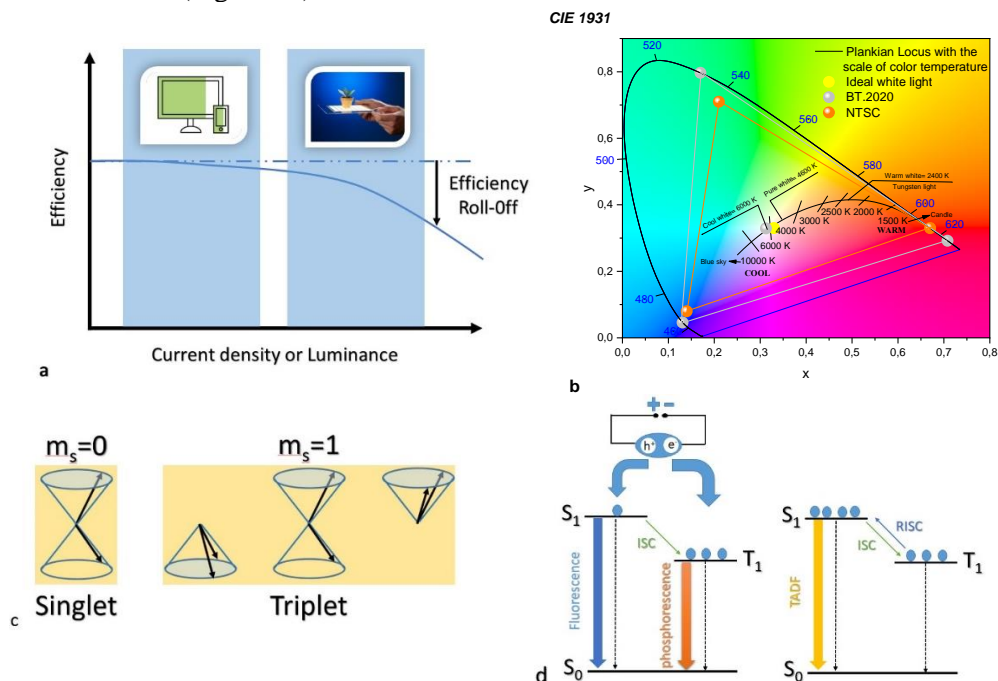
Fig. 1.1. Scheme of efficiency loss (roll-off) in low and high luminance for display and lighting application (a), Planckian locus in the CIE 1931 chromaticity diagram and two different display Color Gamuts and Standards (b) the spin states of singlet and triplet states with their spin quantum numbers (m_s) (c), simplified Jablonski diagram (d)[30]

Considering all that have been mentioned above and aiming to obtain better light quality and higher efficiencies in OLEDs, the urgent need for the synthesis and characterization of novel materials showing good photoluminescence quantum yield (PLQY) and internal quantum efficiency (IQE) are becoming more crucial. Subsequent research has deduced that a huge limitation of fluorescent OLEDs is their large contribution of generated "dark" excited triplet states, which do not have any role in photon generation; thus, in the case of fluorescent compounds, merely emission, which comes from singlet states (25% of all excitons), contributes to the total quantum efficiency. The triplet exciton radiative decays (75% of the total generated excitons) into the electron ground state is not allowed by the quantum

10

theory rules[31] (Fig. 1.1 c). Since 1997, heavy organometallic complexes with emissive triplet states were utilized for harvesting generated singlet and triplet excitons, and an external quantum efficiency (EQE) of 20%, corresponding to potentially 100% IQE, was finally obtained in a phosphorescent OLEDs (PHOLEDs)[32–35]. The strong spin-orbit coupling in the compounds with heavy (high dense) metals can improve the intersystem crossing processes, which can bring about the combination of the singlet and triplet natures of electron excited states. This phenomenon may result in the shortened lifetime of the triplet excited state, and accordingly, the phosphorescence emission can be detected easily[36,37]. Green and red phosphorescent compounds have been extensively exploited in the active-matrix OLEDs (AMOLEDs) display market. However, the stability and lifetime of reported blue PHOLEDs need to be further developed[38–40]. In 2012, a scientific paper by Adachi and co-workers in *Nature* journal revolutionized the entire OLED research area[41]. The first evidence of the mentioned phenomena in a fully organic molecule was rationalized a few decades ago[42–43], and it proposed the solutions for common OLED issues, which attracted the attention of several research groups all around the world, and the process is referred to as thermally activated delayed fluorescence (TADF) phenomenon (Fig. 1.1 d). Over the past 11 years, aiming to tackle both efficiency and stability issues of OLEDs, the researchers have been designing and synthesizing new TADF compounds, which are heavy metal-free emitters[44–46]. TADF compounds allow (similar to the compounds with phosphorescence emission) for the exploitation of all generated excitons to light (100% IQE) and bring hope to fabricate OLEDs with longer device stability and lifetime[47,48]. OLED market sizes are growing quickly, and they are rapidly becoming the next generation of displays and lighting industry due to the ever-growing demands. However, the technology is still emerging, and further research is needed to alleviate a number of major concerns including following ones:

- As it has already been mentioned, higher brightness is needed in OLED lighting panels, and accordingly, applying remarkably higher current densities is a must in comparison with the specifications, which is essential for general display. Higher current densities can lead to the joule self-heating and electrothermal feedback in semiconductor devices. These two phenomena may bring about serious limitations to the OLED lighting industry[49].

- Even a small lighting efficiency enhancement will result in remarkable savings in regards to the cost and energy, thus improving the efficiencies and performances of OLEDs by designing new compounds and optimizing the OLED stacks, which is of importance[50].

- Another main issue that should be addressed is attributed to the scaling up small prototype OLEDs to the large-scale devices. Most high-performance reported OLEDs are based on the small-molecule compounds, and the only downside of these materials is that for device fabrication, the vacuum deposition methods need to be used, which can lead to both a high wastage rate of compounds and the use of expensive equipment. The current trend is moving toward solution-processable materials and methods in order to

fabricate more economical devices and try to bring down the WOLED prices to be able to compete in the mainstream markets[51,52].

- From the compound point of view, there is still an essential need for materials with bipolar properties, which can maintain the carrier balance especially at high current densities. Having this property of a material can help to avoid EQE roll-off and other reducing effects[53].

- Since most of the materials with efficient emission can only emit in a spectral fraction of the visible light, doping luminophores with a complementary color into a suitable host is the main approach for generating white emission. In this approach, the chemical and morphological stability of each material is crucial for the lifetime of the OLED, and the main issue would be the possible differential aging of emitters in the emissive layer. Over the operation range of driving voltage, and due to the energy-transfer processes from short-wavelength emitters to long-wavelength ones, the variation of different color in the final EL spectrum usually changes the stability of the white light and worsens the quality of emission[54,55].

The mentioned issues can be resolved by incorporating new organic semiconductors, as it is proposed in this thesis. The author of this research has expanded the knowledge on the correlation between the photophysical, charge-transporting, thermal, electrochemical, and optoelectrical properties of functional OLED materials and their resulting OLED output performances.

The aim of this work is the characterization of new blue fluorescent emitters for the development and fabrication of efficient OLEDs.

In order to accomplish the aim of the work, **the following objectives** were proposed:

- To study the photophysical, photoelectrical, thermal, charge transport and electroluminescence characteristics of two new phenyl bicarbazole derivatives for developing exciplex-forming systems for oxygen sensors and white hybrid solution-processed OLEDs.
- To investigate two benzophenones derivatives as blue emitters, exciton modulators, and hole-transporting compounds for developing OLED stacks with stable white electroluminescence and good color quality.
- To investigate the effect of a variety of additional acceptors in molecular structure of five multicarbazole and benzonotrile derivatives used as emitters on the performances of blue TADF OLEDs.
- To provide media dependent tuning of blue emission and spin-flip efficiency of multicarbazole-based compounds with different additional acceptors for the improvement of their TADF efficiency.
- To investigate photophysical, photoelectrical, charge transporting and electroluminescent properties of trifluoromethyl benzene-based multidonor–acceptor conjugated derivatives.
- To study the effect of conformational disorder and solid-state solvation on the emission properties of blue OLEDs with non-doped and differently doped emissive layers.

The novelty of the work

- Efficient exciplex-based emitters exhibiting TADF with significant RISC rates up to 5.1×10^7 s^{-1} were designed based on new bicarbazole derivatives substituted by different electron donor moieties (fluoro- or trifluoromethyl). Their applicability was demonstrated for sensing the oxygen and hybrid solution-processable WOLEDs with high color rendering index.
- The spatial exciton allocation strategy was first time used for WOLEDs based on TADF emitters. The strategy allowed modulation and separation of excitons and charges at the exciton recombination region and carrier recombination region resulting in ca. with twice higher EQE and higher quality of white color for developed OLEDs in comparison to the reference OLEDs.
- Enhanced TADF efficiency and high reverse inter-system crossing rates from 4.7×10^4 to 2.32×10^6 s^{-1} were achieved for multicarbazolyl-substituted benzonitriles blue TADF emitters containing a variety of additional acceptors for efficient OLEDs with tunable color variations of blue electroluminescence.
- The minimization of solid-state solvation and conformation disorder corollaries on the performance of blue TADF emitters by multi-donor-acceptor substitution engineering for doping-free and host-based OLEDs with unusually similar electroluminescent performances.

Contribution of the author

The presented dissertation was conducted by the author in collaboration with researchers from Kaunas University of Technology, Lviv Polytechnic National University, University of Malaya, University of Latvia, and National Taiwan Normal University. The author characterized the photophysical, thermal, photoelectrical, charge-transporting, and electroluminescent properties of four groups of newly synthesized blue emitters. Dr. Jonas Keruckas has designed, synthesized and purified two series of bicarbazole and benzophenones-based derivatives. The synthesis and purification of multicarbazole-based TADF emitters were done by Dr. Dalius Gudeika. The oxygen-sensing properties of bicarbazole derivatives were characterized by Mr. Karolis Leitonas. Dr. Viktorija Andrulevičienė has performed and analyzed the DFT calculations of bis(N-naphthyl-N-phenylamino)benzophenones compounds. Dr. Rasa Keruckienė assisted with the synthesis of benzophenone-based derivatives and discussed the obtained results. DFT calculation and Visual Molecular Dynamics (VMD) results of trifluoromethyl phenyl-based multicarbazole were obtained by Dr. Kai Lin Woon (Low Dimensional Material Research Centre, Department of Physics, University of Malaya). Dr. Rita Butkutė measured the mass spectrometry data and helped with the identification of synthesized multicarbazole. Mr. Levani Skhirtladze assisted with the synthesis and purification of multicarbazole TADF compounds. The design and synthesis of sky-blue TADF emitters (PFBP-2b) were performed by Dr. Iryna Danyliv (Department of Electronic Devices, Lviv Polytechnic National University). Mr. Stepan Kutsiy (Department of Electronic Devices, Lviv Polytechnic National University) carried out the cyclic

voltammetry (CV) measurements of bicarbazole materials. Mr. Edgaras Narbutaitis assisted with the synthesis and identifications of two benzophenones-based blue emitters. The ionization potential measurements of one series of compounds were performed by Dr. Yu-Chiang Chao (Department of Physics, National Taiwan Normal University). Prof. Dr. Martins Rutkis (Institute of Solid State Physics, University of Latvia) ran and analyzed the DFT calculation data for one series of compounds. Dr. Dmytro Volyniuk investigated the hole and electron transport properties of the compounds, advised with the measurements and device fabrication, and assisted with the preparation of the manuscript original drafts, and finally, Prof. Dr. Hab. Juozas Vidas Gražulevičius, as a group leader, assisted with funding acquisition, reviewing and editing of the manuscripts.

List of scientific publications on the topic of dissertation

1. **Mahmoudi, Malek**; Keruckas, Jonas; Leitonas, Karolis; Kutsiy, Stepan; Volyniuk, Dmytro; Gražulevičius, Juozas Vidas. Exciplex-forming systems with extremely high RISC rates exceeding 10^7 s^{-1} for oxygen probing and white hybrid OLEDs // *Journal of Materials Research and Technology*. Amsterdam: Elsevier. ISSN: 2238-7854. 2021, vol. 10, p. 711–721. (Web of Science) DOI: 10.1016/j.jmrt.2020.12.058. [IF:6.267; Q1]
2. **Mahmoudi, Malek**; Keruckas, Jonas; Volyniuk, Dmytro; Andrulevičienė, Viktorija; Keruckienė, Rasa; Narbutaitis, Edgaras; Chao, Yu-Chiang; Rutkis, Martins; Grazulevicius, Juozas Vidas. Bis(N-naphthyl-N-phenylamino) benzophenones as exciton-modulating materials for white TADF OLEDs with separated charge and exciton recombination zones // *Dyes and Pigments*. Oxford: Elsevier. ISSN: 0143-7208. 2022, vol. 197, art. no. 109868, p. 1–10. (Web of Science) DOI: 10.1016/j.dyepig.2021.109868. [IF:5.122; Q1]
3. **Mahmoudi, Malek**; Gudeika, Dalius; Volyniuk, Dmytro; Leitonas, Karolis; Butkute, Rita; Danyliv, Iryna; Grazulevicius, Juozas Vidas. Tuning of spin-flip efficiency of blue emitting multicarbazolyl-substituted benzonitriles by exploitation of the different additional electron accepting moieties // *Chemical Engineering Journal*. Amsterdam: Elsevier. ISSN: 1385-8947. 2021, vol. 423, art. no. 130236, p. 1–12. (Web of Science) DOI: 10.1016/j.cej.2021.130236. [IF:16.744; Q1]
4. **Mahmoudi, Malek**; Gudeika, Dalius; Kutsiy, Stepan; Simokaitiene, Jurate; Butkute, Rita; Skhirtladze, Levani; Woon, Kai Lin; Volyniuk, Dmytro; Grazulevicius, Juozas Vidas. Ornamenting of blue thermally activated delayed fluorescence emitters by anchor groups for the minimization of solid-state solvation and conformation disorder corollaries in non-doped and doped organic light-emitting diodes // *ACS Applied Materials & Interfaces*. NW, Washington, DC: American chemical society. ISSN: 1944-8244; 2022, vol. 14, iss. 35, p. 40158–40172. (Web of Science) DOI: 10.1021/acsami.2c12475. [IF:10.383; Q1]

2. REVIEW OF PUBLISHED ARTICLES

The chapter Review of Articles contains the information from articles of the author (see List of publications on the subject of the thesis).

2.1. Exciplex-forming systems with extremely high RISC rates exceeding 10^7 s^{-1} for oxygen probing and white hybrid OLEDs (Scientific publication No. 1, Q1)

This chapter is based on the article published in *Journal of Materials Research and Technology*, 2021, vol. 10, p. 711–72[56]. Due to the fact that 9,9-H or 9,9-diphenyl bicarbazole exhibited excellent application in OLEDs as a donor for making exciplexes[57,58], this work aims to investigate two novel designed diphenyl bicarbazoles substituted by fluoro- or trifluoromethylphenyl moieties as donors for making exciplexes. The molecular structures of compounds **1** and **2** are presented in Fig. 2.1.
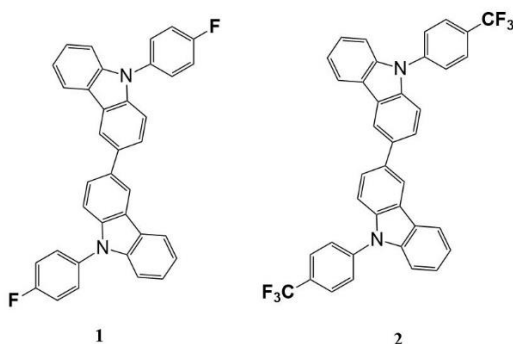
Fig. 2.1. Molecular structures of compounds **1** and **2**

The 5% weight-loss temperatures ($T_{de-5\%}$, ℃) and the thermal transition of the compounds were studied by thermogravimetric analysis (TGA) and differential scanning calorimetry (DSC), respectively. All the data are summarized in Table 2.1. The melting points (T_m, ℃) for both materials were close and situated close to 250 °C when measured by using DSC equipment (sharp endothermic peaks in second heating scans (Fig. 2.2 a, inset)). The synthesized materials formed molecular glasses with glass-transition temperatures (T_g, ℃) of 101 °C for compound **1** and 111 °C for compound **2**. However, the glasses of these compounds tended to crystallize above their glass-transition temperatures. According to the TGA measurements (Fig. 2.2 a), 5% weight-loss temperatures of 374 and 350 °C were observed for **1** and **2**, respectively. Since the materials melted at 250 °C and then experienced complete weight loss at around 450 °C, the detected weight loss may be rather ascribed to the sublimation rather than material decomposition[59].
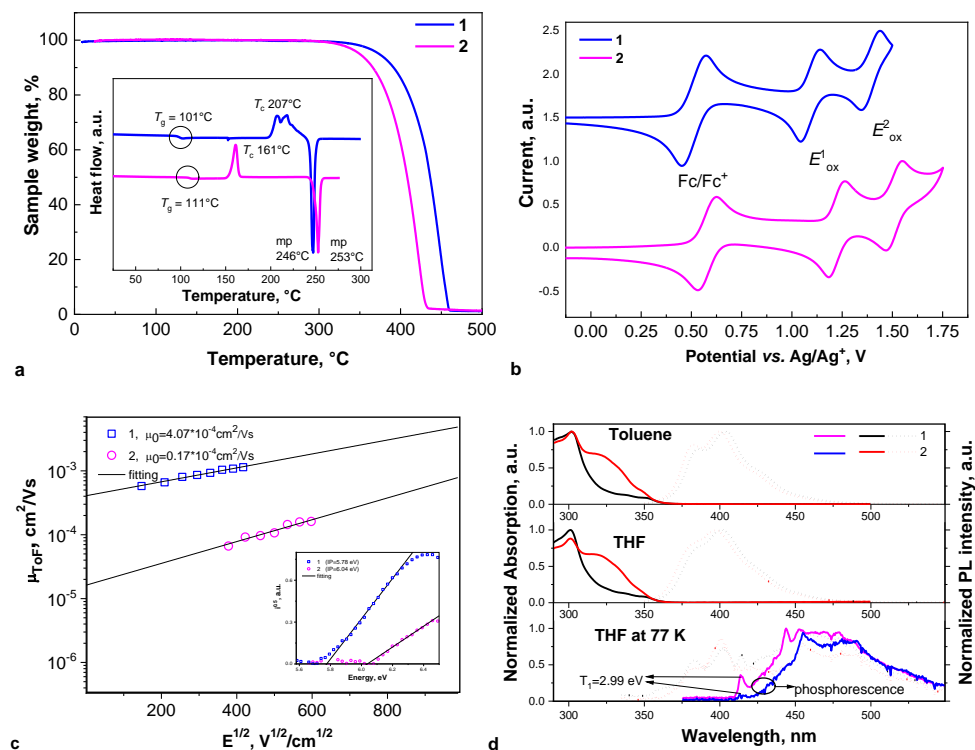
Fig. 2.2. TGA curves and DSC second heating scans (inset) (a), CV voltammograms (b), hole mobility vs. applied electric field and electron photoemission spectra (inset), (c) ultraviolet-visible absorption, PL, and phosphorescence spectra of the dilute solutions of the synthesized compound (d)

The energy levels of the materials were investigated by both cyclic voltammetry (CV) and photoelectron emission spectroscopy (PE) techniques. With the aim of measuring the material electrochemical energy levels, their dichloromethane (DCM) solutions exhibited oxidation half-waves with regard to ferrocene at 0.58 V for compound **1** and 0.65 V for compound **2** (Fig. 2.2 b). Regardless of the small difference (0.07 V) between the oxidation potentials of the compound solutions, a clearly larger difference (0.26 eV) was recorded between their ionization potentials measured by the photoelectron spectroscopy in the air. IP_{PE} of 5.78 eV was detected for the film of compound **1** and 6.04 eV for the film of compound **2**, which are higher than the corresponding values of 5.38 and 5.45 eV measured by CV (Fig. 2.2 c inset and Table 2.1)[60]. As a result of the effective electron withdrawing capacity of CF3 groups compared with that of 4-fluorophenyl groups, for compound **2**, the higher IP_{PE} (deeper HOMO) was observed. The charge carrier characteristics of the materials were tested by the time of flight (TOF) technique, and the results showed low-dispersity positive charge carriers in the compound **1** and **2** films. Hole mobilities (μ_{holes}) of the compounds at different applied electric fields (E) were estimated by taking the transit time values (t_{tr}) at different applied voltages (Fig. 2.2 c, Table 2.1). Compounds **1** and **2** showed only positive charge carrying characteristics apparently

16

due to the not strong enough electron-accepting capability of fluoro or trifluoromethyl moieties[61]. The recorded different values of hole mobilities of the compounds (Table 2.1) could be associated with their dissimilar structure of the layers and their molecular packing, as it was confirmed for other carbazole-containing materials[62,63]. Aiming to study the effect of different substituents on the photophysical characteristics of the materials, photoluminescent (PL) and UV-Vis absorption spectra of the compound THF and toluene solutions (~10^{-5} M) were recorded (Fig. 2.2 d). Since the shape of the absorption spectrum of compound **1** is almost identical to that of carbazole, N-phenylcarbazole, and N,N'-diphenyl(-3,3-)bicarbazole, the carbazole unit is mainly accountable for absorption[64,65]. However, low energy band around 325 nm of compound **2** absorption spectrum could be induced by charge transfer between carbazole and trifluoromethylbenzene units. Vibronically structured fluorescence emission spectra peaked at 385 and 405 nm for dilute toluene solutions of compounds can be ascribed to the locally exited (LE) emission (Fig. 2.2 d, Table 2.1)[66]. Photoluminescence and phosphorescence spectra of dilute THF solutions of compounds were measured as well for obtaining their first excited singlet (E_{S1}) and triplet (E_{T1}) energy states (Fig. 2.2 d, Table 2.1). PLQY values of compounds **1** and **2** neat films and solutions are in the same range of recorded PLQYs of the previously reported N-phenylcarbazoles and N-phenylbicarbazoles (Table 2.1)[67].

As a result of their balanced hole-transporting properties, high triplet levels and emission in the near ultraviolet area of compounds **1** and **2**, they can be considered as high potential donors for making exciplexes with TADF emission. Therefore, two solid-state mixtures by using commercial acceptor 2,4,6-tris[3-(diphenylphosphinyl)phenyl]-1,3,5-triazine (PO-T2T) and compound **1** and **2** as donor units were developed. The samples **1**:PO-T2T and **2**:PO-T2T showed red-shifted exciplex kind emission compared to the pure emission of acceptor and donor units (around 110 nm compared to the donors and 150 nm compared to the acceptor) (Fig. 2.3 a). PL spectra and PL decays at different temperatures proved that about 90% of the whole emission intensity of the developed exciplex samples originated from the thermally activated delayed fluorescence contribution (Fig. 2.3 b, c).

Another confirmation of the existence of TADF in the emission of the obtained exciplex was the small energy gap between singlet state and triplet state (ΔE_{S1T1}), which allowed efficient RISC process (Fig. 2.3 d, Table 2.2). 1:PO-T2T and 2:PO-T2T exciplexes showed similar emission around 520 nm, and their PL decays exhibited a two-component exponential decays with short-lived (τ_{PF} of 69 to 376 ns) and long-lived (τ_{DF} of 1.94 to 4.25 µs) components (Fig. 2.3 a, b). Unlike the previously reported exciplexes[68,69], due to the low non-radiative losses and efficient TADF, PLQY values of the investigated exciplexes linearly increased with rising temperature (Fig. 2.3 e, f).

Table 2.1. Thermal, electrochemical, photoelectrical, hole-mobilities, and photophysical characteristics of materials **1** and **2**

Property	Sample	1	2
T_m, ºC	Powder	246	253
T_g, ºC		101	111
T_{cr}, ºC		206	161
$T_{de-5\%}$, ºC		374	350
$E_{ox\ vs}$ Ag/Ag$^+$, V	DCM solution with TBAPF$_6$	0.58	0.65
IP_{CV}, eV		5.38	5.45
IP_{PE}, eV	Film	5.78	6.04
E_g^{opt}, eV		3.36	3.21
EA_{PE}, V		2.42	2.83
λ_{PL}, nm	Film (THF solution)	390, 409 (385[*], 402)	387, 404 (383[*], 397)
PLQY, %		19 (15)	15 (18)
τ, ns		4.68 (6.09)	4.02 (6.01)
E_{S1}, eV	THF solution at 77 K	3.44	3.38
E_{T1}, eV		2.99	2.99
ΔE_{S1T1}, eV		0.45	0.39
μ_{holes},[a] cm^2/(V·s)	Film	1.1×10^{-3}	7.7×10^{-5}

[*] Shoulder, [a] at applied electric field of 1.6×10^5 V/cm

Taking prompt and delayed fluorescence lifetimes (τ_{PF} and τ_{DF}) and the corresponding quantum yields (η_{PF} and η_{DF}), prompt (k_{PF}) and delayed (k_{DF}) fluorescence radiative rates were calculated. Additionally, non-radiative rates of the singlet (k_{nr}^S) and triplet (k_{nr}^T) states, intersystem crossing rate (k_{ISC}) and reverse intersystem crossing rate (k_{RISC}) were estimated (Table 2.2). k_{RISC}, as an important criterion, is generally assigned to the efficient TADF, and for newly reported intramolecular and intermolecular TADF materials, it is in the order of 10^6 s^{-1} [70,71].

Exciplexes 1:PO-T2T and 2:PO-T2T showed exceptionally high k_{RISC} of 5.1×10^7 and 3.6×10^7 s^{-1}, respectively. The obtained rates are among the highest reported k_{RISC} values until now[70,71]. In spite of the slight difference in the molecular design of compounds **1** and **2**, which basically have no effects on the emission spectra of **1**:PO-T2T and **2**:PO-T2T, quite different non-radiative rate constants (k_{nr}^T) were recorded for these exciplexes. The explanations of this aspect can be related to the different molecular packing due to the presence of various fluoro and trifluoromethyl units in compounds **1** and **2** as well as different hole mobilities of compounds, which can lead to rapid formation of exciplex states. By analyzing the temperature dependences of k_{RISC} and using the Arrhenius equation: $k_{RISC}=A\cdot\exp(-E_a/k_BT)$, the activation energy (E_a) values of 0.052 and 0.127 eV were recorded for exciplex **1**:PO-T2T and **2**:PO-T2T emissions, respectively (Table 2.2)[72].
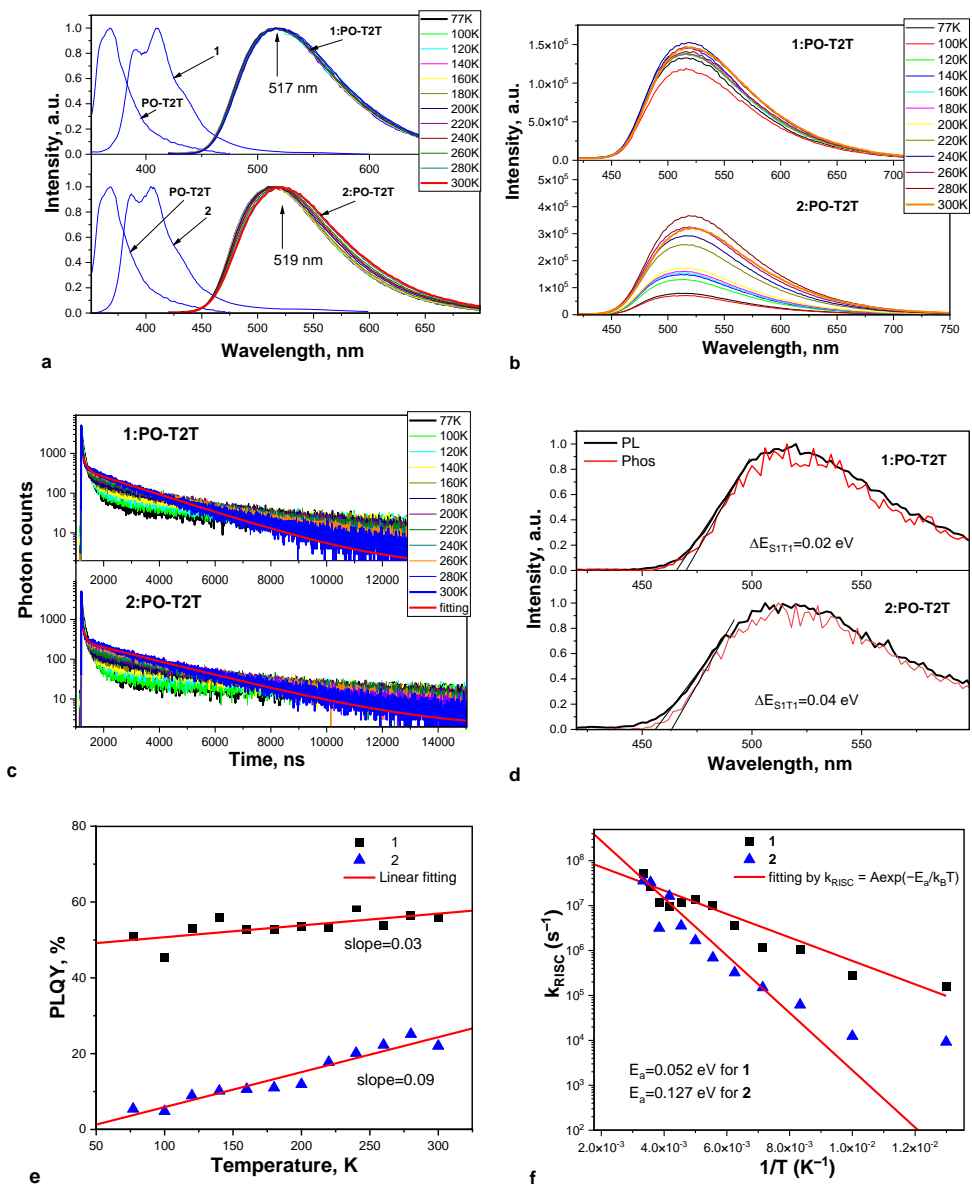
Fig. 2.3. Normalized PL spectra (a) and temperature-dependent PL spectra (b) of the compound **1**, **2**, PO-T2T, **1**:PO-T2T, and **2**:PO-T2T films. The corresponding PL decay curves recorded at different temperatures (c), photoluminescence and phosphorescence spectra measured at 77 K (d) of **1**:PO-T2T and **2**:PO-T2T solid-state mixtures, temperature-dependent PLQY values (e) and k_{RISC} versus 1/T (f) plots for **1**:PO-T2T and **2**:PO-T2T

1:PO-T2T exciplex-forming system was chosen to test its possible application as an oxygen sensor. This sample showed a total PLQY of 56%, which is higher than PLQY of 22% for **2**:PO-T2T exciplex. Since the origin of the **1**:PO-T2T exciplex-forming sample was mainly delayed fluorescence (η_{DF} = 52% versus η_{PF} = 4% (Table

19

2.2)), the oxygen probing capability of this system is more practical if the delayed fluorescence is quenched in the presence of oxygen. Aspiring to check the capability of the 1:PO-T2T exciplex as an active device for oxygen sensing, samples **1**:PO-T2T:Zeonex (1:1:1) with three-component were fabricated. Zeonex matrix was utilized for insuring the oxygen permeability of the films and helping for the good formation of the probe film[73]. The emissions of prepared samples were measured at several different concentrations of oxygen in a continuous circulation of oxygen and nitrogen mixtures (Fig. 2.4 a).

Table 2.2. Photophysical parameters of exciplex-forming molecular mixtures **1**:PO-T2T and **2**:PO-T2T derived at room temperature (300 K)

Exciplex	source/equation	**1:** **PO-T2T**	**2:** **PO-T2T**
λ_{PL}, nm	taken from PL spectra	517	519
FWHM, nm		104	107
E_{S1}, eV	$E_{S1} = 1240/\lambda_{seton}^{PL}$	2.63	2.72
E_{T1}, eV	$E_{T1} = 1240/\lambda_{seton}^{Phos}$	2.64	2.68
ΔE_{S1T1}, eV	$\Delta E_{S1T1} = E_{S1} - E_{T1}$	0.02	0.04
PLQY, %	measured with a sphere	56	22
η_{PF}	$\eta_{PF} = \eta_{PLQY} * PF(\%)/100(\%)$	0.04	0.01
η_{ISC}	$\eta_{ISC} = 1 - \eta_{PF}$	0.96	0.99
η_{DF}	$\eta_{DF} = PLQY * DF(\%)/100(\%)$	0.52	0.21
η_{RISC}	$\eta_{RISC} = \eta_{DF}/(\eta_{PLQY} * \eta_{ISC})$	0.97	0.96
E_a, eV	taken from k_{RISC} fitting by $k_{RISC} = A exp(-E_a/k_B T)$	0.052	0.127
τ_{PF}, ns (%)	from PL decay fitting by	110 (7)	94 (5)
τ_{DF}, μs (%)	$I = A+B1exp(-t/\tau_{PR})+B2exp(-t/\tau_{DF})$	1.94 (93)	2.47 (95)
τ_{PF}^{r}, μs	$\tau_{PF}^{r} = \tau_{PF}/\eta_{PF}$	2.8	9
τ_{PF}^{nr}, ns	$\tau_{PF}^{nr} = \tau_{PF}/(1 - \eta_{PF})$	115	95
k_{PF}, s^{-1}	$k_{PF} = \dfrac{\eta_{PF}}{\tau_{PF}}$	3.6×10^5	1.1×10^5
k_{PF}^{r}, s^{-1}	$k_{PF}^{r} = 1/\tau_{PF}^{r}$	3.6×10^5	1.1×10^5
k_{nr}^{S}, s^{-1}	$k_{PF}^{nr} = 1/\tau_{PF}^{nr}$	8.7×10^6	1.05×10^7
k_{ISC}, s^{-1}	$k_{ISC} = \dfrac{\eta_{DF}}{\eta_{PF}+\eta_{DF}} k_{PF}$	0.25×10^5	0.05×10^5
k_{DF}, s^{-1}	$k_{DF} = \dfrac{\eta_{DF}}{\tau_{DF}}$	2.69×10^5	0.85×10^5
k_{RISC}, s^{-1}	$k_{RISC} = \dfrac{\eta_{DF}}{\eta_{PF}} \cdot \dfrac{k_{PF}.k_{DF}}{k_{ISC}}$	5.1×10^7	3.6×10^7
k_{nr}^{T}, s^{-1}	$k_{nr}^{T} = k_{RISC}/\eta_{RISC} - k_{RISC}$	4.7×10^7	1.35×10^8

The results of Stern–Volmer equation fitting are collected in the inset Table of Fig. 2.4 b, and fitting with R^2 of 0.9652 was obtained[74,75]. In spite of the high ratio η_{DF}/η_{PF} of 13, the ratio of emission intensity under pure nitrogen gas and intensity of emission under pure oxygen atmosphere ($I_{0[100\% N2]}/I_{[100\% O2]}$) of 1.57 was recorded, which proves that the fabricated sample (**1**:PO-T2T:Zeonex) showed relatively low oxygen sensitivity. This measurement is similar to the results of time resolved

20

fluorescence measurements of **1**:PO-T2T:Zeonex film in the air and vacuum proving that this obtained exciplex shows delayed fluorescence even in the presence of oxygen atmosphere (Fig. 2.4 c). It seems that oxygen cannot quench the delayed fluorescence completely when the TADF emitters are characterized by very high k_{RISC} of higher than 10^7 s^{-1}.
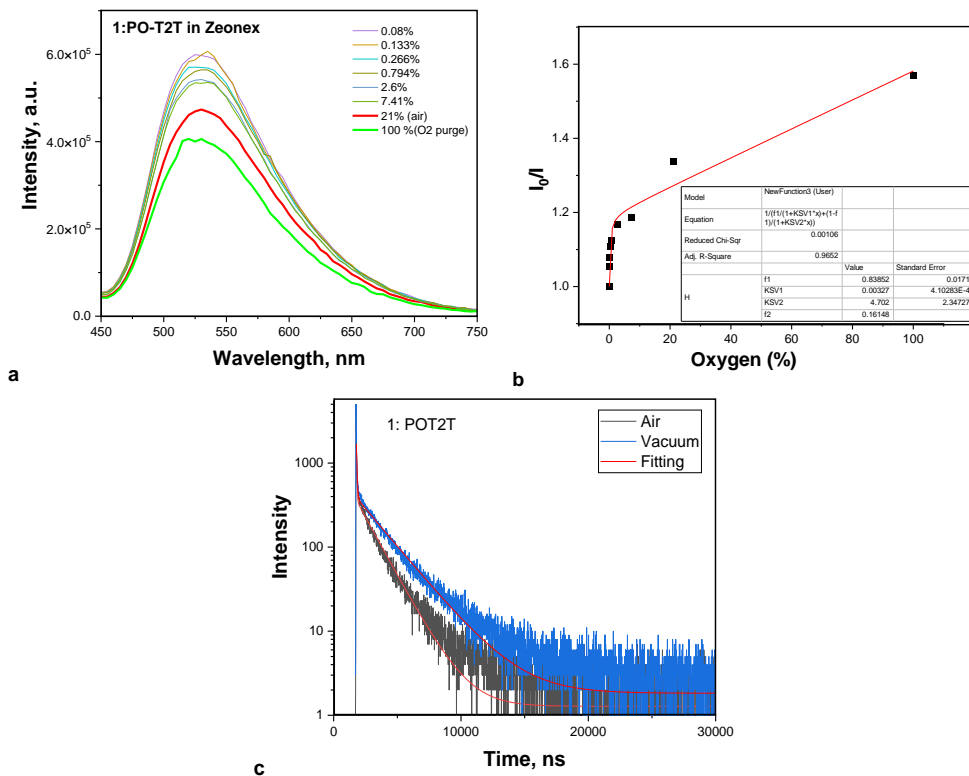
Fig. 2.4. PL spectra (a), Stern–Volmer dependence (b), and PL time decay curves (c) of the **1**:PO-T2T:Zeonex films at different oxygen concentrations

Aiming to obtain natural white emission, two deeply investigated exciplexes, **1**:PO-T2T and **2**:PO-T2T, were selected to use in white OLED structures, and in combination with blue TFB[76] and red (Ir(piq)2(acac))[77] emitters, several solution-based OLED devices were fabricated. The main reason for choosing the solution-based method was that this method could allow to have accurate control on the concentration of emitting compounds in the doped emissive layers, which was essential for WOLEDs fabrication[78]. The OLED device structures consisting of ITO/MoO$_3$ (1 nm)/TFB:Ir(piq)2(acac) (2, 5, or 10 wt%, 30 nm)/**1**:PO-T2T (for the devices named as A2, A5, and A10, respectively) or **2**:PO-T2T (for the devices named as B2, B5, and B10, respectively) (1:1) (20 nm)/ TSPO1 (8 nm)/TPBi (40 nm)/LiF:Al were chosen. Very thin layer of MoO$_3$ was utilized as hole injection layer, TSPO1 compound acted as hole/exciton blocking layer; TPBi material was used as the electron transporting layer, and finally, LiF material was selected to be used in the electron injection layer. By checking the equilibrium energy diagram of the device

structures (Fig. 2.5 a), it can be seen that the recombination zone was principally placed in the emissive layer (EML1, **1**:PO-T2T, or **2**:PO-T2T). The hole-transporting layer of TFB, which was doped by a low concentration of Ir(piq)$_2$(acac), as well played as the second emissive layer (EML2). There are two possibilities for the emission of Ir(piq)2(acac) red emitter. First, when there is a triplet exciton generation in EML1 and then shifting to EML2 and second, when there is a direct recombination of electrons and holes in EML2 [79].
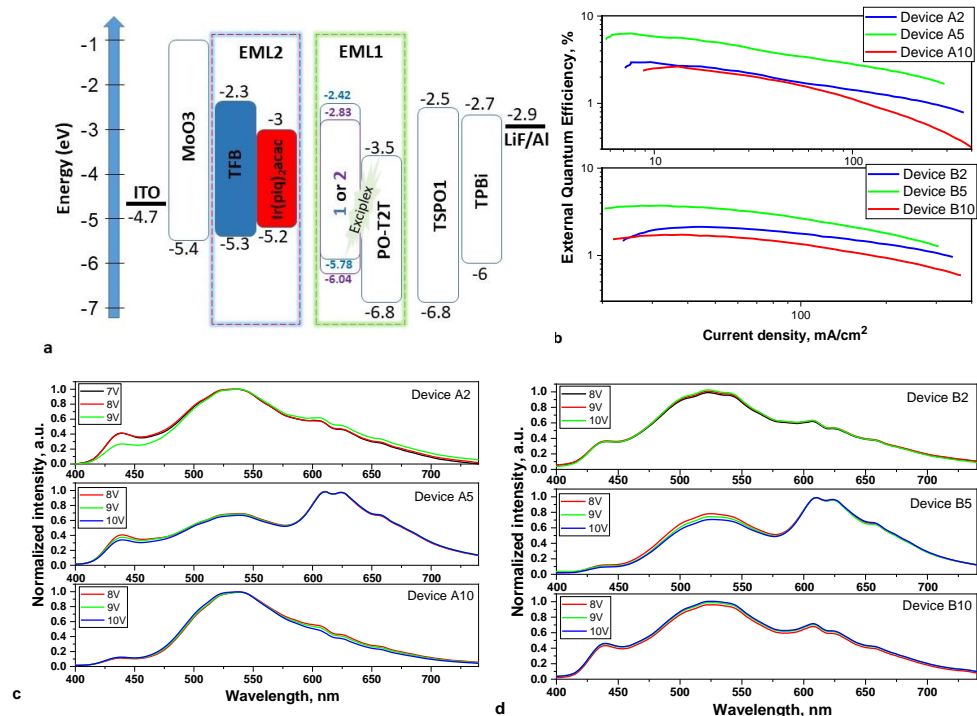

Fig. 2.5. Equilibrium energy diagram of all functional layers (a), EQE versus current density of fabricated OLEDs (b), normalized EL spectra under different voltages for white **1**:PO-T2T (c) and **2**:PO-T2T (d) based devices

As it can be seen in Fig. 2.5 c, d, the EL spectra of fabricated solution-based OLEDs that showed emission bands have references to the emissions of different intensities of Ir(piq)2(acac), **1**:PO-T2T or **2**:PO-T2T, and TFB emitters. This stable electroluminescence of devices A and B at different applied voltages (Fig. 2.5 c, d) can prove the existence of charge balance in the fabricated devices, because by increasing the applied voltages, there is no sign of a shift in the recombination zone from EML1 to EML2. The most intense red emission was observed for devices A5 and B5 with 5% of Ir(piq)2(acac), while the increase of concentration to 10% can result in the decline of red phosphorescence intensity. This can be related to the emission quenching due to the triplet-triplet annihilation (TTA) at a high concentration of the phosphorescence emitter[80]. In terms of color quality, device A5 demonstrated the best combination of intensities of blue, green, and red emissions in its EL spectrum with the best CRI of 92, CIE1931 xy coordinates of (0.384,0.399),

and correlated color temperature (CCT) of 3,655 K. The recorded CIE1931 and color temperature of device A5 can be attributed to warm white light, and at the same time, the CRI value is among the highest values for white OLEDs so far[81,82]. At external voltage of 12 V, the highest brightness of 8,980 cd/m^2 and the lowest brightness of 2,986 cd/m^2 were obtained for devices A5 and A10, respectively. In terms of efficiency, devices A5 and B5 due to the efficient triplet harvesting on phosphorescent emitter Ir(piq)2(acac) and two exciplex-based TADF emitters (**1**:PO-T2T or **2**:PO-T2T) showed the highest efficiencies. The highest CE$_{max}$, PE$_{max}$, and EQE$_{max}$ of 11.6 cd/A, 5.5 lm/W and 6.3% were observed for device A5 with **1**:PO-T2T green exciplex and 5% of Ir(piq)2(acac) (Fig. 2.5 b).

2.2. Bis (N-Naphtyl-N-phenylamino) benzophenones as exciton-modulating materials for white TADF OLEDs with separated charge and exciton recombination zones (Scientific publication No. 2, Q1)

This chapter is based on the published work in *Dyes and Pigments*, 2022, vol. 197, art. no. 109868, p. 1–10[83]. In order to fabricate efficient OLEDs, different approaches were proposed to prevent the exciton quenching and energy loss throughout the energy transfer process in WOLEDs. One of those approaches in the development of efficient hybrid WOLEDs is the use of an appropriate host spacer (exciton modulator). This thin film usually can be placed between the layers of fluorescent and phosphorescent or TADF emitters[84]. This approach, which is known as "spatial exciton allocation strategy", has the capacity to boost the EQE of TADF WOLEDs by preventing non-radiative Dexter energy transfer from blue fluorescent emitter to red-green/orange TADF/Phosphorescence emitters and minimizing the Forster energy transfer within the two layers[85–87]. Up to date, hybrid phosphorescent/TADF WOLEDs are able to obtain EQE of 20%, which is in the same range of full phosphorescent WOLEDs. However, until now, this method was not used for purely TADF WOLEDs[88–90]. In this work, two newly synthesized compounds (compounds **3** and **4**) were used as exciton modulators between blue and orange TADF to fabricate several purely TADF WOLEDs. The molecular structures of compounds **3** and **4** with isomeric (*N*-naphthyl)-*N*-phenylamino donors and benzophenone acceptors are shown in Fig. 2.6.
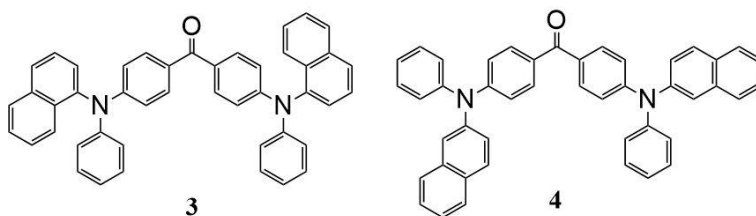
Fig. 2.6. Molecular structures of compounds **3** and **4**

In order to study the photophysical characterization of compounds **3** and **4**, photoluminescence and UV-visible absorption spectra of compound solid layers and dilute THF and toluene solutions were recorded (Fig. 2.7 a, Table 2.3). The compounds **3** and **4** THF solutions exhibited blue emission peaks at 462 nm and 488

nm with Stoke's shifts of 90 and 107 nm. However, the emission of derivative neat films showed the Stoke's shifts of 94 and 113 nm, respectively (Fig. 2.7 a). A slight difference of 22 nm and 34 nm within the emission of toluene and THF solutions of compounds **3** and **4**, respectively, verifies a weak intramolecular charge transfer (CT) between the donor and acceptor units[91]. The optical band gaps were estimated from the onset wavelengths of optical absorption spectra of compound neat films, and the absorption onset wavelengths of **3** and **4** were 429 and 446 nm related to the optical band gaps of 2.89 and 2.78 eV, respectively (Fig. 2.7 a, Table 2.3).
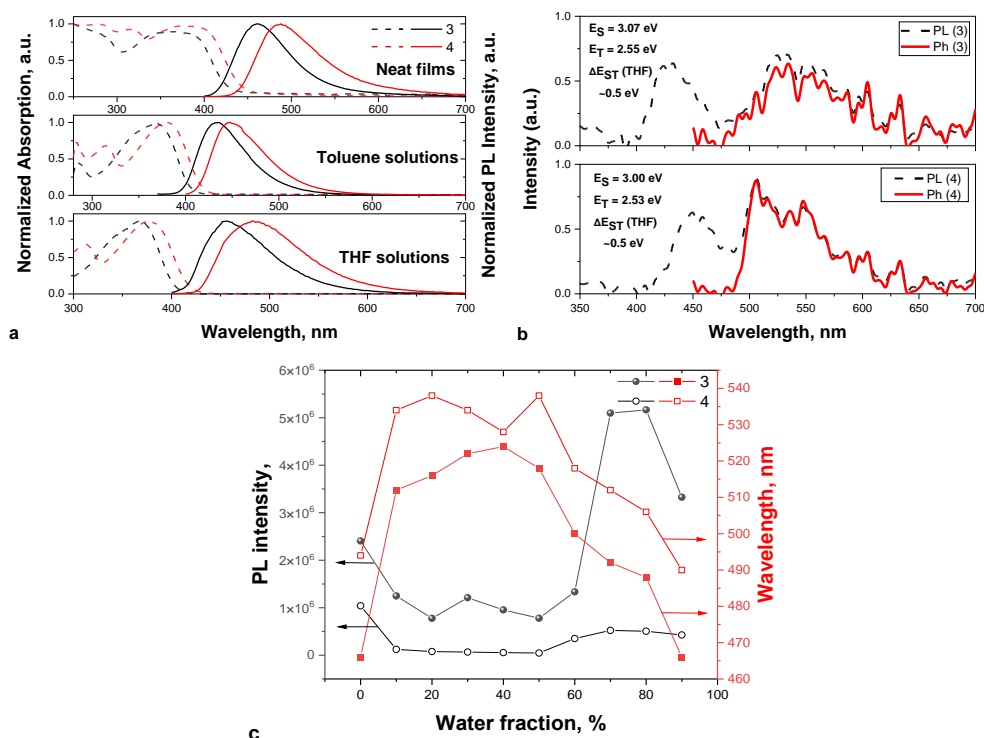
Fig. 2.7. Photoluminescence (right) and normalized UV-absorption spectra (left) (a), PL (black dash lines) and phosphorescence (red lines) spectra of dilute THF solutions of the materials at 77 K (b), wavelength versus water percentage for the dispersions of the compounds in the THF/water mixtures (right) and PL maximum intensities versus water volume percentage of compound dispersions in the mixtures of THF and water (left) (c)

The photophysical properties of compounds **3** and **4** were further investigated by recording the photoluminescence and phosphorescence spectra of their THF solution at 77 K (Fig. 2.7 b). The E_{S1} and E_{T1} energies were obtained and summarized in Table 2.3. LE[3] emissive recombination of N-naphthyl-N-phenylamine units triplet state is the main origin of compound phosphorescence emissions[92]. Since the PLQY of compounds **3** and **4** solid films were higher than those of toluene solutions, the possibility of aggregation-induced emission enhancement (AIEE) characteristics was investigated by measuring the fluorescence spectra of the compounds in different THF/water concentrations (F_W)[93]. Fig. 2.7 c shows the PL intensities (left) and PL-

peaks (right) versus water percentage for the compounds **3** and **4** dispersions. By increasing the percentage of water to 40–50%, which can lead to an increase in the polarity of the mixtures of THF and water, the intensity of emission slowly decreased, and the peak of PL spectra red-shifted till the aggregates were formed. The increase of water fraction can lead to the blue shifts of the PL spectra and an increase of emission intensity owing to the increasing the number of compounds **3** and **4** aggregates. However, during the additional increase of the water percentage from 80–90%, the emission intensities start to decline. Almost the same results were previously reported for the materials with AIEE characteristics due to the precipitation of bigger formed aggregates in the cell with the mixtures of water and THF[94,95].

Using the cyclic voltammetry (CV) technique, it has been found that two materials showed irreversible oxidization approximately at the same potential. The measured IP_{CV} value of **3** was slightly smaller compared to that of **4**, and for both compounds, the electrochemical reduction was not observed[96] (Fig. 2.8 a). A photoelectron emission spectroscopy equipment was utilized to establish the ionization potentials (IP_{PE}) of the compound solid films. IP_{PE} of 5.68 eV was recorded for the compound **3** film and of 5.79 eV for the compound **4** film, proving excellent positive carrier injecting characteristic[97] (Fig. 2.8 b, Table 2.3). The measured IP values with both methods, cyclic voltammetry (CV) and photoelectron emission spectroscopy method, are in good agreement.

The time of flight (TOF) technique was utilized for the estimation of charge carrier characteristics by using the non-doped films of **3** and **4**, which were made by vacuum deposition sandwiched between ITO and Al electrodes[98]. The transit times only were detected when positive voltage was applied to ITO electrode, proving that compounds **3** and **4** only have the hole transport capabilities (Fig. 2.8 c, inset), and the transit times for electrons were not detected. More than two times higher transit time of 4.51 µs was recorded for compound **3** than **4** (1.78 µs) at the same applied electric field (E) of 5×10^5 V/cm. Accordingly, at the mentioned electric field, about two times higher μ_h of 3.5×10^{-4} cm^2/V×s was obtained for compound **3** in comparison to compound **4** (1.8×10^{-4} cm^2/V×s) (Fig. 2.8 c, Table 2.3). By fitting the hole mobilities versus applied electric field diagram of compounds with Poole–Frenkel type mobility, μ_0 which is zero-field hole mobilities of 5.8×10^{-7} and 4.6×10^{-6} cm^2/V×s and field dependence parameters (β) of 8.2×10^{-3} and 6.25×10^{-3} (cm/V)$^{0.5}$ were recorded for compounds **3** and **4**, respectively[98].
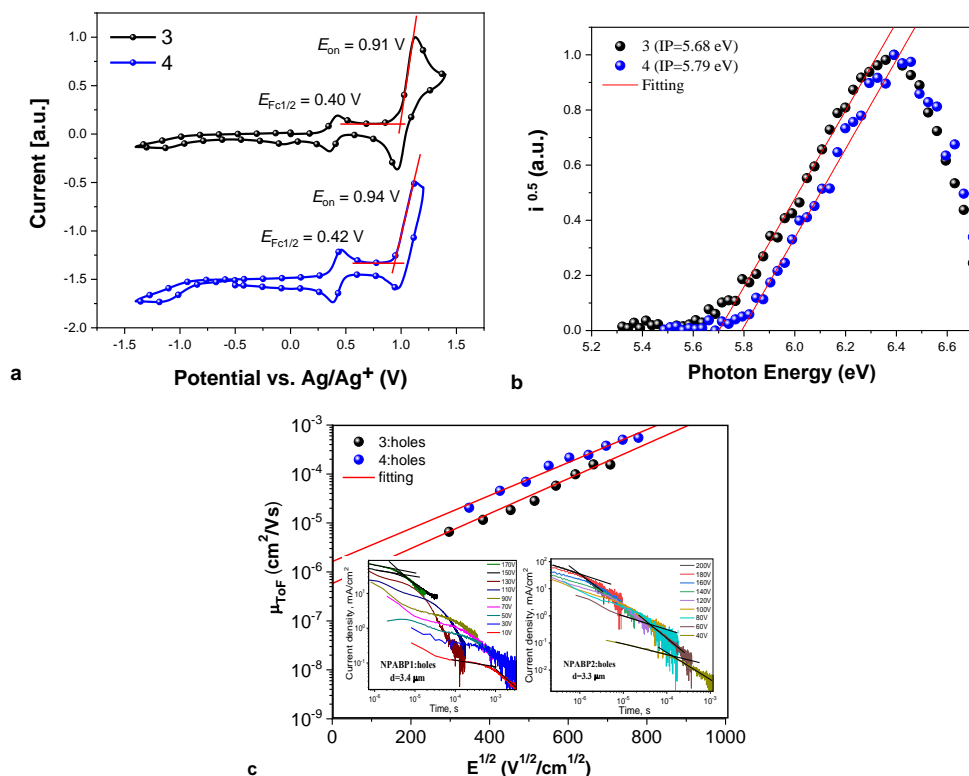
Fig. 2.8. CV curves of dichloromethane dilute solutions of **3** and **4** (a), electron photoemission spectra of **3** and **4** solid samples (b) and their hole mobility versus electric field; insets: TOF pulses for holes in the deposited layers of materials measured at several applied electric fields (c)

Considering good optoelectronic properties of new compounds, materials **3** and **4** were selected for the modulating of exciton in one or two TADF emitters (orange 4CzTPN and blue PFBP-2b) based WOLEDs with separated exciton recombination and hole-electron recombination zones. For the first time, using spatial exciton allocation strategy, two types of purely TADF-based WOLEDs device structures with one resonance blue to orange energy transfer or with two resonance blue to orange and blue to blue energy transfers were fabricated (Fig. 2.9 a).

In the devices with two TADF emitters by two efficient resonance energy transfers, the separation of the recombination area and exciton recombination area can be obtained. However, in the fabricated devices with an exciton blocking layer (EBL), one of the resonance energy transfers may be restricted, which allowed to investigate the effect of one or two resonance energy transfers on the color quality and efficiency of white devices. The OLED designs, which were used are as follows: ITO/ MoO_3 (8 nm)/ NPB(60 nm)/ TAPC(5 nm)/EML/ TSPO1(8 nm)/ TPBi(40 nm)/ LiF(1 nm)/Al (Devices IA(B)1-3) and ITO/MoO_3(8 nm)/ NPB(60 nm)/ TAPC(5 nm)/EML/PFBP-2b (20 wt%):TPBi (40 nm)/ LiF(1nm)/Al (Devices IIA(B)1-3). The OLED device characterizations are written in Table 2.4. The device names with I sign belong to the

first family of OLEDs containing TSPO1 exciton blocking layer with one resonance energy transfers, and device names with II sign are related to the fabricated OLEDs with two efficient resonance energy transfers (Fig. 2.9 a), letter A related to compound **3** and letter B to compound **4**, "1–3" are associated to three different light emissive layers (EML) (Fig. 2.9 a).

Table 2.3. Thermal, photoelectrical, charge carrier, photophysical, and electrochemical parameters of **3** and **4**

Property	Sample	3	4
T_m, ºC	Powder	218	241
T_g, ºC		101	107
T_{cr}, ºC		203	–
$T_{de-5\%}$, ºC		411	428
E_{ox} vs Ag/Ag$^+$, V	DCM solution with TBAPF$_6$	0.91	0.94
IP_{CV}, eV		5.71	5.74
IP_{PE}, eV	Film	5.68	5.79
E_g^{opt}, eV		2.89	2.78
EA_{PE}, eV		2.79	3.01
λ_{PL}, nm	Film (THF solution)	462(456)	488(482)
λ_{abs}, nm		368(366)	375, 314, 281(375, 312)
PLQY, %		12 (9)	13 (18)
E_{S1}, eV	THF solution at 77 K	3.07	3.00
E_{T1}, eV		2.55	2.53
ΔE_{S1T1}, eV		0.52	0.47
μ_{holes},[a] cm^2/(V×s)	Film	1.8×10^{-4}	3.5×10^{-4}
μ_0, cm^2/(V×s)		5.8×10^{-7}	4.6×10^{-6}
β, (cm/V)$^{0.5}$		8.2×10^{-3}	6.25×10^{-3}

[a] At electric field of 5×10^5 V/cm

Devices IA1 and IIA1 (IB1 and IIB1) are based on guest:host type EML of 4CzTPN(5 wt%):**3**(**4**) (20 nm) where compounds **3** and **4** are the matrix for 4CzTPN. Devices IA2 and IIA2 (IB2 and IIB2) are containing guest:host/EML of 4CzTPN(5 wt%):**3**(**4**) (5 nm)/**3**(**4**) (15 nm) where the layers of compounds **3** or **4** without dopant were additionally used as exciton modulators. Devices IA3 and IIA3 (IB3 and IIB3) were based on bi-layered (without dopant) EML of 4CzTPN(1 nm)/**3**(**4**)(15 nm) where dopant-free layers of compounds **3** or **4** were as well used as the exciton modulators. MoO$_3$ was utilized as a hole injection layer; NPB and TAPC were utilized as hole-transporting layers to inject holes, and the high LUMO (-2.0 eV) of TAPC helped to block electrons within EMLs. TSPO1 acted as hole/exciton blocking layer, TPBi was used as an electron transporting layer, and the layer of LiF acted as electron injection layer. The hole-electron recombination area should be located near the electron-transporting layer concerning the devices IIA(B)1-3 (electron-blocking layer

in the case of devices IA(B)1-3) because of the hole-transporting characteristics of compound **3**(**4**) (Fig. 2.9 a).
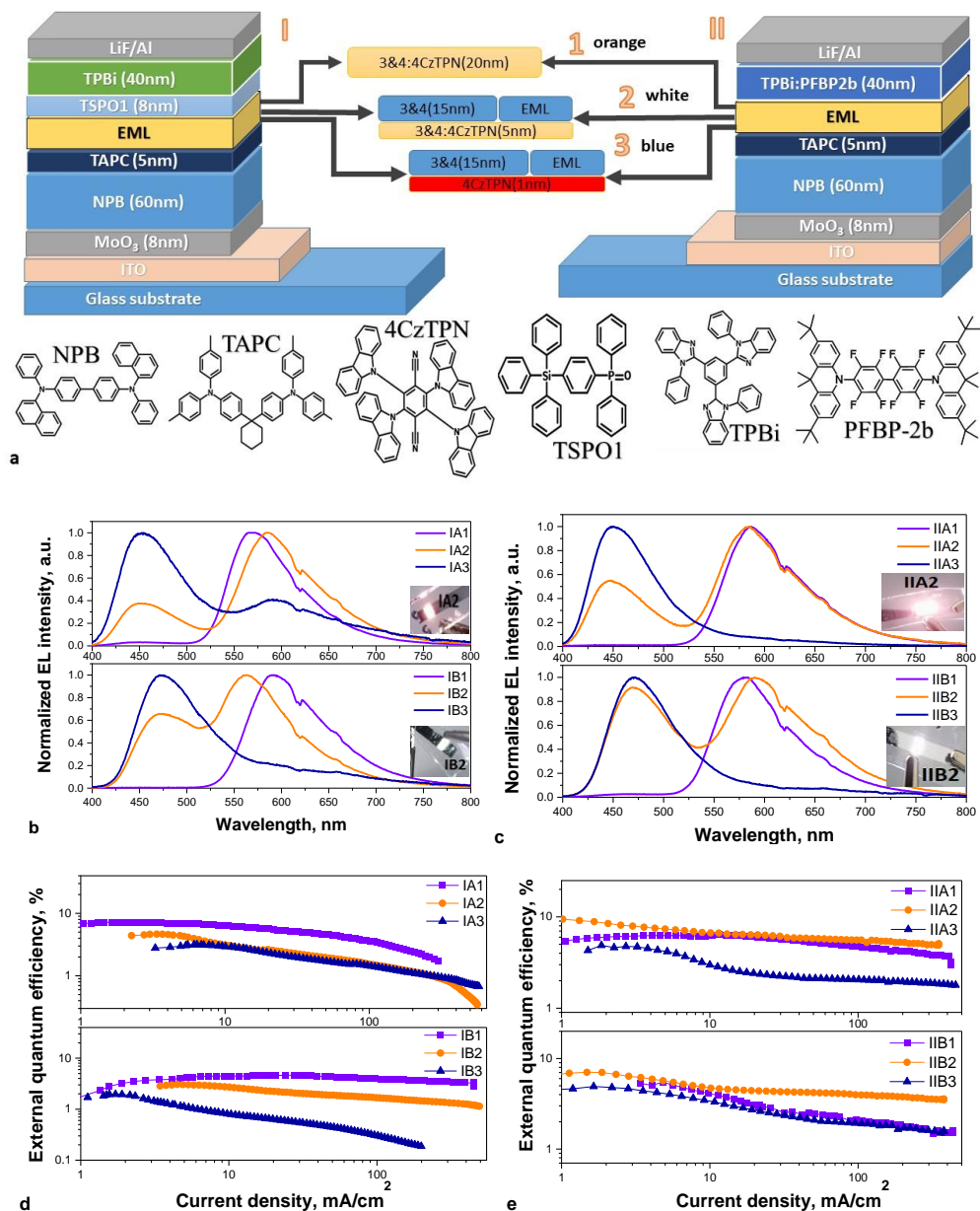
Fig. 2.9. Functional layers in OLED and molecular structures of the materials, which were utilized in the OLEDs (a) EL spectra at 9 V (insets: photographs of WOLEDs at 9 V) (b, c) and EQE versus current density curves of the fabricate OLEDs (d, e)

Material 4CzTPN was chosen as an orange TADF emitter, considering its HOMO/LUMO values, TADF properties, and T_1 state value of 2.44 eV, which is very close to T_1 of compounds **3** and **4** (2.55 and 2.53 eV, respectively)[99]. Compound

28

PFBP-2b was chosen as sky-blue TADF emitter, taking into account its TADF properties, HOMO/LUMO values, and S_1 (2.86 eV), which is in the same range of S_1 states of compounds **3** and **4**, which were about 3.06 and 3.0 eV, respectively (Table 2.3). PFBP-2b was used as the TADF compound in the TPBi:PFBP-2b layer. The combination of the compounds **3** or **4** and 4CzTPN can make good triplet energy resonance T_1(**3** or **4**)→T_1(4CzTPN) that can lead to efficient Dexter energy transfer between them, and the combination of the compounds and PFBP-2b forms an excellent singlet energy resonance S_1(**3** or **4**)→S_1(PFBP-2b) that can cause efficient Förster resonance energy transfer between them[100].

WOLEDs with separated exciton recombination and hole-electron recombination zones could be potentially fabricated by using the 4CzTPN/**3** and **4**/PFBP-2b system. PFBP-2b was used as the TADF emitter in the TPBi:PFBP-2b layer. As it could be seen in Fig. 2.9 a inset, the devices IA2, IB2, IIA2, and IIB2 were characterized by white electroluminescence (EL). The EL spectra of these devices contain two emission bands with different intensities, which consist of blue emission of **3** or **4** (and PFBP-2b in the case of devices IIA2 and IIB2) and orange emission of 4CzTPN (Fig. 2.9 a). This observation can confirm that the hole-electron recombination zone is mainly positioned within a dopant-free layer of **3** or **4**, leading to good exciton modulation between low-energy orange (4CzTPN) and high-energy blue emitters (either **3**, **4**, or PFBP-2b). It should be considered that the contribution of PFBP-2b emitter is evident, since the maximum EQE values of devices IIA2 and IIB2 are almost two times higher than those of devices IA2 and IB2 (Fig. 2.9 d, e, Table 2.4). The devices IA1, IB1, IIA1, and IIB1 showed orange emission originated from 4CzTPN:3(4) layer. However, the devices IA3, IB3, IIA3, and IIB3 demonstrated mostly blue EL because of deficient RET within the layers of **3**(**4**) and 4CzTPN. Due to the extra role of PFBP-2b TADF emitter to the blue emission in fabricated devices with two resonance energy transfers, the band referred to 4CzTPN is stronger for the devices IA3 and IB3 in comparison to IIA3 and IIB3 OLEDs. Due to the really high color standard of white EL fabricated with only two emitters, device IIB2 illustrated the highest CRI of 80 and correlated color temperature (T_C) of 4,490 K, and at the same time, CIE 1931 xy coordinates of (0.32, 0.31), which is nearest to the natural white, were recorded for this device (Table 2.4).

The positive role of PFBP-2b is as well obvious if one would make a comparison between EQEs of blue devices from the first (IA3 and IB3) and the second (IIA3 and IIB3) series of OLEDs. For instance, around two times higher maximum EQE_{max} of 4.9% was recorded for device IIB3 than device IB3 (1.9%). About twice higher efficiency of IIA2 and IIB2 white OLEDs in comparison to that of IA2 and IB2 should be related to the moving of exciton from the modulator layer (**3** or **4**) to TADF emissive layer (PFBP-2b and 4CzTPN) due to the almost similar energy states of S_1(**3** or **4**) with S_1(PFBP-2b) and of T_1(**3** or **4**) with T_1(4CzTPN).

Table 2.4. Electroluminescent parameters of white OLEDs

Device	V_{on},[a] (V)	CE_{max}, cd/A	EQE_{max}, %	CIE (x; y)[b]	CRI[b]	CCT[b]
IA1	4.7	20.8	7.2	(0.47, 0.49)	42	2,932
IA2	4.2	10.2	4.8	(0.40, 0.35)	60	2,751
IA3	5.1	3.9	3.1	(0.26, 0.22)	75	12,520
IB1	5.9	9.4	4.7	(0.55, 0.44)	41	1,840
IB2	5.7	8.3	3.1	(0.36, 0.42)	62	4,220
IB3	4.6	3.7	1.9	(0.20, 0.26)	---	----
IIA1	4.2	13.7	6.3	(0.53, 0.45)	40	2,061
IIA2	3.9	18.6	9.5	(0.36, 0.31)	67	3,332
IIA3	4.6	8.1	4.7	(0.16, 0.13)	-----	-----
IIB1	4	12.4	5.5	(0.49, 0.47)	43	2,515
IIB2	3.6	13.8	7.1	(0.32, 0.31)	80	4,490
IIB3	3.3	7.8	4.9	(0.17, 0.22)	---	-----

[a] Turn-on voltage at luminance of 10 cd m^{-2}, [b] CIE, CRI, and CCT values are referred to EL spectra measured at 9 V

Lower turn-on voltages of 3.3 to 4.6 V were recorded for the fabricated devices using compound **4** than turn-on voltages of 4.2 to 5.9 V for **3** based devices (Table 2.4). This result is in very reasonable approval with the results of the charge mobility measurements, and at the same applied electric fields, material **4** obtained higher hole mobilities (Fig. 2.8 c, Table 2.3). Taking into consideration the mentioned characterization of fabricated devices and making a comparison between the parameters of white OLEDs from the first (IA2 and IB2) and the second (IIA2 and IIB2) series, it could be stated that the remarkable increase in the efficiencies of white TADF OLEDs is because of the effective separation of charge and exciton recombination zones by decreasing the energy losses through the energy transfer mechanism. This process paved the way to obtain more stable blue emission in the total white EL of TADF-based OLEDs, which is mostly essential for the lighting technologies. Additionally, the designed exciton modulators **3** and **4** have the possibility to get utilized in combination with effective blue and orange TADF emitters for obtaining WOLEDs with higher efficiencies.

2.3. Tuning of spin-flip efficiency of blue emitting multicarbazolyl-substituted benzonitriles by exploitation of the different additional accepting moieties (Scientific publication No. 3, Q1)

This section is based on the reported work in *Chemical Engineering Journal*, 2021, Volume 423, art. no. 130236, p. 1–12[101]. As an alternative to phosphorescent blue OLEDs, which have the efficiency and operational stability challenges, TADF

OLEDs by utilizing practical and non-poisonous pure organic compounds can be used to fabricate blue OLEDs with higher efficiencies and stabilities [24,65,102]. After the first published paper on multi-carbazole based materials with two electron-withdrawing benzonitrile units as green and red TADF emitters for OLEDs with high efficiencies[41], the multi-donor-acceptor(s) is one of the widely-used approaches for TADF emitters with blue color, and in order to obtain multi-carbazole based TADF materials with blue emission, few strategies were suggested[103,104]. The reports have shown that efficient TADF compounds could be synthesized using multi donor and acceptor type approach along with a variety of intramolecular forces (for instance, non-covalent or through-space). In this paper, aiming to achieve efficient blue OLEDs, there were used five newly synthesized asymmetrical multi-carbazole-based emitters in doped and non-doped OLED structures. The molecular structures of the compounds **4**–**9** are presented in Fig. 2.10. The compounds contained four 3,6-di-tert-butyl-9H-carbazole as donors and benzonitrile as the general acceptor as well as a variety of extra withdrawing units, i.e., benzonitrile, benzotriazole, 2-benzotrifluoride, methyl 2-benzoate, or methyl 3-methylbenzoate (Fig. 2.10).

The thermal transitions and stabilities of compounds **5**–**9** were recorded by both TGA and DSC techniques (Table 2.5). Throughout the TGA measurements, the compounds experienced complete weight loss indicating sublimation. All of the compounds obtained 5% weight loss temperatures higher than 363 °C. DSC measurements confirmed that the compounds were amorphous compounds, and during the second DSC heating scans of derivatives **5**–**9**, glass transition temperatures of 89, 103, 84, 92, and 109 °C, respectively, were observed. The similar recorded UV-vis absorption spectra for the dilute solutions of the materials in toluene, THF, and neat films can prove almost similar energy levels of ground-states in media with diverse polarity (Fig. 2.11 a). Similar to the previously published multi-carbazole compounds[103,105], the absorption bands in the range of 310–365 nm are related to the π–π* or n–π* transitions of the di-*tert*-butylcarbazole units. The low-energy absorption bands around 365–475 nm of material 6 and around 365–450 nm for the other materials are because of intramolecular CT properties. Unlike the CT states of the previously published materials, containing multi-carbazole with similar benzonitrile withdrawing units[106], for the designed asymmetrical multicarbazole based materials, the broad ICT band with two obvious peaks that are marked by arrows were recorded (Fig. 2.11 a).
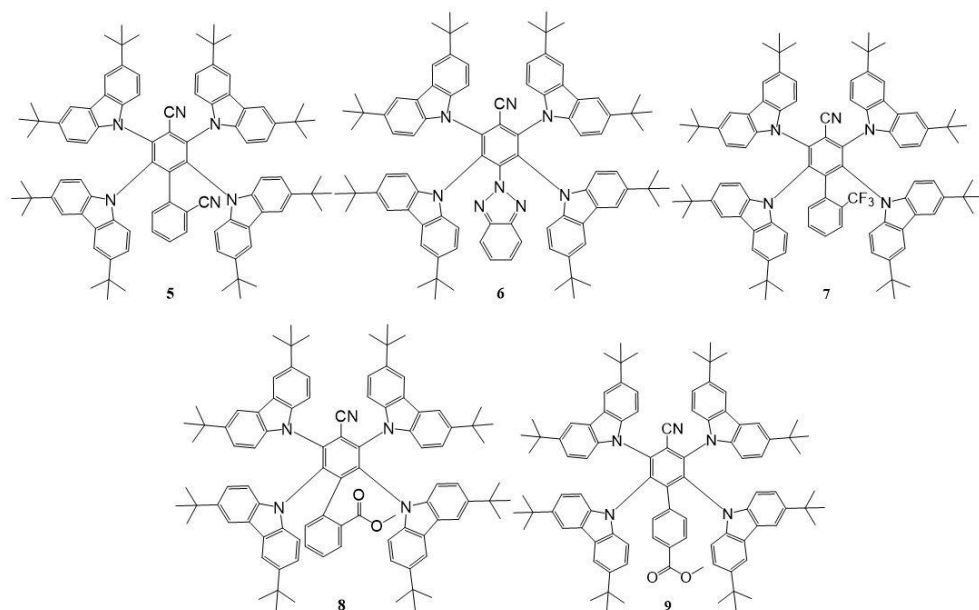
Fig. 2.10. Molecular structures of compounds **5–9**

Apparently, the marked doubled CT bands are due to the transitions among di-tert-butylcarbazolyl units and both withdrawing units. The second low-intensity CT band was earlier detected for other multicarbazole based derivatives and assigned to the existence of excited states with intensified delocalization. This delocalization can increase the mixing between the CT states and local energy (LE), leading to high RISC rates[103]. The red-shifted CT states of material **6**, compared to other investigated compounds in this work, is probably due to the stronger accepting ability of the combination of benzotriazole and benzonitrile moieties (Fig. 2.11 a, b). Because of the excited CT state recombination[107], the emission with unstructured PL spectra, showing maxima at the wavelengths between 457 to 522 nm, was recorded for the solutions and neat films of compounds **5–9** (Fig. 2.11 b). Photoluminescence spectrum of THF solution with high polarity compared to low-polarity toluene solution of material **6** showed the largest red shift. However, PL spectra of the solutions of other investigated materials (compounds **5**, **7–9**) did not show too much difference by increasing the solvent polarity in spite of the CT behavior of their first singlet excited states. There is a possibility that the phenomena can be justified by the weak CT behavior of these materials, possibly with not pure CT or LE emission characteristic[108]. Another possibility can be related to the "stucked" units without dihedral angles freedom of change or without freedom in conformers forming possibilities. The stuck as well may be related to the non-covalent intramolecular forces (for instance, C–H···F, O, N hydrogen bonding)[109].
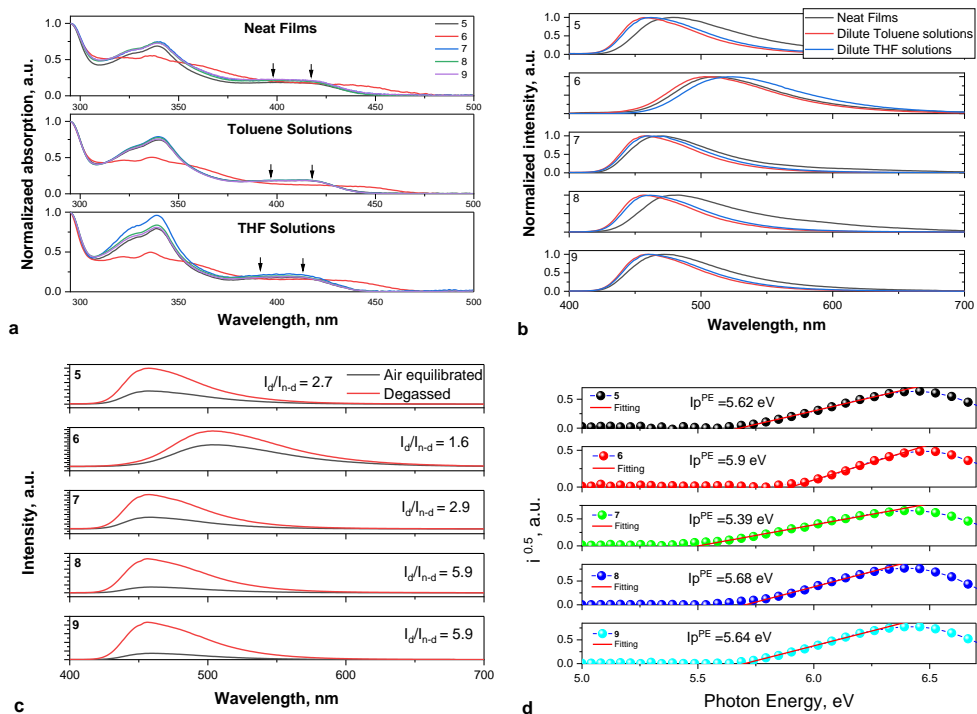
Fig. 2.11. Ultraviolet-visible (a) and PL (b) spectra of toluene or THF solutions and neat films of the investigated materials, PL spectra of toluene solutions before and after removing the oxygen (c), photoelectron emission spectra of the compound solid films measured in the air (d)

PL intensity of compound toluene solutions greatly enhanced when the solutions were deoxygenated by purging with argon gas (Fig. 2.11 c). High absolute PLQY values of 48–82% were measured by using an integrated sphere for deoxygenated toluene solutions of the investigated materials (Table 2.5). This enhancement of the emission is attributed to the emission enhancing of triplet excitons when they are not completely quenched by triplet oxygen. Relatively high PLQY values of 26–50% were recorded for the doped films of the compounds, and the PLQY measurement of the films was conducted under air condition. In order to investigate the hole injecting characteristics of the materials, using the photoelectron emission spectrometry ionization potentials (IP_{PE}) of the material, solid films were investigated (Fig. 2.11 d). Different acceptor moieties led to different ionization potential values, and IP_{PE} values ranged from 5.39 to 5.9 eV, showing various hole-injecting behavior of the compounds. The highest IP_{PE} value of 5.9 eV was measured for the material **6** neat film, and the lowest IP_{PE} value of 5.39 eV was recorded for the material **7** solid layer. Such differences were apparently obtained as a result of different HOMO distributions within solid-state of compounds induced by the different electron accepting properties of acceptors.

Table 2.5. Thermal and photophysical properties of designed materials

| Parameters	Sample	5	6	7	8	9
T_g, °C	Powder	89	103	84	92	109
T_d^{onset}, °C		452	363	457	465	449
λ_{PL}, nm		480	513	470	483	472
FWHM, nm		88	91	75	91	82
PLQY, %	Toluene[a]/THF/neat/doped	77/32/34/50	82/53/17/26	49/32/21/39	48/33/22/37	55/34/26/44
ΔE_{ST}, eV	THF at 77 K	0.11	0.05	0.10	0.13	0.14
ΔE_{S1T1}, eV	Doped film	0.0167	0.025	0.241	0.015	0.021
E_{S1}, eV		2.8	2.607	2.804	2.819	2.813
E_{T1}, eV		2.783	2.582	2.779	2.804	2.792
$k_{RISC} \times 10^6$, s^{-1}	Toluene[a]	0.18	2.32	0.05	0.11	0.07
	Doped film	0.18	2.32	0.047	0.11	0.072

[a] Deoxygenated toluene

The calculation of radiation transition rates of mCP-doped film[110] indicated the effect of acceptor asymmetry, and various reverse intersystem crossing rates (k_{RISC}) that ranged from 0.047×10^6 to 2.32×10^6 s^{-1} were recorded for the investigated compounds **5–9**. Photoluminescence and phosphorescence spectra of the dilute THF solutions of compounds recorded at low temperature (77 K) and really small singlet-triplet splitting of 0.05–0.14 eV were obtained (Fig. 2.12 a, Table 2.5). In order to exclude the role of triplet-triplet annihilation (TTA) process, PL intensity versus excitation density power were recorded, and the slope near to 1 in the linear fitting verified the TADF contribution in delayed fluorescence[111] (Fig. 2.12 c). In order to investigate the mechanism of delayed fluorescence, time-resolved emission and temperature-dependent steady-state measurements were implemented for the doped films of the compounds. As shown in Fig. 2.12 b, photoluminescence decay curves of the compound mCP:**5** film measured at different temperatures showed two obvious elements of prompt fluorescence (PF), which is in the nanosecond scale and delayed fluorescence (DF) in the microsecond scale, and the contribution of long-lived delayed fluorescence element was clearly increased from 77 to 300 K, and again, this observation can confirm the TADF nature of the emission.
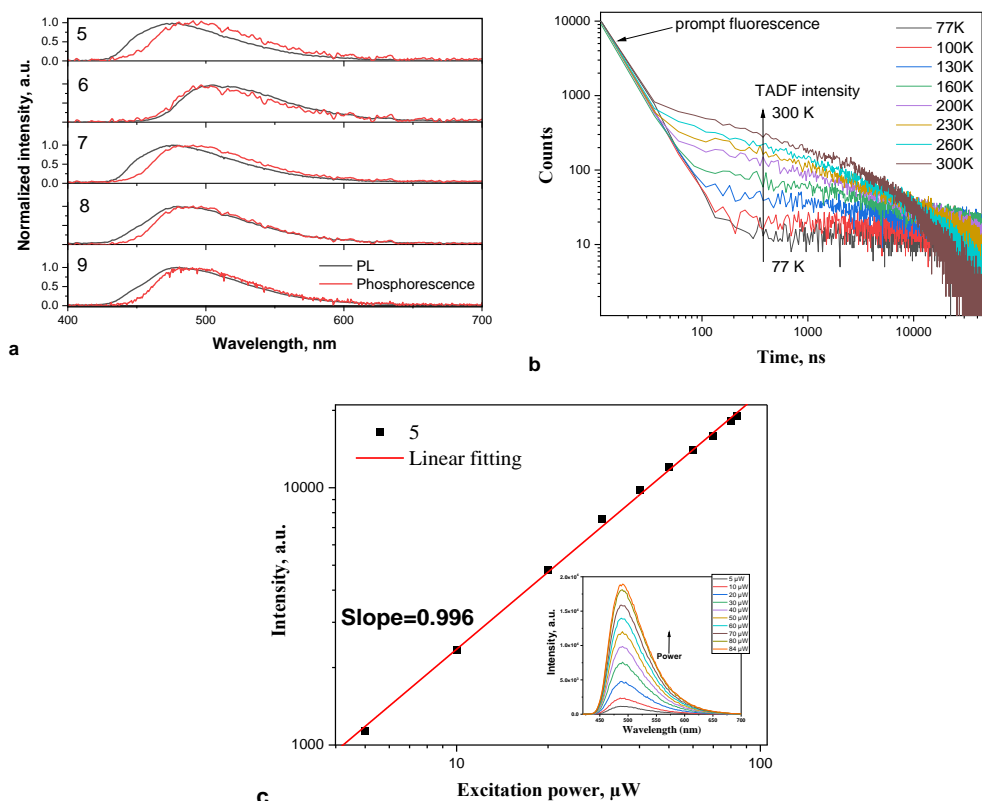
Fig. 2.12. Photoluminescence and phosphorescence spectra of the THF solutions of compounds measured at low temperature (77 K) (a), photoluminescence decay curves of mCP:**5** film measured at different temperatures (b), intensity of recorded delayed emission vs. excitation power for the mCP:**5** solid film (inset illustrates the delayed emission spectra measured at various excitation power) (c)

Electroluminescence characteristics of the materials were studied by using them in several device structures with non-doped and doped emissive layers. The functional organic layers of the fabricated OLEDs were selected to guarantee effective charge carrier injection and transporting and charge the exciton recombination in emissive layers. The OLED layers are as follows: ITO/MoO$_3$ (1 nm)/ NPB (30 nm)/ mCP (4 nm) / light emitting layer (20 nm) / TSPO1 (8 nm)/TPBi (40 nm)/LiF (0.5 nm):Al (100 nm), in which the compounds **5–9** were used in light emitting layers and named n5–n9 for non-doped devices and d5–d9 for doped devices. A very thin layer of MoO$_3$ was utilized as a hole injection layer, NPB for the hole transporting layer, mCP for the exciton blocking layer, TSPO1 for the hole/exciton blocking layer, TPBi for the electron transporting layer, and finally, a thin layer of LiF as an electron injection layer. The obtained HOMO and LUMO are illustrated in the energy diagram of the investigated non-doped (n5–9) and (mCP and mCBP) doped (d5–9) OLEDs in Fig. 2.13 a. As it can be seen in the Jablonski energy diagram for EBL, HBL, and EML triplet levels (T$_1$), mCP and TSPO1 exciton-blocking layers have higher triplet states

35

than that of designed blue TADF emitters, which can lead to the exciton confinement in the emissive layer (Fig. 2.13 a). All of the key criteria of fabricated OLED are summed up in Table 2.6, and the selected electroluminescent properties of optimized OLEDs are illustrated in Fig. 2.13 b.
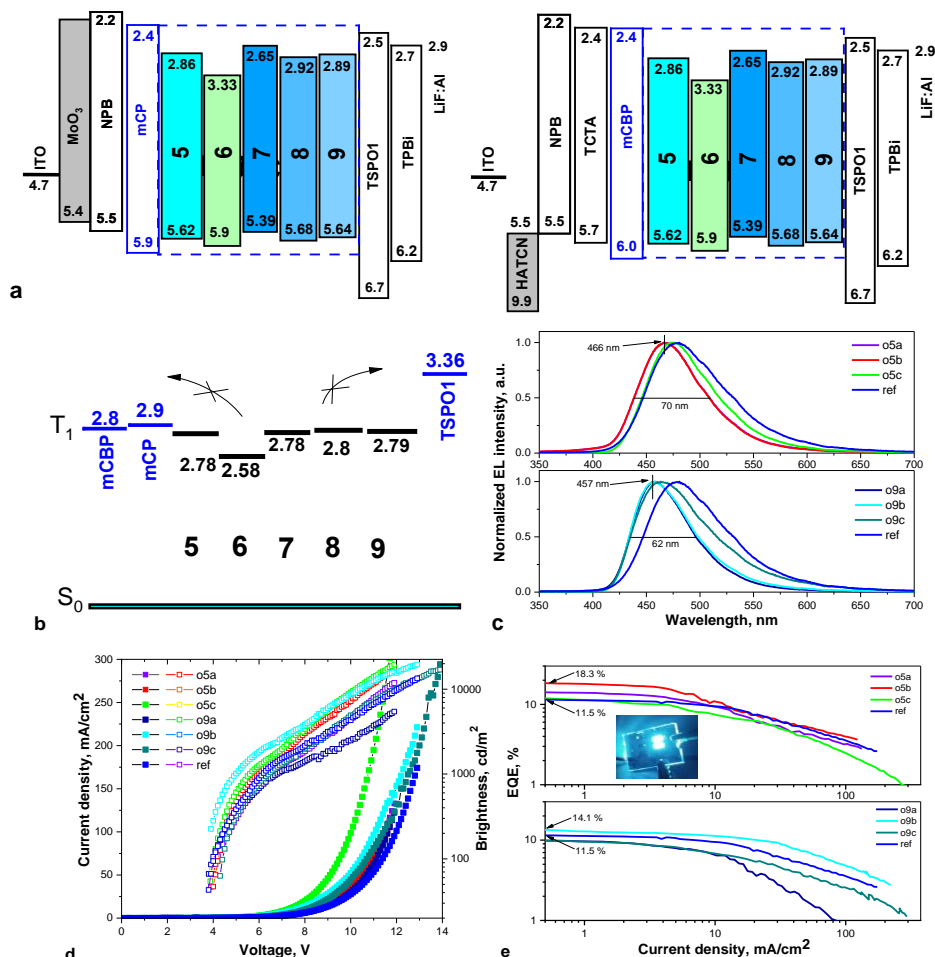
Fig. 2.13. Energy diagram of the non-optimized n5–9, d5–9 and optimized o5a–c, o9a–c devices (a), Jablonski energy diagram of triplet levels (T_1) for the system of EBL and emissive layer (b), EL spectra (c), current density and brightness versus applied voltage curves (d), and EQEs versus current density (e) for the optimized devices (o1a–c, o5a–c, and ref)

All of the non-doped OLEDs illustrated the EL emission in the sky-blue area peaking around 474–495 nm. However, blue-shifts were recorded for devices d5–9 EL emission compared to the corresponding EL emission of n5–9. Consequently, the doped OLEDs obtained blue EL spectra. The CIE1931 xy color coordinates of all fabricated OLEDs can be found in Table 2.6.

Nearly low turn-on voltages were recorded for all obtained devices, showing efficient injection and transport of positive and negative carriers from the electrodes

36

to the light emitting layer. Using mCP as a host led to the small turn-on voltage droppings of devices d1–5 compared to the turn-on voltage values of the corresponding non-doped OLEDs (n1–5). These results can be assigned to the better carrier-transporting characteristics of the emissive layers consisting of ambipolar mCP matrices with good hole and electron transporting capabilities[112]. The highest EQE_{max} of 7.3% and the lowest EQE_{max} of 2% were obtained for the devices n5 and n6, respectively (Table 2.6), and a similar trend was recorded for the doped devices (d5–9). Since devices d5 and d9 showed higher $EQEs_{max}$ of 11.8 and 7.9%, respectively, it has been decided to further improve the OLED device efficiencies by suitable optimization of OLED stack and emitter concentrations in the EML layers.

Table 2.6. OLED characterization results

Device	Emissive layer	$V_{on,}$[a] V	CE_{max} cd/A	$EQE_{max,}$ %	λ nm	Max brightness, cd/m^2
n5	**5**	4.1	19.4	7.3	495	36,000
n6	**6**	4.2	3.8	2	490	2,800
n7	**7**	4.6	6	3.4	474	5,050
n8	**8**	5	7.8	4.3	476	8,243
n9	**9**	6	12.1	5.6	480	16,988
d5	**5** (20wt.%):mCP	3.4	28	11.8	485	39,260
d6	**6** (20wt.%):mCP	4.2	4.8	3.1	470	4,415
d7	**7** (20wt.%):mCP	4.1	12.9	6.6	471	10,144
d8	**8** (20wt.%):mCP	4.6	12.2	5.6	495	14,176
d9	**9** (20wt.%):mCP	4.3	17.5	7.9	481	21,110
o5a	**5** (10wt.%):mCBP	3.9	28.3	15.1	466	11,831
o5b	**5** (20wt.%):mCBP	4	39.3	18.3	468	17,456
o5c	**5** (30wt.%):mCBP	3.9	27.4	12.4	476	19,516
o9a	**9** (10wt.%):mCBP	3.8	22.7	11.6	457	5,453
o9b	**9** (20wt.%):mCBP	3.9	24.8	14.1	457	19,551
o9c	**9** (30wt.%):mCBP	4.3	20.3	10.3	463	17,115
ref	PFBP2b(10wt.%):mCBP	3.8	22.8	11.5	480	13,420

[a] Turn-on voltage at a luminance of 10 cd m^{-2}

Optimized OLED structures with different concentrations of emitters **5** and **9** in the mCBP host contained a layer of HAT-CN as HIL, NPB and TCTA as HTL, and mCBP as EBL. Adding the additional TCTA layer can help to reduce the energy barrier between NPB and mCBP. The optimized device structures were ITO/HAT-CN (5 nm)/NPB (40 nm)/TCTA (10 nm)/mCBP (10 nm)/ light-emitting layer/ TPBi (30 nm)/LiF (0.5 nm)/Al. The devices with **5**:mCBP (10, 20, or 30wt.%) emissive layer were named as o5a, o5b, or o5c, and the devices with emissive layers of **9**:mCBP (10, 20 or 30wt.%) were named as o9a, o9b, o9c. In order to make a comparison between the investigated compounds and those of previously published sky-blue TADF emitters[113 114], PFBP-2b:mCBP (10%) was fabricated in the same conditions

as a reference device[115]. The optimized devices (o5a–c and o9a–c) based on compounds **5** and **9** showed blue-shifted emission in comparison to the doped device (d5 and d9) EL spectra. This shift in EL emission can be related to the lower dielectric constant of mCBP compared to the previous mCP host[116] (Fig. 2.13 b).

Lightly higher turn-on voltages of optimized OLEDs may be assigned either to the larger photon energy of blue shifted EL emission or to the larger total thicknesses of the OLEDs compared to that of OLEDs d1 and d5[117] (Table 2.6). Overall, due to the additional device optimization, excellent EQEs$_{max}$ of 18.3 and 14.1% were obtained for the devices o1b and o5b, respectively. These results can apparently be assigned to the modified charge balance within the emissive layer due to the improved charge carrier mobilities of mCBP host compared to those of mCP matrix. It should be noted that the devices o5b and o9b showed higher EQEs than the corresponding EQE (11.5%) of the reference OLED[115]. The exclusive EQE$_{max}$ (up to 18.3%) of optimized OLEDs verifies the high potential of investigated blue TADF compounds **5** or **9** and well proved the capability of acceptor asymmetry strategy for the future synthesis and design of TADF materials.

2.4. Ornamenting of blue thermally activated delayed fluorescence emitters by anchor group for the minimization of solid-state solvation and conformation disorder corollaries in non-doped and doped organic light emitting diodes (Scientific publication No. 4, Q1)

This section is based on the published work in *ACS Applied Materials & Interfaces*, 2022, 14, 35, 40158–40172[118]. In this paper, aiming to minimize the conformation disorder effect in the solid-state of multi carbazole compounds on emission characteristics, five new efficient asymmetric blue TADF materials with four 3,6-di-*tert*-butylcarbazole donor units and two electron-withdrawing moieties were investigated. Trifluoromethyl phenyl acceptor was common between all of the compounds, and each compound contained additional acceptor. As a result of the low conformational disorder effects, one of the compounds showed identical emission properties (color of the emission) in differently doped and non-doped devices. The molecular structures of compounds **10–14** are illustrated in Fig. 2.14.

UV-visible absorption and PL emission spectra of the compound solid films and dilute solutions are illustrated in Fig. 2.15 a, and summarized information is provided in Table 2.7. Nearly similar absorption profiles for the solutions and neat films of the emitters were recorded. Compounds **10–14** showed absorption bands in the range of 276–287 nm in the high energy region, which can be assigned to the overlapping of π-π^* transitions of electron-accepting and donating moieties. The absorption bands between 316 to 330 nm attributed to n-π^* transitions of di-tert-butylcarbazole units of materials. Additionally, the synthesized compounds exhibited wide absorption bands in the range of 340–425 nm, which can be originated from intramolecular charge (ICT) transition between four donors and two acceptor moieties[119].
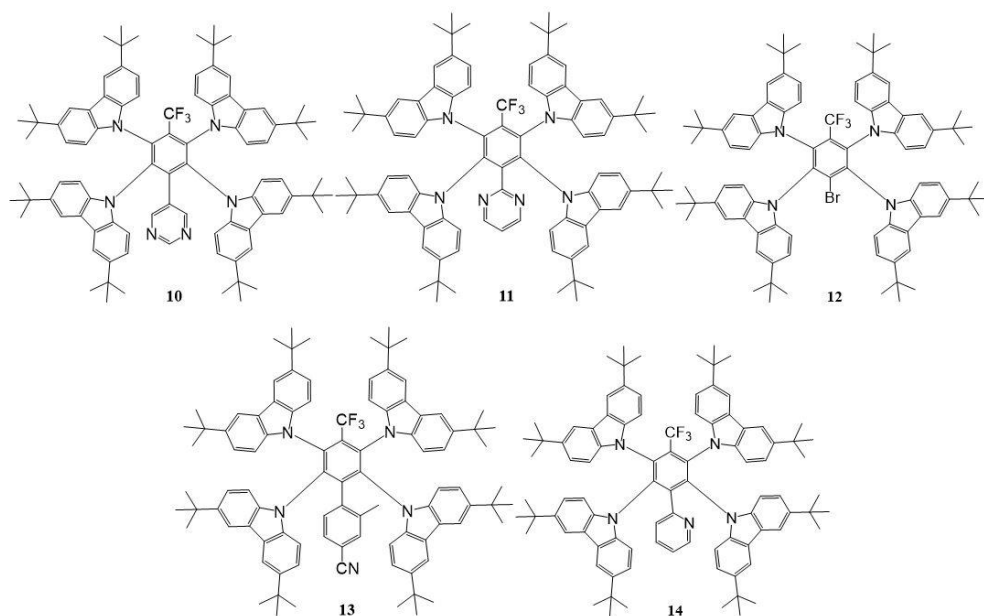
Fig. 2.14. Molecular structures of compound **10**–**14**

Non-structured PL spectra of material **10**–**14** solid films were recorded with the maxima at 482, 508, 482, 490 and 480 nm, respectively (Fig. 2.15 b). Using integrate sphere, PLQY values under atmosphere and vacuum conditions for solid samples and toluene solution of compounds were recorded. The PLQY values of the toluene degassed solutions of **10**–**14** ranged from 7.5–44%, and the PLQY of material 10 solid-state exceeded 75% in the vacuum conditions, which is quite high value for the organic electronic applications (Table 2.7). The PL emissions of the compounds in several different solvents with different polarities were investigated to check the solvatochromic properties of the materials. Since the CT state emission of TADF materials are oversensitive to the polarity of the solvent, these measurements can help to have information about the nature of emission (Fig. 2.15 a)[120,121]. Going from non-polar hexane to highly polar DMF solvents, no visible shifts in absorption profiles but significant red shifts of the emission spectra were observed. Compound **14** showed the largest shift of 68 nm between the PL spectra of solutions in hexane with low-polarity and DMF with high polarity, and the smallest red shift of 14 nm was observed for that of compound **11**. These phenomena probably should be explained by not pure LE or CT emission nature of the materials, and the results can prove that the emissions of compounds **10**–**14** have less tendency to change in media with different polarity compared to that of the previously reported blue TADF emitters[122,123]. PL spectra of air-equilibrated, oxygenated, and degassed toluene solutions of the materials 10–14 were recorded and shown in Fig. 2.15 b. Higher emission intensities for deoxygenated toluene solutions with argon compared to those oxygenated samples were observed for all materials. The oxygen sensitivity and increase of emission after degassing of solutions indicate the triplet state involvements in the emission. The PL intensity of

compound **10** deoxygenated toluene solution was about six times higher than that of the oxygenated dilute toluene solution (Fig. 2.15 b).
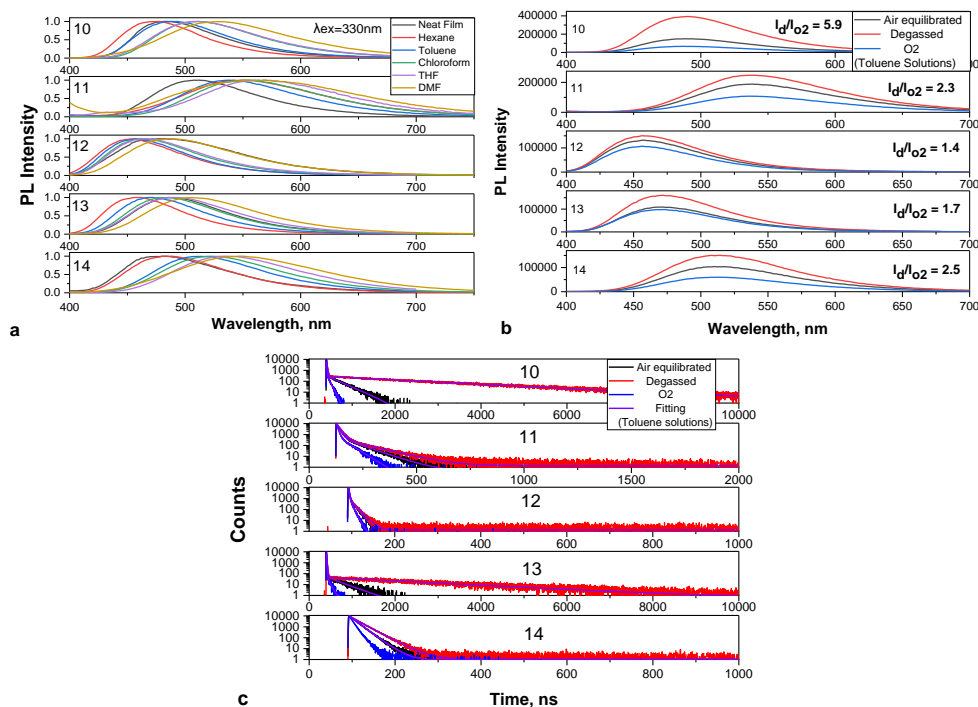
Fig. 2.15. Photoluminescence spectra of several dilute solutions (concentration of 10^{-5} M) and solid films of materials (a), photoluminescence spectra (b) and PL decay curves (c) of oxygenated, air-equilibrated and deoxygenated, dilute toluene solutions of materials **10–14**

The photoluminescence decay curves of the compound toluene solutions at room temperature were recorded as well. The delayed components in the emission of oxygenated toluene solutions of the materials **10–14** were sufficiently annihilated by oxygen molecules (O_2), and it is not detectable in the oxygenated samples. Deoxyginated solutions of compounds **10–14** showed exponential decays with two components, including both prompt fluorescence and delayed fluorescence elements. By using a double exponential decay profile, the τ_{DF} and τ_{PF} (lifetimes of delayed and prompt fluorescence) of oxygenated, air equilibrated, and deoxygenated dilute toluene solutions of materials were estimated (Fig. 2.15 c, Table 2.7). Significantly longer lifetimes of delayed components were recorded for the compounds **10** and **13** toluene solutions in comparison with other compounds: **11**, **12**, and **14**. In case of oxygenated toluene solution of 10, the delayed component was almost negligible ($\tau_{DF} = 56$ ns). However, the photoluminescence decay curve of the deoxygenated dilute solution of compound **10** shows a prompt component with the τ_{PF} of 15 ns (19.9% contribution of PF) together with delayed emission with τ_{DF} of 2.1 µs (80.1% contribution of DF). In accordance with the previously reported approaches[46,124] and concerning that non-radiative decay mostly takes place from the triplet energy states, the measured

40

PLQYs, the ratio of DF/PF intensity and lifetimes were utilized to obtain the k_{RISC}. Compounds **10** and **14** showed really high k_{RISC} of 8×10^5 and 5.5×10^6 s^{-1}, respectively, which can indicate that these compounds have quite fast spin-flip efficiencies. The recorded fast RISC rate can lead to the reduction of the degradation mechanism probabilities, since mostly triplet excitons are involved in the degradation processes[125]. The main reasons for the degradation of TADF OLEDs can be unwanted photophysical parameters and the instability of the TADF emitters, such as a prolonged delayed fluorescence lifetime (τ_{DF}) and relatively small reverse intersystem crossing rate (k_{RISC})[126,127].

**Table 2.7.** Photophysical and thermal properties of **10**–**14**

Parameters	10	11	12	13	14
T_d^{onset}, °C [a]	439	441	433	449	462
λ_{abs}, nm	278/287/316/328	278/288/ 317/329	279/287/ 318/330	277/288/ 317/330	278/288/ 318/330
λ_{PL}, nm	482	508	482	490	480
FWHM, nm	86	104	126	94	106
ΔE_{S1T1}, eV	0.03	0.05	0.04	0.04	0.04
E_{S1}, eV	2.92	2.77	3.04	3.04	2.91
E_{T1}, eV	2.89	2.72	3.00	3.0	2.87
PLQY (%)	44/76	12/51	8/4	17/27	13/49
η_{PF} [b]	0.24	0.16	0.02	0.13	0.07
η_{DF} [b]	0.52	0.35	0.02	0.14	0.42
τ_{PF}, ns (%) [b]	9(31)	13(32)	23(57)	23(48)	21(15)
τ_{DF}, μs (%) [b]	2.4 (69)	1.5 (68)	0.8 (43)	1.8 (52)	2.9 (85)
k_{PF}, s^{-1} [b]	2.6×10^7	1.2×10^7	9.9×10^5	5.7×10^6	3.4×10^6
k_{ISC}, s^{-1} [b]	1.8×10^7	8×10^5	4.2×10^5	2.9×10^6	2.9×10^6
k_{DF}, s^{-1} [b]	2.1×10^5	2×10^5	2.1×10^4	7.6×10^4	1.4×10^5
k_{RISC}, s^{-1} [b]	7×10^5	8×10^5	3.7×10^4	1.6×10^5	1×10^6
k_{RISC}, s^{-1}	8×10^5	5×10^5	6.7×10^4	9.3×10^4	5.5×10^6

[a] T_d^{onset} is the temperature of weight loss onset (heating rate of 20 °C/min at inert nitrogen gas), [b] solid films

Photoluminescence and phosphorescence spectra of dilute THF solution of compounds were recorded at the temperature of 77 K (Fig. 2.16 a). The energy difference between singlet and triplet states (ΔE_{ST}) values in the same range of 0.03 to 0.05 eV were obtained from the onset of photoluminescence and phosphorescence spectra of compound THF solutions, and probably, these minimized singlet-triplet gap is a result of spatially separated frontier orbitals on donor and acceptor moieties (Table 2.7)[128,129].

PL spectra and photoluminescence decay curves of compound films were measured in the air and vacuum. Under the vacuum condition, all of the materials displayed enhancement in the PL emission and the delayed component of PL decay

curves. The (prompt and delayed) efficiencies and rate constants of the important photophysical properties of compound solid films at 300 K were calculated, and the rates belonging to the intersystem crossing (k_{ISC}) are between 4.2×10^5 and 1.8×10^7 s^{-1}, and the rates of reverse intersystem crossing (k_{RISC}) ranging between 3.7×10^4 and 1×10^6 s^{-1} were obtained (Table 2.7).
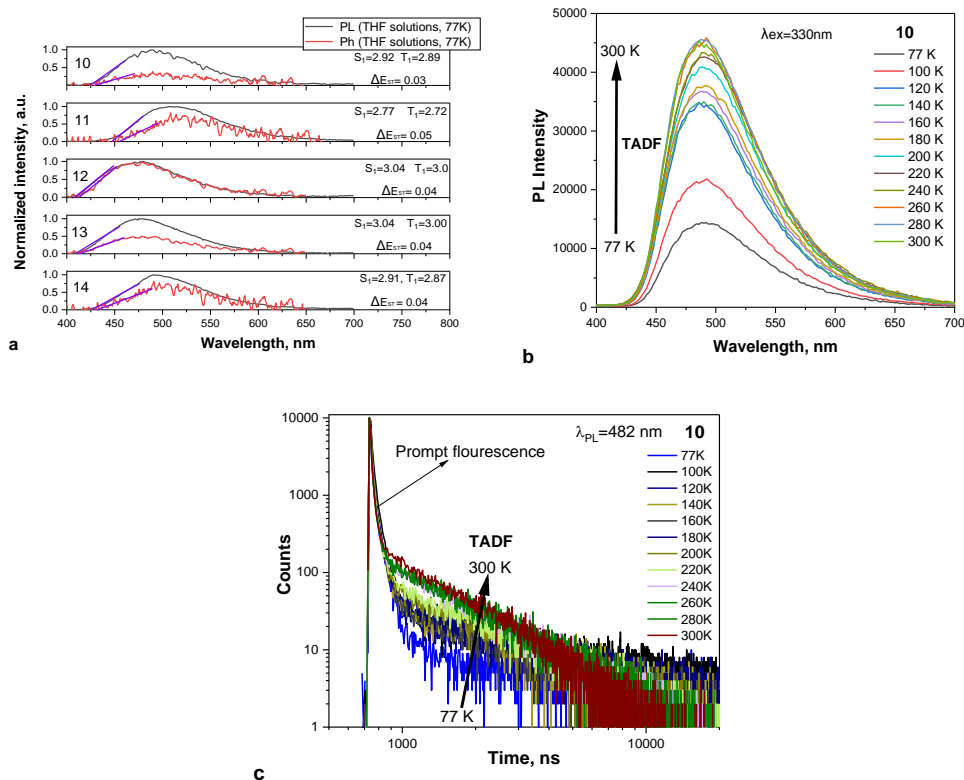
Fig. 2.16. Low temperature (77 K) photoluminescence and phosphorescence spectra of the compound dilute THF solutions (a), photoluminescence spectra (b), photoluminescence decay curves (c) of compound **10** neat film at different temperatures

In order to have a better understanding of the nature of the delayed fluorescence, time-resolved and steady-state emission measurements were conducted in different temperatures for compound neat films (Fig. 2.16 b, c). The thermal activation behavior of the delayed emission in compound **10** neat film was confirmed by the increase of the intensity from 77 to 300 K. Photoluminescence decay curves of the compound **10** solid film measured at several different temperatures show two obvious elements of PF in the nanosecond region and DF in microsecond scale. By increasing of the temperature, the contributions of prompt components are almost constant, but the long-lived DF components show clear temperature-dependent behavior (Fig. 2.16 c). By increasing the temperature and reaching 300 K, the ratio of delayed fluorescence illustrated a remarkable rise from 14 to 51%, proving clear thermally activated DF characteristics of compound **10** (Fig. 2.16 c). For instance, in case of compound **14** neat film, the share of delayed fluorescence in the photoluminescence

decay curves of this material increased from 65.3% to 85.16% after removing the oxygen (Table 2.7). Keeping in mind that the charge transporting abilities of functional materials are extremely important for the OLED applications and in order to investigate the capability of compounds **10**–**14** as emitters in the emissive layers of OLEDs, their charge mobility properties were investigated by the time of flight technique[130,131]. In order to study the hole transport characteristics of the materials after applying the voltages to the ITO substrate of thick fabricated samples, transit time (t_{tr}) for compounds **10**, **12**–**14** were easily detected in time-of-flight transients of currents (in logarithmic scale). However, the charge mobility of the compound **11** was not recorded by the time of flight measurement most probably due to the relatively strong charge recombination[132] (Fig. 2.17 a). At the same time, by applying the negative voltages, transit time was only detected for compound **10**, proving its electron-transporting capability. By applying several different electric fields, charge mobilities were determined using transit time values from the corresponding TOF current transients. The hole/electron mobility values of compound **10** were in the range of highest reported values among the TADF emitters[133,134]. Compound **10** was characterized by the hole mobility value of 8.9×10^{-4} cm^2 V^{-1} s^{-1} and electron mobility value of 5.8×10^{-4} cm^2 V^{-1} s^{-1} at the same electric field of 4.7×10^5 V/cm, proving the balanced charge mobilities for non-doped OLED applications. Conformer formation and hosting effects of compounds **10**–**14** on their emission characteristic were investigated as well. Several spectra measured at various delays after the excitation for compounds **10** and **12** obtained from time-resolved emission spectra (TRES) measurement show the PL emission shift, which may be assigned to various conformational disorder[135] (Fig. 2.17 b, c). Compound **12** with no additional accepting moiety showed the highest conformational disorder (largest PL shift of 0.19 eV in different delay time from 0 to 900 ns), and compound **10** obtained the lowest conformational disorder (the lowest photoluminescence spectra shift of 0.06 eV was detected). The obtained results regarding the conformational disorder of compounds **10**–**14** indicated that the existence of additional acceptors can lead to an increase of steric hindrance effect within the donors and extra accepting units, and an increase of steric effect can result in decreasing of the torsional disorder freedom between the donors and acceptors[136].
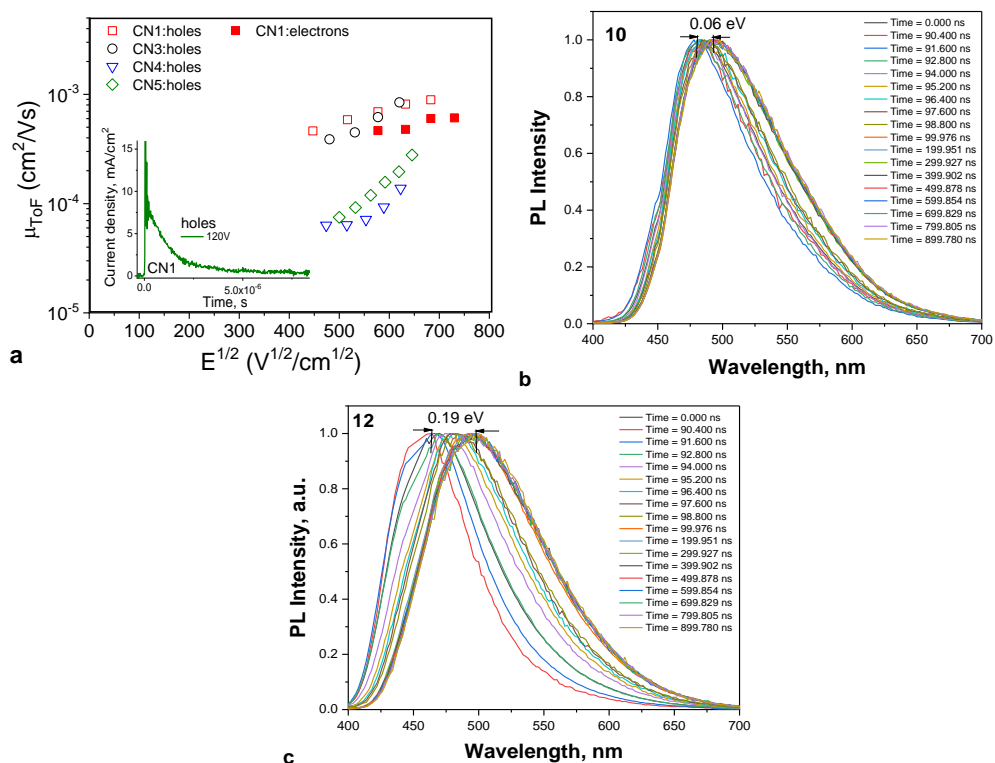
Fig. 2.17. Electron (solid symbols) and hole (open symbols) mobilities of the evaporated films of **10**–**14** versus the electric field[137] (inset illustrates the time of flight signal in linear ranges for holes in compound **10** solid film measured at 120 V) (a), 2D TRES data of compound **10** (b) and **12** (c)

In order to compare the EL performance of blue TADF compounds, non-doped and doped devices were fabricated and investigated with the following structures: ITO / HAT-CN (HIL) / NPB (HTL) / TCTA (EBL) / mCBP (ExBL) / **10**–**14** (emissive layer) / TPBi (ETL) / LiF:Al (EIL and cathode) for non-doped and ITO / HAT-CN / NPB / TCTA / mCBP / mCBP: **10**–**14** (mCBP as a host) / TPBi / LiF:Al for doped devices. The equilibrium energy graphs of provided OLED devices are schematically illustrated in Fig. 2.18 a, in which the energy levels IP$_{PE}$ and EA$_{PE}$ of the **10**–**14** films measured by using photoemission spectroscopy were utilized for providing the schematic energy diagrams of emissive layers. The mCBP matrix was chosen because of its wide bandgap, which it requires for blue emitter hosts as well as its high triplet (2.9 eV) and singlet (3.6 eV) energies[138]. Vacuum-deposited layers were prepared by step-by-step deposition for the non-doped and doped devices, and regarding the doped emissive layers, 10% doping concentration of compounds **10**–**14** were doped in the mCBP matrix. Aiming to fabricate efficient and optimized devices, different concentrations of emitter **10** (10, 20, and 30 wt%), which showed superior photophysical and charge-transporting properties in the mCBP matrix were fabricated as well. The selected key parameters of device characteristics, such as (EQE), turn on

voltage, current efficiency, peak wavelength of EL spectra and CIE xy coordinates, are summarized in Table 2.8. Fabricated non-doped OLEDs using materials **10**–**14** were denoted as n10–n14, mCBP-doped OLEDs based on materials **11**–**14** denoted as d10–d14, and optimized doped devices with different concentrations 10, 20, and 30 wt% of compound **10** named as d10a, d10b, and d10c, respectively. EL spectra of the fabricated devices were very similar to the PL emission of the compound neat films, and the unstructured blue emissions with λ_{EL} between 473 to 497 nm were recorded. Blue-shifted EL spectra were recorded for the doped devices as a result of the sensitivity of CT state to the polarity and different polarity of mCBP matrix[139]. The CIEx color coordinates of the fabricated blue TADF OLEDs ranged from 0.16 to 0.21, and CIEy color coordinates ranged from 0.19 to 0.4 (Table 2.8). Relatively low turn-on voltages of 5.2 to 7.9 V for fabricated devices with non-doped (n10–n14) and even lower voltages of 4.1 to 5 V for doped devices (d10–d14) were recorded, and these results can prove the efficient injection from the selected cathodes and transport of carriers to the emissive layers. Lower turn on voltage for doped devices can be ascribed to good charge transport capabilities of mCBP matrix, which was utilized as a host in the light emitting layer[140].
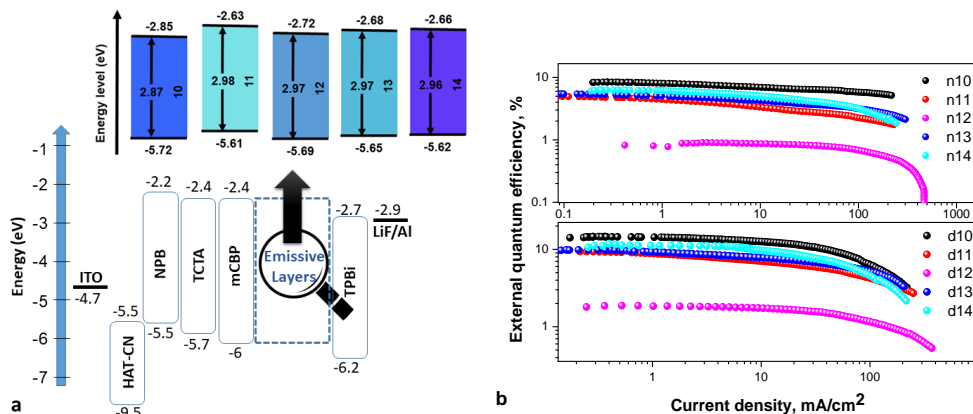
Fig. 2.18. Visualized fabricated OLED structures with an illustration of energy states of all utilized materials (a) and EQE vs. current density (CE) of the OLEDs (b)

OLED n1, which had the compound **10** in the emissive layer emitted sky-blue emission with CIE xy coordinate of 0.16, 0.27, PE_{max} of 12.4 lm/W, and EQE_{max} of 8.4% (Table 2.8). The highest device efficiency was obtained by d10b with 20% doping concentration of compound **10**. This device (d10b) showed blue emission of 477 nm, the highest current efficiency of 42.6 cd/A and EQE of 15.9% (Fig. 2.18 b, Table 2.8). The recorded lower efficiencies of the device with higher concentration (30 wt%) of an emitter are probably because of the exciton annihilation and concentration quenching effects[141]. The fabricated devices with 30 wt% of compound **10** (o10c) showed EQE_{max} of 12.8%, and EL spectra peaked at 479 nm, which is lightly red-shifted in comparison with the other two devices. Further optimization of OLEDs can be achieved by using the novel host materials or functional layers, since compounds **10**–**14** showed really high triplet levels, and the host or electron transporting layer should be replaced with other compounds with at least 0.2 eV

higher triplet states[142]. In conclusion, it should be considered that similar EL characteristics of non-doped and mCBP-doped devices of compound **10**–**14**, particularly fabricated devices based on compound **10**, can be a sign of introduced concept, which is the effect of low conformation disorder on the emission characteristics of TADF compounds. Compound **10** showed the smallest difference of 4 nm between the EL spectra peaks of non-doped and mCBP-doped OLEDs.

Table 2.8. Parameters of OLED

Device	Light emitting layer	$V_{on,}$[a] V	CE_{max} cd/A	$EQE_{max,}$ %	$\lambda,$ nm	Max brightness, cd/m^2
n10	**10**	5.8	20.5	8.4	481	19,735
n11	**11**	5.4	10.8	4.9	497	10,496
n12	**12**	7.9	2.5	0.9	491	2,387
n13	**13**	5.2	11.5	5.5	476	12,634
n14	**14**	5.5	14.6	6.3	488	15,975
d10a	mCBP: **10** (10wt.%)	4.6	37.7	14.6	473	34,500
d10b	mCBP: **10** (20wt.%)	4.1	42.6	15.9	477	39,226
d10c	mCBP: **10** (30wt.%)	4.9	33.9	12.8	479	30,928
d11	mCBP: **11** (10wt.%)	4.9	24	9.4	494	20,154
d12	mCBP: **12** (10wt.%)	5	4.3	1.9	470	4,958
d13	mCBP: **13** (10wt.%)	4.5	26.5	9.8	469	21,963
d14	mCBP: **14** (10wt.%)	4.8	30	11.7	483	28,129

[a] Turn-on voltage at a luminance of 10 cd m^{-2}

3. CONCLUSIONS

1. In order to unclose the effects of photophysical, photoelectrical, charge carrier mobility, electrochemical parameters of two new diphenyl bicarbazoles substituted with fluoro and trifluoromethyl acceptors on their electroluminescence characteristics, they were studied by many experimental methods, including steady-state and time-resolved spectroscopy at different temperatures, thermogravimetric analysis, differential scanning calorimetry, photoemission spectroscopy, and time-of-flight charge-transporting measurements.

1.1. By mixing diphenyl bicarbazole substituted compounds as donors and commercial PO-T2T as acceptor, two exceptional exciplexes with very high RISC rates exceeding 10^7 s^{-1} were developed for using in white OLEDs and oxygen sensors. Exciplex-forming system with fluoro-substituted diphenyl bicarbazole showed higher TADF efficiency owing to its higher hole mobility and lower activation energy.

1.2. Because of extremely high RISC rates of the developed exciplexes, they were used as active oxygen-sensing materials. The fabricated oxygen sensor based on green exciplex, which showed a higher RISC rate, was as well characterized by non-linear behavior oxygen probing properties (3.27×10^{-3} and 4.7 ppm^{-1} were recorded for Stern–Volmer constants).

1.3. Due to the broad photoluminescence spectra of developed exciplex-forming systems, they were utilized in the emissive layers of several solution-based white OLEDs, and the fabricated devices showed electroluminescence resulting in EQE$_{max}$ of 6.3% as well as very high-quality white color with CIE xy coordinates of (0.384, 0.399) and color rendering index of 92.

2. Stable and efficient white OLEDs were developed using two new benzophenone-based isomers as blue emitters, hosts, and modulators of the exciton in their structures.

2.1. These two compounds showed high thermal stabilities, and for one of the compounds, 5% weight-loss temperature reached 428 °C. Hole mobilities higher than 10^{-4} cm$^2 \cdot$(V$\cdot$s)$^{-1}$ and suitable charge injecting characteristics (ionization potential values ranged from 5.68 to 5.79 eV) were detected.

2.2. By engineering the layers of fabricated OLEDs, either in devices with one (orange color) or two (orange and blue colors) TADF emitters, the generated excitons were efficiently transferred after hole-electron recombination, and due to higher resonant energy transfers of fabricated devices with two TADF emitters, almost two times higher EQE of 9.5% was recorded.

2.3. High-quality white emission with CRI of 80, CIE xy coordinates of 0.32, 0.31 and CCT of 4490 K were recorded for the device with EQE of 7.1%. This observation can be assigned to the very good quality of white EL spectra, which was closest to the natural white light, and it was based on only two emitters.

3. Efficient blue OLEDs were developed exploiting new multi-carbazole-based blue TADF emitters with two non-similar accepting units, benzonitrile

accepting moiety as the general acceptor along with different additional conjugated acceptor moieties for each compound.

3.1. DSC measurements proved that all of the synthesized TADF emitters were amorphous compounds, and TGA results showed that 5% weight loss temperatures of the materials were between 363 and 457 °C.

3.2. Very different TADF properties and spin-flip capabilities were recorded for the new investigated compounds, in which reverse intersystem crossing rates were between 4.7×10^4 and 2.32×10^6 s^{-1}, which is displaying the effect of acceptor asymmetry, and the PLQY values of the degassed dilute toluene solutions of materials were from 55 to 82%.

3.3. The effect of additional acceptor moieties was as well obvious in the electroluminescent characteristics of the fabricated devices with the investigated TADF compounds in the emissive layers. EQEs of fabricated non-doped devices ranged from 2 to 7.3%, while the EQEs of mCP-doped devices ranged from 3.1 to 11.8%.

3.4. The fabricated optimized devices based on compound with benzonitrile additional moiety and compound with methyl 3-methylbenzoate extra acceptor obtained the practical EQEs$_{max}$ of 18.3 and 14.1%, respectively, which proves the potential of the acceptor asymmetry strategy for the design of TADF emitters.

4. The minimization of solid-state solvation and conformation disorder corollaries in non-doped and doped OLEDs was achieved by involving several efficient multicarbazole-based TADF compounds with four donor units (tert-butylcarbazole), two acceptor moieties were deeply investigated, and the effects of changing one of the acceptors in the optoelectronic characteristics of the new materials were studied.

4.1 The values for ionization potentials (IP$_{PE}$) of the investigated materials were almost in the same range, i.e., from 5.61 to 5.72 eV. Their 5% weight loss temperatures were between 433 to 462 °C, proving the excellent thermal stability of these multicarbazole-based compounds, and during the TGA experiments, the compounds showed complete weight losses, indicating sublimation.

4.2 Due to the multi-channel charge-transfer characters, the investigated materials showed quite efficient blue TADF with RISC rate of 1×10^6 s^{-1}, and high neat film PLQY of 76% was recorded.

4.3 During the time-resolved emission spectra measurements, the compound with pyrimidine additional acceptor showed the lowest shift of 0.06 eV, and the compound without additional accepting moiety was characterized with the highest shift and as a result the highest conformation disorder.

4.4 Surprisingly, due to the very low disorder and solvation effects in the film form of the compounds, approximately the same electroluminescent performances (including EL spectra) of mCBP-doped and non-doped devices were recorded.

4.5 The highest maximum EQE of 15.9%, maximum PE of 24.1 lm W^{-1}, and maximum CE of 42.6 cd A^{-1} were recorded for the one of the fabricated devices with high color quality sky blue EL spectra that peaked at 477 nm.

4. SANTRAUKA

Organiniai puslaidininkiai sulaukia išskirtinio dėmesio dėl savo puikių optoelektroninių savybių, turinčių gausų potencialą[1-3]. Organines medžiagas dėl jų reguliuojamų savybių galima naudoti įvairiuose prietaisuose, pavyzdžiui, fotovoltiniuose elementuose (PV), lauko tranzistoriuose (FET) ir šviesos dioduose (LED)[4,5]. Be to, organines medžiagas galima plačiai pritaikyti įvairiuose gamybos metoduose (pavyzdžiui, vakuuminio nusodinimo, sukamojo dengimo, ritininio dengimo ar rašalinio spausdinimo), suteikiant įvairių komercializavimo galimybių[6,7]. Nuo tada, kai 1987 m. Tang ir VanSlyke paskelbė mokslinį straipsnį[8], aprašantį pirmuosius pasaulyje veikiančius organinius šviesos diodus (OLED), kuriuose tarp dviejų elektrodų įterpdami du ploni organinių medžiagų sluoksniai, šie diodai sulaukė didelio pramonės tyrėjų ir akademinių mokslininkų susidomėjimo, o OLED-ai tapo nusistovėjusia ir brandžia ekranų technologija. Beveik pusė 2021 m. parduotų mobiliųjų telefonų turėjo OLED-inius ekranus[9]. OLED-ų gamybai reikia žemesnės temperatūros[10] ir mažiau pavojingų medžiagų nei dirbant su neorganinėmis medžiagomis. Vietoj siauro matymo kampo suteikiamo skystųjų kristalų ekranų (LCD), OLED-ai paprastai pasižymi lambertiniu spinduliuotės paskirstymu ir reikalauja mažiau aktyvių komponentų, palyginti su LCD-ais[11,12]. Praktiškiau gaminti mikroOLED-inius ekranus, skirtus akims draugiškiems ekranams, sumažinus OLED-inių pikselių dydį iki kelių mikrometrų[13]. Proveržis kuriant efektyvius aukštos kokybės šviesos šaltinius, kuriuos galima panaudoti dirbtiniam apšvietimui, buvo mėlynos spalvos šviesos diodų pristatymas, kuris 2014 m. buvo apdovanotas Nobelio fizikos premija[14]. Be baltos spalvos organinių šviesos diodų (WOLED), kurie turi didelį potencialą tapti pramoniniais kietaisiais šviesos šaltiniais, vienspalviai OLED-ai taip pat gali būti naudojami kaip šviesos šaltiniai automobilių pramonėje[15,16]. Dvi pagrindinės praktinės organinių šviesos diodų taikymo sritys – kietakūnis apšvietimas ir ekranai – yra įmanomos dėl dviejų pagrindinių sukurtų prietaisų ir organinių puslaidininkinių medžiagų savybių. Plonasluoksniai OLED-ai yra plotiniai šviesos šaltiniai ir gali suteikti naujų galimybių įvairioms reikmėms. Dėl gana mažo organinių medžiagų standumo nanosluoksniai leidžia gaminti OLED-us ant sulankstomų ir lanksčių substraktų[17,18]. Be to, organinių puslaidininkių spinduliuotės spektro spalvą ir plotį galima reguliuoti organinių junginių sintezės metu. Naudojant daugiau nei vieną spinduolį emisiniame sluoksnyje, galima efektyviausiai sukurti akims nekenksmingą natūralią šviesą[19,20]. Nauji pagaminti efektyvūs OLED-ai pasiekė tokį pat efektyvumą, kaip fluorescencinės lempos[21,22]. O prietaiso eksploatavimo trukmė tampa suderinama su kitais komerciniais šviesos šaltiniais, ir jau pranešta apie OLED-us, kurių veikimo trukmė viršija 100 000 valandų[23]. Tačiau vis dar sunku rasti tinkamų medžiagų derinių, kurie užtikrintų ilgą OLED-ų eksploatavimo trukmę, didelį efektyvumą ir gerą spalvų perteikimą. Vienas iš pagrindinių paaiškinimų, kodėl OLED-ai plačiai paplito ekranų technologijų rinkoje, o ne apšvietimo srityje, yra efektyvumo kritimas, t. y. gana greitas efektyvumo sumažėjimas esant dideliam srovės tankiui arba ryškumui[24,25].

Šio darbo tikslas – naujų mėlynos spalvos fluorescencinių spinduolių elektroliuminescencinių savybių tyrimas.

Darbo tikslui pasiekti buvo pasiūlytos šios **užduotys**:

- Ištirti dviejų naujų fenildikarbazolo darinių fotofizines, fotoelektrines, termines, krūvio pernašos ir elektroliuminescencines charakteristikas, siekiant sukurti eksipleksus sudarančias sistemas, skirtas deguonies jutikliams ir baltos spalvos hibridiniams liejimo iš tirpalo metodu formuojamiems OLED-ams.
- Ištirti du benzfenonų darinius kaip mėlynos spalvos spinduolius, eksitono moduliatorius ir skyles pernešančius junginius, skirtus sukurti OLED-us, pasižyminčius stabilia balta elektroliuminescencija ir gera spalvų kokybe.
- Ištirti įvairių papildomų akceptorių, esančių penkių daugiakarbazolo ir benznitrilo darinių molekulinėje struktūroje, įtaką mėlynos spalvos TADF OLED-ų veikimui, kai junginiai naudojami kaip spinduoliai.
- Pateikti nuo terpės priklausomą mėlynosios emisijos ir sukinio apvertimo efektyvumo nustatymą daugiakarbazoliniuose junginiuose su skirtingais papildomais akceptoriais siekiant pagerinti jų TADF efektyvumą.
- Ištirti konjuguotų daugiadonorų-akceptorių darinių, turinčių trifluormetilbenzeno fragmentus, fotofizikines, fotoelektrines, krūvio pernašos ir elektroliuminescencines savybes.
- Ištirti konformacinės netvarkos ir kietosios būsenos tirpinimo poveikį mėlynos šviesos OLED-ų, turinčių nelegiruotus ir skirtingai legiruotus emisinius sluoksnius, emisijos savybėms.

Darbo naujumas:

- Panaudojant naujus dikarbazolo darinius, pakeistus skirtingais elektrondonoriniais (fluor- arba trifluormetil-) fragmentais, sukurti veiksmingi eksipleksiniai spinduoliai, pasižymintys termiškai aktyvuojamąja uždelstąja fluorescencija (TADF) ir reikšmingais atvirkštinės interkombinacinės konversijos (RISC) greičiais iki $5,1 \times 10^7$ s^{-1}. Buvo įrodyta, kad juos galima naudoti deguonies jutikliams ir hibridiniams liejimo iš tirpalo metodu formuojamiems WOLED-ams su aukštu spalvų perteikimo indeksu.
- Erdvinio eksitonų paskirstymo strategija pirmą kartą buvo panaudota WOLED-ams, turintiems TADF spinduolius. Ši strategija leido moduliuoti ir atskirti eksitonus bei krūvininkus eksitonų rekombinacijos ir krūvininkų rekombinacijos srityse, todėl sukurtų OLED-ų išorinis kvantinis efektyvumas (EQE) bei baltos spalvos kokybė, palyginti su etaloniniais OLED-ais, buvo maždaug du kartus didesnė.
- Naudojant daugiakarbazolilpakeistus benznitrilo mėlynos spalvos TADF spinduolius, turinčius įvairių papildomų akceptorių, siekiant sukurti efektyvius OLED-us su derinamais mėlynos elektroliuminescencijos spalvų

variantais, buvo pasiektas didesnis TADF efektyvumas ir didelis RISC greitis nuo $4,7 \times 10^4$ iki $2,32 \times 10^6$ s⁻¹.

- Kietosios būsenos tirpimo ir konformacijos netvarkos pasekmių minimizavimas mėlynos spalvos TADF emiterių veikimui taikant kelių donorų ir akceptorių pakeitimo inžineriją, siekiant sukurti nelegiruotus ir legiruotus OLED-us, pasižyminčius neįprastai panašiomis elektroliuminescencinėmis savybėmis.

4.1 Eksipleksus formuojančios sistemos su itin dideliu RISC greičiu, viršijančiu 10^7 s⁻¹, skirtos deguonies jutikliams ir baltos spalvos hibridiniams OLED-ams

Šiame darbe siekėme ištirti du naujai sumodeliuotus fluor- arba trifluormetilfenilpakeistus difenildikarbazolus kaip donorus eksipleksams sudaryti. Junginių **1** ir **2** molekulinės struktūros pateiktos **4.1 pav**.
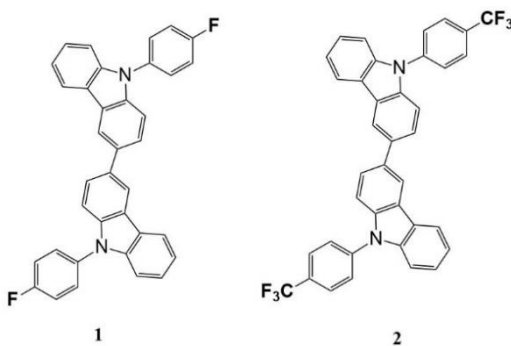
4.1 pav. Junginių **1** ir **2** molekulinės struktūros

Junginiai **1** ir **2** dėl subalansuotų skylių pernašos savybių, aukšto tripletinio lygio ir emisijos artimoje ultravioletinėje srityje gali būti laikomi potencialiais donorais eksipleksams, pasižymintiems TADF emisija, gaminti. Todėl buvo sukurti du kietieji tirpalai, naudojant komercinį akceptorių 2,4,6-tris[3-(difenilfosfinil)fenil]-1,3,5-triaziną (PO-T2T) bei junginius **1** ir **2** kaip donorus. Bandiniai **1**:PO-T2T ir **2**:PO-T2T pasižymėjo raudonų bangų pusėn pasislinkusia eksipleksine emisija, palyginti su grynąja akceptoriaus ir donoro emisija (apie 110 nm, palyginti su donorais, ir 150 nm, palyginti su akceptoriumi) (**4.2 pav., a**). Bandinių fotoliuminescencijos (PL) spektrai ir PL gesimai esant skirtingoms temperatūroms parodė, kad apie 90% skleidžiamos eksipleksinės emisijos intensyvumo susidaro dėl termiškai aktyvuojamos uždelstosios fluorescencijos (**4.2 pav. b, c**). Kitas TADF egzistavimo mūsų gautų eksipleksų emisijoje patvirtinimas buvo mažas energetinis tarpas tarp singletinės ir tripletinės būsenų (ΔE_{S1T1}), kuris leido efektyviai vykdyti RISC procesą (**4.2 pav., d**). Eksipleksai **1**:PO-T2T ir **2**:PO-T2T pasižymėjo panašia emisija maždaug ties 520 nm bangos ilgiu, o jų PL gesimas aprašomas dieksponentine funkcija su trumpai gyvuojančiu (τ_{PF} nuo 69 iki 376 ns) ir ilgai gyvuojančiu (τ_{DF} nuo 1,94 iki 4,25 µs) komponentais (**4.2 pav., a, b**). Eksipleksai **1**:PO-T2T ir **2**:PO-T2T pasižymėjo itin

dideliu k_{RISC}, atitinkamai $5{,}1×10^7$ ir $3{,}6×10^7$ s^{-1}. Gautos k_{RISC} vertės yra vienos didžiausių iki šiol aprašytų[70,71].
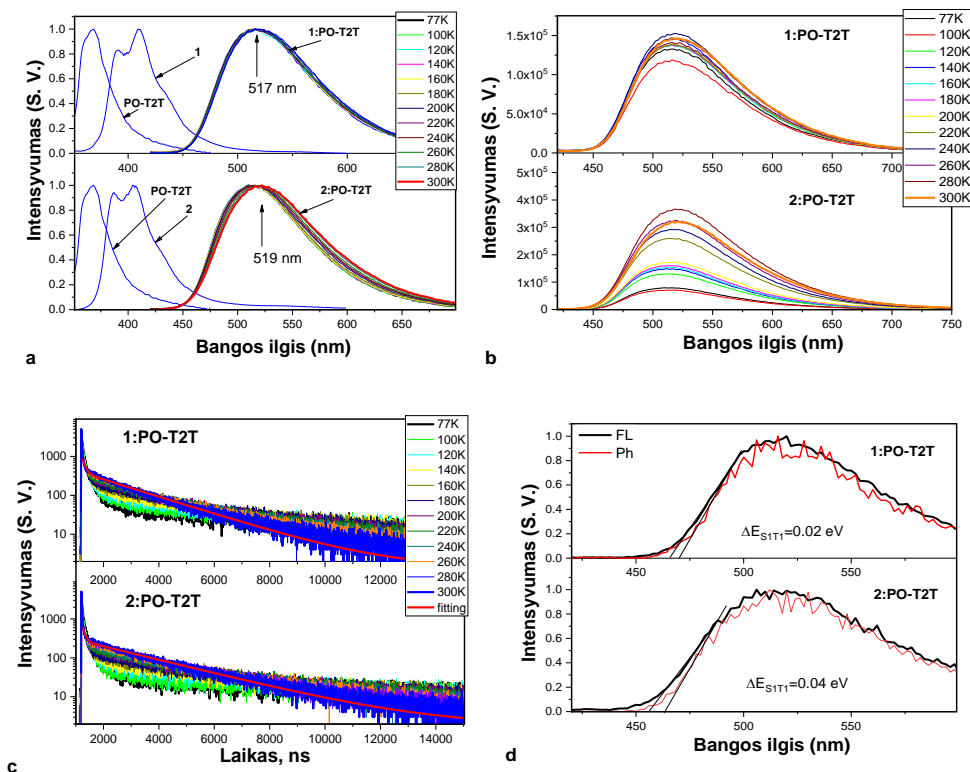

4.2 pav. Bandinių **1**, **2**, PO-T2T, **1**:PO-T2T ir **2**:PO-T2T sluoksnių normalizuoti PL spektrai (a) ir nuo temperatūros priklausantys PL spektrai (b). Kietųjų tirpalų **1**:PO-T2T ir **2**:PO-T2T PL gesimo kreivės, užregistruotos esant skirtingoms temperatūroms (c), ir fotoliuminescencijos ir fosforescencijos spektrai, išmatuoti esant 77 K temperatūrai (d)

Siekiant išgauti natūralią baltą šviesą, eksipleksai **1**:PO-T2T ir **2**:PO-T2T kartu su mėlynu TFB[76] ir raudonu (Ir(piq)2(acac))[77] spinduoliais buvo pasirinkti keliems liejimo iš tirpalo metodu formuojamiems baltos spalvos OLED prietaisams pagaminti. Pagrindinė priežastis, kodėl pasirinkome liejimo iš tirpalo metodą, nes šis metodas leidžia tiksliai kontroliuoti spinduolių koncentraciją legiruotuose emisiniuose sluoksniuose, kurie buvo labai svarbūs gaminant WOLED[78]. Pasirinktos OLED prietaisų struktūros: ITO/MoO$_3$ (1 nm)/TFB:Ir(piq)$_2$(acac) (2, 5 arba 10%, 30 nm)/**1**:PO-T2T (atitinkamai prietaisų A2, A5 ir A10) arba **2**:PO-T2T (atitinkamai prietaisų B2, B5 ir B10) (1:1) (20 nm)/TSPO1 (8 nm)/TPBi (40 nm)/LiF:Al. Labai plonas MoO$_3$ sluoksnis buvo naudojamas kaip skylių injekcijos sluoksnis, junginys TSPO1 veikė kaip skylių ir eksitonų blokavimo sluoksnis, TPBi buvo naudojamas kaip elektronų pernešimo sluoksnis, o elektronų injekcijos sluoksniui buvo pasirinktas LiF. Rekombinacijos zona iš esmės yra emisiniame sluoksnyje (EML1, **1**:PO-T2T arba **2**:PO-T2T), kaip matyti prietaisų struktūrų pusiausvyros energijos diagramoje (**4.3 pav., a**). Skyles pernešantis TFB sluoksnis, kuris buvo legiruotas mažos

koncentracijos Ir(piq)$_2$(acac), taip pat naudojamas kaip antrasis emisinis sluoksnis (EML2). Yra dvi raudonojo spinduolio Ir(piq)2(acac) emisijos galimybės: kai EML1 susidaro tripletiniai eksitonai, kurie persikelia į EML2, ir kai EML2 vyksta tiesioginė elektronų ir skylių rekombinacija[79].
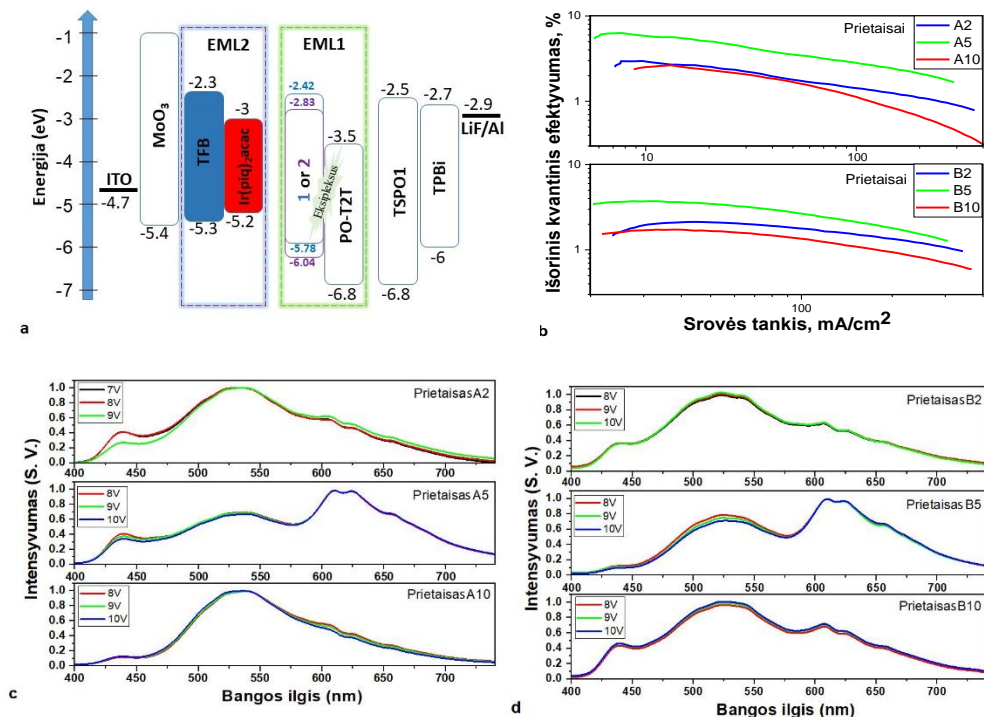
4.3 pav. Prietaisų visų funkcinių sluoksnių pusiausvyros energijos diagrama (a), pagamintų OLED *EQE* priklausomybė nuo srovės tankio (b), baltų prietaisų, sudarytų naudojant **1**:PO-T2T (c) ir **2**:PO-T2T (d), normalizuoti EL spektrai esant skirtingoms įtampoms

Kaip matyti **4.3 pav., c, d,** liejimo iš tirpalo metodu pagamintų OLED-ų elektroliuminescencijos (EL) spektruose matomos skirtingo intensyvumo Ir(piq)2(acac), **1**:PO-T2T arba **2**:PO-T2T ir TFB spinduolių emisijos juostos. Tokia stabili A ir B prietaisų EL esant skirtingoms įtampoms (**4.3 pav., c, d**) gali įrodyti, kad pagamintuose prietaisuose yra krūvininkų pusiausvyra, nes didinant įtampas nepastebimas rekombinacinės zonos poslinkis iš EML1 į EML2. Intensyviausia raudona emisija buvo prietaisuose A5 ir B5 su 5% Ir(piq)2(acac), o koncentraciją padidinus iki 10%, raudonos fosforescencijos intensyvumas gali sumažėti. Tai gali būti susiję su emisijos gesimu dėl tripleto-tripleto anihiliacijos (TTA) esant didelei fosforescencinio spinduolio koncentracijai[80]. Kalbant apie spalvų kokybę, prietaisas A5 turėjo geriausią mėlynos, žalios ir raudonos emisijos intensyvumo derinį savo EL spektre su geriausiomis CRI – 92, CIE1931 xy koordinatėmis (0,384,0,399) ir koreliuojamąja spalvų temperatūra (CCT) 3655 K. Užregistruota CIE1931 ir įrenginio A5 spalvos temperatūra gali būti priskirta šiltai baltai šviesai, o CRI reikšmė iki šiol yra viena didžiausių baltų OLED verčių[81,82]. Esant 12 V išorinei įtampai, didžiausią

8980 cd/m² ir mažiausią 2986 cd/m² skaistį pasiekė atitinkamai prietaisai A5 ir A10. Didžiausiu efektyvumu pasižymėjo prietaisai A5 ir B5, kuriuose fosforescencinis spinduolis Ir(piq)2(acac) ir du eksipleksai TADF spinduoliai (**1**:PO-T2T arba **2**:PO-T2T) tripletinius eksitonus efektyviai verčia singuletiniais. Didžiausios CE_{max}, PE_{max} ir EQE_{max} vertės atitinkamai 11,6 cd/A, 5,5 lm/W ir 6,3% pastebėtos prietaise A5 su **1**:PO-T2T žaliu eksipleksu ir 5% Ir(piq)2(acac) (**4.3 pav., b**).

4.2 Bis(*N*-naftil-*N*-fenilamin)benzfenonai kaip eksitonus moduliuojančios medžiagos, skirtos baltos šviesos TADF OLED-ams su atskirtomis krūvininkų ir eksitonų rekombinacijos zonomis

Šiame darbe du naujai susintetinti junginiai **3** ir **4** panaudoti kaip mėlyno ir oranžinio TADF eksitonų moduliatoriai gaminant keletą grynai TADF WOLED-ų. Junginių **3** ir **4** su izomeriniais (*N*-naftil)-*N*-fenilamino donorainiais ir benzfenono akceptoriniais fragmentais molekulinės struktūros pateiktos **4.4 pav.**
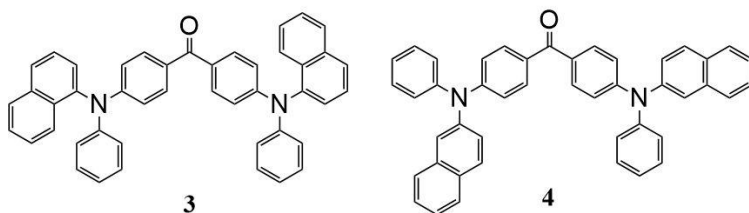

4.4 pav. Junginių **3** ir **4** struktūros

Siekiant ištirti junginių **3** ir **4** fotofizikines savybes, užregistruoti junginių kietųjų sluoksnių ir praskiestų tirpalų THF bei toluene fotoliuminescencijos ir UV absorbcijos spektrai (**4.5 pav., a**). Junginių **3** ir **4** tirpalų THF emisijos maksimumai atitinkamai ties 462 nm ir 488 nm, o Stoko poslinkiai buvo 90 ir 107 nm. Junginių sluoksnių Stoko poslinkiai atitinkamai buvo 94 ir 113 nm (**4.5 pav., a**). Nedidelis, atitinkamai 22 nm ir 34 nm, skirtumas tarp junginių **3** ir **4** tirpalų toluene ir THF emisijos patvirtina silpną intramolekulinę krūvio perdavą (CT) tarp donorinių ir akceptorinių fragmentų[91]. Optinės draustinės juostos tarpai buvo apskaičiuoti pagal junginių sluoksnių absorbcijos spektrų pradžios bangos ilgius, taigi junginių **3** ir **4** absorbcijos pradžios bangos ilgiai buvo 429 ir 446 nm, jie atitinka 2,89 ir 2,78 eV optinius draustinės juostos tarpus (**4.5 pav., a**). Junginių **3** ir **4** fotofizikinės savybės toliau tirtos registruojant jų tirpalų THF fotoliuminescencijos ir fosforescencijos spektrus 77 K temperatūroje (**4.5 pav.**, b). Gautos E_{S1} ir E_{T1} energijos apibendrintos **2.3 lentelėje**. *N*-naftil-*N*-fenilamino fragmentų tripletinės būsenos LE³ emisijos rekombinacija yra pagrindinis junginių fosforescencinės emisijos šaltinis[92].
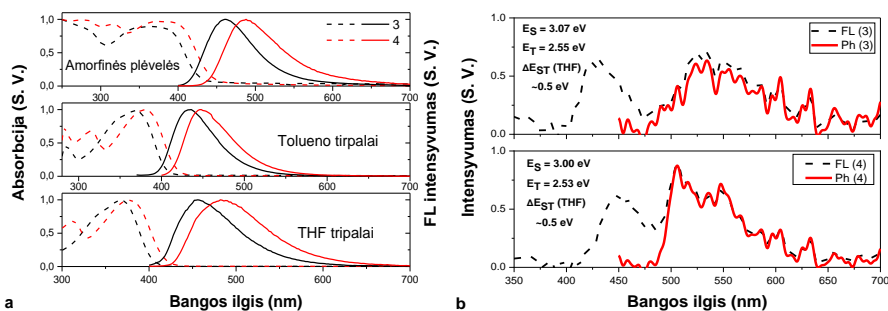
4.5 pav. Junginių **3** ir **4** PL (dešinėje) ir normalizuoti UV absorbcijos spektrai (kairėje) (a) bei jų praskiestų tirpalų THF PL (juodos brūkšninės linijos) ir fosforescencijos (Ph, raudonos linijos) spektrai 77 K temperatūroje (b)

Atsižvelgiant į geras naujųjų junginių optoelektronines savybes, junginiai **3** ir **4** parinkti moduliuoti eksitonams viename arba dviejuose TADF spinduoliuose (oranžiniame 4CzTPN ir mėlyname PFBP-2b), skirtuose WOLED-ams su atskirtomis eksitonų ir krūvininkų rekombinacijos zonomis. Pirmą kartą, taikant erdvinę eksitonų paskirstymo strategiją, pagamintos dviejų tipų grynai TADF WOLED prietaisų struktūros su vienu rezonansiniu energijos perdavimu iš mėlynos į oranžinę arba su dviem rezonansiniais energijos perdavimais iš mėlynos į oranžinę ir iš mėlynos į mėlyną spalvą. Mūsų prietaisuose su dviem TADF emiteriais, naudojant du efektyvius rezonansinius energijos perdavimus, galima atskirti krūvininkų ir eksitonų rekombinacijos zonas. Tačiau pagamintuose prietaisuose su eksitonus blokuojančiu sluoksniu (EBL) vienas iš rezonansinių energijos perdavimų gali būti apribotas, todėl galėjome ištirti vieno ar dviejų rezonansinių energijos perdavimų poveikį baltų prietaisų spalvų kokybei ir efektyvumui. Naudotos šios OLED konstrukcijos: ITO/ MoO_3 (8nm)/ NPB(60nm)/ TAPC(5nm)/EML/ TSPO1(8nm)/ TPBi(40nm)/ LiF(1nm)/Al (prietaisai IA(B)1-3) ir ITO/MoO_3(8nm)/ NPB(60nm)/ TAPC(5nm)/EML/PFBP-2b (20%):TPBi (40 nm)/ LiF(1nm)/Al (prietaisai IIA(B)1-3). OLED prietaisų charakteristikos pateiktos **4.1 lentelėje**. Prietaisų pavadinimai su ženklu I priklauso pirmajai OLED-ų šeimai, kurioje yra TSPO1 kaip eksitonus blokuojantis sluoksnis, su vienu rezonansinės energijos perdavimu, o prietaisai su ženklu II turi du efektyvius rezonansinės energijos perdavimus, A raidė žymi struktūroje esantį junginį **3**, o B raidė – junginį **4**, "1-3" yra susiję su trimis skirtingais emisiniais sluoksniais (EML). Naudojant 4CzTPN/3 ir 4/PFBP-2b sistemas, galima pagaminti WOLED-us su atskirtomis eksitonų ir skylių-elektronų rekombinacijos zonomis. TPBi:PFBP-2b sluoksnyje kaip TADF spinduolis naudotas PFBP-2b. Prietaisai IA2, IB2, IIA2 ir IIB2 charakterizuoti balta elektroliuminescencija. Šių prietaisų EL spektruose yra dvi skirtingo intensyvumo emisijos juostos, kurias sudaro mėlynos spalvos junginių **3** arba **4** (ir PFBP-2b prietaisų IIA2 ir IIB2 atveju) emisija ir oranžinės spalvos 4CzTPN emisija (**4.6 pav.**, a, b).
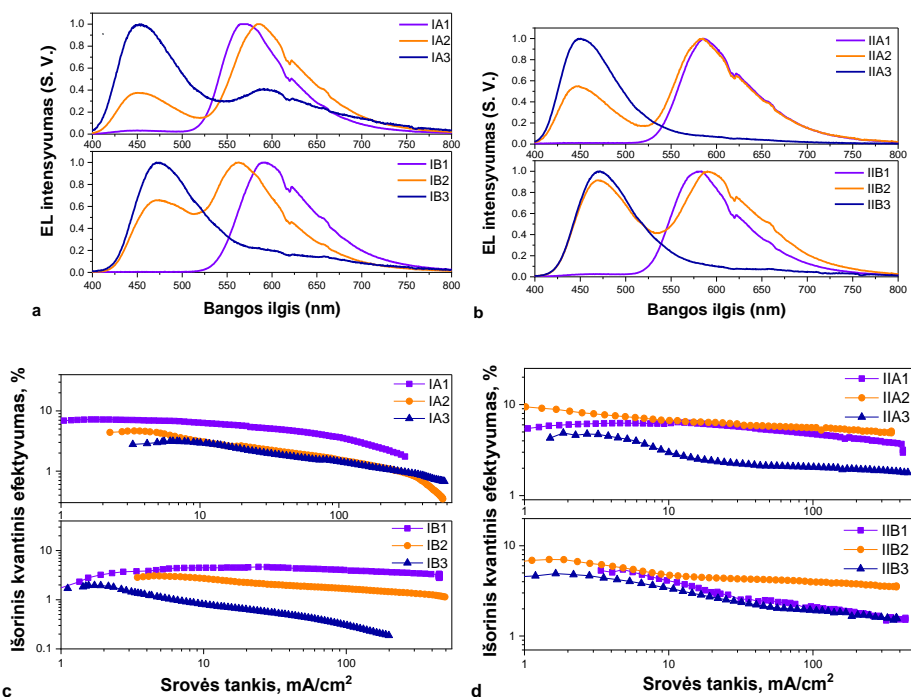
4.6 pav. Pagamintų OLED-ų EL spektrai esant 9 V įtampai (a, b) bei EQE priklausomybės nuo srovės tankio kreivės (c, d)

Prietaisai IA1, IB1, IIA1 ir IIB1 pasižymėjo oranžinės spalvos emisija, kilusia iš 4CzTPN:3(4) sluoksnio. Tačiau prietaisai IA3, IB3, IIA3 ir IIB3 dėl nepakankamo RET 3(4) ir 4CzTPN sluoksniuose rodė daugiausia mėlynos spalvos EL. Dėl papildomo PFBP-2b TADF spinduolio vaidmens mėlynajai emisijai pagamintuose prietaisuose su dviem rezonansiniais energijos perdavimais emisijos juosta, susijusi su 4CzTPN, yra stipresnė IA3 ir IB3 prietaisuose, palyginti su IIA3 ir IIB3 OLED-ais. Dėl tikrai aukšto baltos spalvos elektroliuminescencijos standarto, gauto naudojant tik du emiterius, prietaisas IIB2 pasižymėjo aukščiausiu CRI (80) ir koreliacine spalvine temperatūra (T_C) 4490 K, o CIE 1931 xy koordinatės (0,32, 0,31) yra artimiausios natūraliai baltai spalvai (**4.1 lentelė**). Teigiamas PFBP-2b vaidmuo akivaizdus ir palyginus pirmosios (IA3 ir IB3) ir antrosios (IIA3 ir IIB3) OLED-ų serijos mėlynos spalvos prietaisų EQE (**4.6 pav.**, c, d).

4.1 lentelė. Baltų OLED elektroliuminescencijos charakteristikos

Prietaisas	$V_{įjungti,}$ [a] V	CE_{maks}, cd/A	EQE_{maks}, %	CIE (x; y)[b]	CRI[b]	CCT[b]
IA1	4,7	20,8	7,2	(0,47, 0,49)	42	2932
IA2	4,2	10,2	4,8	(0,40, 0,35)	60	2751
IA3	5,1	3,9	3,1	(0,26, 0,22)	75	12520

IB1	5,9	9,4	4,7	(0,55, 0,44)	41	1840
IB2	5,7	8,3	3,1	(0,36, 0,42)	62	4220
IB3	4,6	3,7	1,9	(0,20, 0,26)	---	----
IIA1	4,2	13,7	6,3	(0,53, 0,45)	40	2061
IIA2	3,9	18,6	9,5	(0,36, 0,31)	67	3332
IIA3	4,6	8,1	4,7	(0,16, 0,13)	-----	-----
IIB1	4	12,4	5,5	(0,49, 0,47)	43	2515
IIB2	3,6	13,8	7,1	(0,32, 0,31)	80	4490
IIB3	3,3	7,8	4,9	(0,17, 0,22)	---	-----

[a] Įjungimo įtampa esant 10 cd m^{-2} skaisčiui, [b]CIE, CRI ir CCT vertės nustatytos, kai EL spektrai išmatuoti esant 9 V įtampai

4.3 Mėlyną spalvą emituojančių daugiakarbazolilpakeistų benznitrilų sukinio apvertimo efektyvumo derinimas panaudojant skirtingus papildomus akceptorinius fragmentus

TADF junginiai gali būti sintetinami naudojant multidonorinį ir akceptorinį tipą bei įvairias intramolekulines jėgas (pvz., nekovalentines arba erdvines). Šiame darbe, siekdami sukurti efektyvius mėlynos spalvos OLED-us, panaudojome penkis naujai susintetintus asimetrinius daugiakarbazolinius spinduolius legiruotose ir nelegiruotose OLED-ų struktūrose. Junginių **5**–**9** molekulinės struktūros pateiktos **4.7 pav**.
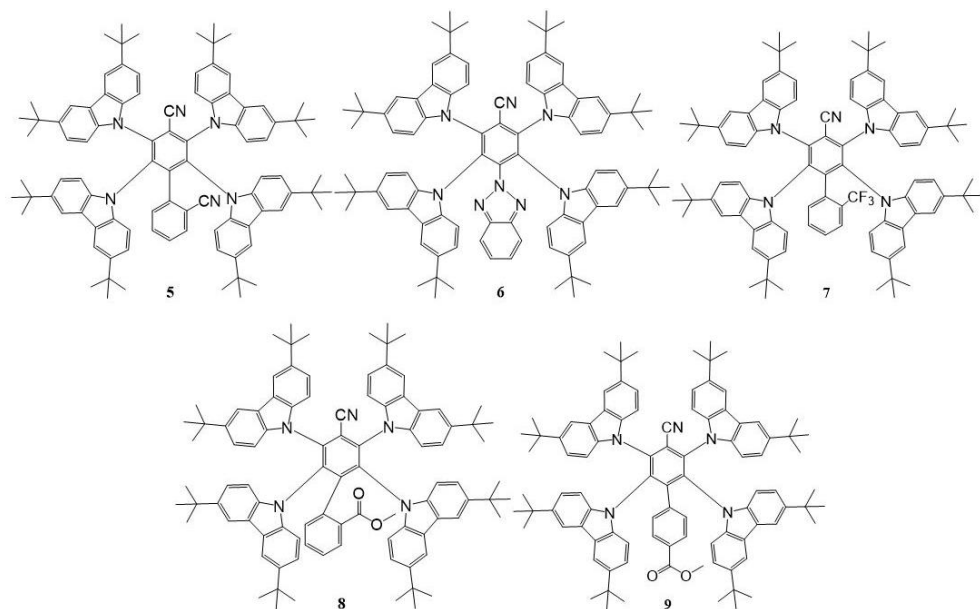
4.7 pav. Junginių **5**–**9** molekulinės struktūros

Panašiai kaip ir anksčiau paskelbtuose daugiakarbazoliniuose junginiuose[103,105], UV absorbcijos juostos 310–365 nm diapazone yra susijusios su di-*tret*-butilkarbazolo fragmento π–π* arba n–π* šuoliais. Junginio **6** spektre mažos energijos absorbcijos juostos apie 365–475 nm ir kitų junginių spektruose apie 365–450 nm atsiranda dėl intramolekulinės CT savybių. Dėl sužadintosios CT būsenos rekombinacijos[107] junginių **5**–**9** tirpaluose ir sluoksniuose užregistruota emisija su nestruktūrizuotais PL spektrais, kurių maksimumai yra 457–522 nm (**4.8 pav.**, b). Junginių didelio poliškumo THF tirpalų PL spektrai, palyginti su mažo poliškumo tolueno tirpalų spektrais, parodė didžiausią poslinkį raudonos spalvos link. Junginių tirpalų toluene PL intensyvumas labai padidėjo, kai tirpalai buvo prapūsti argono dujomis pašalinant deguonį (**4.8 pav., c**). Norint ištirti junginių skylių injektavimo savybes, naudojant elektronų fotoemisijos spektrometriją, ištirti junginių sluoksnių jonizacijos potencialai (IP_{PE}) (**4.8 pav.**, d). Skirtingi akceptoriniai fragmentai lėmė skirtingas jonizacijos potencialo vertes: jos svyravo nuo 5,39 iki 5,9 eV, o tai rodo, kad junginiai pasižymi skirtinga skylių injektavimo elgsena.
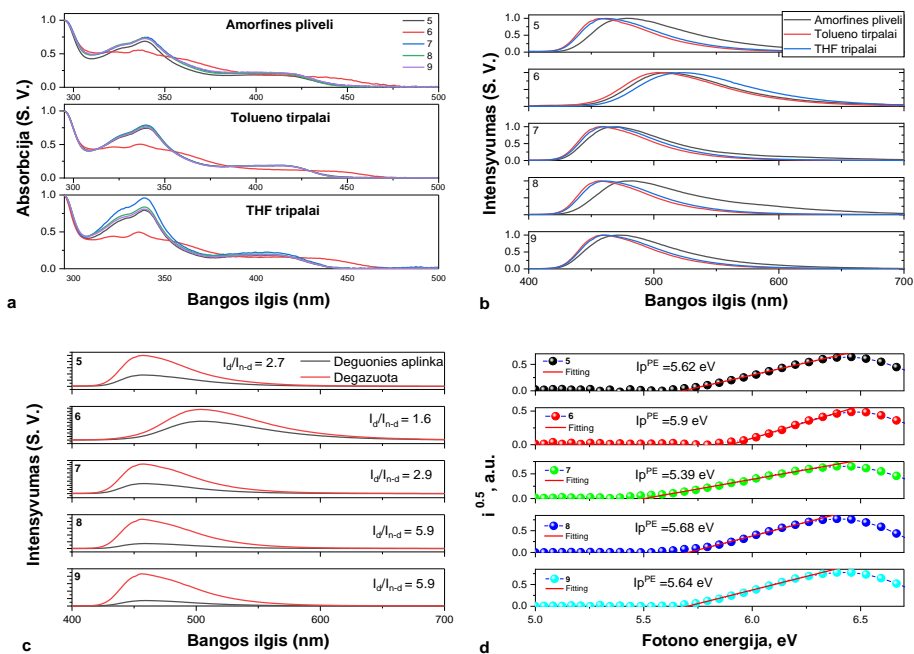
4.8 pav. Tiriamų junginių tirpalų toluene arba THF bei sluoksnių UV absorbcijos (a) ir PL (b) spektrai, junginių tirpalų toluene PL spektrai prieš ir po deguonies pašalinimo (c), junginių sluoksnių elektronų fotoemisijos spektrai, matuoti ore (d)

Junginių elektroliuminescencinės savybės tirtos naudojant jas keliose prietaisų struktūrose su nelegiruotais ir legiruotais emisiniais sluoksniais. Pagamintų OLED-ų funkciniai organiniai sluoksniai parinkti taip, kad būtų užtikrintas efektyvus krūvininkų injektavimas ir pernaša, taip pat krūvininkų ir eksitonų rekombinacija emisiniuose sluoksniuose. Suformuotų OLED-ų sluoksniai buvo tokie: ITO/MoO₃ (1 nm)/ NPB (30 nm)/ mCP (4 nm) / emisinis sluoksnis (20 nm) / TSPO1 (8 nm)/TPBi

(40 nm)/LiF (0,5 nm):Al (100 nm), kuriuose junginiai **5–9** naudoti emisiniuose sluoksniuose ir atitinkamai pavadinti n5–n9 neleguotuose prietaisuose ir d5–d9 legiruotuose prietaisuose. Visi pagrindiniai pagamintų OLED-ų kriterijai yra apibendrinti **4.2 lentelėje**. Visuose gautuose prietaisuose užfiksuotos beveik mažos įjungimo įtampos, rodančios, kad teigiami ir neigiami krūvininkai iš elektrodų į emisinį sluoksnį yra efektyviai injektuojami ir pernešami. Didžiausias 7,3% EQE_{max} ir mažiausias 2% EQE_{max} gauti prietaisuose n5 ir n6 (**4.2 lentelė**), taip pat panaši tendencija užfiksuota ir legiruotuose prietaisuose (d5–9). Kadangi prietaisai d5 ir d9 pasižymėjo didesniais EQE_{max}, atitinkamai 11,8 ir 7,9%, nusprendėme toliau didinti OLED-ų prietaisų efektyvumą, tinkamai optimizuodami OLED struktūrą ir spinduolių koncentracijas EML sluoksniuose. Optimizuotos OLED struktūros su skirtingomis spinduolių **5** ir **9** koncentracijomis mCBP matricoje turėjo HAT-CN sluoksnį kaip HIL, NPB ir TCTA kaip HTL ir mCBP kaip EBL. Apskritai dėl papildomo prietaiso optimizavimo prietaisuose o1b ir o5b pavyko pasiekti puikius 18,3 ir 14,1% EQE_{max}. Šiuos rezultatus galima priskirti pakitusiam krūvininkų balansui emisiniame sluoksnyje dėl geresnio krūvininkų judrumo mCBP sluoksnyje.

4.2 lentelė. OLED charakteristikos

Prietaisas	Emisinis sluoksnis	$V_{ijungti}$, [a] **V**	CE_{maks} cd/A	EQE_{maks}, %	Λ, nm	*Maks skaistis*, cd/m²
n5	**5**	4,1	19,4	7,3	495	36000
n6	**6**	4,2	3,8	2	490	2800
n7	**7**	4,6	6	3,4	474	5050
n8	**8**	5	7,8	4,3	476	8243
n9	**9**	6	12,1	5,6	480	16988
d5	**5** (20wt.%):mCP	3,4	28	11,8	485	39260
d6	**6** (20wt.%):mCP	4,2	4,8	3,1	470	4415
d7	**7** (20wt.%):mCP	4,1	12,9	6,6	471	10144
d8	**8** (20wt.%):mCP	4,6	12,2	5,6	495	14176
d9	**9** (20wt.%):mCP	4,3	17,5	7,9	481	21110
o5a	**5** (10wt.%):mCBP	3,9	28,3	15,1	466	11831
o5b	**5** (20wt.%):mCBP	4	39,3	18,3	468	17456
o5c	**5** (30wt.%):mCBP	3,9	27,4	12,4	476	19516
o9a	**9** (10wt.%):mCBP	3,8	22,7	11,6	457	5453
o9b	**9** (20wt.%):mCBP	3,9	24,8	14,1	457	19551
o9c	**9** (30wt.%):mCBP	4,3	20,3	10,3	463	17115
ref	PFBP2b(10wt.%): mCBP	3,8	22,8	11,5	480	13420

[a] Įjungimo įtampa esant 10 cd m⁻² skaisčiui

4.4 Mėlynos spalvos TADF spinduolių elementų dekoravimas inkarine grupe, siekiant sumažinti kietosios solvatacijos ir konformacijos netvarkos padarinius nelegiruotuose ir legiruotuose OLED-uose

Šiame darbe, siekiant kuo labiau sumažinti daugiakarbazolinių junginių konformacijos netvarkos kietoje būsenoje poveikį emisijos charakteristikoms, buvo ištirtos penkios naujos efektyvios asimetrinės mėlynos spalvos TADF medžiagos su keturiais donoriniais 3,6-di-*tret*-butilkarbazilfragmentais ir dviem elektronus atitraukiančiais pakaitais. Junginių **10**–**14** molekulinės struktūros pavaizduotos **4.9 pav**.
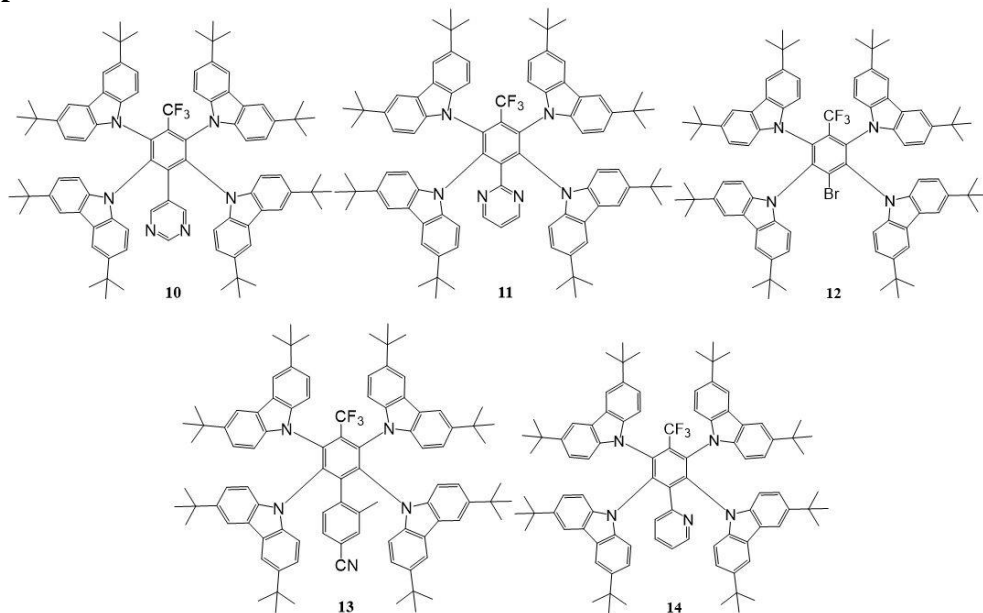
4.9 pav. Junginių **10**–**14** molekulinės struktūros

Junginių sluoksnių ir praskiestų tirpalų UV absorbcijos ir PL emisijos spektrų apibendrinta informacija pateikta **4.3 lentelėje**. Užfiksuoti beveik panašūs spinduolių tirpalų ir sluoksnių sugerties profiliai. Užregistruoti medžiagų **10**–**14** sluoksnių nestruktūrizioti PL spektrai, kurių maksimumai atitinkamai ties 482, 508, 482, 490 ir 480 nm. Naudojant integruotąją sferą užfiksuotos junginių kietųjų sluoksnių ir tirpalų toluene PLQY vertės atmosferos ir vakuumo sąlygomis. Junginių **10**–**14** degazuotų tirpalų toluene PL kvantinio našumo (PLQY) vertės svyravo nuo 7,5 iki 44 %, taip pat medžiagos **10** kietojo būsenos PLQY vakuume viršijo 75 %, o tai yra gana didelė vertė organinės elektronikos reikmėms (**4.3 lentelė**). Visose medžiagose pastebėtas didesnis bedeguonių tirpalų toluene emisijos intensyvumas, palyginti su deguonies prisotintais mėginiais. Jautrumas deguoniui ir emisijos padidėjimas degazavus tirpalus rodo, kad emisijoje dalyvauja tripletinė būsena. Junginio **10** bedeguonio tirpalo toluene PL intensyvumas buvo maždaug šešis kartus didesnis nei deguonies prisotinto praskiesto tirpalo toluene PL intensyvumas. Remiantis anksčiau praneštais metodais[46,124] ir atsižvelgiant į tai, kad nespindulinis gesimas dažniausiai vyksta iš

tripletų energijos lygmenų, norint gauti k_{RISC} buvo panaudoti išmatuoti PLQY bei intensyvumo ir eksploatavimo trukmės santykis DF/PF. Junginiai **10** ir **14** pasižymėjo tikrai dideliu k_{RISC}, atitinkamai 8×10^5 ir 5.5×10^6 s^{-1}, tai rodo, kad šie junginiai pasižymi gana greitu sukinio apvertimo efektyvumu. Junginių praskiestų tirpalų THF fotoliuminescencijos ir fosforescencijos spektrai užregistruoti 77 K temperatūroje. Junginių singuletinės ir tripletinės energijų skirtumo (ΔE_{ST}) vertės išsidėsto diapazone nuo 0,03 iki 0,05 eV, kurios gautos iš iš junginių tirpalų THF PL ir fosforescencijos spektrų pradžios, ir tikėtina, kad šis minimalus singuleto-tripleto atotrūkis yra erdviškai atskirtų donorinių ir akceptorinių fragmentų molekulinių orbitų rezultatas (**4.3 lentelė**)[128,129].

**4.3 lentelė.** Junginių **10**–**14** fotofizikinės ir terminės savybės

Parameteras	10	11	12	13	14
T_d^{onset}, °C [a]	439	441	433	449	462
λ_{abs}, nm	278/287/316/328	278/288/ 317/329	279/287/ 318/330	277/288/ 317/330	278/288/ 318/330
λ_{PL}, nm	482	508	482	490	480
$FWHM$, nm	86	104	126	94	106
ΔE_{S1T1}, eV	0,03	0,05	0,04	0,04	0,04
E_{S1}, eV	2,92	2,77	3,04	3,04	2,91
E_{T1}, eV	2,89	2,72	3,00	3,0	2,87
$PLQY$ (%)	44/76	12/51	8/4	17/27	13/49
η_{PF} [b]	0,24	0,16	0,02	0,13	0,07
η_{DF} [b]	0,52	0,35	0,02	0,14	0,42
τ_{PF}, ns (%) [b]	9(31)	13(32)	23(57)	23(48)	21(15)
τ_{DF}, μs (%) [b]	2,4 (69)	1,5 (68)	0,8 (43)	1,8 (52)	2,9 (85)
k_{PF}, s^{-1} [b]	$2,6 \times 10^7$	$1,2 \times 10^7$	$9,9 \times 10^5$	$5,7 \times 10^6$	$3,4 \times 10^6$
k_{ISC}, s^{-1} [b]	$1,8 \times 10^7$	8×10^5	$4,2 \times 10^5$	$2,9 \times 10^6$	$2,9 \times 10^6$
k_{DF}, s^{-1} [b]	$2,1 \times 10^5$	2×10^5	$2,1 \times 10^4$	$7,6 \times 10^4$	$1,4 \times 10^5$
k_{RISC}, s^{-1} [b]	7×10^5	8×10^5	$3,7 \times 10^4$	$1,6 \times 10^5$	1×10^6
k_{RISC}, s^{-1}	8×10^5	5×10^5	$6,7 \times 10^4$	$9,3 \times 10^4$	$5,5 \times 10^6$

[a] T_d^{onset} – terminės destrukcijos pradžios temperatūra (kaitinimo greitis 20 °C/min esant azoto atmosferai), [b] kieti sluoksniai

Norėdami palyginti mūsų mėlynos spalvos TADF junginių EL charakteristikas, pagaminome ir ištyrėme nelegiruotus ir legiruotus prietaisus su šiomis struktūromis: ITO / HAT-CN (HIL) / NPB (HTL) / TCTA (EBL) / mCBP (ExBL) / **10**–**14** (emisinis sluoksnis) / TPBi (ETL) / LiF:Al (EIL ir katodas) nelegiruotiems ir ITO / HAT-CN / NPB / TCTA / mCBP / mCBP: **10**–**14** (mCBP – matrica) / TPBi / LiF:Al legiruotiems prietaisams. Prietaisų sluoksniai ruošti juos vakuuminiu būdu laipsniškai nusodinant

nelegiruotuose ir legiruotuose prietaisuose, o legiruotiems emisiniams sluoksniams į mCBP matricą legiruoti 10% junginių **10**–**14**. Siekiant pagaminti efektyvius ir optimizuotus prietaisus, taip pat pagaminti prietaisai su skirtingomis spinduolio **10** koncentracijomis (10, 20 ir 30%), jis pasižymėjo geresnėmis fotofizikinėmis ir krūvininkų pernašos savybėmis mCBP matricoje. Pagamintų prietaisų EL spektrai buvo labai panašūs į junginių sluoksnių PL emisiją ir užregistruoti nestruktūrizuota mėlyna emisija su λ_{EL} nuo 473 iki 497 nm. OLED n1, kurio emisiniame sluoksnyje yra junginys **10**, skleidė dangaus mėlynumo emisiją, kurios CIE xy koordinatės yra (0,16, 0,27), PE_{max} – 12,4 lm/W, o EQE_{max} – 8,4%. Didžiausias prietaiso efektyvumas pasiektas d10b, kuriame legiruota 20% junginio **10**. Šis prietaisas (d10b) pasižymėjo mėlyna 477 nm emisija, didžiausiu srovės efektyvumu 42,6 cd/A ir EQE – 15,9% (**4.10 pav.**, b).

Užfiksuotas mažesnis prietaiso su didesne emiterio koncentracija (30%) efektyvumas tikriausiai yra susijęs su eksitonų anihiliacijos ir koncentracijos gesinimo poveikiu[141]. Pagamintas prietaisas su 30% junginio **10** (o10c) pasižymėjo 12,8% EQE_{max} ir EL spektro maksimumu ties 479 nm, kuris, palyginti su kitais dviem prietaisais, yra šiek tiek pasislinkęs raudonos spalvos kryptimi (**4.10 pav.**, b). Toliau optimizuoti OLED-us galima naudojant naujas matricines medžiagas arba funkcinius sluoksnius, nes junginiai **10**–**14** pasižymėjo tikrai aukštais tripletiniais lygmenimis, todėl matricinį arba elektronus pernešantį sluoksnį reikėtų pakeisti kitais junginiais, kurių tripletinės būsenos yra bent 0,2 eV aukštesnės[142]. Apibendrinant reikėtų manyti, kad panašios EL charakteristikos nelegiruotų ir mCBP legiruotų prietaisų su junginiais **10**–**14**, ypač pagamintų prietaisų, kurių sudėtyje yra junginys **10**, gali būti mūsų pristatytos koncepcijos, t. y. mažos konformacijos netvarkos poveikio TADF junginių emisijos charakteristikoms, požymis. Junginio **10** prietaisai pasižymėjo mažiausiu 4 nm skirtumu tarp nelegiruotų ir mCBP legiruotų OLED-ų EL spektrų maksimumų.
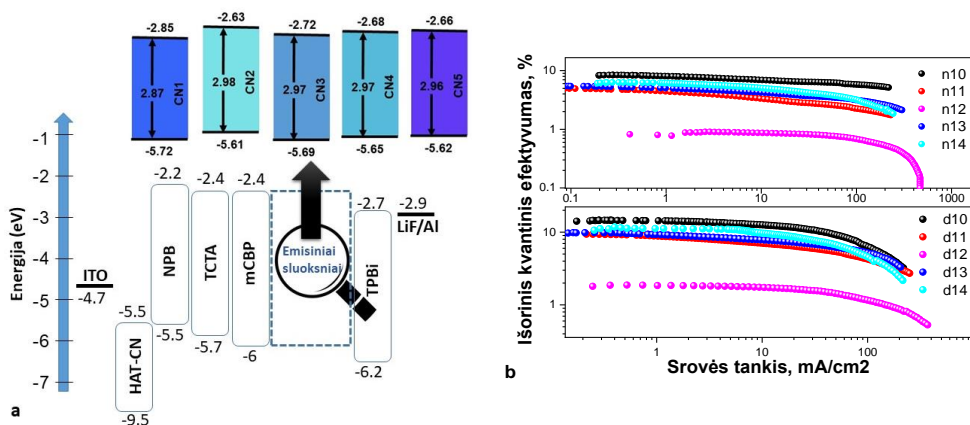
4.10 pav. Vizualizuotos pagamintos OLED struktūros su visų panaudotų medžiagų energinių būsenų lygmenimis (a) ir OLED-ų EQE priklausomybė nuo srovės tankio (b)

4.5 IŠVADOS

1. Siekiant atskleisti dviejų naujų fluor- ir trifluormetilpakeistų difenilbikarbazolų fotofizikinių, fotoelektrinių, krūvininkų judrio, elektrocheminių parametrų įtaką jų elektroliuminescencijos charakteristikoms, jie buvo tiriami daugeliu eksperimentinių metodų, įskaitant nuostoviosios būsenos ir laikinės skyros emisiją skirtingose temperatūrose, termogravimetrinę analizę, diferencinę skenuojamąją kalorimetriją, fotoemisijos spektroskopiją ir lėkio trukmės metodą.

    1.1. Donorinius difenilbikarbazolilpakeistus junginius sumaišius su komerciniu akceptoriniu PO-T2T sukurti du išskirtiniai eksipleksai, pasižymintys labai dideliu atvirkštinės interkombinacinės konversijos (RISC) greičiu, viršijančiu 10^7 s^{-1}, ir skirti naudoti baltos spalvos OLED-uose ir deguonies jutikliuose.

    1.2. Sukurti eksipleksai panaudoti kaip aktyviosios medžiagos deguonies pajutimui. Pagamintas deguonies jutiklis, turintis žalią eksipleksą, kuris pasižymėjo didesniu RISC greičiu, taip pat pasižymėjo nelinijinėmis deguonies zondavimo savybėmis (užfiksuotos Stern-Volmer konstantos – $3,27\times10^{-3}$ ir 4,7 ppm^{-1}).

    1.3. Gautos eksipleksus formuojančios sistemos panaudotos liejimo iš tirpalo metodu formuojamų baltų OLED-ų emisiniuose sluoksniuose, o pagaminti prietaisai pasižymėjo elektroliuminescencija, kurios išorinis kvantinis efektyvumas (EQE) siekė 6,3%, taip pat labai aukštos kokybės balta spalva, kurios CIE xy koordinatės yra (0,384, 0,399), o spalvų perteikimo indeksas – 92.

2. Sukurti stabilūs ir efektyvūs baltos spalvos OLED-ai, jų struktūroje naudojant du naujus benzfenono izomerus kaip mėlynos spalvos spinduolius, matricas ir moduliatorius eksitonų.

    2.1. Šie du benzfenono junginiai pasižymėjo dideliu terminiu stabilumu, o vieno iš jų 5% masės nuostolio temperatūra siekė 428 °C. Junginiuose nustatytas didesnis nei 10^{-4} cm^2·(V·s)$^{-1}$ skylių judris ir tinkamos krūvininkų injekcijos charakteristikos (junginių jonizacijos potencialo vertės 5,68 ir 5,79 eV).

    2.2. Suprojektavus pagamintų OLED sluoksnius, prietaisuose su vienu (oranžinės spalvos) arba dviem (oranžinės ir mėlyno spalvos) termiškai aktyvuotosios uždelstosios fluorescencijos (TADF) spinduoliais generuojami eksitonai buvo efektyviai perduodami po skylės-elektrono rekombinacijos, o dėl didesnio rezonansinės energijos perdavimo pagamintuose prietaisuose su dviem TADF emiteriais užfiksuotas beveik du kartus didesnis *EQE* – 9,5%.

    2.3. Prietaisas skleidė aukštos kokybės baltą emisiją, kurios CRI – 80, CIE xy koordinatės (0,32, 0,31) ir koreliuojamąja spalvų temperatūra – 4490 K, o *EQE* – 7,1%.

3. Efektyvūs mėlynos spalvos OLED-ai sukurti naudojant naujus daugiakarbazolinius mėlynos spalvos TADF emiterius su dviem nepanašiomis akceptorinėmis grupėmis, akceptoriniu benznitrilo fragmentu kaip bendruoju

akceptoriumi ir skirtingomis papildomais konjuguotais akceptoriniais fragmentais kiekviename junginyje.

3.1. Diferencinės skenuojamosios kalorimetrijos matavimai parodė, kad visi susintetinti TADF emiteriai – amorfiniai junginiai, o termogravimetrinės analizės metu nustatytos medžiagų 5% masės nuostolių temperatūros buvo nuo 363 iki 457 °C.

3.2. Užfiksuotos labai skirtingos naujų tirtų junginių TADF savybės ir sukinio apsisukimo galimybės, kai RISC greičiai buvo nuo $4,7{\times}10^4$ iki $2,32{\times}10^6$ s^{-1}, taip pat junginių degazuotuose praskiestuose tirpaluose toluene fotoliuminescencijos kvantinio našumo (*PLQY*) vertės buvo nuo 55 iki 82 %.

3.3. Papildomų akceptorinių fragmentų ir akceptorių asimetrijos poveikis buvo akivaizdus pagamintų prietaisų su tirtais TADF junginiais emisiniuose sluoksniuose elektroliuminescencinėms charakteristikoms. Pagamintų nelegiruotų prietaisų EQE svyravo nuo 2 iki 7,3%, o mCP-legiruotų prietaisų *EQE* svyravo nuo 3,1 iki 11,8%.

3.4. Pagaminti optimizuoti prietaisai, sudaryti su papildomai benznitrililpakeistu junginiu ir su papildomai metil-3-metilbenzoatpakeistu junginiu, pasiekė atitinkamai 18,3 ir 14,1% praktinį EQE_{max}.

4. Kietosios būsenos tirpimo ir konformacijos netvarkos pasekmių minimizavimas nelegiruotuose ir legiruotuose OLED-uose pasiektas įtraukiant kelis efektyvius daugiakarbazolinius TADF junginius su keturiais donoriniais (*tret*-butilkarbazolil) fragmentais bei dviem akceptoriniais fragmentais, prietaisai nuodugniai ištirti ir ištirtas vieno iš akceptorinių fragmentų poveikis naujųjų medžiagų optoelektroninėms savybėms.

4.1. Tirtų junginių jonizacijos potencialų vertės buvo beveik vienodos – nuo 5,61 iki 5,72 eV. Jų 5% masės nuostolių temperatūra buvo nuo 433 iki 462 °C, o tai rodo puikų šių daugiakarbazolinių junginių terminį stabilumą.

4.2. Ištirtos medžiagos pasižymėjo gana efektyviu mėlynos spalvos TADF su $1{\times}10^6$ s^{-1} RISC greičiu, taip pat buvo užfiksuotas didelis junginio su papildomu akceptoriniu pirimidino fragmentu (**10**) grynojo sluoksnio *PLQY* – 76%.

4.3. Atliekant laikinės skyros emisijos matavimus, junginys su papildomu akceptoriniu pirimidino fragmentu (**10**) pasižymėjo mažiausiu 0,06 eV poslinkiu, o junginys be papildomo akceptorinio fragmento (**12**) pasižymėjo didžiausiu poslinkiu ir dėl to didžiausia konformacijos netvarka.

4.4. Dėl labai mažos netvarkos ir tirpinimo efektų junginių sluoksniuose užfiksuoti maždaug vienodi mCBP-legiruotų ir nelegiruotų prietaisų elektroliuminescenciniai parametrai (įskaitant EL spektrus).

4.5. Didžiausias maksimalus *EQE* – 15,9%, didžiausias *PE* – 24,1 lm W^{-1} ir didžiausias *CE* – 42,6 cd A^{-1} užfiksuoti viename iš pagamintų prietaisų su

aukštos kokybės dangaus mėlynos spalvos EL spektru, kurio maksimumas buvo ties 477 nm.

5. REFERENCES

1   Bronstein, H. *et al.* The role of chemical design in the performance of organic semiconductors. *Nature Reviews Chemistry 2020 4:2* [interactive]. 2020, vol. 4 (2), 66–77. Access via the Internet: <https://doi.org/10.1021/10.1038/s41570-019-0152-9>.

2   Reineke, S. *et al.* White organic light-emitting diodes with fluorescent tube efficiency. *Nature* [interactive]. 2009, vol. 459. Access via the Internet: <https://doi.org/10.1021/10.1038/nature08003>.

3   Bré das, J.L. *et al.* Organic semiconductors: A theoretical characterization of the basic parameters governing charge transport. *PNAS Nexus* [interactive]. 2002, vol. 30 (9), 5804–5809. Access via the Internet: <https://doi.org/10.1021/10.1073/pnas.09214339>.

4   Nayak, P.K. *et al.* Photovoltaic solar cell technologies: analysing the state of the art. *Nature Reviews Materials 2019 4:4* [interactive]. 2019, vol. 4 (4), 269–285. Access via the Internet: <https://doi.org/10.1021/10.1038/s41578-019-0097-0>.

5   Lüssem, B. *et al.* Doped Organic Transistors. *Chemical Reviews* [interactive]. 2016, vol. 116 (22), 13714–13751. Access via the Internet: <https://doi.org/10.1021/10.1021/acs.chemrev.6b00329>.

6   Abbel, R. *et al.* Toward high volume solution based roll-to-roll processing of OLEDs. *Journal of Materials Research* [interactive]. 2017, vol. 32 (12), 2219–2229. Access via the Internet: <https://doi.org/10.1021/10.1557/jmr.2017.204>.

7   Teichler, A. *et al.* Inkjet printing of organic electronics-comparison of deposition techniques and state-of-the-art developments. *Journal of Materials Chemistry C* [interactive]. 2012, vol. 1, 1910–1925. Access via the Internet: <https://doi.org/10.1021/10.1039/c2tc00255h>.

8   Tang, C.W. *et al.* Organic electroluminescent diodes. *Applied Physics Letters* [interactive]. 1987, vol. 51 (12), 913–915. Access via the Internet: <https://doi.org/10.1021/10.1063/1.98799>.

9   Yang, X. *et al.* Organic semiconductors: commercialization and market. *Journal of Semiconductors,* [interactive]. 2021, vol. 42 (9), 090201-090201–3. Access via the Internet: <https://doi.org/10.1021/10.1088/1674-4926/42/9/090201>.

10 Dong, H. *et al.* Low-temperature vacuum deposition of green phosphorescent OLED devices using close-space sublimation of spirobifluorene hosts. *Journal of Luminescence* [interactive]. 2022, vol. 252, 119360. Access via the Internet: <https://doi.org/10.1021/10.1016/J.JLUMIN.2022.119360>.

11 Koden, M. OLED Display and Lighting. *OLED Display and Lighting* [interactive]. 2016, 1–222. Access via the Internet: <https://doi.org/10.1021/10.1002/9781119040477>.

12 Tsujimura, T. *OLED display fundamentals and applications*. 2017. Access via the Internet: <https://doi.org/10.1021/10.1002/9781119187493>.

13   Huang, Y. *et al.* Mini-LED, Micro-LED and OLED displays: present status and future perspectives. *Light: Science & Applications* [interactive]. 2020, vol. 9 (1), 1–16. Access via the Internet: <https://doi.org/10.1021/10.1038/s41377-020-0341-9>.

14   Bergström, L. *et al.* Blue LEDs-Filling the world with new light. *The Royal Swedish Academy of Sciences* [interactive]. 2014. Access via the Internet: <https://doi.org/10.1021/https://kva.se>.

15   Mahon, J.K. History and Status of Organic Light Emitting Device (OLED) Technology for Vehicular Applications. *The Society for Information Display* [interactive]. 2001, vol. 32 (1), 22–25. Access via the Internet: <https://doi.org/10.1021/10.1889/1.1831838>.

16   Pode, R. Organic light emitting diode devices: An energy efficient solid state lighting for applications. *Renewable and Sustainable Energy Reviews* [interactive]. 2020, vol. 133, 110043. Access via the Internet: <https://doi.org/10.1021/10.1016/J.RSER.2020.110043>.

17   Park, J.S. *et al.* Thin film encapsulation for flexible AM-OLED: a review. *Semiconductor Science and Technology* [interactive]. 2011, vol. 26 (3), 034001. Access via the Internet: <https://doi.org/10.1021/10.1088/0268-1242/26/3/034001>.

18   Sugimoto, A. *et al.* Flexible OLED displays using plastic substrates. *IEEE Journal on Selected Topics in Quantum Electronics* [interactive]. 2004, vol. 10 (1), 107–114. Access via the Internet: <https://doi.org/10.1021/10.1109/JSTQE.2004.824112>.

19   Kiprof, P. *et al.* Systematic color tuning of a family of luminescent azole -based organoboron compounds suitable for OLED applications. *Dalton Transactions* [interactive]. 2013, vol. 42 (42), 15120–15132. Access via the Internet: <https://doi.org/10.1021/10.1039/C3DT51853A>.

20   Mo, H.W. *et al.* Color Tuning of Avobenzone Boron Difluoride as an Emitter to Achieve Full-Color Emission. *Advanced Functional Materials* [interactive]. 2016, vol. 26 (37), 6703–6710. Access via the Internet: <https://doi.org/10.1021/10.1002/ADFM.201601257>.

21   Vasilopoulou, M. *et al.* High efficiency blue organic light-emitting diodes with below-bandgap electroluminescence. *Nature Communications* [interactive]. 2021, vol. 12, 4868. Access via the Internet: <https://doi.org/10.1021/10.1038/s41467-021-25135-z>.

22   Lee, Y.H. *et al.* Achieving over 36% EQE in blue OLEDs using rigid TADF emitters based on spiro-donor and spiro-B-heterotriangulene acceptors. *Chemical Engineering Journal* [interactive]. 2023, vol. 452, 139387. Access via the Internet: <https://doi.org/10.1021/10.1016/J.CEJ.2022.139387>.

23   He, G. *et al.* White stacked OLED with 38 lm/W and 100,000-hour lifetime at 1000 cd/m2 for display and lighting applications. *Journal of the Society for Information Display* [interactive]. 2009, vol. 17 (2), 159–165. Access via the Internet: <https://doi.org/10.1021/10.1889/JSID17.2.159>.

24   Scholz, S. *et al.* Degradation mechanisms and reactions in organic light-emitting devices. *Chemical Reviews* [interactive]. 2015, vol. 115 (16), 8449–8503. Access via

the Internet: <https://doi.org/10.1021/https://doi.org/10.1021/cr400704v>.

25   Murawski, C. *et al.* Efficiency Roll-Off in Organic Light-Emitting Diodes 1. Introduction. *Adv. Mater* [interactive]. 2013, vol. 25, 6801–6827. Access via the Internet: <https://doi.org/10.1021/10.1002/adma.201301603>.

26   Sasabe, H. *et al.* Development of high performance OLEDs for general lighting. *Journal of Materials Chemistry C* [interactive]. 2013, vol. 1 (9), 1699–1707. Access via the Internet: <https://doi.org/10.1021/10.1039/C2TC00584K>.

27   Kanno, H. *et al.* Development of OLED with high stability and luminance efficiency by co-doping methods for full color displays. *IEEE Journal on Selected Topics in Quantum Electronics* [interactive]. 2004, vol. 10 (1), 30–36. Access via the Internet: <https://doi.org/10.1021/10.1109/JSTQE.2004.824076>.

28   Geffroy, B. *et al.* Organic light-emitting diode (OLED) technology: materials, devices and display technologies. *Polymer International* [interactive]. 2006, vol. 55 (6), 572–582. Access via the Internet: <https://doi.org/10.1021/10.1002/PI.1974>.

29   *Parameter values for ultra-high definition television systems for production and international programme exchange*. *BT Series Broadcasting service (television)* [interactive]. 2015. Available from: http://www.itu.int/ITU-R/go/patents/en

30   Mahoro, G.U. *et al.* Recent Advances in Solid-State Lighting Devices Using Transition Metal Complexes Exhibiting Thermally Activated Delayed Fluorescent Emission Mechanism. *Advanced Optical Materials* [interactive]. 2020, vol. 8 (16), 2000260. Access via the Internet: <https://doi.org/10.1021/10.1002/ADOM.202000260>.

31   Kang, S.W. *et al.* Green phosphorescent organic light-emitting diode exhibiting highest external quantum efficiency with ultra-thin undoped emission layer. *Scientific Reports* [interactive]. 2021, vol. 11 (1), 1–8. Access via the Internet: <https://doi.org/10.1021/10.1038/s41598-021-86333-9>.

32   Xia, D. *et al.* Self-Host Blue-Emitting Iridium Dendrimer with Carbazole Dendrons: Nondoped Phosphorescent Organic Light-Emitting Diodes. *Angewandte Chemie International Edition* [interactive]. 2014, vol. 53 (4), 1048–1052. Access via the Internet: <https://doi.org/10.1021/10.1002/ANIE.201307311>.

33   Cui, R. *et al.* Highly efficient green phosphorescent organic electroluminescent devices with a terbium complex as the sensitizer. *Dyes and Pigments* [interactive]. 2017, vol. 136, 361–367. Access via the Internet: <https://doi.org/10.1021/10.1016/J.DYEPIG.2016.08.068>.

34   Xiao, L. *et al.* Nearly 100% Internal Quantum Efficiency in an Organic Blue-Light Electrophosphorescent Device Using a Weak Electron Transporting Material with a Wide Energy Gap. *Advanced Materials* [interactive]. 2009, vol. 21 (12), 1271–1274. Access via the Internet: <https://doi.org/10.1021/10.1002/ADMA.200802034>.

35   Adachi, C. *et al.* Nearly 100% internal phosphorescence efficiency in an organic light-emitting device. *Journal of Applied Physics* [interactive]. 2001, vol. 90, 5048–5051. Access via the Internet: <https://doi.org/10.1021/10.1063/1.1409582>.

36 Baldo, M.A. *et al.* Very high-efficiency green organic light-emitting devices based on electrophosphorescence. *Applied Physics Letters* [interactive]. 1999, vol. 75 (1), 4–6. Access via the Internet: <https://doi.org/10.1021/10.1063/1.124258>.

37 O'Brien, D.F. *et al.* Improved energy transfer in electrophosphorescent devices. *Applied Physics Letters* [interactive]. 1999, vol. 74 (3), 442–444. Access via the Internet: <https://doi.org/10.1021/10.1063/1.123055>.

38 Song, W. *et al.* Degradation Mechanism and Lifetime Improvement Strategy for Blue Phosphorescent Organic Light-Emitting Diodes. *Advanced Optical Materials* [interactive]. 2017, vol. 5 (9), 1600901. Access via the Internet: <https://doi.org/10.1021/10.1002/ADOM.201600901>.

39 Sun, J. *et al.* Exceptionally stable blue phosphorescent organic light-emitting diodes. *Nature Photonics* [interactive]. 2022, vol. 16 (3), 212–218. Access via the Internet: <https://doi.org/10.1021/10.1038/s41566-022-00958-4>.

40 Lin, C.J. *et al.* High Energy Gap OLED Host Materials for Green and Blue PHOLED Materials. *Journal of Display Technology* [interactive]. 2009, vol. 5 (6), 236–240. Access via the Internet: <https://doi.org/10.1021/10.1109/JDT.2008.2007750>.

41 Uoyama, H. *et al.* Highly efficient organic light-emitting diodes from delayed fluorescence. *Nature* [interactive]. 2012, (7428), 2012–2024. Access via the Internet: <https://doi.org/10.1021/10.1038/nature11687>.

42 Endo, A. *et al.* Efficient up-conversion of triplet excitons into a singlet state and its application for organic light emitting diodes. *Chinese Journal of Chemical Physics* [interactive]. 2011, vol. 98, 83302. Access via the Internet: <https://doi.org/10.1021/10.1063/1.3558906>.

43 Parker, C.A. *et al.* Triplet-singlet emission in fluid solutions. Phosphorescence of eosin. *Transactions of the Faraday Society* [interactive]. 1961, vol. 57 (0), 1894–1904. Access via the Internet: <https://doi.org/10.1021/10.1039/TF9615701894>.

44 Shi, Y.Z. *et al.* Recent progress in thermally activated delayed fluorescence emitters for nondoped organic light-emitting diodes. *Chemical Science* [interactive]. 2022, vol. 13 (13), 3625–3651. Access via the Internet: <https://doi.org/10.1021/10.1039/D1SC07180G>.

45 Bryden, M.A. *et al.* Organic thermally activated delayed fluorescence (TADF) compounds used in photocatalysis. *Chemical Society Reviews* [interactive]. 2021, vol. 50 (13), 7587–7680. Access via the Internet: <https://doi.org/10.1021/10.1039/D1CS00198A>.

46 Skhirtladze, L. *et al.* 1,4-Bis(trifluoromethyl)benzene as a new acceptor for the design and synthesis of emitters exhibiting efficient thermally activated delayed fluorescence and electroluminescence: experimental and computational guidance. *Journal of Materials Chemistry C* [interactive]. 2022, vol. 10 (12), 4929–4940. Access via the Internet: <https://doi.org/10.1021/10.1039/D1TC05420A>.

47 Adachi, C. Third-generation organic electroluminescence materials. *Japanese Journal of Applied Physics* [interactive]. 2014, vol. 53, 060101. Access via the

Internet: <https://doi.org/10.1021/10.7567/JJAP.53.060101>.

48   Volz, D. Review of organic light-emitting diodes with thermally activated delayed fluorescence emitters for energy-efficient sustainable light sources and displays. *Journal of Photonics for Energy* [interactive]. 2016, vol. 6 (2), 020901. Access via the Internet: <https://doi.org/10.1021/10.1117/1.JPE.6.020901>.

49   Nayak, D. *et al.* A survey of the structure, fabrication, and characterization of advanced organic light emitting diodes. *Microelectronics Reliability* [interactive]. 2023, vol. 144, 114959. Access via the Internet: <https://doi.org/10.1021/10.1016/j.microrel.2023.114959>.

50   Mullemwar, S.Y. *et al.* OLEDs: Emerging technology trends and designs. *Phosphor Handbook* [interactive]. 2023, 307–328. Access via the Internet: <https://doi.org/10.1021/10.1016/B978-0-323-90539-8.00005-X>.

51   Kamtekar, K.T. *et al.* Recent Advances in White Organic Light-Emitting Materials and Devices (WOLEDs). *Advanced Materials* [interactive]. 2010, vol. 22, 572–582. Access via the Internet: <https://doi.org/10.1021/10.1002/adma.200902148>.

52   Zeng, X.Y. *et al.* Solution-processed OLEDs for printing displays. *Materials Chemistry Frontiers* [interactive]. 2023, vol. 7 (7), 1166–1196. Access via the Internet: <https://doi.org/10.1021/10.1039/D2QM01241C>.

53   Duan, L. *et al.* Strategies to Design Bipolar Small Molecules for OLEDs: Donor-Acceptor Structure and Non-Donor-Acceptor Structure. *Advanced Materials* [interactive]. 2011, vol. 23 (9), 1137–1144. Access via the Internet: <https://doi.org/10.1021/10.1002/ADMA.201003816>.

54   Panigrahi, K. *et al.* Challenges and Strategies to Design Phosphors for Future White Light Emitting Diodes. *Journal of Physical Chemistry C* [interactive]. 2022, vol. 126 (20), 8553–8564. Access via the Internet: <https://doi.org/10.1021/10.1021/acs.jpcc.2c01679>.

55   Stanitska, M. *et al.* Exciplex-Forming Systems of Physically Mixed and Covalently Bonded Benzoyl-1 H-1,2,3-Triazole and Carbazole Moieties for Solution-Processed White OLEDs. *Journal of Organic Chemistry* [interactive]. 2022, vol. 87 (6), 4040–4050. Access via the Internet: <https://doi.org/10.1021/10.1021/acs.joc.1c02784>.

56   Mahmoudi, M. *et al.* Exciplex-forming systems with extremely high RISC rates exceeding 107 s−1 for oxygen probing and white hybrid OLEDs. *Journal of Materials Research and Technology* [interactive]. 2021, vol. 10, 711–721. Access via the Internet: <https://doi.org/10.1021/10.1016/J.JMRT.2020.12.058>.

57   Zhao, X. *et al.* Room-Temperature Observation for Reverse Intersystem Crossing in Exciplex-Based OLEDs with Balanced Charge Injection. *ACS Applied Electronic Materials* [interactive]. 2021, vol. 2021, 3043. Access via the Internet: <https://doi.org/10.1021/10.1021/acsaelm.1c00259>.

58   Hisahiro Sasabe, C. *et al.* 3,3′-Bicarbazole-Based Host Materials for High-Efficiency Blue Phosphorescent OLEDs with Extremely Low Driving Voltage. *Advanced Materials* [interactive]. 2012, vol. 24 (24), 3212–3217. Access via the Internet: <https://doi.org/10.1021/10.1002/ADMA.201200848>.

70

59   Li, J. *et al.* Decomposing or subliming? An investigation of thermal behavior of l-leucine. *Thermochimica Acta* [interactive]. 2006, vol. 447 (2). Access via the Internet: <https://doi.org/10.1021/10.1016/j.tca.2006.05.004>.

60   Bredas, J.L. Mind the gap! *Materials Horizons* [interactive]. 2013, vol. 1 (1), 17–19. Access via the Internet: <https://doi.org/10.1021/10.1039/C3MH00098B>.

61   Jiang, X. *et al.* Trifluoromethylthiolation, Trifluoromethylation, and Arylation Reactions of Difluoro Enol Silyl Ethers. *Journal of Organic Chemistry* [interactive]. 2020, vol. 85 (13), 8311–8319. Access via the Internet: <https://doi.org/10.1021/10.1021/acs.joc.0c01030>.

62   Ivaniuk, K. *et al.* Highly luminous sky-blue organic light-emitting diodes based on the bis[(1,2)(5,6)]indoloanthracene emissive layer. *Journal of Physical Chemistry C* [interactive]. 2016, vol. 120 (11), 6206–6217. Access via the Internet: <https://doi.org/10.1021/10.1021/acs.jpcc.6b00696>.

63   Lin, T.C. *et al.* Probe exciplex structure of highly efficient thermally activated delayed fluorescence organic light emitting diodes. *Nature Communications* [interactive]. 2018, vol. 9 (1), 3111–3111. Access via the Internet: <https://doi.org/10.1021/10.1038/S41467-018-05527-4>.

64   Sarma, M. *et al.* Exciplex: An Intermolecular Charge-Transfer Approach for TADF. *ACS Applied Materials and Interfaces* [interactive]. 2018, vol. 10 (23), 19279–19304. Access via the Internet: <https://doi.org/10.1021/10.1021/acsami.7b18318>.

65   Lee, J.H. *et al.* Blue organic light-emitting diodes: current status, challenges, and future outlook. *Journal of Materials Chemistry C* [interactive]. 2019, vol. 7 (20), 5874–5888. Access via the Internet: <https://doi.org/10.1021/10.1039/C9TC00204A>.

66   Galievsky, V.A. *et al.* Ultrafast Intramolecular Charge Transfer with N-(4-Cyanophenyl)carbazole. Evidence for a LE Precursor and Dual LE + ICT Fluorescence. *Journal of Physical Chemistry A* [interactive]. 2010, vol. 114 (48), 12622–12638. Access via the Internet: <https://doi.org/10.1021/10.1021/jp1070506>.

67   Rettig, W. *et al.* On twisted intramolecular charge transfer (TICT) states in N-aryl carbazoles. *Chemical Physics Letters* [interactive]. 1982, vol. 87 (3), 229–234. Access via the Internet: <https://doi.org/10.1021/10.1016/0009-2614(82)83131-X>.

68   Bunzmann, N. *et al.* Optically and electrically excited intermediate electronic states in donor:acceptor based OLEDs †. *1126 | Mater. Horiz* [interactive]. 2020, vol. 7, 1126. Access via the Internet: <https://doi.org/10.1021/10.1039/c9mh01475f>.

69   Kim, K.-H. *et al.* Boosting Triplet Harvest by Reducing Nonradiative Transition of Exciplex toward Fluorescent Organic Light-Emitting Diodes with 100% Internal Quantum Efficiency. *Chem. Mater* [interactive]. 2016, vol. 28 (6), 1936–1941. Access via the Internet: <https://doi.org/10.1021/10.1021/acs.chemmater.6b00478>.

70   Chapran, M. *et al.* Realizing 20% External Quantum Efficiency in Electroluminescence with Efficient Thermally Activated Delayed Fluorescence from an Exciplex. *ACS Applied Materials and Interfaces* [interactive]. 2019, vol. 11 (14),

13460–13471. Access via the Internet: <https://doi.org/10.1021/10.1021/acsami.8b18284>.

71   Duan, L. *et al.* Development of Red Exciplex for Efficient OLEDs by Employing a Phosphor as a Component. *Frontiers in Chemistry | www.frontiersin.org* [interactive]. 2019, vol. 1, 16. Access via the Internet: <https://doi.org/10.1021/10.3389/fchem.2019.00016>.

72   Nikolaenko, A.E. *et al.* Thermally Activated Delayed Fluorescence in Polymers: A New Route toward Highly Efficient Solution Processable OLEDs. *Advanced Materials* [interactive]. 2015, vol. 27 (44), 7236–7240. Access via the Internet: <https://doi.org/10.1021/10.1002/ADMA.201501090>.

73   Yamazaki, M. Industrialization and application development of cyclo-olefin polymer. *Journal of Molecular Catalysis A: Chemical* [interactive]. 2004, vol. 213 (1), 81–87. Access via the Internet: <https://doi.org/10.1021/10.1016/J.MOLCATA.2003.10.058>.

74   Wu, Y.C. *et al.* Improved oxygen optical sensing performance from Re(I) complex doped MCM-41 composite samples by incorporating oxadiazole ring into diamine ligand: Synthesis, characterization and sensing response. *Sensors and Actuators B: Chemical* [interactive]. 2017, vol. 244, 1113–1120. Access via the Internet: <https://doi.org/10.1021/10.1016/J.SNB.2017.01.128>.

75   Carraway, E.R. *et al.* Photophysics and Photochemistry of Oxygen Sensors Based on Luminescent Transition-Metal Complexes. *Analytical Chemistry* [interactive]. 1991, vol. 63 (4), 337–342. Access via the Internet: <https://doi.org/10.1021/10.1021/ac00004a007>.

76   Sekine, C. *et al.* Recent progress of high performance polymer OLED and OPV materials for organic printed electronics. *Science and Technology of Advanced Materials* [interactive]. 2014, vol. 15 (3), 034203. Access via the Internet: <https://doi.org/10.1021/10.1088/1468-6996/15/3/034203>.

77   Su, Y.J. *et al.* Highly efficient red electrophosphorescent devices based on iridium isoquinoline complexes: Remarkable external quantum efficiency over a wide range of current. *Advanced Materials* [interactive]. 2003, vol. 15 (11), 884–888. Access via the Internet: <https://doi.org/10.1021/10.1002/ADMA.200304630>.

78   Arias, A.C. *et al.* Materials and Applications for Large Area Electronics: Solution-Based Approaches. *Chemical Reviews* [interactive]. 2010, vol. 110 (1), 3–24. Access via the Internet: <https://doi.org/10.1021/10.1021/cr900150b>.

79   Sarma, M. *et al.* Exciplexes in OLEDs: Principles and promises. *Materials Science and Engineering: R: Reports* [interactive]. 2022, vol. 150, 100689. Access via the Internet: <https://doi.org/10.1021/10.1016/J.MSER.2022.100689>.

80   Giebink, N.C. *et al.* Intrinsic luminance loss in phosphorescent small-molecule organic light emitting devices due to bimolecular annihilation reactions. *Journal of Applied Physics* [interactive]. 2008, vol. 103 (4), 044509. Access via the Internet: <https://doi.org/10.1021/10.1063/1.2884530>.

81   Jou, J.H. *et al.* High-efficiency, very-high color rendering white organic light-

emitting diode with a high triplet interlayer. *Journal of Materials Chemistry* [interactive]. 2011, vol. 21 (46), 18523–18526. Access via the Internet: <https://doi.org/10.1021/10.1039/C1JM13975D>.

82   Miao, Y. *et al.* High-efficiency/CRI/color stability warm white organic light-emitting diodes by incorporating ultrathin phosphorescence layers in a blue fluorescence layer. *Nanophotonics* [interactive]. 2018, vol. 7 (1), 295–304. Access via the Internet: <https://doi.org/10.1021/10.1515/nanoph-2017-0021>.

83   Mahmoudi, M. *et al.* Bis(N-naphthyl-N-phenylamino)benzophenones as exciton-modulating materials for white TADF OLEDs with separated charge and exciton recombination zones. *Dyes and Pigments* [interactive]. 2022, vol. 197. Access via the Internet: <https://doi.org/10.1021/10.1016/J.DYEPIG.2021.109868>.

84   Sun, Y. *et al.* Management of singlet and triplet excitons for efficient white organic light-emitting devices. *Nature 2006 440:7086* [interactive]. 2006, vol. 440 (7086), 908–912. Access via the Internet: <https://doi.org/10.1021/10.1038/nature04645>.

85   Liu, B.-Q. *et al.* Color-stable, reduced efficiency roll-off hybrid white organic light emitting diodes with ultra high brightness. *Chinese Physics B* [interactive]. 2013, vol. 22 (7), 077303. Access via the Internet: <https://doi.org/10.1021/10.1088/1674-1056/22/7/077303>.

86   Zhao, F. *et al.* Spatial exciton allocation strategy with reduced energy loss for high-efficiency fluorescent/ phosphorescent hybrid white organic light-emitting diodes. *Materials Horizons* [interactive]. 2017, vol. 4, 641–648. Access via the Internet: <https://doi.org/10.1021/10.1039/c7mh00131b>.

87   Duan, L. *et al.* Controlling the Recombination Zone of White Organic Light-Emitting Diodes with Extremely Long Lifetimes. *Advanced Functional Materials* [interactive]. 2011, vol. 21 (18), 3540–3545. Access via the Internet: <https://doi.org/10.1021/10.1002/ADFM.201100943>.

88   Li, X.L. *et al.* High-Efficiency WOLEDs with High Color-Rendering Index based on a Chromaticity-Adjustable Yellow Thermally Activated Delayed Fluorescence Emitter. *Advanced Materials* [interactive]. 2016, vol. 28 (23), 4614–4619. Access via the Internet: <https://doi.org/10.1021/10.1002/ADMA.201505963>.

89   Han, C. *et al.* Host engineering based on multiple phosphorylation for efficient blue and white TADF organic light-emitting diodes. *Chemical Engineering Journal* [interactive]. 2021, vol. 405, 126986. Access via the Internet: <https://doi.org/10.1021/10.1016/J.CEJ.2020.126986>.

90   Zhang, J. *et al.* High-Power-Efficiency White Thermally Activated Delayed Fluorescence Diodes Based on Selectively Optimized Intermolecular Interactions. *Advanced Functional Materials* [interactive]. 2020, vol. 30 (45), 2005165. Access via the Internet: <https://doi.org/10.1021/10.1002/adfm.202005165>.

91   Huang, R. *et al.* Balancing charge-transfer strength and triplet states for deep-blue thermally activated delayed fluorescence with an unconventional electron rich dibenzothiophene acceptor. *Journal of Materials Chemistry C* [interactive]. 2019, vol. 7 (42), 13224–13234. Access via the Internet: <https://doi.org/10.1021/10.1039/C9TC02175B>.

92   Song, J. *et al.* Rational design of high efficiency green to deep red/near-infrared emitting materials based on isomeric donor-acceptor chromophores. *J. Mater. Chem. C* [interactive]. 2019, vol. 7, 1887. Access via the Internet: <https://doi.org/10.1021/10.1039/c8tc05383a>.

93   Chen, Y. *et al.* Aggregation-induced emission: fundamental understanding and future developments. *Materials Horizons* [interactive]. 2019, vol. 6, 428–433. Access via the Internet: <https://doi.org/10.1021/10.1039/c8mh01331d>.

94   Yang, Z. *et al.* High-Tg carbazole derivatives as a new class of aggregation-induced emission enhancement materials. *Journal of Materials Chemistry* [interactive]. 2010, vol. 20 (35), 7352–7359. Access via the Internet: <https://doi.org/10.1021/10.1039/C0JM00712A>.

95   Zhang, X. *et al.* End-group effects of piezofluorochromic aggregation-induced enhanced emission compounds containing distyrylanthracene. *Journal of Materials Chemistry* [interactive]. 2012, vol. 22 (35), 18505–18513. Access via the Internet: <https://doi.org/10.1021/10.1039/C2JM33140C>.

96   Climent, V. *et al.* Cyclic Voltammetry. *Encyclopedia of Interfacial Chemistry: Surface Science and Electrochemistry* [interactive]. 2018, 48–74. Access via the Internet: <https://doi.org/10.1021/10.1016/B978-0-12-409547-2.10764-4>.

97   Sasaki, T. *et al.* Unravelling the electron injection/transport mechanism in organic light-emitting diodes. *Nature Communications 2021 12:1* [interactive]. 2021, vol. 12 (1), 1–8. Access via the Internet: <https://doi.org/10.1021/10.1038/s41467-021-23067-2>.

98   Bassler, H. Charge Transport in Disordered Organic Photoconductors A Monte Carlo Simulation Study. *physica status solidi (b)* [interactive]. 1993, vol. 175, 15–56. Access via the Internet: <https://doi.org/10.1021/10.1002/pssb.2221750102>.

99   Yokoyama, M. *et al.* Trifluoromethane modification of thermally activated delayed fluorescence molecules for high-efficiency blue organic light-emitting diodes. *Chem. Commun* [interactive]. 2018, vol. 54, 8261–8264. Access via the Internet: <https://doi.org/10.1021/10.1039/c8cc03425g>.

100   Meredith, P. *et al.* Electronic and optoelectronic materials and devices inspired by nature. *Reports on Progress in Physics* [interactive]. 2013, vol. 76 (3), 034501. Access via the Internet: <https://doi.org/10.1021/10.1088/0034-4885/76/3/034501>.

101   Mahmoudi, M. *et al.* Tuning of spin-flip efficiency of blue emitting multicarbazolyl-substituted benzonitriles by exploitation of the different additional electron accepting moieties. *Chemical Engineering Journal* [interactive]. 2021, vol. 423. Access via the Internet: <https://doi.org/10.1021/10.1016/J.CEJ.2021.130236>.

102   Fleetham, T.B. *et al.* Tetradentate Pt(II) Complexes with 6-Membered Chelate Rings: A New Route for Stable and Efficient Blue Organic Light Emitting Diodes. *Chemistry of Materials* [interactive]. 2016, vol. 28 (10), 3276–3282. Access via the Internet: <https://doi.org/10.1021/10.1021/acs.chemmater.5b04957>.

103   Zhang, D. *et al.* Efficient and Stable Deep-Blue Fluorescent Organic Light-Emitting Diodes Employing a Sensitizer with Fast Triplet Upconversion. *Advanced Materials*

[interactive]. 2020, vol. 32 (19), 1908355. Access via the Internet:
<https://doi.org/10.1021/10.1002/ADMA.201908355>.

104   Kreiza, G. *et al.* Suppression of benzophenone-induced triplet quenching for
       enhanced TADF performance. *Journal of Materials Chemistry C* [interactive]. 2019,
       vol. 7, 11522. Access via the Internet:
       <https://doi.org/10.1021/10.1039/c9tc02408e>.

105   Zheng, X. *et al.* Achieving 21% External Quantum Efficiency for Nondoped
       Solution-Processed Sky-Blue Thermally Activated Delayed Fluorescence OLEDs by
       Means of Multi-(Donor/Acceptor) Emitter with Through-Space/-Bond Charge
       Transfer. *Advanced Science* [interactive]. 2020, vol. 7 (7), 1902087. Access via the
       Internet: <https://doi.org/10.1021/10.1002/ADVS.201902087>.

106   Jayakumar, J. *et al.* Pyridine-Carbonitrile−Carbazole-Based Delayed Fluorescence
       Materials with Highly Congested Structures and Excellent OLED Performance. *ACS
       Appl. Mater. Interfaces* [interactive]. 2019, vol. 11, 21042–21048. Access via the
       Internet: <https://doi.org/10.1021/10.1021/acsami.9b04664>.

107   Hall, D. *et al.* Substitution Effects on a New Pyridylbenzimidazole Acceptor for
       Thermally Activated Delayed Fluorescence and Their Use in Organic Light-Emitting
       Diodes. *Advanced Optical Materials* [interactive]. 2021, vol. 9 (20). Access via the
       Internet: <https://doi.org/10.1021/10.1002/ADOM.202100846>.

108   Wong, M.Y. *et al.* Purely Organic Thermally Activated Delayed Fluorescence
       Materials for Organic Light-Emitting Diodes. *Advanced Materials* [interactive].
       2017, vol. 29 (22), 1605444. Access via the Internet:
       <https://doi.org/10.1021/10.1002/ADMA.201605444>.

109   Li, B. *et al.* Role of the Intramolecular-Locking Strategy in the Construction of
       Organic Thermally Activated Delayed Fluorescence Emitters with Rotation-
       Restricted Acceptors. *Advanced Optical Materials* [interactive]. 2023, vol. 11 (7),
       2202610. Access via the Internet:
       <https://doi.org/10.1021/10.1002/ADOM.202202610>.

110   Han, C. *et al.* Dipole-Dipole Interaction Management for Efficient Blue Thermally
       Activated Delayed Fluorescence Diodes. *Chem* [interactive]. 2018, vol. 4 (9), 2154–
       2167. Access via the Internet:
       <https://doi.org/10.1021/10.1016/J.CHEMPR.2018.06.005>.

111   Qiao, X. *et al.* Nonlinear optoelectronic processes in organic optoelectronic devices:
       Triplet-triplet annihilation and singlet fission. *Materials Science and Engineering R:
       Reports* [interactive]. 2020, vol. 139. Access via the Internet:
       <https://doi.org/10.1021/10.1016/J.MSER.2019.100519>.

112   Tsuboi, T. *et al.* Spectroscopic and electrical characteristics of highly efficient
       tetraphenylsilane-carbazole organic compound as host material for blue organic light
       emitting diodes. *Organic Electronics* [interactive]. 2009, vol. 10 (7), 1372–1377.
       Access via the Internet: <https://doi.org/10.1021/10.1016/J.ORGEL.2009.07.020>.

113   Chan, C.Y. *et al.* Efficient and stable sky-blue delayed fluorescence organic light-
       emitting diodes with CIEy below 0.4. *Nature Communications 2018 9:1*
       [interactive]. 2018, vol. 9 (1), 1–8. Access via the Internet:

<https://doi.org/10.1021/10.1038/s41467-018-07482-6>.

114 Fu, Y. *et al.* Boosting external quantum efficiency to 38.6% of sky-blue delayed fluorescence molecules by optimizing horizontal dipole orientation. *Science Advances* [interactive]. 2021, vol. 7 (43). Access via the Internet: <https://doi.org/10.1021/10.1126/sciadv.abj2504>.

115 Hladka, I. *et al.* Polymorphism of derivatives of tert-butyl substituted acridan and perfluorobiphenyl as sky-blue OLED emitters exhibiting aggregation induced thermally activated delayed fluorescence. *J. Mater. Chem. C* [interactive]. 2018, vol. 6, 13179. Access via the Internet: <https://doi.org/10.1021/10.1039/c8tc04867c>.

116 Naqvi, B.A. *et al.* What Controls the Orientation of TADF Emitters? *Frontiers in Chemistry* [interactive]. 2020, vol. 8. Access via the Internet: <https://doi.org/10.1021/10.3389/fchem.2020.00750>.

117 Keruckiene, R. *et al.* Power Efficiency Enhancement of Organic Light-Emitting Diodes Due to the Favorable Horizontal Orientation of a Naphthyridine-Based Thermally Activated Delayed Fluorescence Luminophore. *ACS Applied Electronic Materials* [interactive]. 2023, vol. 5 (2), 1013–1023. Access via the Internet: <https://doi.org/10.1021/10.1021/acsaelm.2c01529>.

118 Mahmoudi, M. *et al.* Ornamenting of Blue Thermally Activated Delayed Fluorescence Emitters by Anchor Groups for the Minimization of Solid-State Solvation and Conformation Disorder Corollaries in Non-Doped and Doped Organic Light-Emitting Diodes. *ACS Applied Materials & Interfaces* [interactive]. 2022, vol. 14, 40172. Access via the Internet: <https://doi.org/10.1021/10.1021/acsami.2c12475>.

119 Macionis, S. *et al.* Does Through-Space Charge Transfer in Bipolar Hosts Affect the Efficiency of Blue OLEDs? *Advanced Optical Materials* [interactive]. 2021, vol. 9 (7), 2002227. Access via the Internet: <https://doi.org/10.1021/10.1002/ADOM.202002227>.

120 Gudeika, D. *et al.* Oxygen sensing and OLED applications of di-tert-butyl-dimethylacridinyl disubstituted oxygafluorene exhibiting long-lived deep-blue delayed fluorescence. *Journal of Materials Chemistry C* [interactive]. 2020, vol. 8 (28), 9632–9638. Access via the Internet: <https://doi.org/10.1021/10.1039/D0TC01648A>.

121 Divac, V.M. *et al.* Solvent effects on the absorption and fluorescence spectra of Zaleplon: Determination of ground and excited state dipole moments. *Spectrochimica Acta Part A: Molecular and Biomolecular Spectroscopy* [interactive]. 2019, vol. 212, 356–362. Access via the Internet: <https://doi.org/10.1021/10.1016/J.SAA.2019.01.023>.

122 Chen, D.-G. *et al.* Optically Triggered Planarization of Boryl-Substituted Phenoxazine: Another Horizon of TADF Molecules and High-Performance OLEDs. 2018. Access via the Internet: <https://doi.org/10.1021/10.1021/acsami.8b00053>.

123 Rybauskaite-Kaminskiene, G. *et al.* Aggregation-EnhancedE mission and Thermally ActivatedD elayed Fluorescence of Derivativeso f9-Phenyl-9H-Carbazole:E ffectso f Methoxyand tert-Butyl Substituents. *Chemistry - A European Journal* [interactive].

2018, vol. 24 (38), 9581–9591. Access via the Internet: <https://doi.org/10.1021/10.1002/chem.201800822>.

124 Goushi, K. *et al.* Organic light-emitting diodes employing efficient reverse intersystem crossing for triplet-to-singlet state conversion. *Nature Photonics 2012 6:4* [interactive]. 2012, vol. 6 (4), 253–258. Access via the Internet: <https://doi.org/10.1021/10.1038/nphoton.2012.31>.

125 Tanaka, M. *et al.* Understanding degradation of organic light-emitting diodes from magnetic field effects. *Communications Materials 2020 1:1* [interactive]. 2020, vol. 1 (1), 1–9. Access via the Internet: <https://doi.org/10.1021/10.1038/s43246-020-0019-0>.

126 Kim, M. *et al.* Stable Blue Thermally Activated Delayed Fluorescent Organic Light-Emitting Diodes with Three Times Longer Lifetime than Phosphorescent Organic Light-Emitting Diodes. *Advanced Materials* [interactive]. 2015, vol. 27 (15), 2515–2520. Access via the Internet: <https://doi.org/10.1021/10.1002/adma.201500267>.

127 Kyu Jeon, S. *et al.* Recent Progress of the Lifetime of Organic Light-Emitting Diodes Based on Thermally Activated Delayed Fluorescent Material. *Advanced Materials* [interactive]. 2019, vol. 31 (34), 1803524. Access via the Internet: <https://doi.org/10.1021/10.1002/ADMA.201803524>.

128 Hatakeyama, T. *et al.* Ultrapure Blue Thermally Activated Delayed Fluorescence Molecules: Efficient HOMO–LUMO Separation by the Multiple Resonance Effect. *Advanced Materials* [interactive]. 2016, vol. 28 (14), 2777–2781. Access via the Internet: <https://doi.org/10.1021/10.1002/ADMA.201505491>.

129 Tuč, L. *et al.* On the origin of the inverted singlet-triplet gap of the 5th generation light-emitting molecules. *Phys. Chem. Chem. Phys* [interactive]. 2022, vol. 24, 18713. Access via the Internet: <https://doi.org/10.1021/10.1039/d2cp02364d>.

130 Lee, S. *et al.* The Role of Charge Balance and Excited State Levels on Device Performance of Exciplex-based Phosphorescent Organic Light Emitting Diodes. *Scientific Reports* [interactive]. 2017, vol. 7 (1), 1–9. Access via the Internet: <https://doi.org/10.1021/10.1038/s41598-017-12059-2>.

131 Kang, S. *et al.* Highly efficient deep-blue fluorescence OLEDs with excellent charge balance based on phenanthro[9,10-d]oxazole-anthracene derivatives. *Journal of Materials Chemistry C* [interactive]. 2020, vol. 8 (32), 11168–11176. Access via the Internet: <https://doi.org/10.1021/10.1039/D0TC01811B>.

132 Juška, G. *et al.* Charge carrier transport and recombination in disordered materials. *Lithuanian Journal of Physics* [interactive]. 2016, vol. 56 (3), 182–189. Access via the Internet: <https://doi.org/10.1021/10.3952/PHYSICS.V56I3.3367>.

133 Lee, H. *et al.* Analysis of interrelationship between efficiency and charge transport properties of green TADF organic light-emitting diodes with mixed host by impedance spectroscopy. *Organic Electronics* [interactive]. 2020, vol. 84, 105816. Access via the Internet: <https://doi.org/10.1021/10.1016/J.ORGEL.2020.105816>.

134 Ghasemi, M. *et al.* Effects of the change of isomers on room-temperature phosphorescence, thermally activated delayed fluorescence, and long persistent

luminescence of organic hole-transporting materials with the selective potential for the application in electronic devices and optical sensors of oxygen. *Chemical Engineering Journal* [interactive]. 2023, 145004. Access via the Internet: <https://doi.org/10.1021/10.1016/J.CEJ.2023.145004>.

135   Serevič ius, T. *et al.* Single-exponential solid-state delayed fluorescence decay in TADF compounds with minimized conformational disorder. [no date]. Access via the Internet: <https://doi.org/10.1021/10.1039/d0tc05503d>.

136   Huo, J. *et al.* Molecular engineering of blue diphenylsulfone-based emitter with aggregation-enhanced emission and thermally activated delayed fluorescence characteristics: impairing intermolecular electron-exchange interactions using steric hindrance. *Chemical Engineering Journal* [interactive]. 2023, vol. 452, 138957. Access via the Internet: <https://doi.org/10.1021/10.1016/J.CEJ.2022.138957>.

137   Pautmeier, L. *et al.* Poole-Frenkel behavior of charge transport in organic solids with off-diagonal disorder studied by Monte Carlo simulation. *Synthetic Metals* [interactive]. 1990, vol. 37 (1–3), 271–281. Access via the Internet: <https://doi.org/10.1021/10.1016/0379-6779(90)90158-H>.

138   Ihn, S.G. *et al.* An Alternative Host Material for Long-Lifespan Blue Organic Light-Emitting Diodes Using Thermally Activated Delayed Fluorescence. *Advanced Science* [interactive]. 2017, vol. 4 (8). Access via the Internet: <https://doi.org/10.1021/10.1002/ADVS.201600502>.

139   Han, J. *et al.* Narrowband blue emission with insensitivity to the doping concentration from an oxygen-bridged triarylboron-based TADF emitter: nondoped OLEDs with a high external quantum efficiency up to 21.4%. *Chemical Science* [interactive]. 2022, vol. 13 (12), 3402–3408. Access via the Internet: <https://doi.org/10.1021/10.1039/D2SC00329E>.

140   Bagnich, S.A. *et al.* Triplet energies and excimer formation in meta- and para-linked carbazolebiphenyl matrix materials. *Philosophical transactions. Series A, Mathematical, physical, and engineering sciences* [interactive]. 2015, vol. 373 (2044). Access via the Internet: <https://doi.org/10.1021/10.1098/RSTA.2014.0446>.

141   Godumala, M. *et al.* Recent breakthroughs in thermally activated delayed fluorescence organic light emitting diodes containing non-doped emitting layers. *Journal of Materials Chemistry C* [interactive]. 2019, vol. 7, 2172. Access via the Internet: <https://doi.org/10.1021/10.1039/c8tc06293e>.

142   Tsutsui, T. Progress in electroluminescent devices using molecular thin films. *MRS Bulletin* [interactive]. 1997, vol. 22 (6), 39–45. Access via the Internet: <https://doi.org/10.1021/10.1557/S0883769400033613/METRICS>.

6. CURRICULUM VITAE

Personal information

Name, Surname	**Malek Mahmoudi Sharabiani**
Date of birth:	August 23, 1988
Nationality:	Iranian
Email:	malek.mahmoudi@ktu.lt

Work experience

2020.04–2020.12	Kaunas University of Technology, Junior Researcher
2020.08–2023.09	Kaunas University of Technology, Project Engineer

Education

2019–2024	Kaunas University of Technology PhD studies, Materials Engineering
2011–2014	Shahid Beheshti University, Laser and Plasma Research Institute Master of Photonics
2007–2011	Basic Science University of Damghan Bachelor of Physics

Internships

2022.09–2022.12	Guest researcher at Dresden University of Technology, Dresden, Germany. Research supervisor: Prof. Dr. Sebastian Reineke Heavy metal free emitters for new-generation light "MEGA"
2023.01–2023.04	Guest researcher at Dresden University of Technology, Dresden, Germany. Research supervisor: Prof. Dr. Sebastian Reineke Heavy metal free emitters for new-generation light "MEGA"

Languages

Persian, English, Azerbaijani.

7. LIST OF AUTHOR'S PUBLICATIONS AND CONFERENCES

List of publications on the subject of the thesis

1. **Mahmoudi, Malek**; Keruckas, Jonas; Leitonas, Karolis; Kutsiy, Stepan; Volyniuk, Dmytro; Gražulevičius, Juozas Vidas. Exciplex-forming systems with extremely high RISC rates exceeding 10^7 s^{-1} for oxygen probing and white hybrid OLEDs // *Journal of Materials Research and Technology*. Amsterdam: Elsevier. ISSN: 2238-7854. 2021, vol. 10, p. 711–721. (Web of Science) DOI: 10.1016/j.jmrt.2020.12.058. [IF:6.267; Q1]
2. **Mahmoudi, Malek**; Keruckas, Jonas; Volyniuk, Dmytro; Andrulevičienė, Viktorija; Keruckienė, Rasa; Narbutaitis, Edgaras; Chao, Yu-Chiang; Rutkis, Martins; Grazulevicius, Juozas Vidas. Bis(N-naphthyl-N-phenylamino) benzophenones as exciton-modulating materials for white TADF OLEDs with separated charge and exciton recombination zones // *Dyes and Pigments*. Oxford: Elsevier. ISSN: 0143-7208. 2022, vol. 197, art. no. 109868, p. 1–10. (Web of Science) DOI: 10.1016/j.dyepig.2021.109868. [IF:5.122; Q1]
3. **Mahmoudi, Malek**; Gudeika, Dalius; Volyniuk, Dmytro; Leitonas, Karolis; Butkute, Rita; Danyliv, Iryna; Grazulevicius, Juozas Vidas. Tuning of spin-flip efficiency of blue emitting multicarbazolyl-substituted benzonitriles by exploitation of the different additional electron accepting moieties // *Chemical Engineering Journal*. Amsterdam: Elsevier. ISSN: 1385-8947. 2021, vol. 423, art. no. 130236, p. 1–12. (Web of Science) DOI: 10.1016/j.cej.2021.130236. [IF:16.744; Q1]
4. **Mahmoudi, Malek**; Gudeika, Dalius; Kutsiy, Stepan; Simokaitiene, Jurate; Butkute, Rita; Skhirtladze, Levani; Woon, Kai Lin; Volyniuk, Dmytro; Grazulevicius, Juozas Vidas. Ornamenting of blue thermally activated delayed fluorescence emitters by anchor groups for the minimization of solid-state solvation and conformation disorder corollaries in non-doped and doped organic light-emitting diodes // *ACS Applied Materials & Interfaces*. NW, Washington, DC: American chemical society. ISSN: 1944-8244; 2022, vol. 14, iss. 35, p. 40158–40172. (Web of Science) DOI: 10.1021/acsami.2c12475. [IF:10.383; Q1]

List of other publications

1. **Mahmoudi, Malek**; Urbonas, Ervinas; Volyniuk, Dmytro; Gudeika, Dalius; Dabrovolskas, Kestutis; Simokaitiene, Jurate; Dabuliene, Asta; Keruckiene, Rasa; Leitonas, Karolis; Guzauskas, Matas; Skhirtladze, Levani; Stanitska, Mariia; Grazulevicius, Juozas Vidas. Indolocarbazoles with Sterically Unrestricted Electron-Accepting Anchors Showcasing Aggregation-Induced Thermally Activated Delayed Mechanoluminescence for Host-Free Organic Light-Emitting Diodes // *Molecules*. Basel: MDPI. ISSN: 1420-3049. 2023, vol. 28, iss. 16, art. no. 5999, p. 1–17. (Web of Science) DOI: 10.3390/molecules28165999 [IF: 4.927]
2. Khan, Faizal; **Mahmoudi, Malek**; Volyniuk, Dmytro; Grazulevicius, Juozas Vidas; Misra, Rajneesh. Stimuli-responsive phenothiazine-S,S-dioxide-based nondoped OLEDs with color-changeable electroluminescence // *Journal of*

Physical Chemistry C. NW, Washington, DC : American chemical society. ISSN: 1932-7447; eISSN: 1932-7455. 2022, vol. 126, iss. 37, p. 15573–15586. (Web of Science) DOI: 10.1021/acs.jpcc.2c04123 [IF:4.177; Q1]

3. Khan, Faizal; **Mahmoudi, Malek**; Gupta, Pankaj Kumar; Volyniuk, Dmytro; Grazulevicius, Juozas Vidas; Misra, Rajneesh. Mechanochromic materials based on tetraphenylethylene-substituted phenothiazines: substituent-dependent hypsochromic and bathochromic switching of emission // *Journal of Physical Chemistry C.* Washington, DC: American chemical society. ISSN: 1932-7447; eISSN: 1932-7455; 2023, vol. 127, iss. 3, p. 1643–1654. (Web of Science) DOI: 10.1021/acs.jpcc.2c07010 [IF:4.177; Q1]

List of conferences

1. **Mahmoudi, Malek**; Gudeika, Dalius; Volyniuk, Dmytro; Grazulevicius, Juozas Vidas. Efficient non-doped OLEDs based on multi-carbazole derivatives substituted by different acceptors // Open readings 2020: 63rd international conference for students of physics and natural sciences, March 17–20, Vilnius, Lithuania: abstract book 2020. P1-106, p. 210.
2. **Mahmoudi, Malek**; Keruckas, Jonas; Volyniuk, Dmytro; Simokaitiene, Jurate; Grazulevicius, Juozas Vidas. Solution-processed white organic light-emitting diode based on two emissive layers // ICEPOM -12 conference abstracts: Electronic processes in organic and inorganic materials, June 1–5, 2020, Kamianets-Podilskyi, Ukraine. Kamianets-Podilskyi: Kamianets-Podilskyi National Ivan Ohiienko University. 2020. p. 325.
3. **Mahmoudi, Malek**; Keruckas, Jonas; Volyniuk, Dmytro; Simokaitiene, Jurate; Gražulevičius, Juozas Vidas. Highly efficient green exciplex-based OLEDs utilizing bicarbazole derivatives. ISSN: 1822-7759. Advanced materials and technologies: book of abstracts of 22nd international conference-school, 24–28 August 2020, Palanga, Lithuania. Kaunas: Kaunas University of Technology. 2020, B-P56, p. 82.
4. **Mahmoudi, Malek**; Keruckas, Jonas; Volyniuk, Dmytro; Simokaitiene, Jurate; Helzhynskyy, Igor; Stakhira, Pavlo; Grazulevicius, Juozas Vidas. Developments of hybrid white organic light emitting diodes with high efficiency and colour quality exploiting exciton allocation strategy. 63rd electronic materials conference (EMC 2021), June 23–25, 2021, Columbus, USA. Columbus: Ohio State University. 2021, PS2.15, p. 73.
5. **Mahmoudi, Malek**; Gudeika, Dalius; Volyniuk, Dmytro; Kutsiy, Stepan; Simokaitiene, Jurate; Grazulevicius, Juozas Vidas. Effect of different additional electron accepting moieties on electroluminescent properties of trifluoromethyl-containing multicarbazoles. ISSN: 2669-1930; DOI: 10.5755/e01.2669-1930.2021. Advanced materials and technologies: book of abstracts of 23rd international conference-school, 23–27 August 2021, Palanga, Lithuania. Kaunas: Kaunas University of Technology. 2021, A-P69, p. 100.
6. **Mahmoudi, Malek**; Gudeika, Dalius; Volyniuk, Dmytro; Kutsiy, Stepan; Grazulevicius, Juozas Vidas. Thermally activated delayed fluorescence of multicarbazole derivatives with different acceptor moieties. Chemistry and

chemical technology: 16th international conference of Lithuanian chemical society, 24 September 2021, Vilnius, Lithuania: book of abstracts. Vilnius: Lithuanian chemical society. 2021, O008, p. 107.

7. **Mahmoudi, Malek**; Urbonas, Ervinas; Gudeika, Dalius; Volyniuk, Dmytro; Grazulevicius, Juozas Vidas. Pluses and minuses of differently substituted indolocarbazole isomers used in non-doped organic light emitting diodes. Open readings 2022: 65th international conference for students of physics and natural sciences, March 15–18: abstract book / editors: Š. Mickus, S. Pūkienė, L. Naimovičius. Vilnius: Vilnius University Press. 2022, P3-41, p. 251.

8. **Mahmoudi, Malek**; Masimukku, Naveen; Volyniuk, Dmytro; Bezvikonnyi, Oleksandr; Dabuliene, Asta; Grazulevicius, Juozas Vidas. TADF hosting effects on the performances of glassforming 1,8-naphthalimide derivatives as red fluorescent OLED emitters, IPOE2022, University of Málaga, Malaga, Spain, June 13–16, 2022.

9. **Mahmoudi, Malek**; Gudeika, Dalius; Volyniuk, Dmytro; Urbonas, Ervinas; Simokaitiene, Jurate; Grazulevicius Juozas Vidas. Multifunctional indolocarbazole-based derivatives as TADF emitters for non-doped blue OLEDs, 16th International Summer Schools N&N, Organic Electronics & Nanomedicine, (ISSON22), Thessaloniki, Greece, July 2–9, 2022.

10. **Mahmoudi, Malek**; Skhirtladze, Levani; Volyniuk, Dmytro; Simokaitienė, Jūratė; Gražulevičius, Juozas Vidas. Donor substitution effects on the properties of 6-(trifluoromethyl)quinoxaline-based green emitters. ISSN: 2669-1930; DOI: 10.5755/e01.2669-1930.2022. Advanced materials and technologies: book of abstracts of 24rd international conference-school, 22–26 August 2022, Palanga, Lithuania. Kaunas: Kaunas University of Technology. 2022, B-P55, p. 92.

8. COPIES OF PUBLICATIONS

Original Article

Exciplex-forming systems with extremely high RISC rates exceeding 10^7 s^{-1} for oxygen probing and white hybrid OLEDs

Malek Mahmoudi [a], Jonas Keruckas [a], Karolis Leitonas [a], Stepan Kutsiy [b], Dmytro Volyniuk [a,**], Juozas V. Gražulevičius [a,*]

[a] Department of Polymer Chemistry and Technology, Kaunas University of Technology, Baršausko Str. 59, LT, 51423, Kaunas, Lithuania
[b] Department of Electronic Devices, Lviv Polytechnic National University, S. Bandera 12, 79013, Lviv, Ukraine

ARTICLE INFO

ABSTRACT

A rare example of exciplex-forming systems with highly efficient thermally activated delayed fluorescence (TADF) exhibiting reverse intersystem crossing (RISC) yields of 97 and 96% and RISC rates of 5.1×10^7 and 3.6×10^7 s^{-1} at 300 K are developed for oxygen probing and organic light-emitting diodes (OLEDs). The exciplexes forming systems consist of a commercial acceptor 2,4,6-tris [3-(diphenylphosphinyl)phenyl]-1,3,5-triazine and a donor diphenyl bicarbazole substituted by electron withdrawing fluoro- or trifluoromethyl units. Affected by the donor modification, exciplex-forming system containing fluoro-substituted diphenyl bicarbazole demonstrated higher TADF efficiency due to its higher hole mobility ($\mu_h = 1.1 \cdot 10^{-3}$ cm^2/V·s at $1.6 \cdot 10^5$ V/cm) and lower activation energy (E_a) of 52 meV for exciplex formation in comparison to E_a of 127 meV observed for exciplex formation of trifluoromethyl-substituted diphenyl bicarbazole which is characterized by μ_h of $7.7 \cdot 10^{-5}$ cm^2/V at the same electric field. Due to extremely high RISC rates (one of the highest for TADF emitters observed up to now to the best of our knowledge), TADF was detected even under oxygen atmosphere. The developed exciplex emission based oxygen probes are characterised by non-linear oxygen sensitivity with the Stern–Volmer constants of ca. $3.27 \cdot 10^{-3}$ and 4.7 ppm^{-1}. In order to demonstrate possible OLED applications of the developed exciplex-forming systems, solution-processed white hybrid OLEDs with very high colour rendering index (CRI) of 92, colour temperature of 3655 K and CIE1931 co-ordinates of (0.384, 0.399) were fabricated using exciplex-forming emitters.

© 2020 The Authors. Published by Elsevier B.V. This is an open access article under the CC BY-NC-ND license (http://creativecommons.org/licenses/by-nc-nd/4.0/).

1. Introduction

Exciplex-forming organic donor–acceptor systems have big potential for electroluminescent devices such as organic-light-emitting diodes (OLEDs) and vertical light-emitting

transistors [1,2]. Particularly, big interest to exciplex emission is mainly grounded on:

- Possibility to harvest "dark" triplets via reverse intersystem crossing (RISC) of thermally activated delayed fluorescence (TADF) phenomenon; [3,4].
- Ability to decrease energy barriers for transported charges in device structures via formation of an "active" pn-heterojunction resulting in low turn-on voltage, thus high OLED power efficiency (exceeding of 100 l m/W); [5].
- Simplicity of obtaining of exciplex emission by mixing of electron donating and electron accepting molecules in solid state; [6].
- Versatility of different types of device structures since exciplex-forming systems are utilized as emitters, hosts, and they can be formed/transferred through relatively long distance; [7—10].
- Broad emission spectra and dual/multi-peak emission of exciplexes are suitable for realization of white OLEDs [11].

Among the best cases, exciplex emission characterized by very high reverse intersystem crossing (RISC) rates of 7.3×10^6 s^{-1} for TSBPA:POT2T [12] or 1.42×10^6 s^{-1} for DBT-SADF:PO-T2T:CDBP [13] was observed. It allowed to obtain exciplex emission based OLEDs with external quantum efficiency (EQE) higher than 20%. The abbreviation TSBPA is used for 4,4′-(diphenylsilanediyl)bis (N,N-diphenylaniline, PO-T2T is used for 2,4,6-tris [3-(diphenylphosphinyl)phenyl]-1,3,5-triazine, DBT-SADF is used for 2-(spiro [acridine-9,9′ -fluoren]-10-l)dibenzo [b,d]thiophene 5,5-dioxide, and CDBP is used for 4,4′-bis(9-carbazolyl)-2,2′-dimethylbiphenyl. Such RISC rates (k_{RISC}) observed for exciplex forming systems are comparable or even higher than RISC rates of state-of-art TADF emitters exhibiting k_{RISC} values of ca.10^6 s^{-1} [14,15]. However, TADF efficiencies of exciplex-based emitters are typically low at room temperature (RT) which affects EQE of electroluminescent devices. For instance, OLED based on exciplex-forming molecular mixture mMTDATA:3TPYMB exhibited lower EQE of 6.3% at RT than at 248 K (11%) [16]. Here, m-MTDATA is 4,4′,4″-tris [phenyl (m-tolyl)amino]triphenylamine and 3TPYMB is tris(2,4,6-trimethyl-3-(pyridin-3-yl)phenyl) borane. The similar observation was previously attributed to high non-radiative singlet and triplet transition rates (k_{nr}^S and k_{nr}^T, respectively) of exciplexes at room temperature [17]. It was concluded that not only high RISC rates but also low non-radiative transition rates are required for efficient exciplex based TADF [17].

In this work, we aimed to find out whether high k_{RISC} and high k_{RISC}/k_{nr}^T relation can be obtained for exciplexes when exciplex-forming donor diphenyl bicarbazole is modified by electron withdrawing fluoro- or trifluoromethyl units. 9,9-H or 9,9-diphenyl bicarbazole showed good performances in OLEDs as exciplex-forming donors [18—20]. We expected that substitution of diphenyl bicarbazole by acceptor units will result at least in higher ionization potentials compared to unsubstituted ones. Thus, knowing that the exciplex emission maximum wavelength can be described by formula $h\nu_{ex}^{max} \simeq I_P^D - E_A^A - E_C$, where I_P^D is the ionization potential of a donor, E_A^A is the electron affinity of an acceptor, and E_C is the

electron—hole Coulombic attraction energy [21], we expected that the attachment of accepting moieties to diphenyl bicarbazole may result in the shift of emission of exciplexes to the higher-energy region. In addition, bipolar charge transport, which is required for functional OLED materials (e.g. for hosts and emitters), can be expected for compounds containing donor and acceptor units [22,23]. Taking into account these considerations, we synthesized two new diphenyl bicarbazoles (**bFPC** and **bTfPC** in Scheme 1). At RT, solid-state mixtures **bFPC**:PO-T2T and **bTfPC**:PO-T2T demonstrated efficient exciplex emission with the similar k_{RISC} of 5.1×10^7 and 3.6×10^7 s^{-1} but different k_{RISC}/k_{nr}^T of 1.1 and 0.27, respectively. Because of that, different photoluminescence quantum yields (PLQY) of 56 and 22% were recorded for exciplex-forming molecular mixtures **bFPC**:PO-T2T and **bTfPC**:PO-T2T, respectively. Despite extremely high k_{RISC} and relatively high k_{RISC}/k_{nr}^T their PLQYs were still much below 100%. Relatively low PLQYs can be explained by relatively low relationship of rates of prompt fluorescence to non-radiative singlet transition rates (k_{pr}/k_{nr}^S) of 41.4×10^{-3} observed for **bFPC**:PO-T2T and 10.5×10^{-3} recorded for **bTfPC**:PO-T2T. Thus, not only TADF efficiency but also efficiency of prompt fluorescence has to be increased for exciplex-forming systems. Nevertheless, having exciplexes with RISC yields of 97 and 96%, it is possible to employ them in optical sensors of oxygen. Naturally, quenching of TADF under presence of oxygen is expected. Several examples of TADF emitters were reported as active oxygen sensing materials [24,25] but to the best of our knowledge, the systems exhibiting exciplex based TADF were not yet used for this purpose. In addition, we used exciplex-forming molecular mixtures **bFPC**:PO-T2T and **bTfPC**:PO-T2T as green emitters in solution-processed hybrid white OLEDs based on polymeric host which acted also as a blue emitter doped by low concentration of a red phosphorescent emitter. Mixing blue fluorescence, green exciplex emission and red phosphorescence we achieved high colour rendering index (CRI) of 92, low correlated colour temperature of 3655 K and CIE1931 coordinates of (0.384, 0.399).

Originality of the proposed approach for the fabrication of white hybrid OLEDs is based on the distribution of electrical excitation energy between two light emitting layers, namely between green exciplex-based TADF and blue/red fluorescent/phosphorescent ones. The hole—electron recombination zone was mainly situated within the green exciplex-based light-emitting layer while part of electrical excitation energy was transferred to the blue/red emitting layer by direct hole—electron recombination and by exciton energy transfer. Such allocation of exciton energy resulted in relatively stable white emission under different external voltages.

2.   Experimental

Materials. Molybdenum (VI) oxide (MoO₃), poly (9,9-dioctylfluorene-alt-N-(4-sec-butylphenyl)-diphenylamine) (TFB), bis(1-phenylisoquinoline) (acetylacetonate)iridium (III) (Ir (piq)₂ (acac)), 2,4,6-tris [3-(diphenylphosphinyl)phenyl]-1,3,5-triazine (PO-T2T), diphenyl-4-triphenylsilylphenyl-phosphine oxide (TSPO1), 2,2′,2″-(1,3,5-benzinetriyl)-tris(1-

phenyl-1-H-benzimidazole) (TPBi), and lithium fluoride (LiF) were purchased from Sigma−Aldrich or Lumtec companies and used without additional purification.

OLED fabrication. Electroluminescent devices with the structures of ITO/MoO$_3$/TFB:Ir (piq)$_2$ (acac) (EML2)/**BFPC**:PO-T2T or **BTfPC**:PO-T2T (EML1)/TSPO1/TPBi/LiF:Al were fabricated by a spin-coating/evaporation hybrid method. Indium-tin-oxide (ITO)-coated substrates were consecutively cleaned in an ultra-sonic bath containing acetone solution, distilled water and treated by UV-ozone for 15 min. Then, the devices were prepared by step-by-step depositions of different organic layers. The first (EML1) (**BFPC**:PO-T2T or **BTfPC**:PO-T2T) and the second (EML2) (TFB:Ir (piq)$_2$ (acac)) light-emitting layers were spin-coated while the other layers were vacuum-evaporated. The layers EML1 and EML2 were deposited from toluene solutions (4 mg/ml) of the corresponding compound mixtures under inert gas atmosphere inside a glove box. After spin-coating of EML1 and EML2, the samples were thermally annealed at 90 °C for 30 min (in case of EML1) or 180 °C for 40 min (in case of EML2). The vacuum-evaporated layers (MoO$_3$, TSPO1, TPBi, LiF and Al) were prepared under the vacuum of 10^{-6} mBar. All of the vacuum-evaporated layers were deposited at a rate of 1 Å s^{-1} except the LiF layer which was deposited at 0.1 Å s^{-1}. The size of emissive pixel was of 6 mm^2.

Additional information on materials, instrumentation and device testing are presented in the Supplementary Information.

3. Results and discussion

3.1. Synthesis and common characterizations

Compounds **bFPC** and **bTfPC** were prepared by two-step synthetic procedure starting from 9H-carbazole as it is shown in Scheme 1. In the first step, carbazole was substituted at N-position by 4-fluorophenyl or 4-trifluoromethylphenyl groups using the respective aryl iodides under the modified Ullmann conditions [26]. The intermediate compounds **FPC** and **TfPC** were isolated by re-crystallization in good yields of ca. 70−90%. In the second step, the intermediates were coupled by oxidative method [27] using iron (III) chloride. The target compounds, 3,3′-bis [9-(4-fluorophenyl)carbazole] (**bFPC**) and 3,3′-bis [9-(4-trifluoromethylphenyl)carbazole] (**bTfPC**) were isolated after column chromatography and re-crystallization in sufficient yields of 67% and 52%, respectively (see ESI for the procedures).

While proceeding with our research, we have discovered more efficient synthetic procedure for **bFPC** compared to that reported by other authors [28]. Interestingly, the melting point of 86−88 °C reported for **bFPC** in ref. [28] is close to glass-transition temperature established by ourselves for this compound (Fig. 1a, Table 1). Thus, we assume that **bFPC** reported in ref. [28] was rather isolated as amorphous solid than crystalline material. However, the structural data for **bFPC** (NMR, IR, MS) well match with those reported previously.

Compounds **bFPC** and **bTfPC** were isolated as crystalline solids which was proved by their well-defined melting points (mp) (Table 1). The mp values for both materials were close

and situate around 245 °C when measured in capillary (see ESI) and around 250 °C as established by DSC (sharp endothermic peaks in Fig. 1a, inset). Both the compounds formed molecular glasses with glass-transition temperatures (T$_g$) of 101 °C for **bFPC** and 111 °C for **bTfPC**. However, the glasses of these compounds tended to crystallize above their glass-transition temperatures (exothermic peaks at ca. 205 and 160 °C in Fig. 1a) and melted again at the same temperature as before.

According to the data of thermogravimetric analysis (TGA, Fig. 1a), five percent weight-loss temperatures established for **bFPC** and **bTfPC** were 374 and 350 °C, respectively. Since the compounds melted at 250 °C and their sample weights went down to zero even at not very high temperature (around 450 °C), the weight loss can be rather attributed to evaporation than to chemical decomposition.

In order to determine electrochemical energy levels of compounds **bFPC** and **bTfPC,** they were examined by cyclic voltammetry (CV). Their dichloromethane (DCM) solutions with tetra-n-butylammonium hexafluorophosphate (TBAPF$_6$) as supporting electrolyte showed oxidation half-waves with respect to ferrocene at 0.58 V for **bFPC** and 0.65 V for **bTfPC** (Fig. 1b, Table 1). Both compounds exhibited double reversible CV oxidation but no expressed reduction waves were observed for DCM solutions even when strong electron withdrawing CF$_3$ groups were present. Despite the small difference (0.07 V) between oxidation potentials of the solutions of **bFPC** and **bTfPC**, a noticeably bigger difference (0.26 eV) was observed between their ionization potentials estimated by photoelectron spectroscopy (PESA) in air. I_p^{PESA} of 5.78 eV was observed for the film of **bFPC** and 6.04 eV for the film of **bTfPC**(Fig. 1c inset, Table 1). I_p^{PESA} values of **bFPC** and **bTfPC** were found to be higher than corresponding values measured by CV. I_p^{CV} values of 5.38 and 5.45 eV respectively were recorded. Such discrepancy is typically observed due to the different physical meaning of I_p^{CV} and I_p^{PESA} [29]. Due to stronger electron accepting ability of CF$_3$ groups in comparison to that of F, the higher I_p^{PESA} (deeper HOMO) was obtained for compound **bTfPC** relative to that observed for **bFPC**.

Time of flight (TOF) experiment disclosed low-dispersity hole transport in the layers of **bFPC** and **bTfPC**. The transit times (t$_{tr}$) for holes were easily identified from TOF current transients at different external voltages (V) in log−log scales for the vacuum-deposited films (Fig. S1). Despite the presence of electron accepting fluoro- or trifluoromethyl substituents, electron transport ability was detected for the layers of **bFPC** and **bTfPC** by the TOF measurements (Fig. S1). Taking the t$_{tr}$ values for holes at different external voltages, hole mobility (μ$_h$) at different electric fields (E) were calculated for **bFPC** and **bTfPC** (Fig. 1c). Dependences log (μ$_h$) versus $\sqrt{E}$ were well fitted by the Poole−Frenkel formula $\mu = \mu_0 e^{\alpha E^{1/2}}$ [30].

By the fitting, zero-field mobilities (μ$_0$) and field dependence parameter (α) were obtained. Slightly higher value of α observed for **bTfPC** was apparently due to its more dispersive charge transport. Higher by ca. 20 times μ$_0$ value observed for **bFPC** can apparently be explained by favourable molecular packing (Fig. 1c). Lower field dependence parameter α of 2.5·10^{-3} cm/V was obtained for **bFPC** compared to that observed for **bTfPC** (3.9·10^{-3} cm/V) indicates lower charge dispersity in the layer of **bFPC** than in that of **bTfPC**.

85

**Table 1 – Thermal, electrochemical, photoelectrical, hole-transporting and photophysical parameters of bFPC and bTfPC.**

Property	Sample	bFPC	bTfPC
T_m, °C	Powder	246	253
T_g, °C		101	111
T_{cr}, °C		206	161
$T_{de-5\%}$, °C		374	350
E_{ox} vs Ag/Ag$^+$, V	DCM solution with TBAPF$_6$	0.58	0.65
IP_{CV}, eV		5.38	5.45
IP_{PE}, eV	Film	5.78	6.04
E_g^{opt}, eV		3.36	3.21
EA_{PE}, V		2.42	2.83
λ^{PL}, nm	Film (THF solution)	390, 409 (385[b], 402)	387, 404 (383[b], 397)
PLQY, %		19 (15)	15 (18)
τ, ns		4.68 (6.09)	4.02 (6.01)
E_{S1}^{THF}, eV	THF solution at 77 K	3.44	3.38
E_{T1}^{THF}, eV		2.99	2.99
ΔE_{S1T1}^{THF}, eV		0.45	0.39
μ_{holes},[a] cm^2/(V·s)	Film	$1.1 \cdot 10^{-3}$	$7.7 \cdot 10^{-5}$

[a] At electric field of $1.6 \cdot 10^5$ V/cm.
[b] Shoulder.

Apparently, the presence of trifluoromethyl units hinders hoping of holes between HOMO–HOMO molecular orbitals of neighbouring molecules. In addition, more efficient formation of hydrogen bonds C–H···F in the layer of bTfPC than in the layer of bFPC can be the reason of the above described observations. The different values of hole mobility of bFPC and bTfPC might be also related to their molecular packing and/or

different structure of the layers as it was proved for other carbazole-containing compounds [31]. Notably, μ_h of 1.1×10^{-3} cm^2/V·s recorded at electric field of 1.6×10^5 V/cm is by two orders of magnitude higher than hole mobility of efficient exciplex-forming bicarbazoles containing CN groups at the same electric fields (Table 1) [32,33]. In contrast to those CN-substituted bicarbazoles which showed bipolar charge
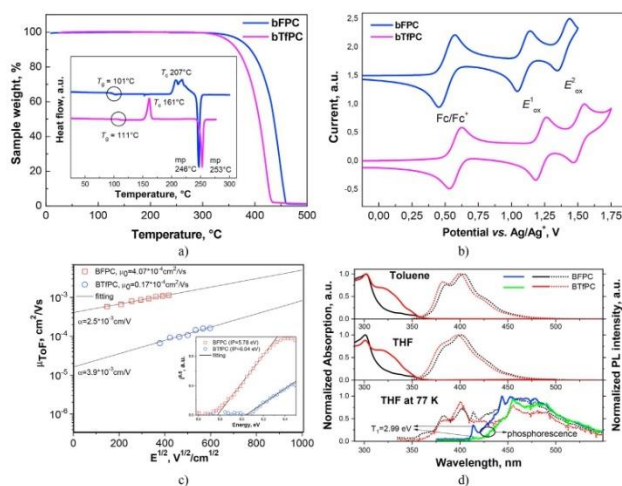
Fig. 1 – (a) DSC second heating scans (inset) and TGA curves; (b) CV voltammograms ("Fc" stands for ferrocene, E^{ox}_1 and E^{ox}_2 stand respectively for the first and the second oxidation waves); (c) hole mobility versus electric field and electron photoemission spectra (inset); (d) UV absorption, PL and phosphorescence spectra of the dilute solutions of bFPC and bTfPC. Phosphorescence spectra were recorded at 77 K with the delay of 50 ms after excitation turn-off.

transport, compounds **bFPC** and **bTfPC** exhibited only hole-transporting properties apparently because of the weak electron withdrawing ability of fluoro or trifluoromethyl units.

In order to investigate the effect of the different substituents on photophysical properties of the compounds, absorption and photoluminescent (PL) spectra of the dilute solutions ($\sim$10^{-5} M) of **bFPC** and **bTfPC** in toluene and THF were recorded (Fig. 1d). Carbazole unit is mainly responsible for absorption of the solutions of compound **bFPC** since the shape of its absorption spectrum is similar to that of carbazole, N-phenylcarbazole, and N,N'-diphenyl(-3,3-)bicarbazole [1,2,18]. The additional energy band around 325 nm can be recognized in the low-energy region of absorption spectra of the solutions of compound **bTfPC**. It was not observed in the spectra of the solutions of **bFPC** and N-phenylcarbazole [35]. The similar absorption band was observed for benzonitrile-substituted carbazole N-(4-cyanophenyl)carbazole (NP4CN) and was attributed to S$_0$→charge transfer (CT) absorption [34]. Charge transfer between carbazole and trifluoromethylbenzene units induced that additional absorption band. Vibronically structured fluorescence spectra with two maxima at 385 and 405 nm were recorded for toluene solutions of **bFPC** and **bTfPC**. The similar fluorescence spectrum was previously reported for N-phenylcarbazoles and was attributed to locally exited (LE) emission (Fig. 1d) [34]. PL decays of the toluene solutions of the compounds were adequately represented by single-exponential fitting with the lifetimes of ca. 6 ns? The lifetimes slightly differed with the change of polarity of media (Fig. S2, Table S2). This effect is apparently related to different non-radiative rates of the compounds in different media. LE emission was also detected for the solutions of compounds **bFPC** and **bTfPC** in more polar

TFH. A weak intramolecular CT (ICT) contribution can be recognised in the emission of compounds **bFPC** and **bTfPC** as it was shown for CF$_3$-substituted N-phenylcarbazole [35]. However, no any strong ICT emission was observed even for the films of compounds **bFPC** and **bTfPC**, as it was for reported for compound NP4CN with a relatively strong benzonitrile acceptor (Fig. 2a) [34]. Photoluminescence quantum yield (PLQY) values of the solutions and neat films of compounds **bFPC** and **bTfPC** (Table 1) are in agreement with PLQYs of the previously studied N-phenylcarbazoles and N-phenyl-bicarbazoles [18,33,35].

PL and phosphorescence spectra of THF solutions of **BFPC** and **BTfPC** were also recorded for getting their first excited singlet (E_{S1}) and triplet (E_{T1}) energy levels (taken from the first highest-energy peak) (Fig. 1d, Table 1). The compounds emit intense phosphorescence which is mainly related to the LE^3 emissive recombination of triplet state of carbazole moiety [36,37]. The differences observed in phosphorescence spectra of **bFPC** and **bTfPC** are apparently caused be weak influence of ICT^3 emission in case of **bTfPC**. Nevertheless, both compounds were characterized be the same energy of the first excited triplet states of 2.99 eV (Table 1).

3.2. Exciplex-forming properties

Compounds **bFPC** and **bTfPC** can be regarded as promising candidates as exciplex-forming donors for TADF emitters due to their high triplet levels, high hole mobilities, and fluorescence in near UV region. Indeed, solid-state mixtures **bFPC**:PO-T2T and **bTfPC**:PO-T2T demonstrated exciplex type emission which was typically red-shifted in comparison to pure emission of donor and acceptor compounds (Fig. 2a). PL
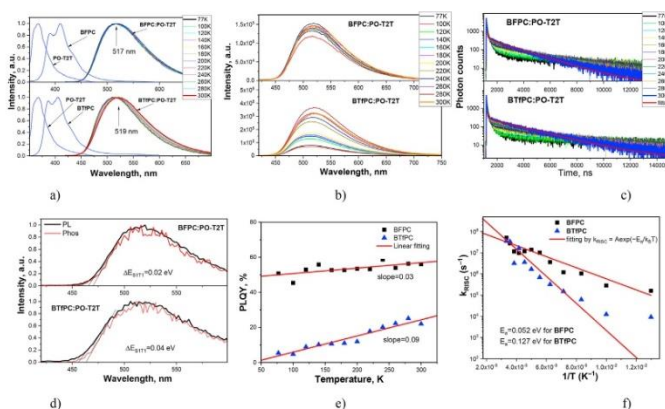
Fig. 2 – Normalized PL spectra (a) and intensity dependences on the temperature of PL spectra (b) of the films of bFPC, bTfPC, PO-T2T, bFPC:PO-T2T, and bTfPC:PO-T2T. The corresponding PL decay curves recorded at the indicated temperatures (c), PL and phosphorescence spectra recorded at 77K (d) of molecular mixtures bFPC:PO-T2T and bTfPC:PO-T2T. PLQY versus temperature (e) and k_{RISC} versus 1/T (f) plots for bFPC:PO-T2T and bTfPC:PO-T2T.

spectra of **bFPC**:PO-T2T and **bTfPC**:PO-T2T are peaked at the similar wavelength near 520 nm. Their PL decays were adequately fitted by double exponential law giving short-lived (τ_{PF} of 69—376 ns)) and long-lived (τ_{DF} of 1.94—4.25 μs) components (Table 2). More than 90% of total emission intensity of exciplexes was related to delayed fluorescence which is thermally activated by nature. This statement was proved by the measurements of PL spectra and PL decays at the different temperatures (Fig. 2b,c). The presence of TADF is in the emission of the exciplex forming systems was confirmed by small singlet-triplet energy differences (ΔE_{S1T1}) which allowed RISC process and thus TADF (Fig. 2d) [4]. Having absolute PLQY values of exciplexes at RT and dependences of PL spectra on the temperature (Table 2, Fig. 2b), it was possible to plot PLQY versus temperature for exciplex emitters **bFPC**:PO-T2T and **bTfPC**:PO-T2T (Fig. 2e). In contrast to previously studied exciplexes which showed the highest efficiency at low temperatures [16,17], PLQY values of the studied exciplexes linearly increased with increasing temperature due to the efficient TADF and low non-radiative losses.

Solid molecular mixtures **bFPC**:PO-T2T and **bTfPC**:PO-T2T were also studied by the time-resolved luminescence spectrometry at the different temperatures (Tables 2 and S2) [4,5,38]. The values of prompt (η_{PF}) and delayed (η_{DF}) fluorescence quantum yields were obtained from PL decays fitting assuming that the total integral of PL transients is attributed to the absolute PLQYs of exciplexes **bFPC**:PO-T2T and **bTfPC**:PO-T2T (Table S2). Taking lifetimes of prompt and delayed fluorescence (τ_{PF} and τ_{DF}) and the corresponding quantum yields (η_{PF} and η_{DF}), radiative rates of prompt (k_{PF}) and delayed (k_{DF}) fluorescence were estimated (Tables 2 and

S2). In addition, non-radiative rates of the singlet (k_{nr}^S) and triplet (k_{nr}^T) states were calculated. Non-radiative rate k_{nr}^S is mainly related to the intersystem crossing (ISC) with the quantum efficiency η_{ISC} and rate constant k_{ISC}. The RISC process is responsible for the population of the first singlet state (S1) resulting to the long-living component of PL transients. Rate constant k_{RISC} as a key parameter is generally attributed to efficient TADF and is in the order of 10^6 s^{-1} for state-of-art intramolecular and intermolecular TADF emitters [12—15]. Notably, exciplexes **bFPC**:PO-T2T and **bTfPC**:PO-T2T were characterized by extremely high k_{RISC} of 5.1×10^7 and 3.6×10^7 s^{-1} respectively, which are among the highest values to the best of our knowledge. Despite of the close k_{RISC} values, exciplex emission of **bFPC**:PO-T2T was found to be more efficient than emission of **bTfPC**:PO-T2T. The respective absolute PLQY values were found to be different, i.e. of 56% and 22% at room temperature (Table 2). This observation can be explained by the different non-radiative rate constants k_{nr}^T of 4.7×10^7 for **bFPC**:PO-T2T and of 1.35×10^8 for **bTfPC**:PO-T2T resulting in the different k_{RISC}/k_{nr}^T ratio of 1.1 and 0.27, respectively. Despite of the small difference in the molecular structures of compounds **bFPC** and **bTfPC** which practically have no effects on the exciplex emission spectra of **bFPC**:PO-T2T and **bTfPC**:PO-T2T, the different non-radiative rate constants k_{nr}^T were obtained for these exciplexes.

This observation may be attributed to the different molecular packing caused by the presence of the different fluoro- and trifluoromethyl substituents in **bFPC** and **bTfPC**. The presence of trifluoromethyl groups may be the reason of higher intermolecular distances in solid films leading to the higher non-radiative rate constant k_{nr}^T and to the less efficient

Table 2 — Photophysical parameters of exciplex-forming molecular mixtures bFPC:PO-T2T and bTfPC:PO-T2T derived at room temperature (300 K).

Exciplex	source/equation	bFPC: PO-T2T	bTfPC:PO-T2T
λ^{PL}_{max}, nm	taken from PL spectra	517	519
FWHM, nm		104	107
E_{S1}, eV	$E_{S1} = 1240/\lambda^{PL}_{seton}$	2.63	2.72
E_{T1}, eV	$E_{T1} = 1240/\lambda^{Phos}_{seton}$	2.64	2.68
ΔE_{S1T1}, eV	$\Delta E_{S1T1} = E_{S1} - E_{T1}$	0.02	0.04
PLQY, %	measured with a sphere	56	22
η_{PF}	$\eta_{PF} = \eta_{PLQY} * PF(\%)/100(\%)$	0.04	0.01
η_{ISC}	$\eta_{ISC} = 1 - \eta_{PF}$	0.96	0.99
η_{DF}	$\eta_{DF} = PLQY * DF(\%)/100(\%)$	0.52	0.21
η_{RISC}	$\eta_{RISC} = \eta_{DF}/(\eta_{PLQY} * \eta_{ISC})$	0.97	0.96
E_a, eV	taken from k_{RISC} fitting by $k_{RISC} = A\exp(-E_a/k_BT)$	0.052	0.127
τ_{PF}, ns (%)	from PL decay fitting by $I = A + B1\exp(-t/\tau_{PR}) + B2\exp(-t/\tau_{DF})$	110 (7)	94 (5)
τ_{DF}, μs (%)		1.94 (93)	2.47 (95)
τ^r_{PF}, μs	$\tau^r_{PF} = \tau_{PF}/\eta_{PF}$	2.8	9
τ^{nr}_{PF}, ns	$\tau^{nr}_{PF} = \tau_{PF}/(1 - \eta_{PF})$	115	95
k_{PF}, s^{-1}	$k_{PF} = \dfrac{\eta_{PF}}{\tau_{PF}}$	3.6×10^5	1.1×10^5
k^r_{PF}, s^{-1}	$k^r_{PF} = 1/\tau^r_{PF}$	3.6×10^5	1.1×10^5
k^s_{nr}, s^{-1}	$k^{nr}_{PF} = 1/\tau^{nr}_{PF}$	8.7×10^6	1.05×10^7
k_{ISC}, s^{-1}	$k_{ISC} = \dfrac{\eta_{DF}}{\eta_{PF} + \eta_{DF}} k_{PF}$	0.25×10^5	0.05×10^5
k_{DF}, s^{-1}	$k_{DF} = \dfrac{\eta_{DF}}{\tau_{DF}}$	2.69×10^5	0.85×10^5
k_{RISC}, s^{-1}	$k_{RISC} = \dfrac{\eta_{DF}}{\eta_{PF}} \dfrac{k_{PF} \cdot k_{DF}}{k_{ISC}}$	5.1×10^7	3.6×10^7
k^T_{nr}, s^{-1}	$k^T_{nr} = k_{RISC}/\eta_{RISC} - k_{RISC}$	4.7×10^7	1.35×10^8

TADF of **bTfPC**:PO-T2T in comparison to that of **bFPC**:PO-T2T. In case of exciplex formed by **bFPC**:PO-T2T, the lower non-radiative energy loss can be explained by a relatively large HOMO—LUMO orbital overlap since molecules of **bFPC** and PO-T2T in their solid molecular mixture are apparently closer to each other in comparison to distance between the molecules of **bTfPC** and PO-T2T in the solid molecular mixture. Thus, the different intermolecular distances between the molecules in the solid molecular mixtures of **bFPC**:PO-T2T and **bTfPC**:PO-T2T causing the different HOMO—LUMO overlaps apparently lead to the different radiative decay probabilities from excited spin-singlet states [11,12,32].

The different hole mobilities of **bFPC** and **bTfPC** have also to be taken into account. Since higher hole mobility of 1.1×10^{-3} cm^2/V·s was observed for compound **bFPC** (Fig. 1c, Table 1), it could be the reason of faster formation of hole—electron excited states (exciplexes). On the other, the probability of dissociation of hole—electron pairs into free charges may be increased for the exciplex **bFPC**:PO-T2T due to the high hole mobility of **bFPC** [12,32]. Free charges (positive and negative polarons) may lead to non-radiative energy loss of the exciplex states as it was concluded by the authors of ref. [32]. However, the authors of study [12] noted that formation of free charges not necessarily leads to the non-radiative energy loss of the exciplex states when the energy of local excited (LE) states of exciplex-forming compounds are above their CT exciplex states. It was presumed that "new" CT exciplex states could be formed by the dissociated free holes and electrons [12]. Despite the dissociation, when the triplet CT exciplex state lives long enough, efficient RISC can occur which is required for efficient TADF [12]. It is the case of exciplexes **bFPC**:PO-T2T and **bTfPC**:PO-T2T since their singlet and triplet LE states are higher than their CT exciplex states (Fig. 1 d, Tables 1 and 2). It shout be noted the faster formation of the "new" CT exciplex states from the dissociated charges is expected for the exciplex based on the compound **bFPC** with higher hole mobility in comparison to the **bTfPC**-based exciplex. Taking into account, the probability of dissociation of hole—electron pairs into free charges for both **bFPC**:PO-T2T and **bTfPC**:PO-T2T exciplexes, the lower non-radiative energy losses are expected for **bFPC**-based exciplex due to the fast formation of the "new" CT exciplex states followed by their emissive recombination.

Having k_{RISC} values at different temperatures, Arrhenius plots were plotted and fitted (in the range of T > 200K where phosphorescence is absent (limited)) according to Arrhenius equation: $k_{RISC} = A \cdot \exp (-E_a/k_B T)$, where A is the frequency factor involving the spin—orbit coupling constant, E_a is activation energy and k_B is Boltzmann constant [39]. By analysing the temperature dependences of k_{RISC}, E_a values of 0.052 and 0.127 eV were obtained for emission of exciplexes **bFPC**:PO-T2T and **bTfPC**:PO-T2T, respectively. These E_a values are in good agreement with their singlet-triplet splitting ΔE_{S1T1} allowing population of the emissive singlet exciplex state via RISC from the triplet exciplex state.

3.3. Oxygen probing

Exciplex-formig system **bFPC**:PO-T2T was selected for testing its applicability as oxygen probe. This system was characterized by higher total PLQY (56%) than BTfPC:PO-T2T (22%). Since exciplex emission of **bFPC**:PO-T2T was mainly characterized by delayed fluorescence (η_{DF}=52% versus η_{PF} = 4% (Table 2)), oxygen sensitivity of this system can be predicted if the delayed fluorescence is quenched under presence of oxygen (Table 2). This prediction is supported by the relation η_{DF}/η_{PF} = 13, which may be obtained from the relation of emission intensities estimated in the presence and in the absence of oxygen. Aiming to test exciplex-forming system **bFPC**:PO-T2T as active component for oxygen probing, three-component samples **bFPC**:PO-T2T:Zeonex (1:1:1) were fabricated. Zeonex 480 was used for the improvement of film-forming properties of the probe and for insuring oxygen permeability of the films [40]. PL spectra of the films of the mixtures **bFPC**:PO-T2T:Zeonex were recorded under different concentration of oxygen in constant flow of nitrogen:oxygen mixture when emission intensity was stabilized (Fig. 3a). Dependence of integrated emission intensity versus concentration of oxygen was then analysed by the Stern—Volmer equation which describes nonlinear curve [41,42].

$$\frac{I_0}{I} = \frac{1}{\frac{f_1}{1+K_{SV1}[O_2]} + \frac{f_2}{1+K_{SV2}[O_2]}}, \tag{1}$$

where I_0 and I are emission intensities under nitrogen and at the different concentrations of oxygen; f_1 and f_2 are fractional contributions of different sensing sites; K_{SV1} and K_{SV2} are Stern—Volmer constants. The results of fitting are collected in the inset Table of Fig. 3b. The fitting with relatively high accuracy (R^2 = 0.9652) was performed using formula (1). The fitting data can be used for determination of specific concentration of oxygen measuring ratiometric properties of the samples of the mixtures **bFPC**:PO-T2T:Zeonex. Despite the
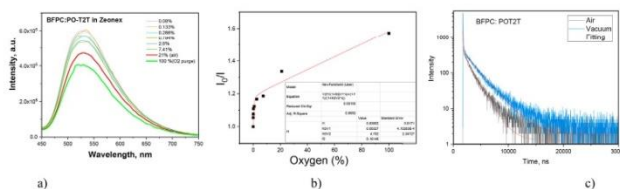

Fig. 3 — PL spectra (a), Stern—Volmer dependence (b), and PL decays (c) of the films of bFPC:PO-T2T:Zeonex under different concentration of oxygen.

high ratio η_{DF}/η_{PF} of 13, the ratio of emission intensity under pure nitrogen and emission intensity under pure oxygen ($I_{0\,[100\%\,N_2]}/I_{[100\%\,O_2]}$) of 1.57 was obtained which indicates relatively low oxygen sensitivity of the mixture bFPC:PO-T2T:Zeonex. This observation is in agreement with the results of PL decay measurements of the films of bFPC:PO-T2T:Zeonex under vacuum and under air demonstrating that this exciplex-forming system is characterized by delayed fluorescence even in the presence of oxygen. Apparently, delayed fluorescence cannot be totally quenched by oxygen when TADF emitters are characterized by extremely high k_{RISC}, which exceeds 10^7 s^{-1} (Table 2).

3.4. Solution processed white hybrid organic light-emitting diodes

Taking into account the green TADF with broad PL spectra of the studied exciplex-forming systems bFPC:PO-T2T and bTfPC:PO-T2T, they can be regarded as good candidates for getting white electroluminescence (EL) in combination with appropriate blue and red emitters. Blue emitting poly (9,9-dioctylfluorene-alt-N-(4-sec-butylphenyl)-diphenylamine) (TFB) [43] and red emitting bis(1-phenylisoquinoline) (acetylacetonate)iridium (III) (Ir (piq)$_2$ (acac)) [44] emitters were selected as one possible set of emitters which may enable to obtain natural white emission mixing their emission with the green exciplex emission of bFPC:PO-T2T and bTfPC:PO-T2T (Fig. 4a). The total spectrum (Fig. 4, orange line) obtained by mixing three emission spectra of TFB, bFPC:PO-T2T (or

bTfPC:PO-T2T) and Ir (piq)$_2$ (acac) covers the whole visible region. This observation confirmed that the combinations of red, green, and blue emitters were well selected. The polymeric material TFB was selected aiming to fabricate partly solution processable white OLEDs. In addition to practical interest in solution-processing [45], this solution-based method allows precise control of concentration of an emitter in doped light-emitting layers which are required for the fabrication of white OLEDs. To get white electroluminescence, the device structure ITO/MoO$_3$ (1 nm)/TFB:Ir (piq)$_2$ (acac) (2, 5 or 10 wt%, 30 nm)/bFPC:PO-T2T (for the devices named as A2, A5 and A10, respectively) or bTfPC:PO-T2T (for the devices named as B2, B5 and B10, respectively) (1:1) (20 nm)/TSPO1 (8 nm)/TPBi (40 nm)/LiF:Al was selected, where the layer of MoO$_3$ was employed as hole injection layer, the layer of diphenyl-4-triphenylsilylphenyl-phosphine oxide (TSPO1) acted as hole/exciton blocking layer, the layer of 2,2′,2″-(1,3,5-benzinetriyl)-tris(1-phenyl-1-H-benzimidazole) (TPBi) acted as electron transporting layer, and the layer of LiF acted as electron injection layer. The effect of concentration of the red phosphorescent emitter Ir (piq)$_2$ (acac) on the quality of white electroluminescence was investigated for devices A (A2, A5 and A10) and B (B2, B5 and B10), with the concentration of Ir (piq)$_2$ (acac) of 2, 5 and 10% respectively (Table 2). Such concentrations of the dopant in light-emitting layers based on the host-guest system were simply attainable because the layers were fabricated by spin-coating method.

Analysis of the equilibrium energy diagram of the device structures (Fig. 4b) revealed that the recombination zone of
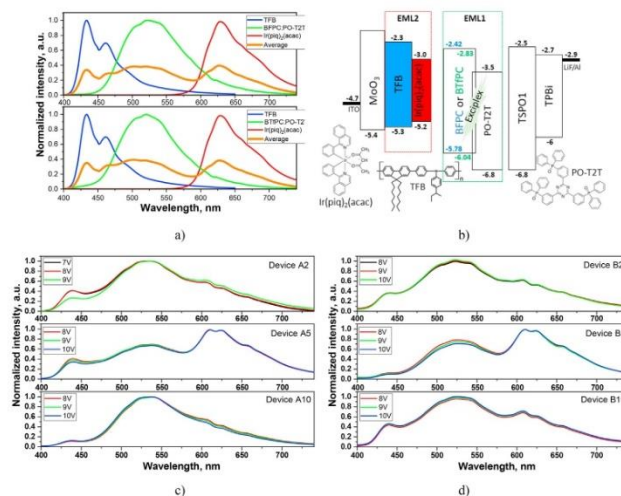

Fig. 4 − PL spectra of blue emitting TFB, green emitting bFPC:PO-T2T or bTfPC:PO-T2T, and red emitting Ir (piq)$_2$ (acac) and the total spectrum of the three emitters (a); visualized device structure with indication of energy levels of all functional layers (b); normalized electroluminescence spectra under different applied voltages for white bFPC:PO-T2T (c) and bTfPC:PO-T2T (d) based devices.

Table 3 – Electroluminescent parameters of white OLEDs.

Device	Emissive layers	$V_{on,}$[a] (V)	Max. brightness, cd/m²[b]	CE_{max},cd/A[c]	EQE_{max}, %[d]	CIE (x; y)[e]	CRI[f]	T_C, K[g]
A2	TFB:Ir (piq)₂ (acac) (98:2)/bFPC:POT2T (1-1)	3.4	6381	6.5	2.9	(0.311; 0.424)	76	5654
B2	TFB:Ir (piq)₂ (acac) (98:2)/bTfPC:POT2T (1-1)	3.4	7513	4.8	2.1	(0.327; 0.471)	78	5625
A5	TFB:Ir (piq)₂ (acac) (95:5)/bFPC:POT2T (1-1)	4.2	8980	11.6	6.3	(0.384; 0.399)	92	3655
B5	TFB:Ir (piq)₂ (acac) (95:5)/bTfPC:POT2T (1-1)	4.5	7647	7.3	3.7	(0.396; 0.452)	89	3538
A10	TFB:Ir (piq)₂ (acac) (90:10)/bFPC:POT2T (1-1)	4.6	2986	5.8	2.6	(0.331; 0.516)	60	5080
B10	TFB:Ir (piq)₂ (acac) (90:10)/bTfPC:POT2T (1-1)	4.2	4761	3.8	1.7	(0.316; 0.415)	83	5461

[a] Turn-on voltage at luminance of 10 cd m⁻².
[b] Maximum brightness.
[c] Maximum current efficiency.
[d] Maximum external quantum efficiency.
[e] Commission Internationale de l'Eclairage (CIE) 1931 colour coordinates.
[f] Colour rendering index.
[g] Colour temperature (CIE, CRI and T_C values are related to EL spectra recorded at 9 V).

holes and electrons was mainly situated in the light-emitting layers (EML1), thus in the layers of **bFPC**:PO-T2T or **bTfPC**:PO-T2T. In the hole-transporting layer of TFB doped by Ir (piq)₂ (acac) of low concentration that additionally acted as the second light-emitting layer (EML2), hole and electron recombination was practically not expected because of high energy barrier (1.2 eV) for electrons on TFB/PO-T2T interface and due to favourable hole-transporting properties of compounds **bFPC** and **bTfPC** (Fig. 1c). According to this approach, hole and electron recombination on the low-energy emitter Ir (piq)₂ (acac) was prevented. Contribution of red phosphorescence from Ir (piq)₂ (acac) in devices A and B is expected when triplet excitons generated in EML1 either reach EML2 or recombination of holes and electrons occurs directly in EML2.

EL spectra of devices A and B were characterized by the bands related to the emissions of the different intensities of emitters Ir (piq)₂ (acac), **bFPC**:PO-T2T or **bTfPC**:PO-T2T and TFB (Fig. 4c). The most intensive green exciplex emission was detected for devices A2 and B2 with the lowest concentration of Ir (piq)₂ (acac). Apparently, blue TFB emission was caused by direct recombination of holes and electrons in EML2 and red Ir (piq)₂ (acac) emission resulted from diffusion of triplet excitons from EML1 to EML2. This consideration is supported by stable EL spectra of devices A and B at different external voltages (Fig. 4c). This observation indicates that charge disbalance practically did not occurr in the device structure due to the shift of charge-recombination zone from EML1 to EML2 with increasing applied voltages. With the increase of
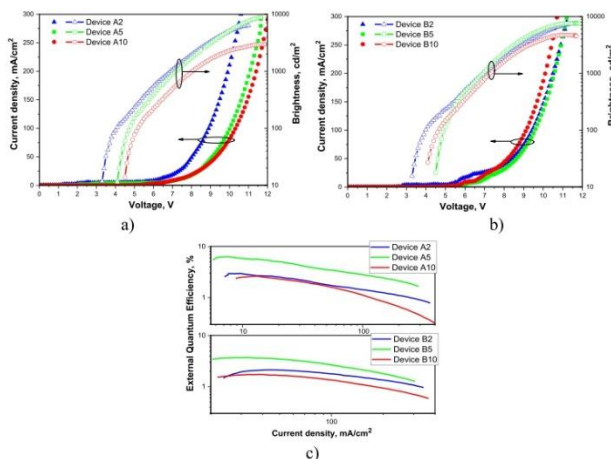
Fig. 5 – Current density/brightness versus applied voltage (a, b), external quantum efficiency versus current density (c) for the studied OLEDs.
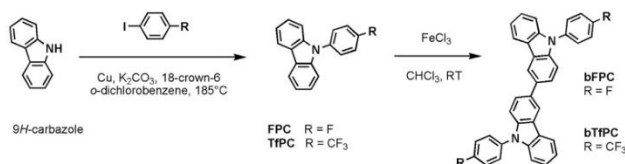
Scheme 1 — The synthetic path to fluoro- and trifluoromethyl-substituted 9,9′-diphenyl-3,3′-bicarbazole derivatives.

concentration of Ir (piq)$_2$ (acac) from 2 to 5%, the most intensive red phosphorescence was detected for devices A5 and B5. The increase of concentration of Ir (piq)$_2$ (acac) to 10% lead to the decrease of intensity of red phosphorescence which apparently was related to quenching of emission due to the triplet–triplet annihilation at high concentration of the emitter [46].

The highest colour rendering index (CRI) of 92 was observed for device A5 demonstrating the best combination of intensities of blue, green and red emissions in its EL spectrum with CIE1931 coordinates of (0.384, 0.399) and colour temperature (T$_C$) of 3655 K attributed to warm white light. The value of CRI is among the best values for white OLEDs [47,48]. Due to the broad emission spectra of the studied exciplexes and contribution of blue emission of TFB and red phosphorescence of Ir (piq)$_2$ (acac) to EL spectra of devices A and B, their CRI values are relatively high (Table 3).

Current density and brightness versus voltage curves are given in Fig. 5a, b. The efficient injection of charge carriers from electrodes and the following transport to emitting layers is confirmed by the low turn-on voltages (3.4–4.6 V) of all the fabricated OLEDs (Table 3). In addition to high quality of white colour of electroluminescence, high EQEs were observed for devices A5 and B5 due to the efficient triplet harvesting on two exciplex-based TADF emitters (bFPC:PO-T2T or bTfPC:PO-T2T) and phosphorescent emitter Ir (piq)$_2$ (acac). The highest maximum power, current, and quantum efficiencies of respectively 5.5 l m/W, 11.6 cd/A and 6.3% were observed for device A5 (Fig. 5c, Table 2). This device also showed the highest brightness of ca. 9000 cd/m^2 at 11.5 V.

4. Conclusions

Using the newly synthesized diphenyl bicarbazoles substituted by electron withdrawing fluoro- or trifluoromethylphenyl units as exciplex-forming donors and 2,4,6-tris [3-(diphenylphosphinyl)phenyl]-1,3,5-triazine as exciplex-forming acceptor, exciplex-forming emitters with efficient thermally activated delayed fluorescence were obtained. Exciplex-forming molecular mixture containing fluoro-substituted diphenyl bicarbazole demonstrated good performance in OLEDs mainly due to high hole mobility of $1.1 \cdot 10^{-3}$ cm^2/V·s at $1.6 \cdot 10^5$ V/cm of and lower activation energy of emission of 52 meV. The newly developed exciplex-forming systems were applied as active components of white hybrid electroluminescent diodes. The devices demonstrated high external quantum efficiency of 6.3% as for

solution processable white OLEDs. High quality of warm-white electroluminescence with colour rendering index of 92, colour temperature of 3655 K and CIE1931 coordinates of (0.384, 0.399) was relatively stable under different voltages.

Declaration of Competing Interest

The authors declare that they have no known competing financial interests or personal relationships that could have appeared to influence the work reported in this paper.

Acknowledgement

Appendix ASupplementary data

REFERENCES

[1] Sarma M, Wong KT. ACS Appl Mater Interfaces 2018;10:19279–304.
[2] Lee JH, Chen CH, Lee PH, Lin HY, Leung MK, Chiu TL, et al. J Mater Chem C 2019;7:5874–88.
[3] Goushi K, Yoshida K, Sato K, Adachi C. Nat Photon 2012;6:253–8.
[4] Jankus V, Data P, Graves D, McGuinness C, Santos J, Bryce MR, et al. Adv Funct Mater 2014;24:6178–86.
[5] Chen D, Liu K, Gan L, Liu M, Gao K, Xie G, et al. Adv Mater 2016;28:6758–65.
[6] Wei X, Liu Y, Hu T, Li Z, Liu J, Wang R, et al. Front Chem 2019;7.
[7] Regnat M, Pernstich KP, Kim KH, Kim JJ, Nüesch F, Ruhstaller B. Adv Electron Mater 2020;6:1–8.
[8] Nakanotani H, Furukawa T, Morimoto K, Adachi C. Sci Adv 2016;2:1–8.
[9] Pu YJ, Koyama Y, Otsuki D, Kim M, Chubachi H, Seino Y, et al. Chem Sci 2019;10:9203–8.
[10] Feng D, Dong D, Lian L, Wang H, He G. Org Electron 2018;56:216–20.

[11] Moon CK, Huh JS, Kim JM, Kim JJ. Chem Mater 2018;30:5648–54.

[12] Chapran M, Pander P, Vasylieva M, Wiosna-Salyga G, Ulanski J, Dias FB, et al. ACS Appl Mater Interfaces 2019;11:13460–71.

[13] Zhang M, Liu W, Zheng CJ, Wang K, Shi YZ, Li X, et al. Adv Sci 2019;6.

[14] Zhang D, Song X, Gillett AJ, Drummond BH, Jones STE, Li G, et al. Adv Mater 2020;32:1–9.

[15] Kreiza G, Banevičius D, Jovaišaitė J, Maleckaitė K, Gudeika D, Volyniuk D, et al. J Mater Chem C 2019;7:11522–31.

[16] Bunzmann N, Weissenseel S, Kudriashova L, Gruene J, Krugmann B, Grazulevicius JV, et al. Mater Horizons 2020;7:1126–37.

[17] Kim KH, Yoo SJ, Kim JJ. Chem Mater 2016;28:1936–41.

[18] Sasabe H, Toyota N, Nakanishi H, Ishizaka T, Pu YJ, Kido J. Adv Mater 2012;24:3212–7.

[19] Shih C-J, Lee C-C, Yeh T-H, Biring S, Kesavan KK, Al Amin NR, et al. ACS Appl Mater Interfaces 2018;10:24090–8.

[20] Al Amin NR, Kesavan KK, Biring S, Lee C-C, Yeh T-H, Ko T-Y, et al. ACS Appl Electron Mater 2020;2:1011–9.

[21] Kalinowski J. Mater Sci Pol 2009;27:735–56.

[22] Hung WY, Chi LC, Chen WJ, Chen YM, Chou SH, Wong KT. J Mater Chem 2010;20:10113–9.

[23] Duan L, Qiao J, Sun Y, Qiu Y. Adv Mater 2011;23:1137–44.

[24] Zieger SE, Steinegger A, Klimant I, Borisov SM. ACS Sens 2020;5:1020–7.

[25] Tonge CM, Paisley NR, Polgar AM, Lix K, Algar WR, Hudson ZM. ACS Appl Mater Interfaces 2020;12:6525–35.

[26] Gauthier S, Fréchet JMJ. Synth Met 1987:383–5.

[27] Vaitkeviciene V, Grigalevicius S, Grazulevicius JV, Jankauskas V, Syromyatnikov VG. Eur Polym J 2006;42:2254–60.

[28] Mallick S, Maddala S, Kollimalayan K, Venkatakrishnan P. J Org Chem 2019;84:73–93.

[29] Bredas JL. Mater Horizons 2014;1:17–9.

[30] Arkhipov VI, Fishchuk II, Kadashchuk A, Bässler H. .. In: Photophysics mol. Mater. Weinheim, FRG: Wiley-VCH Verlag GmbH & Co. KGaA; 2006. p. 261–366.

[31] Ivaniuk K, Cherpak V, Stakhira P, Hotra Z, Minaev B, Baryshnikov G, et al. J Phys Chem C 2016;120:6206–17.

[32] Lin TC, Sarma M, Chen YT, Liu SH, Lin KT, Chiang PY, et al. Nat Commun 2018;9:1–8.

[33] Sych G, Guzauskas M, Volyniuk D, Simokaitiene J, Starykov H, Grazulevicius JV. J Adv Res 2020;24:379–89.

[34] Galievsky VA, Druzhinin SI, Demeter A, Mayer P, Kovalenko SA, Senyushkina TA, et al. J Phys Chem A 2010;114:12622–38.

[35] Rettig W, Zander M. Chem Phys Lett 1982;87:229–34.

[36] Brunner K, Van Dijken A, Börner H, Bastiaansen JJAM, Kiggen NMM, Langeveld BMW. J Am Chem Soc 2004;126:6035–42.

[37] Holmes RJ, Forrest SR, Tung YJ, Kwong RC, Brown JJ, Garon S, et al. Appl Phys Lett 2003;82:2422–4.

[38] Han C, Zhang Z, Ding D, Xu H. Inside Chem 2018;4:2154–67.

[39] Nikolaenko AE, Cass M, Bourcet F, Mohamad D, Roberts M. Adv Mater 2015;27:7236–40.

[40] Yamazaki M. J Mol Catal A Chem 2004;213:81–7.

[41] Wu YC, Yang XF, Hao L. Sensor Actuator B Chem 2017;244:1113–20.

[42] Carraway ER, Demas JN, DeGraff BA, Bacon JR. Anal Chem 1991;63:337–42.

[43] Sekine C, Tsubata Y, Yamada T, Kitano M, Doi S. Sci Technol Adv Mater 2014;15.

[44] Su YJ, Huang HL, Le Li C, Chien CH, Tao YT, Chou PT, et al. Adv Mater 2003;15:884–8.

[45] Arias AC, MacKenzie JD, McCulloch I, Rivnay J, Salleo A. Chem Rev 2010;110:3–24.

[46] Giebink NC, D'Andrade BW, Weaver MS, MacKenzie PB, Brown JJ, Thompson ME, et al. J Appl Phys 2008;103.

[47] Jou JH, Chou YC, Shen SM, Wu MH, Wu PS, Lin CR, et al. J Mater Chem 2011;21:18523–6.

[48] Miao Y, Wang K, Zhao B, Gao L, Tao P, Liu X, et al. Nanophotonics 2018;7:295–304.

93

Bis(N-naphthyl-N-phenylamino)benzophenones as exciton-modulating materials for white TADF OLEDs with separated charge and exciton recombination zones

Malek Mahmoudi [a], Jonas Keruckas [a], Dmytro Volyniuk [a,**], Viktorija Andrulevičienė [a], Rasa Keruckienė [a], Edgaras Narbutaitis [a], Yu-Chiang Chao [b], Martins Rutkis [c], Juozas V. Grazulevicius [a,*]

[a] Department of Polymer Chemistry and Technology, Kaunas University of Technology, Bariausko Str. 59, LT-51423, Kaunas, Lithuania
[b] Department of Physics, National Taiwan Normal University, 88, Sec.4, Ting-Chou Rd., Taipei, 116, Taiwan
[c] Institute of Solid State Physics, University of Latvia, 8 Kengaraga St., Riga, LV-1063, Latvia

ABSTRACT

Organic semiconductors were employed as exciton modulators, blue emitters, hole-transporting materials and hosts with resonant-appropriate singlet and triplet energies for efficient and stable white organic light emitting diodes (OLEDs). Two 4,4'-bis(N-naphthyl-N-phenylamino)benzophenones were synthesized using isomeric N-naphthyl-N-phenylamines as the donors and benzophenone as the acceptor moiety. Molecular design of new compounds allowed to obtain required combination of properties, i.e. blue prompt fluorescence in solid state with singlet energies close to those of the selected blue emitter exhibiting thermally activated delayed fluorescence (TADF), low triplet energies of 2.32 and 2.45 eV which are close to those of orange TADF emitter, good charge injecting properties (ionization potentials of 5.68 and 5.79 eV), good charge transporting properties with hole mobilities exceeding 10^{-4} cm^2 (V s)$^{-1}$ and high thermal stability with five percent weight loss temperatures up to 428 °C. The blue-emitting compounds were used as exciton modulators between the known blue and orange TADF emitters for fabrication of white OLEDs exploiting spatial exciton allocation strategy. In the frame of this strategy, resonant energy transfers: **NPABP** emitters → blue TADF and **NPABP** emitters → orange TADF emitters were investigated using different device structures towards efficient white electroluminescence. About twice higher external quantum efficiency was obtained for devices with two resonant energy transfers in comparison to that of the reference devices with one resonant energy transfer proving efficiency of spatial exciton allocation strategy for white TADF OLEDs. The best quality of white electroluminescence is characterized by CIE coordinates of (0.32, 0.31), colour temperature of 4490 K and colour rendering index of 80. Similar stability of blue and orange emission bands in white electroluminescence spectra was achieved due to the separation of charge and exciton recombination zones in the device structure.

1. Introduction

Organic light-emitting diodes (OLEDs) have been studied in academic institutions and industry for the last thirty years due to their remarkable advantages of flexibility, high contrast, low power consumption, ultrathin device structure, as well as fast on/off responses [1, 2]. Nowadays, white OLEDs (WOLEDs) have been regarded to be one of the most auspicious candidates for meeting the requirements of

high-quality displays and energy-efficient lighting [3,4]. Since the pioneer WOLEDs made by Kido and his colleagues, WOLED technology is incredibly developed. [5,6] During the past two decades, the power efficiency (PE) of WOLEDs was enhanced and exceeded 100 lm W^{-1} [7–9]. In regards to lighting applications, WOLEDs should meet the requirement of high efficiency, long lifetime and bright luminance [10–12]. In the meantime, the color rendering index (CRI) above 80 is more appropriate for the indoor lighting and the Commission

---

* Corresponding author.
** Corresponding author.
E-mail addresses: dmytro.volyniuk@ktu.lt (D. Volyniuk), juozas.grazulevicius@ktu.lt (J.V. Grazulevicius).

International de L'Eclairage (CIE) chromaticity coordinates of WOLEDs need to be settled near white light equal-energy point (0.33, 0.33) [13, 14]. Other parameters, such as color stability and correlated color temperature (CCT) of WOLEDs also should be taken into account for developing of high-quality lighting devices [15].

WOLEDs can be fabricated by mainly using materials exhibiting fluorescence, phosphorescence or thermally activated delayed fluorescence (TADF) [16]. Phosphorescent materials are the dominant candidates due to their potential for achievement of 100% internal quantum efficiency [17]. However, negligible number of blue phosphorescent materials could be regarded as suitable candidates for WOLEDs so far owing to the high energy gap which leads to problems in maintaining color stability and finding appropriate host matrices [18,19].

Fluorescent/phosphorescent hybrid WOLEDs combining blue fluorophores and green/red (or yellow) phosphors are considered to be more acceptable for possible applications due to their technological benefit of high efficiency and high stability [20,21]. To reach the device efficiency equal to the theoretically expected value, efficient approaches were proposed for overcoming problems attributed to the energy loss during the energy transfer mechanism and exciton quenching in WOLEDs. A significant breakthrough in the efficiency of hybrid fluorescent/phosphorescent WOLEDs and reducing energy loss was made by Sun et al. [22]. An important stage in the development of this kind of devices is the selection of a proper host spacer (exciton modulator), the layer of which is located between the layers of fluorescent emitter and phosphorescent or TADF emitters. Playing the crucial role in hybrid WOLEDs, exciton modulators can not only minimize Forster energy transfer from blue fluorescent emitter to red-green/orange TADF emitters but also prevent non-radiative Dexter energy transfer between the two layers. Moreover, emission color and color quality can also be tuned by changing the thickness of spacers [23]. This approach (so-called "spatial exciton allocation strategy" [24]) has potential also for TADF WOLEDs. One of the aims of this work was to prove it. The improvement of both efficiency and stability of WOLEDs can be reached by reasonable design of the structures of devices [25].

TADF of fully organic emitters has attracted attention of researchers as a promising route to harvest non-radiative triplet excitons in OLEDs. [26,27] Theoretically, the internal quantum efficiency of the TADF-based OLEDs can reach 100% since both singlet and triplet excitons of TADF materials can be exploited for light emission [28,29]. As a result, triplet states can be harvested as delayed fluorescence using effective reverse intersystem crossing (RISC) through their up-conversion from a lowest triplet state to a lowest singlet state. Recently, there have been several significant types of research on TADF-based hybrid WOLEDs. Their efficiencies have been step-by-step enhanced [30,31]. Until now, hybrid TADF/phosphorescent WOLEDs can achieve external quantum efficiency (EQE) of ca 20% [32], which is close to that of thoroughly designed phosphorescent WOLEDs. Purely TADF-based WOLEDs are also known [33–35]. To the best of our knowledge, spatial exciton allocation strategy was not used yet for purely TADF WOLEDs.

Herein, aiming to demonstrate the potential of the spatial distribution of singlet and triplet excitons between blue and orange TADF emitters, purely TADF WOLEDs were designed using two newly synthesized compounds (**NPABP1** and **NPABP2** in Scheme 1) as exciton modulators. Two types of device structures with one resonant blue-→orange energy transfer (RET1) or with two resonant blue→orange (RET1) and blue→blue energy transfers (RET2) were investigated in the frame of spatial exciton allocation strategy for the first time for purely TADF-based WOLEDs (Fig. 1). In the structures of WOLEDs, hole-electron recombination zone (exciton generation zone) can be formed within exciton-modulating layer (EModL). In this case, the first singlet (S_1) and first triplet (T_1) levels of EModL are respectively equal to S_1 of blue TADF emitter (TADF2) and to T_1 of orange TADF emitter (TADF1). Two resonant energy transfers (RET2 and RET1) are possible. Thus, separation of hole-electron recombination zone and exciton
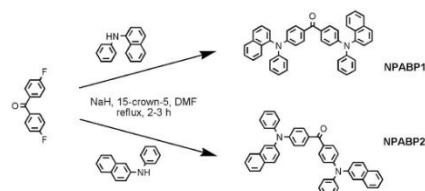
Scheme 1. Synthesis of 4,4'-bis(*N*-naphthyl-*N*-phenylamino)benzophenones (**NPABPs**).
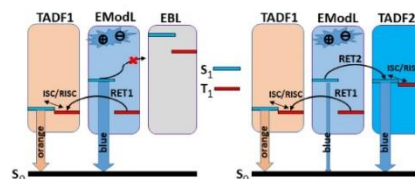

Fig. 1. Schematic Jablonski diagrams for light-emitting systems of white OLEDs based on one (left) and two (right) resonant energy transfers. The given schematic Jablonski diagrams do not show all possible energy transfers, just resonant ones between the respectively equal energy levels S1–S1 and T1-T1 are shown.

recombination zone can be realized within three layers when efficient RET1 and RET2 are achieved. In the case when exciton blocking layer (EBL) is used, RET2 can be restricted allowing to study the effect of one or two resonant energy transfers on out-put parameters of white devices.

Taking into account S_1 and T_1 values of **NPABP1** and **NPABP2** which are in good agreement with S_1 of blue and T_1 of orange TADF emitters, they were used for EModLs in the device structures of purely TADF-based WOLEDs described above. As the proof of the concept, devices with two resonant energy transfers showed approximately twice higher values of maximum EQE in comparison to that of devices with one resonant energy transfer. This observation shows that all singlet and triplet excitons were harvested along completely independent channels and therefore nearly resonant energy transfer from host (either from singlet or from triplet states) to dopants was achieved.

2. Results and discussion

2.1. Synthesis and characterization

Two new compounds, 4,4'-bis(*N*-naphthyl-*N*-phenylamino)benzophenones were prepared by nucleophilic substitution reaction of 4,4'-difluorobenzophenone with *N*-naphthyl-*N*-phenylamines (either 1- or 2-) in refluxing *N*,*N*-dimethylformamide (DMF) using NaH as a base together with 15-crown-5 (Scheme 1). After all the purification procedures, the products were obtained in satisfactory yields of ca. 60 and 70%. The materials showed good solubility in chloroform and THF.

The theoretical geometries of **NPABP1** and **NPABP2** presented in Fig. 2 demonstrate that (*N*-naphthyl)-*N*-phenylamino and benzophenone fragments have propeller-like structure. The naphthalene moiety shows dihedral angle of 57° and −45° with respect to N–C bond in **NPABP1** and **NPABP2**, respectively. In the case of **NPABP2**, the phenyl and benzophenone fragments are more twisted with respect to the N–C bond comparing to the analogous moieties of **NPABP1**. These structural differences result in the different spatial distribution of electron density.
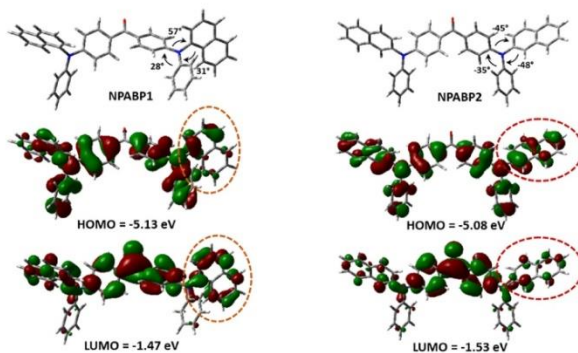
Fig. 2. Theoretical geometries and frontier molecular orbitals of **NPABP1** and NPABP2 (B3LYP/6-31d,p).
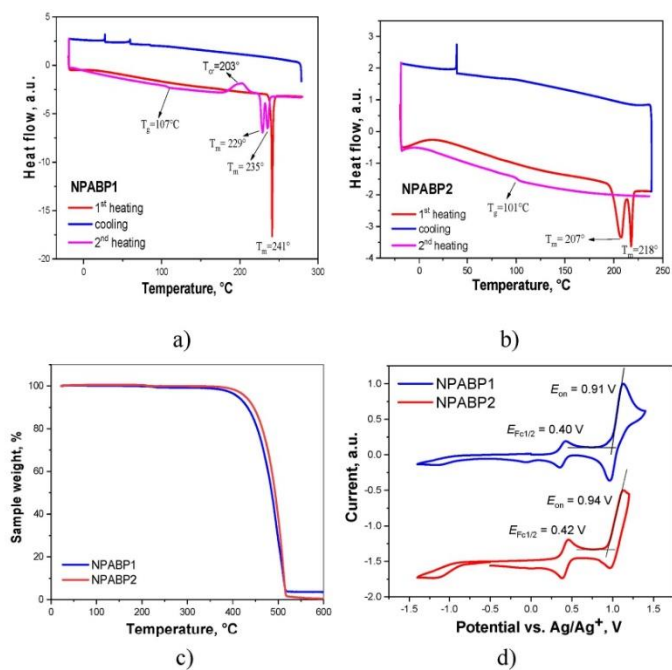

Fig. 3. DSC trace of **NPABP1**(a), DSC curves of NPABP2 (heating and cooling rates 10 °C/min) (b), TGA curves of **NPABP1** and NPABP2 compounds (heating rate 20 °C/min) (c), Cyclic voltammetry (CV) curves of **NPABP1** and **NPABP2** dilute solutions in dichloromethane at room temperature (d).

3

The highest occupied molecular orbitals (HOMO) of both compounds are localized on the whole molecular backbone. However, **NPABP2** has a smaller distribution of electronic cloud of HOMO on naphthalene moiety comparing that with **NPABP1**. Accordingly, the HOMO level of **NPABP1** (-5.13 eV) is somewhat lower compared to that of **NPABP2** (-5.08 eV). The lowest unoccupied molecular orbitals (LUMO) of the compounds are localized over electron deficient benzophenone fragment with a larger contribution from the naphthalene substituent in **NPABP1**. The LUMO levels of **NPABP1** and **NPABP2** are -1.47 eV and -1.53 eV, respectively.

Compounds **NPABP1** and NPABP2 are characterized by close melting points (of ca. 240 and 220 °C respectively) and close glass-transition temperatures (T_g) slightly above 100 °C, as measured by DSC (Fig. 3 a, b). Compound **NPABP1**, which contains naphthalene moieties attached at 1- position, has a higher tendency to crystallize from its melt (an exothermic ridge at ca. 200 °C). However, just after the crystallization, it shows double DSC melting peak which might appear due to different crystalline forms. Theoretical calculations revealed that **NPABP1** can adopt different conformers with energy differences of less than 0.5 kcal/mol (Fig. S1). The conformers of **NPABP1** may lead to the formation of two types of crystalline forms. NPABP2 also shows double melting. The **NPABP2** showed slightly lower melting point and T_g value as well as stable molecular glass (at least during DSC measurements). Both compounds exhibit high thermal stability as indicated by TGA experiments (Fig. 3c). Their 5% weight-loss temperatures are above 400 °C. Complete weight loss observed by TGA indicates sublimation of the compounds.

As it can be seen from cyclic voltammetry (CV) results, both

compounds were oxidized irreversibly nearly at the same potential (Fig. 3d). Their oxidation potentials vs. ferrocene standard are established as $+0.51$ V for **NPABP1** and $+0.52$ V for **NPABP2** (see ESI for more details). The data were in quite good agreement with their solid-state IP values which situate near 5.7 and 5.8 eV, respectively. Any waves of electrochemical reduction were not observed. The measured IP value of **NPABP2** was slightly larger comparing to that of **NPABP1**. Probably, the trend of HOMO energies is not consistent with the trend of IP due to possibility of the molecules to form various conformers. The CV data and frontier molecular orbitals of **NPABP1** and NPABP2 imply that the molecular orbitals of donor and acceptor units are not separated well enough and therefore balanced bipolar charge transport or TADF properties are hardly expectable.

To investigate the photophysical properties of compounds **NPABP1** and NPABP2, steady-state UV−VIS absorption and photoluminescence spectra of their dilute solutions ($\sim10^{-5}$ M in toluene and THF) and of solid layers were recorded (Fig. 4a, for the summarized data see Table 1). Theoretical calculations using TDDFT were performed to identify the nature of the experimental absorption bands of **NPABP1** and NPABP2. The absorption bands with maxima at 366 and 375 nm observed in the UV spectra of THF solutions of **NPABP1** and NPABP2, respectively, correspond to the electron transition from HOMO to LUMO (Figure S2 a). The lowest energy absorption band of NPABP2 is red shifted in comparison with that of NPABP1 due to the different position of attachments of naphthalene moiety as seen in Fig. 2. The additional energy band around 312 nm can be identified in the high-energy region of absorption spectra of the solutions of compound NPABP2. However, it was not observed in the spectra of the solutions of **NPABP1**. Based on the

a)

b)

c)   d)   e)
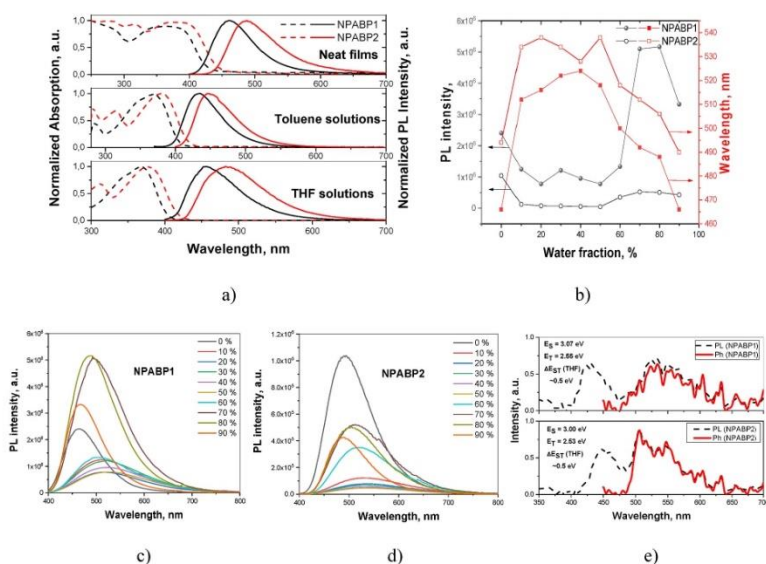
Fig. 4. Normalized absorption (left) and photoluminescence spectra (right, $\lambda_{exc} = 330$ nm) (a), PL maximum intensities versus water volume fraction of the dispersions of the compounds in THF/water mixtures (left) and wavelength versus water fraction for the dispersions of the compounds in the mixtures of THF and water (right)(b); PL spectra of the dispersions of **NPABP1** (c) and **NPABP2** in the THF/water mixtures (d), PL and phosphorescence spectra for the dilute THF solutions of the compounds recorded at 77 K (e).

4

Table 1

Thermal, electrochemical, photoelectrical, hole-transporting and photophysical parameters of **NPABP1** and **NPABP2**.

Property	Sample	NPABP1	NPABP2
T_m, °C	Powder	218	241
T_g, °C		101	107
T_{cr}, °C		203	–
$T_{de-5\%}$, °C		411	428
$E_{ox\ vs}$ Ag/Ag$^+$, V	DCM solution with	0.91	0.94
IP_{CV}, eV	TBAPF$_6$	5.71	5.74
IP_{PE}, eV	Film	5.68	5.79
E_g^{opt}, eV		2.89	2.78
EA_{PE}, eV		2.79	3.01
λ^{PL}, nm	Film (THF solution)	462 (456)	488 (482)
λ^{abs}, nm		368 (366)	375, 314, 281 (375, 312)
PLQY, %		12 (9)	13 (18)
E_{S1}^{THF}, eV	THF solution at 77 K	3.07	3.00
E_{T1}^{THF}, eV		2.55	2.53
ΔE_{S1T1}^{THF}, eV		0.52	0.47
μ_{holes},[a] cm^2/(V × s)	Film	1.8×10^{-4}	3.5×10^{-4}
μ_0, cm^2/(V × s)		5.8×10^{-7}	4.6×10^{-6}
β, (cm/V)$^{0.5}$		8.2×10^{-3}	6.25×10^{-3}

[a] at electric field of 5×10^5 V/cm.

theoretical results, this band can be attributed to the combination of electronic transitions towards S_8 and S_9 excited states. According to the natural transition orbitals (NTOs) shown in Fig. S2 b, the transitions $S_0{\rightarrow}S_8$ and $S_0{\rightarrow}S_9$ of NPABP2 can be characterized as the local electronic excitations. The optical band gaps were evaluated from the onset wavelength of optical absorption spectra by the formula $E_g = 1240/\lambda_{edge}$, in which λ_{edge} is the onset wavelength of absorption spectrum in the longwave direction. The absorption onset wavelengths of **NPABP1** and NPABP2 were found to be 429 and 446 nm, which correspond to the optical band gaps of 2.89 and 2.78 eV, respectively (Fig. 4a, Table 1).

The THF solutions of **NPABP1** and NPABP2 exhibited blue emission with the intensity maxima at 462 nm and 488 nm with Stoke's shifts of 90 and 107 nm respectively. The Stoke's shifts of 94 and 113 nm were found for the emission of neat films of derivatives **NPABP1** and NPABP2, respectively. A small difference of 22 nm and 34 nm between the wavelengths of PL maxima of toluene and THF solutions of NPABP1 and NPABP2, respectively, confirms a weak intramolecular charge transfer between the donor and acceptor moieties [36]. Prompt fluorescence was observed for **NPABP1** and NPABP2. Their PL decays of their toluene solutions and solid films were in nanosecond region and were practically not sensitive to the presence of oxygen (Figs. S3 and S4).

PLQY values of the solid films of compounds **NPABP1** and NPABP2 were found to be higher than those of toluene solutions. This observation can apparently be attributed to aggregation-induced emission enhancement (AIEE) which may be observed owing to the constraint of movements (restriction of rotation and vibration) of molecular units in the solid-state leading to the reduction of nonradiative decay [37]. To confirm this assumption, fluorescence spectra of the compounds dispersed in the THF/water co-solvent system with different water volume fractions (F_W) were recorded (Fig. 4 b–d, S3). Relative dependencies of PL intensities (left) and wavelengths (right) of PL peaks versus water fractions for the dispersions of compounds **NPABP1** and NPABP2 are shown in Fig. 4b. Upon increasing water fraction up to ca. 40–50%, emission intensity gradually decreased and PL maximum wavelength red-shifted until the aggregates were formed (Fig. 4 c,d). These effects could arise from increasing polarity of the THF-water mixtures to which fluorescence (which resulted from recombination of intramolecular charge transfer states) is very sensitive. The increase of F_W leads to the increase of emission intensity and blue shifts of PL spectra owing to the increasing amount of aggregates. However, upon a

further increase of the water fraction from 80% to 90%, maximum emission intensity of compounds began to decrease. Similar observation was previously observed for compounds with AIEE effects causing by the precipitation of big-size aggregates in cuvette with the THF/water mixture. [38,39].

To further investigate the photophysical properties of **NPABP1** and NPABP2, photoluminescence (PL) and phosphorescence spectra of their THF solutions were recorded at the liquid nitrogen temperature (Fig. 4e.) The S_1 (E_S) and T_1 (E_T) energies were obtained from the onsets of the fluorescence and phosphorescence spectra, respectively. They are summarized in Table 1. Phosphorescence of the compounds is mainly related to the LE^3 emissive recombination of triplet state of N-naphthyl-N-phenylamine moiety [40]. It should be pointed out that compounds **NPABP1** and NPABP2 were characterized by nearly the same singlet-triplet splitting of 0.5 eV. The singlet and triplet values of **NPABP1** and NPABP2 are appropriate for resonant blue→orange and blue→blue energy transfers as it will be discussed in the device section.

A photoelectron emission spectroscopy method was employed to establish the ionization potentials (IP$_{PE}$) of the solid films of the compounds. IP$_{PE}$ of 5.68 eV was observed for the film of **NPABP1** and 5.79 eV for the film of NPABP2 indicating good hole-injecting properties (Fig. 5a, Table 1). These IP$_{PE}$ values are in very good agreement with corresponding IP$_{CV}$ values. Subtracting of the optical band gaps taken for films from IP$_{PE}$ values, electron affinities (EA$_{PE}$) of 2.79 and 3.01 eV were obtained for **NPABP1** and NPABP2 showing also good electron-injecting properties (Table 1).

The vacuum-deposited films of **NPABP1** and NPABP2 sandwiched between ITO and Al electrodes were used for estimation of charge-transporting properties by time of flight (TOF) method [41]. When positive voltage was applied to ITO electrode through which the layers were excited by laser beam, transit times (t_{tr}) were well seen for holes proving the hole-transport in both **NPABP1** and NPABP2 (Fig. 4b, insets). In contrast, electron-transport was not detected in the compounds by TOF measurements. The transit times were not observed when negative voltages were applied to ITO. At the same electric field (E) of ca. 5×10^5 V/cm, about twice higher transit time (t_{tr}) of 4.51 µs was obtained for **NPABP1** than for NPABP2 (1.78 µs) indicating more efficient hole transport in NPABP2 (Fig. S6a). As a result, about twice higher hole mobility (μ_h) of 3.5×10^{-4} cm^2/V × s was calculated for **NPABP2** than for NPABP1 (1.8×10^{-4} cm^2/V × s) at the same electric field (Fig. 5b, Table 1). Taking into account the similar shapes and lengths of the tails of the TOF signals at the same electric fields (Fig. S6), both the compounds demonstrated similar dispersive character of hole transport. Predictively, electric field hole mobility dependences of **NPABP2** and NPABP1 were in very good agreement with the Poole–Frenkel type mobility ($\mu = \mu_0 e^{\beta E^{1.2}}$ (1)) [42]. According to the fitting by formula (1), zero-field hole mobilities (μ_0) of 5.8×10^{-7} and 4.6×10^{-6} cm^2/V × s and field dependence parameters (β) of 8.2×10^{-3} and 6.25×10^{-3} (cm/V)$^{0.5}$ were obtained for NPABP2 and NPABP1, respectively (Table 1). Such relatively high values of field dependence parameters are typically observed for dispersive charge-transport [43]. The above described differences in hole mobility parameters of **NPABP2** and **NPABP1** result from their different HOMO distributions as well as HOMO-HOMO overlapping between neighboring molecules in the solid films (Fig. 2).

Compounds **NPABP1** or NPABP2 were identified as hole transporters by the TOF measurements (Fig. 5b). Meanwhile, electron-transporting abilities were not observed for them by TOF. It is worth to note that electron-transporting properties were previously detected for conventional organic hole transport layers of 4,4'-bis[N-(1-naphthyl)-N-phenylamino]biphenyl (NPB) despite absence of electron-accepting moieties in their molecular structures [44]. Thus, having the electron-accepting benzophenone moiety in the molecular structures, electron-transporting properties were expected for **NPABP1** or **NPABP2**. To additionally investigate the charge-transporting properties of the synthesized compounds, the hole only devices (HODs) and
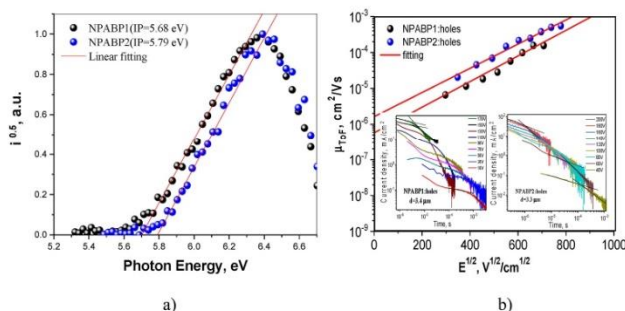
Fig. 5. Electron photoemission spectra of the solid samples of **NPABP1** and **NPABP2** (a) and their hole mobility dependences on electric field. Insets: TOF pulses for holes in the deposited layers of compounds **NPABP1** and **NPABP2** recorded at different electric fields (b).

electron only devices (EODs) were fabricated and studied comparing the results with those of the corresponding devices based on well-known hole-transporting compound NPB. Comparison of the voltage-current density characteristics of the corresponding HODs and EODs based on **NPANP1** and **NPABP2** (Fig. S7), shows that their hole-transporting properties are considerably better than their electron-transporting properties which is in very good agreement with the results of TOF measurements. Meanwhile, electron-transporting properties of NPB were better than those of **NPANP1** and **NPABP2**.

2.2. White organic light-emitting diodes

Taking into account the hole transporting properties, S_1/T_1, and HOMO/LUMO values of **NPABP1** and **NPABP2**, they were used for the preparation of exciton modulator layers in one or two TADF emitters (orange 4CzTPN and blue PFBP-2b) based WOLEDs with separated hole-electron recombination and exciton recombination zones. For comparison, two devices with the structures ITO/MoO₃ (8 nm)/NPB(60 nm)/TAPC(5 nm)/EML/TSPO1(8 nm)/TPBi(40 nm)/LiF (1 nm)/Al (Devices IA(B)1–3) and ITO/MoO₃(8 nm)/NPB (60 nm)/TAPC(5 nm)/EML/PFBP-2b (20 wt%):TPBi (40 nm)/LiF(1 nm)/Al (Devices IIA(B)1–3) were fabricated. Abbreviations of all functional materials are unclosed in the Supporting Information. The names of devices contain signs "I(II)" which are respectively related to the first(second) device families, "A (B)" to **NPABP1(NPABP2)**, "1–3" are related to three different light-emitting layers (EML) (Fig. S8). The first device structure (I) contained exciton blocking layer TSPO1 between EML and electron transporting layer of TPBi. Devices IA1, IB1, IIA1, and IIB1 are based on guest:host type EML of 4CzTPN(5 wt%):**NPABP1(NPABP2)** (20 nm) where **NPABP1** and **NPABP2** are the hosts for 4CzTPN. Devices IA2, IB2, IIA2, and IIB2 are based on bi-layered guest:host/EML of 4CzTPN (5 wt%):**NPABP1(NPABP2)**(5 nm)/**NPABP1(NPABP2)**(15 nm) where doping-free layers of **NPABP1** or **NPABP2** were additionally used as exciton modulators.

Devices IA3, IB3, IIA3, and IIB3 were based on bi-layered dopant-free EML of 4CzTPN(1 nm)/**NPABP1(NPABP2)**(15 nm) where dopant-free layers of **NPABP1** or **NPABP2** was also used as the exciton modulators. The electron-transporting layer of PFBP-2b (20 wt%):TPBi (40 nm) of devices IIA1, IIA2, IIA3 and IIB1, IIB2, IIB3 were doped by sky-blue TADF emitter PFBP-2b aiming to obtain RET from EML to PFBP-2b.
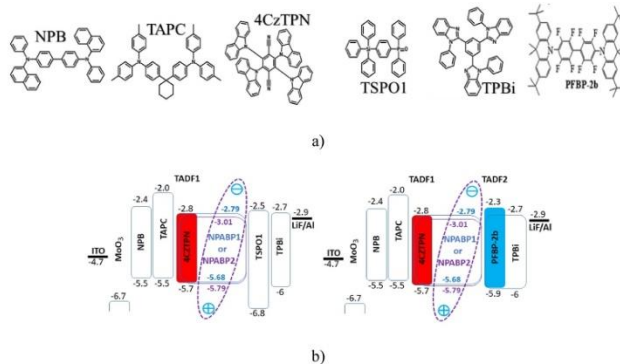

Fig. 6. Abbreviations of functional materials (a) as well as equilibrium energy diagrams (b) with (left) and without (right) exciton-blocking layer of TSPO1.

6

The names and detailed structures of all fabricated OLEDs are collected in Table S1. The role of layer MoO₃ is widely known [45]. Hole-transporting layers of NPB and TAPC were used to inject holes to EML of **NPABP1**(**NPABP2**) within which hole-electron recombination zone is expected as it can be concluded analysing equilibrium energy diagrams of the devices (Fig. 6b). High LUMO (−2.0 eV) of TAPC allowed to block electrons within EMLs. The hole-electron recombination zone should be placed close to electron-blocking layer in the case of devices IA(B)1–3 (electron-transporting layer in the case of devices IIA (B)1–3) due to the hole-transporting properties of **NPABP1**(**NPABP2**) (Fig. 5b).

Compound 4CzTPN was selected as orange TADF emitter taking into account its TADF properties, HOMO/LUMO values and T₁ (2.44 eV) which is very close to T₁ of **NPABP1** and **NPABP2**, (2.55 and 2.53 eV, respectively) (Table 1) [46]. Thus, the combination of **NPABPs** and 4CzTPN forms an excellent triplet energy resonance T₁(**NPABP1** or **NPABP2**)→T₁(4CzTPN) which can cause an efficient Dexter energy transfer between them. In addition, compounds **NPABP1** and **NPABP2** with wide band-gaps (ca. 2.8 eV) can be used as hosts for 4CzTPN (Fig. 6b). Compound PFBP-2b was selected as sky-blue TADF emitter taking into account its TADF properties, HOMO/LUMO values and S₁ (2.86 eV) which is very close to S₁ of **NPABP1** and **NPABP2**, which were found to be of 3.06 and 3.0 eV, respectively (Table 1) [47]. Thus, the combination of **NPABPs** and PFBP-2b forms an excellent singlet energy resonance S₁(**NPABP1** or **NPABP2**)→S₁(PFBP-2b) which can cause an efficient Förster resonance energy transfer between them [48]. Exploiting systems 4CzTPN/**NPABPs**/PFBP-2b, WOLEDs with separated hole-electron recombination and exciton recombination zones can be predictively fabricated as it is schematically shown in Fig. 1. PFBP-2b showed strongly dispersive hole transport as it was previously reported [47]. Electron transport was not detected for PFBP-2b by the TOF measurements. Thus, PFBP-2b acts as the TADF emitter in the TPBi: PFBP-2b layer. Electron-transport properties of the layer of TPBi: PFBP-2b should be even worse than those of the layer of TPBi taking into account that molecules of PFBP-2b act as additional traps.

Indeed, devices IA2, IB2, IIA2, and IIB2 were characterized by white electroluminescence (EL) (Fig. 7a insets, S9). Their EL spectra contain two emission bands of different intensities which correspond to blue emission of **NPABP1** or NPABP2 (and PFBP-2b in the case of devices IIA2, and IIB2) and to orange emission of 4CzTPN, respectively (Fig. 7a). This observation proves that the hole-electron recombination zone is mainly placed within dopant-free layer of **NPABP1** or NPABP2 causing good exciton modulation between high-energy blue (either **NPABP1**, NPABP2 or PFBP-2b) and low-energy orange (4CzTPN) emitters. It should be noted that the contribution of emitter PFBP-2b (thus S₁(**NPABP1** or NPABP2)→S₁(PFBP-2b) RET) is evident since maximum EQE values of devices IIA2 and IIB2 are approximately twice higher than those of devices IA2 and IB2 (Fig. 7b, Table 2).

In contrast, devices IA1, IB1, IIA1, and IIB1 demonstrated orange EL from EML of 4CzTPN:**NPABP1**(NPABP2). Meanwhile, devices IA3, IB3, IIA3, and IIB3 showed mainly blue EL due to inefficient RET between the layers of **NPABP1**(NPABP2) and 4CzTPN. The band related to 4CzTPN is more intensive for devices IA3 and IB3 than for devices IIA3 and IIB3. This observation can be explained by additional contribution of PFBP-2b to blue emission resulting in more intensive high-energy blue band. If to plot a line between Commission Internationale de I'Eclairage (CIE)
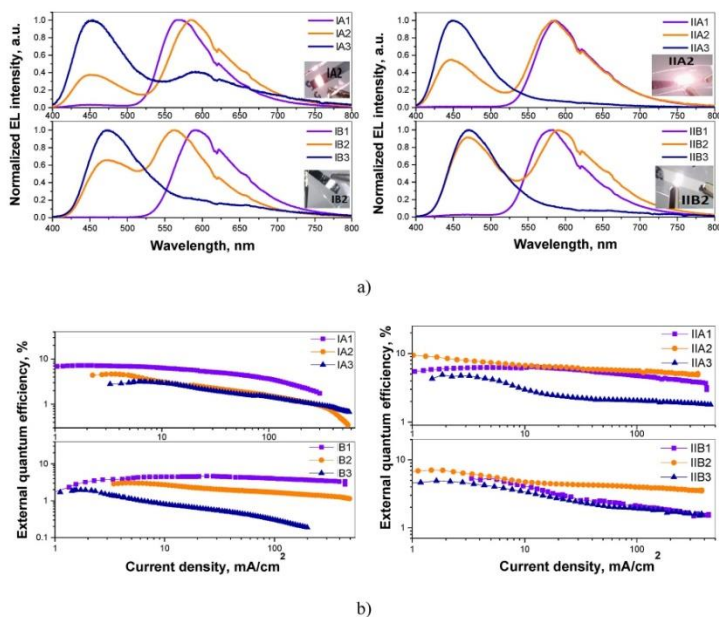

a)

b)

Fig. 7. EL spectra at 9 V (a) and external quantum efficiency versus current density curves of the studied devices (b). Insets: photographs of WOLEDs at 9 V.

7

100

Table 2
Electroluminescent parameters of white OLEDs.

Device	V_{on},[a] V	Max. brightness, cd/m^2	CE_{max}, cd/A[b]	EQE_{max}, %[c]	CIE (x; y)[d]	CRI[e]	T_C, K[f]
First device family (IA1- IB3)							
IA1	4.7	23680	20.8	7.2	(0.47, 0.49)	42	2932
IA2	4.2	6163	10.2	4.8	(0.40, 0.35)	60	2751
IA3	5.1	1351	3.9	3.1	(0.26, 0.22)	75	12520
IB1	5.9	12340	9.4	4.7	(0.55, 0.44)	41	1840
IB2	5.7	8409	8.3	3.1	(0.36, 0.42)	62	4220
IB3	4.6	1015	3.7	1.9	(0.20, 0.26)	–	–
Second device family (IIA1- IIB3)							
IIA1	4.2	22644	13.7	6.3	(0.53, 0.45)	40	2061
IIA2	3.9	29922	18.6	9.5	(0.36, 0.31)	67	3332
IIA3	4.6	5482	8.1	4.7	(0.16, 0.13)	–	–
IIB1	4	17868	12.4	5.5	(0.49, 0.47)	43	2515
IIB2	3.6	15350	13.8	7.1	(0.32, 0.31)	80	4490
IIB3	3.3	5700	7.8	4.9	(0.17, 0.22)	–	–

[a] Turn-on voltage at luminance of 10 cd m^{-2}.
[b] Maximum current efficiency.
[c] Maximum external quantum efficiency.
[d] Commission Internationale de l'Eclairage (CIE) 1931 colour coordinates.
[e] Colour rendering index.
[f] Colour temperature (CIE, CRI and T_C values are related to EL spectra recorded at 9 V).

coordinates of blue and orange devices, it is seen that CIE coordinates of WOLEDs with close to natural white values of (0.33, 0.33) can be achieved (Fig. S10). This observation proves good selection of blue and orange emitters for getting white electroluminescence by mixing their individual emissions. The CIE coordinates of (0.32, 0.31) closest to the natural white light were obtained for device IIB2 (Table 2). This device also showed the highest color rendering index (CRI) of 80 and color temperature (T_C) of 4490 K. This observation can be attributed to the very good quality of white EL based on only two emitters. Devices IA2 and IIA2 were characterized by T_C values of 2751 and 3332 K

a)

b)

c)
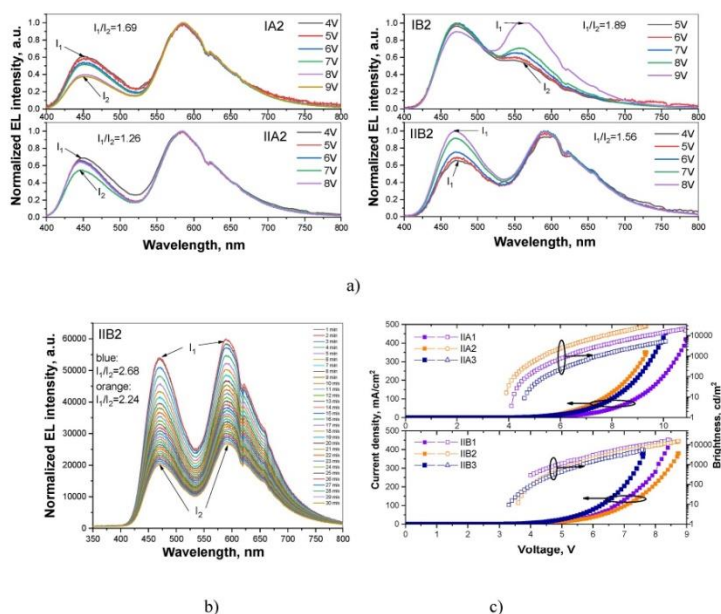
Fig. 8. EL spectra of white OLEDs at different voltages (a), EL spectra of non-passivated device IIB2 in air at continues voltage of 9 V recorded with time step of 1 min (b), and current density/brightness versus applied voltage dependences of the second family of devices (c).

8

101

respectively which show eye-friendly warm white light emission.

In should be noted, that the better stability of EL spectra under different voltages was obtained for devices IIA2 and IIB2 than for devices IA2 and IB2, respectively (Fig. 8a). For example, the lower ratio of EL intensities I_1/I_2 of 1.26 was obtained for device IIA2 than for device IA2 which showed I_1/I_2 of 1.69 (I_1 and I_2 are the intensities of the selected EL band at different voltages (Fig. 8a)). This result is attributed to the better separation of charge and exciton recombination zones in devices IIA2 and IIB2 than in devices IA2 and IB2 with EBL. The relative stability of blue and orange EL were additionally checked for device IIB2 with the best quality of white EL recording its EL spectra under continuous voltage of 9 V in air without passivation (Fig. 8b). The similar ratios I_1/I_2 2.68 and 2.24 were obtained for the blue and the orange bands of EL spectra of device IIB2 recorded after 1 and 30 min of continuous work. This result can be attributed to the similar stability of blue and orange TADF emitters when spatial exciton allocation strategy is utilized, thus charge and exciton recombination zones are well separated. The similar EL spectra were recorded at different voltages for the corresponding single-color devices (Fig. S8).

As it was noted above, maximum EQE values of devices IIA2 and IIB2 with exciton distribution (modulation) between two TADF emitters (4CzTPN and PFBP-2b) are approximately twice higher than maximum EQE values of devices IA2 and IB2 with exciton distribution (modulation) between **NPABP1**(**NPABP2**) and 4CzTPN (Fig. 7b, Table 2). This result indicates contribution of PFBP-2b to the total efficiency of IIA2 and IIB2. Contribution of PFBP-2b is also evident if to compare maximum EQEs of blue devices from the first (IA3 and IB3) and the second (IIA3 and IIB3) families of devices. For example, about twice lower maximum EQE of 1.9% was obtained for device IB3 than for device IIB3 (4.9%). In contrast, close maximum EQE values of the orange devices of the first (IA1 and IB1) and the second (IIA1 and IIB1) families were obtained. This observation can be explained by the prevailing contribution of orange emission of 4CzTPN in both cases. For example, close maximum EQE values of 4.7 and 5.5% were obtained for devices IB1 and IIB1 showing the similar charge recombination abilities of the first and the second families of devices. Approximately twice higher efficiency of white OLEDs IIA2 and IIB2 in comparison to that of white OLEDs IA2 and IB2 can be mainly attributed to exciton movement (resonant energy transfers) from exciton modulator layer (**NPABP1** or **NPABP2**) to TADF emitters (PFBP-2b and 4CzTPN) due to the similarities of S_1(**NPABP1** or **NPABP2**) with S_1(PFBP-2b) and of T_1(**NPABP1** or **NPABP2**) with T_1(4CzTPN).

Lower turn-on voltages of 3.3–4.6 V were observed for **NPABP2** based devices than turn-on voltages (4.2–5.9 V) of **NPABP1** based devices (Fig. 8c, Table 2). This result is in very good agreement with the results of the measurements of charge mobilities, which showed higher hole mobilities of **NPABP2** at the same electric fields (Fig. 5b). One more exploitation in favor of spatial exciton allocation strategy for TADF-based OLEDs is higher maximum brightness observed for devices IIA2 and IIB2 relative to that of devices IA2 and IB2. It exceeded 10000 cd/m^2. Taking into account the above presented analyses of output parameters of white devices from the first (IA2 and IB2) and the second (IIA2 and IIB2) families, it can be concluded that the significant performance improvement of white TADF OLEDs is due to the effective separation of charge and exciton recombination zones with minimized energy losses during energy transfer processes. This approach allows to get more stable blue emission in the total white EL of TADF-based OLEDs needed for illumination and display back lighting technologies. In addition, the developed exciton modulators **NPABP1** and **NPABP2** can be used in combination with even more efficient blue and orange TADF emitters for getting even more efficient WOLEDs.

3. Conclusions

Motivated to develop exciton-modulating functional materials for white TADF-based OLEDs, two new bis(N-naphthyl-N-phenylamino)

benzophenones were synthesized. They were characterized by blue aggregation-enhanced emission, triplet energies of 2.32–2.45 eV, ionization potentials of 5.68–5.79 eV, hole mobilities exceeding 10^{-4} cm^2 (V s)$^{-1}$ at high electric fields and five percent weight loss temperature reaching 428 °C. They were used as exciton modulators for the fabrication of white TADF-based OLEDs with one or two TADF emitters. After hole-electron recombination/exciton generation within the dopant-free exciton-modulating layers, excitons were efficiently transferred either to one orange or to both orange and blue TADF emitters distributed as guests in neighboring layers separating charge and exciton recombination zones. Approximately twice higher efficiency was obtained for white electroluminescent devices based on two TADF emitters due to double efficient resonant energy transfers. Efficiency of those resonant energy transfers depends on combinations of singlet-singlet and triplet-triplet levels between exciton modulator and respectively blue/orange TADF emitters. Warm-white and white electroluminescences with CIE coordinates of (0.36, 0.31) and (0.32, 0.31), color temperatures 3332 and 4490 K, CRI of 67 and 80 respectively were observed for the best devices with external quantum efficiencies reaching 9.5 and 7.1%. The proposed approach has big potential for the design of efficient and stable OLEDs with high quality of white electroluminescence.

CRediT authorship contribution statement

Malek Mahmoudi: carried out device fabrication and characterization, performed photoluminescence measurements and interpretation, Writing – original draft. **Jonas Keruckas:** designed and synthesized the materials, Writing – original draft. **Dmytro Volyniuk:** investigated hole-transporting properties of the compounds, advised with device fabrication, Writing – original draft. **Viktorija Andruleviciene:** performed DFT calculations. **Rasa Keruckiene:** discussed the results, Writing – review & editing. **Edgaras Narbutaitis:** assisted with synthesis and identifications of materials. **Yu-Chiang Chao:** performed ionization potential measurements, assisted with device fabrication. **Martins Rutkis:** assisted and analyzed of DFT calculation data. **Juozas V. Grazulevicius:** the team leader of the project, discussed the results obtained, Writing – review & editing.

Declaration of competing interest

The authors declare that they have no known competing financial interests or personal relationships that could have appeared to influence the work reported in this paper.

Appendix A. Supplementary data

Supplementary data to this article can be found online at https://doi.org/10.1016/j.dyepig.2021.109868.

References

[1] Udagawa K, Sasabe H, Cai C, Kido J. Low-driving-voltage blue phosphorescent organic light-emitting devices with external quantum efficiency of 30. Adv Mater 2014;26:5062–6. https://doi.org/10.1002/adma.201401621.

9

[2] Reineke S, Lindner F, Schwartz G, Seidler N, Walzer K, Lüssem B, et al. White organic light-emitting diodes with fluorescent tube efficiency. Nature 2009;459: 234–8. https://doi.org/10.1038/nature08003.

[3] Yin Y, Ali MU, Xie W, Yang H, Meng H. Evolution of white organic light-emitting devices: from academic research to lighting and display applications. Mater Chem Front 2019;3:970–1031. https://doi.org/10.1039/c9qm00042a.

[4] Ma D. White OLED devices. Handb. Adv. Light. Technol. Springer International Publishing; 2014. p. 1–34. https://doi.org/10.1007/978-3-319-00295-8_24-1.

[5] Kido J, Kimura M, Nagai K. Multilayer white light-emitting organic electroluminescent device. 80 Science 1995;267:1332–4. https://doi.org/10.1126/science.267.5202.1332.

[6] Kido J, Hongawa K, Okuyama K, Nagai K. White light-emitting organic electroluminescent devices using the poly(N-vinylcarbazole) emitter layer doped with three fluorescent dyes. Appl Phys Lett 1994;64:815–7. https://doi.org/10.1063/1.111023.

[7] Ou Q-D, Zhou L, Li Y-Q, Shen S, Chen J-D, Li C, et al. Light-emitting diodes: extremely efficient white organic light-emitting diodes for general lighting (adv. Funct. Mater. 46/2014). Adv Funct Mater 2014;24:7392. https://doi.org/10.1002/adfm.201470301, 7392.

[8] Liu B, Wang L, Xu M, Tao H, Gao D, Zou J, et al. Extremely stable-color flexible white organic light-emitting diodes with efficiency exceeding 100 lm W-1. J Mater Chem C 2014;2:9836–41. https://doi.org/10.1039/c4tc01582g.

[9] Jou J-H, Hsieh C-Y, Tseng J-R, Peng S-H, Jou Y-C, Hong JH, et al. Candle light-style organic light-emitting diodes. Adv Funct Mater 2013;23:2750–7. https://doi.org/10.1002/adfm.201203209.

[10] Kamtekar KT, Monkman AP, Bryce MR. Recent advances in white organic light-emitting materials and devices (WOLEDs). Adv Mater 2010;22:572–82. https://doi.org/10.1002/adma.200902148.

[11] Gather MC, Köhnen A, Meerholz K. White organic light-emitting diodes. Adv Mater 2011;23:233–48. https://doi.org/10.1002/adma.201002636.

[12] Sasabe H, Kido J. Development of high performance OLEDs for general lighting, n. d. https://doi.org/10.1039/c2tc00584k.

[13] Jou J-H, Hsieh C-Y, Chen P-W, Kumar S, Hong JH. Candlelight style organic light-emitting diode: a plausibly human-friendly safe night light. J Photon Energy 2014; 4:043598. https://doi.org/10.1117/1.JPE.4.043598.

[14] Chang CH, Tien KC, Chen CC, Lin MS, Cheng HC, Liu SH, et al. Efficient phosphorescent white OLEDs with high color rendering capability. Org Electron 2010;11:412–8. https://doi.org/10.1016/j.orgel.2009.11.020.

[15] Jou J-H, Wu R-Z, Yu H-H, Li C-J, Jou Y-C, Peng S-H, et al. Artificial Dusk-light based on organic light emitting diodes. 2013. https://doi.org/10.1021/ph400007w.

[16] Zhang L, Li XL, Luo D, Xiao P, Xiao W, Song Y, et al. Strategies to achieve high-performance white organic light-emitting diodes. Materials 2017;10. https://doi.org/10.3390/ma10121378.

[17] Baldo MA, O'Brien DF, You Y, Shoustikov A, Sibley S, Thompson ME, et al. Highly efficient phosphorescent emission from organic electroluminescent devices. Nature 1998;395:151–4. https://doi.org/10.1038/25954.

[18] Kim S, Bae HJ, Park S, Kim W, Kim J, Kim JS, et al. Degradation of blue-phosphorescent organic light-emitting devices involves exciton-induced generation of polaron pair within emitting layers. Nat Commun 2018;9:1–11. https://doi.org/10.1038/s41467-018-02025-4.

[19] Scholz S, Kondakov D, Bjö Rn, Lü §, Leo K. Degradation mechanisms and reactions in organic light-emitting devices. 2015. https://doi.org/10.1021/cr400704v.

[20] Chen Y, Zhu J, Wu Y, Yao J, Yang D, Qiao X, et al. Highly efficient fluorescence/phosphorescence hybrid white organic light-emitting devices based on a bipolar blue emitter to precisely control charges and excitons. J Mater Chem C 2020;8: 7543–51. https://doi.org/10.1039/d0tc01549k.

[21] Schwartz G, Fehse K, Pfeiffer M, Walzer K, Leo K. Highly efficient white organic light emitting diodes comprising an interlayer to separate fluorescent and phosphorescent regions. Appl Phys Lett 2006;89:083509. https://doi.org/10.1063/1.2338588.

[22] Sun Y, Giebink NC, Kanno H, Ma B, Thompson ME, Forrest SR. Management of singlet and triplet excitons for efficient white organic light-emitting devices. Nature 2006;440:908–12. https://doi.org/10.1038/nature04645.

[23] Liu BQ, Tao H, Su YJ, Gao DY, Lan LF, Zou JH, et al. Color-stable, reduced efficiency roll-off hybrid white organic light emitting diodes with ultra high brightness. Chin Phys B 2013;22. https://doi.org/10.1088/1674-1056/22/7/077303.

[24] Zhao F, Wei Y, Xu H, Chen D, Ahamad T, Alshehri S, et al. Spatial exciton allocation strategy with reduced energy loss for high-efficiency fluorescent/phosphorescent hybrid white organic light-emitting diodes. Mater Horiz 2017;4:641–8. https://doi.org/10.1039/c7mh00131b.

[25] Duan L, Zhang D, Wu K, Huang X, Wang L, Qiu Y. Controlling the recombination zone of white organic light-emitting diodes with extremely long lifetimes. Adv Funct Mater 2011;21:3540–5. https://doi.org/10.1002/adfm.201100943.

[26] Yersin H, Rausch AF, Czerwieniec R, Hofbeck T, Fischer T. The triplet state of organo-transition metal compounds. Triplet harvesting and singlet harvesting for efficient OLEDs. Coord Chem Rev 2011;255:2622–52. https://doi.org/10.1016/j.ccr.2011.01.042.

[27] Higuchi T, Nakanotani H, Adachi C. High-efficiency white organic light-emitting diodes based on a blue thermally activated delayed fluorescent emitter combined with green and red fluorescent emitters. Adv Mater 2015;27:2019–23. https://doi.org/10.1002/adma.201404967.

[28] Luo D, He Z, Xiao P, Liu Q, Liu B. White organic light-emitting diodes with thermally activated delayed fluorescence emitters. Light. Diode - an Outlook Empir. Featur. Its recent Technol. Adv. InTech; 2018. https://doi.org/10.5772/intechopen.75564.

[29] Lin L, Fan J, Wang CK. Theoretical perspective for internal quantum efficiency of thermally activated delayed fluorescence emitter in solid phase: a QM/MM study. Org Electron 2017;51:349–56. https://doi.org/10.1016/j.orgel.2017.09.021.

[30] Zhang D, Duan L, Li Y, Zhang D, Qiu Y. Highly efficient and color-stable hybrid warm white organic light-emitting diodes using a blue material with thermally activated delayed fluorescence. J Mater Chem C 2014;2:8191–7. https://doi.org/10.1039/c4tc01289e.

[31] Gao F, Du R, Wei Y, Xu H. Optimizing energy transfer for highly efficient single-emissive-layer white thermally activated delayed fluorescence organic light-emitting diodes. Opt Lett 2019;44:5727. https://doi.org/10.1364/ol.44.005727.

[32] Li XL, Xie G, Liu M, Chen D, Cai X, Peng J, et al. High-efficiency WOLEDs with high color-rendering index based on a chromaticity-adjustable yellow thermally activated delayed fluorescence emitter. Adv Mater 2016;28:4614–9. https://doi.org/10.1002/adma.201505963.

[33] Han C, Zhang J, Ma P, Yang W, Xu H. Host engineering based on multiple phosphorylation for efficient blue and white TADF organic light-emitting diodes. Chem Eng J 2021;405:126986. https://doi.org/10.1016/j.cej.2020.126986.

[34] Wang T, Li K, Yao B, Chen Y, Zhan H, Xie Z, et al. Rigidity and polymerization amplified red thermally activated delayed fluorescence polymers for constructing red and single-emissive-layer white thermally activated delayed fluorescence polymers for constructing red and single-emissive-layer white. Adv Funct Mater 2020;30:2002493. https://doi.org/10.1002/adfm.202002493.

[35] Zhang J, Han C, Du F, Duan C, Wei Y, Xu H. High-power-efficiency white thermally activated delayed fluorescence diodes based on selectively optimized intermolecular interactions. Adv Funct Mater 2020;30:2005165. https://doi.org/10.1002/adfm.202005165.

[36] Huang R, Kukhta NA, Ward JS, Danos A, Batsanov AS, Bryce MR, et al. Balancing charge-transfer strength and triplet states for deep-blue thermally activated delayed fluorescence with an unconventional electron rich dibenzothiophene acceptor. J Mater Chem C 2019;7:13224–34. https://doi.org/10.1039/c9tc02175b.

[37] Chen Y, Lam JWY, Kwok RTK, Liu B, Tang BZ. Aggregation-induced emission: fundamental understanding and future developments. Mater Horiz 2019;6:428–33. https://doi.org/10.1039/c8mh01331d.

[38] Yang Z, Chi Z, Xu B, Li H, Zhang X, Li X, et al. High-T g carbazole derivatives as a new class of aggregation-induced emission enhancement materials, † n.d. https://doi.org/10.1039/c0jm00712a.

[39] Zhang X, Chi Z, Xu B, Chen C, Zhou X, Zhang Y, et al. End-group effects of piezofluorochromic aggregation-induced enhanced emission compounds containing distyrylanthracene. J Mater Chem 2012;22:18505–13. https://doi.org/10.1039/c2jm33140c.

[40] Zhang Y, Zhao Z, Song J, He J, Wang X, Wu J, et al. Rational design of high efficiency green to deep red/near-infrared emitting materials based on isomeric donor-acceptor chromophores. J Mater Chem C 2019;7:1880–7. https://doi.org/10.1039/c8tc05383a.

[41] Bässler H. Charge transport in disordered organic photoconductors a Monte Carlo simulation study. Phys Status Solidi 1993;175:15–56. https://doi.org/10.1002/pssb.2221750102.

[42] Pope M. Vol. vol. 49 Optical Engineering Series By Paul M. Borsenberger and David S. Weiss. Marcel Dekker, Inc.: New York. 1998. xxiv + 768 pp. $195.00. ISBN 0-8247-0173-9. J Am Chem Soc. Organic Photoreceptors in Xerography, vol. 122; 2000. p. 3986. https://doi.org/10.1021/ja995764x, 3986.

[43] Arkhipov VI, Fishchuk II, Kadashchuk A, Bässler H. Charge transport in Disordered organic semiconductors. Photophysics mol. Mater. Weinheim, FRG: Wiley-VCH Verlag GmbH & Co. KGaA; 2006. p. 261–366. https://doi.org/10.1002/3527607323.ch6.

[44] Khademi S, Song JY, Wyatt PB, Kreouzis T, Gillin WP. Ambipolar charge transport in "traditional" organic hole transport layers. Adv Mater 2012;24:2278–83. https://doi.org/10.1002/adma.201103830.

[45] Meyer J, Hamwi S, Kröger M, Kowalsky W, Riedl T, Kahn A. Transition metal oxides for organic electronics: energetics, device physics and applications. Adv Mater 2012;24:5408–27. https://doi.org/10.1002/adma.201201630.

[46] Yokoyama M, Inada K, Tsuchiya Y, Nakanotani H, Adachi C. Trifluoromethane modification of thermally activated delayed fluorescence molecules for high-efficiency blue organic light-emitting diodes. Chem Commun 2018;54:8261–4. https://doi.org/10.1039/c8cc03425g.

[47] Hladka I, Volyniuk D, Bezvikonnyi O, Kinzhybalo V, Bednarchuk TJ, Danyliv Y, et al. Polymorphism of derivatives of tert-butyl substituted acridan and perfluorobiphenyl as sky-blue OLED emitters exhibiting aggregation induced thermally activated delayed fluorescence. J Mater Chem C 2018;6:13179. https://doi.org/10.1039/c8tc04867c.

[48] Deibel C, Dyakonov V. Reports on Progress in Physics Electronic and optoelectronic materials and devices inspired by nature Related content Polymer-fullerene bulk heterojunction solar cells. Rep Prog Phys 2013;76:34501. https://doi.org/10.1088/0034-4885/76/3/034501.

Tuning of spin-flip efficiency of blue emitting multicarbazolyl-substituted benzonitriles by exploitation of the different additional electron accepting moieties

Malek Mahmoudi [a], Dalius Gudeika [a], Dmytro Volyniuk [a], Karolis Leitonas [a], Rita Butkute [a], Iryna Danyliv [b], Juozas V. Grazulevicius [a,*]

[a] Department of Polymer Chemistry and Technology, Kaunas University of Technology, Radvilenu pl. 19, LT-50254 Kaunas, Lithuania
[b] Department of Electronic Devices, Lviv Polytechnic National University, Stepan Bandera 12, 79013 Lviv, Ukraine

ARTICLE INFO

ABSTRACT

Aiming to improve spin-flip efficiency of emitters exhibiting thermally activated delayed fluorescence (TADF), to five derivatives of tetra-tert-butyl-carbazolyl-substituted benzonitriles the different additional electron accepting moieties were attached, i.e. benzonitrile, benzotriazole, 2-benzotrifluoride, methyl 2-benzoate or methyl 3-methylbenzoate (compounds named as CNCN, CN4T, CNCF3, CNCOA and CNCOAM, respectively). The selection of the additional acceptor moieties provided not only different electron accepting abilities but also enabled different non-covalent intramolecular interactions (e.g., due to C-H···F, O, N hydrogen bonds) which affected emission intensity. Despite the similarity of the molecule structures of the compounds, they demonstrated very different TADF efficiencies with reverse intersystem crossing rates in the wide range from 0.047×10^6 to 2.32×10^6 s^{-1} observed for their oxygen-free toluene solutions. These solutions exhibited photoluminescence spectra peaking in the range from 456 to 506 nm and photoluminescence quantum yields reaching 82%. The effect of the additional acceptor substituents was on electroluminescent properties of OLEDs based on the designed TADF emitters was observed. External quantum efficiencies of non-doped and doped devices based on the newly synthesized emitters decreased in order of CNCN > CNCOAM > CNCOA > CNCF3 > CN4T. The best blue devices exhibiting electroluminescence peaked at 468 and 457 nm with CIE coordinates of (0.15, 0.17) and (0.15, 0.13), respectively, showed external quantum efficiency of 18.3 and 14.1% which was considerably higher than 11.5% observed for the reference device which was fabricated using a previously published TADF emitter and showed electroluminescence intensity maximum at 480 nm.

1. Introduction

Well competing with conventional light sources, organic light-emitting diodes (OLEDs) have found own niche in lighting and display technologies owing to high brightness, low power consumption, large viewing angle, low cost and simpler design that enables ultra-thin, flexible, foldable and transparent displays, [1,2]. In the last few years, extremely efficient deep-blue phosphorescent OLEDs with narrow electroluminescence spectra were developed using rigid tetradentate Pt (II) complexes [3] and N-heterocyclic carbene coordinated Ir(III) complexes.[4] However, their efficiency and operational stability are still major challenges in display technology. In practice, the utilization of blue emitters is still behind that of green and red emitters in terms of

efficiency.[5] Even though blue phosphorescent OLEDs demonstrate high efficiency, they suffer from a lack of colour purity, short operational lifetimes and high cost in comparison to blue fluorescent OLEDs [6]. As an alternative, blue thermally activated delayed fluorescence (TADF) OLEDs exploiting cost-effective and non-toxic pure organic materials can reach high efficiencies and exert comparable outcome to phosphorescent OLEDs [7]. TADF compounds are generally designed with the aid of twisted electron-donating and accepting groups to provide the spatially decoupled HOMO and LUMO, which subsequently leads to a small singlet–triplet energy gap ΔE_{ST}.[8] According to the dependence between the first-order mixing coefficient (λ) and the spin–orbit coupling (H_{SO}) value and ΔE_{ST} ($\lambda \sim H_{SO}/\Delta E_{ST}$) which expresses spin-flip processes between singlet and triplet states [9,10], the

---

small ΔE_{ST} is of importance for achieving efficient thermally-assisted reverse intersystem crossing (RISC) from triplet to singlet manifold. [11] The replacement of noble metal-containing phosphors with metal-free pure organic fluorophores is a big challenge and one of the priorities for development of cost-effective OLEDs.

Since the first report on multi-carbazole based compounds containing two electron accepting benzonitrile moieties as green–red TADF emitters for efficient OLEDs [12], the multi-donor–acceptor(s) design strategy is among the best ones for blue TADF emitters. To achieve blue emission of multi-carbazole based TADF compounds few approaches were proposed [11–13]. The replacement of strong acceptor benzonitrile moiety by the weaker ones was among the most efficient methods. When weaker acceptors, cyanophenyls, were used, blue TADF emitters with RISC rates reaching $2.36 \times 10^6 \, \text{s}^{-1}$ were obtained [13]. In OLEDs, such emitters showed electroluminescence peak at 456 nm. The device exhibited maximum EQE of 22.8%, and life-time T80 (time to 80% of the initial luminance) exceeding 60 h at an initial luminance of 1000 cd $\times$ m^{-2}. Using one benzophenone or methyl benzoate electron-accepting moiety and five electron donating carbazolyl groups, two TADF emitters were synthesized with RISC rates of 3.81×10^6 and $4.44 \times 10^6 \, \text{s}^{-1}$, as well as with great electroluminescent properties. OLEDs showed maximum EQEs of 24.6 and 12.5% and greenish blue electroluminescence peaked at ca. 481 and 497 nm, respectively [14]. Using three di-*tert*-butylcarbazolyl groups as donors and three difluorocyanobenzene units as acceptors linked through a benzene π-bridge, blue multi-(donor/acceptor)-type TADF emitters with RISC rates in the range of 0.12×10^5–$5.07 \times 10^5 \, \text{s}^{-1}$ were obtained due to the coexistence of through-space charge transfer and through bond charge transfer effects [15]. These emitters allowed fabrication of non-doped OLEDs with EL maxima at 484 nm and maximum EQEs of up to 21%. It was shown that TADF efficiency with RISC rates over $10^6 \, \text{s}^{-1}$ can be effectively improved fixing molecular configuration by intramolecular C–H⋯F hydrogen bonds [16]. TADF emitter containing seven carbazole moieties as donors and two difluorocyanobenzene units as acceptors linked through a diphenylene bridge was reported [14]. F atom was introduced for fixing the molecular configuration through formation of intramolecular C–H⋯F hydrogen bonds. Using TADF emitters with and without intramolecular interactions, green doped OLEDs with maximum EQEs of 20.8 and 9.5% respectively were fabricated, demonstrating advantages of intramolecular non-covalent interaction. Taking into account that multiple donor moieties cause formation of charge-resonance-type hybrid triplet states, the authors of study [7] synthesized 9,9′,9″,9‴,9⁗-(6-(4,6-diphenyl-1,3,5-triazine-2-yl)benzene-1,2,3,4,5-pentayl)pentakis(9H-carbazole) (5Cz-TRZ). Compound 5Cz-TRZ exhibited blue TADF with extremely fast spin-flip (RISC rate of $1.5 \times 10^7 \, \text{s}^{-1}$). It was used for fabrication of sky-blue OLEDs with electroluminescence spectra peaking at 486 nm, maximum EQE of 29.3% and superior device life-time T90 (time to 90% of the initial luminance) of ca.600 h at brightness of 1000 cd $\times$ m^{-2} as for sky-blue TADF devices. The above analysis shows, that state-of-art blue TADF emitters can be obtained exploiting multi-(donor/acceptor) design strategy in combination with variety of intramolecular interactions (*via* through-space and non-covalent). For realization of spin-flip tuning and emission blue-shifts of TADF emitters, additional modifications of multi-donor containing compounds are required, e.g., by introduction of acceptor asymmetry, which was the aim of this study. Examples of asymmetrical multi-donor-based TADF emitters were not reported in the literature yet to the best of our knowledge.

In this work, aiming to develop efficient blue OLEDs, we introduced asymmetry to multi-carbazole-based emitters by exploiting two different types of accepting moieties which allowed to improve their spin-flip abilities and to achieve blue-shifts of emission. The compounds contain benzonitrile as the general accepting unit and the different additional acceptor moieties, i.e. benzonitrile, benzotriazole, 2-benzotrifluoride, methyl 2-benzoate or methyl 3-methylbenzoate. The motivation of selection of additional acceptor unit was based not only on their

accepting abilities but also on possibility to take part in the different non-covalent intramolecular interactions, e.g. C–H⋯π, F, O, N hydrogen bonds or repulsive N⋯N interactions. Five compounds with asymmetrical A-multi-D-A* structures were designed, synthesised, identified and characterized by the different theoretical and experimental techniques. Comparison of external quantum efficiencies of non-doped and doped OLEDs and their electroluminescent spectra demonstrates the effect of spin-flip tuning and emission blue-shifts induced by different acceptor moieties. With respect of efficiency of OLEDs, the additional acceptor units of the synthesized emitters can be laid out in the order benzonitrile > methyl 3-methylbenzoate > methyl 2-benzoate > 2-benzotrifluoride > benzotriazole. Although the main aim of the work was comparison of spin-flip tuning of five A-multi-D-A* type compounds, relatively high maximum EQEs of 18.3 and 14.1% were obtained for the blue devices electroluminescence intensity of which peaked at 468 and 457 nm, respectively.

2. Results and discussion

### 2.1. Synthesis and characterization

As it is shown in Scheme 1, intermediate compounds **CN1**, **CN3-5** were synthesized by Pd-catalyzed direct arylation of 2,3,5,6-tetrafluorobenzonitrile with aryl iodides i.e., 2-iodobenzonitrile, 2-iodobenzotrifluoride, methyl 2-iodobenzoate and methyl 4-iodo-3-methylbenzoate. The reactions make use of triphenylphosphine as ligand and afford high yields. Intermediate compound **CN2** was prepared according to the previously reported procedure [17]. Five target TADF emitters **CNCN**, **CN4T**, **CNCF3**, **CNCOA** and **CNCOAM** were prepared in a catalyst free aromatic nucleophilic substitution reactions of **CN1-5** and 3,6-di-*tert*-butyl-9H-carbazole. The target materials were fully characterized by ^{1}H NMR, ^{13}C NMR, mass spectrometries and elemental analysis. Synthetic procedures and characterization data for **CNCN**, **CN4T**, **CNCF3**, **CNCOA** and **CNCOAM** can be found in Supporting Information.

2.2. Geometries and frontier orbitals

The frontier molecular orbital distribution and molecular configuration of **CNCN**, **CN4T**, **CNCF3**, **CNCOA** and **CNCOAM** were analyzed by density functional theory (DFT) calculations using Gaussian 16 software. Initial geometries of molecules as well as the energies of their frontier molecular orbitals were calculated at B3LYP/6-31G (d,p) level in vacuum. The calculated dihedral angles between benzonitrile and 2-benzonitrile, benzotriazole, 2-benzotrifluoride, methyl 2-benzoate or methyl 3-methylbenzoate rings were found to be of 90, 67, 90, 82 and 90°, respectively (Fig. 1). The theoretical geometries and the distribution of HOMO and LUMO of derivatives **CNCN**, **CN4T**, **CNCF3**, **CNCOA** and **CNCOAM** are shown in Fig. 1. HOMOs are localized on di-*tert*-butyl carbazolyl moieties, while LUMOs are mainly located on benzonitrile and 2-benzonitrile, benzotriazole, 2-benzotrifluoride, methyl 2-benzoate or methyl 3-methylbenzoate units. The clear separation of HOMO and LUMO molecular orbitals determined small calculated ΔE_{ST} values for **CNCN**, **CN4T**, **CNCF3**, **CNCOA** and **CNCOAM** of 0.09, 0.01, 0.07, 0.06 and 0.02 eV respectively. The HOMO energy levels of the compounds were found to be in the close range of -5.35 - -5.25 eV due to the presence of the same donor moieties. The LUMO energy levels of the **CNCN**, **CNCF3**, **CNCOA** and **CNCOAM** were also found to be close (-2.31 - -1.95).

Natural transition orbitals (NTO) for the S_1 state were generated (Figure S1). The calculations showed that for compounds **CNCN**, **CN4T**, **CNCF3**, **CNCOA** and **CNCOAM** the $S_1 \rightarrow S_0$ transitions occur due to electron transfer from the acceptor fragment to the donor moiety. However, there is also some overlap of varying degree on the cyanophenyl ring. This observation shows the mixed nature of the transition with a prevailing charge transfer (CT) character.

The absorption bands were calculated to correspond to HOMO →
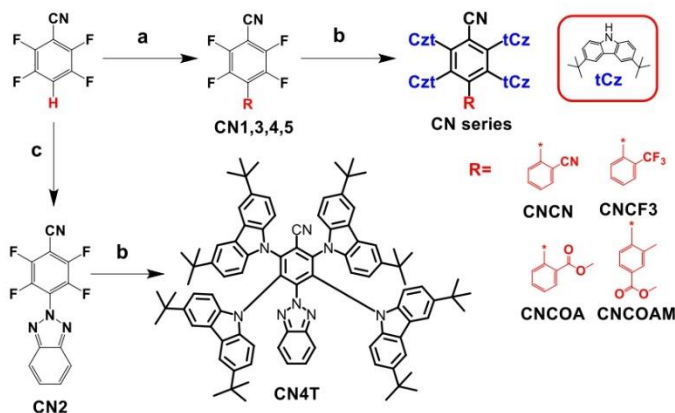
Scheme 1. Synthesis of **CNCN, CN4T, CNCF3, CNCOA** and **CNCOAM**. Reagents and conditions: a) aryl iodides, Pd(OAc)$_2$, PPh$_3$, Ag$_2$CO$_3$, DMF, 70 °C, 24 h; b) Cs$_2$CO$_3$, DMF, 120 °C, 24 h.

LUMO transitions for all the studied derivatives. The theoretical transition wavelengths for compounds **CNCN, CN4T, CNCF3, CNCOA** and **CNCOAM** were 484, 503, 476, 462 and 473 nm, respectively (Figure S2).

2.3. Experimental energy levels and thermal properties

To characterize hole injecting properties of the compounds, thus to obtain the minimum energy necessary to create a positive charge carrier in the materials, ionization potentials (IP$_{PE}$) of the solid layers of the compounds were investigated by photoelectron emission spectrometry (Fig. 2a, Table 1). The IP$_{PE}$ values were obtained from the intersection points of the fit lines to the linear parts of the spectra with the horizontal axis. Despite the same electron donating units of the compounds, their IP$_{PE}$ values were found to be in a relatively broad range of 5.39–5.9 eV indicating to the different hole injecting properties. The highest IP$_{PE}$ value of 5.9 eV was recorded for the solid layer of compound **CN4T** containing benzonitrile and benzotriazole units. The lowest IP$_{PE}$ value of 5.39 eV was measured for the solid film of compound **CNCF3** containing benzonitrile and 2-benzotrifluoride units. Such differences were apparently obtained due to the different HOMO distributions within molecules in solid-state induced by the different electron accepting abilities of acceptors (Fig. 1). Taking into account that all the designed molecules contain the same multicarbazolyl-substituted benzonitrile moiety, it can be presumed that the order of electron accepting ability of acceptor units is as follows: benzotriazole > methyl 3-methylbenzoate ~ benzonitrile ~ methyl 2-benzoate > 2-benzotrifluoride. The same order was observed for Ip values of compounds **CN4T, CNCOAM, CNCN, CNCOA, CNCF3** containing the corresponding acceptor moieties: 5.9 > 5.68 ~ 5.64 ~ 5.62 > 5.39 eV, respectively (Table 1). In contrast, ionization potential (IP$_{CV}$) values in the range of 5.76–5.79 eV were estimated for the compounds by cyclic voltammetry (CV) from the onset potentials versus the Fc/Fc$^+$ of their oxidation curves (Fig. 2b, S3, Table 1). This observation shows that IP$_{CV}$ values of the studied compounds mainly depend the donor used, thus on the oxidation of di-*tert*-butyl carbazolyl moieties, without effect of acceptor substitutions. Taking into account the IP$_{PE}$ values of compounds **CNCN, CN4T, CNCF3, CNCOA,** and **CNCOAM,** it can be presumed that for efficient hole injection from commonly used anode indium tin oxide (ITO) hole-injecting/

transporting layers will be required for adjusting their IP$_{PE}$ values to the work function of ITO (4.7 eV).

To characterize electron injecting properties of the compounds, electron affinities (EA$_{PE}$) were estimated for the compounds by the formula EA$_{PE}$ = IP$_{PE}$-E$_g$, where E$_g$ is the optical band-gap taken from onset of low energy band of absorption spectra of the layers (Fig. 3a). The EA$_{PE}$ values were obtained in the range of 2.66–3.34 eV being well appropriate for the electron injection from the commonly used cathodes uses for OLED fabrication (e.g. LiF:Al, Ca:Al). Due to slightly different IP$_{PE}$ and IP$_{CV}$ values, the different electron affinity (EA$_{CV}$) values were determined according to the equation EA$_{CV}$ = −(|IP$_{CV}$|− E$_g$) using the optical band gap energies taken from absorption spectra of the materials (Table 1).

The temperatures of thermal transitions of compounds **CNCN, CN4T, CNCF3, CNCOA** and **CNCOAM** were measured by thermogravimetric analysis (TGA) and differential scanning calorimetry (DSC). During the TGA experiments, the weight of most of the compounds decreased to 0 indicating sublimation and inability to determine the temperatures of onsets of thermal degradation (Figure S4a). Very close values of 5% weigh loss temperatures ranging from 449 to 457 °C were observed for the studied compounds except that of compound **CN4T** with benzotriazole moiety (363 °C, Table 2). This observation indicates temperature sensitivity of benzotriazole moiety resulting in the appearance of additional high-energy emission band in electroluminescence spectra of **CN4T**-based devices which will be discussed in the last section.

DSC measurements approved that **CNCN, CN4T, CNCF3, CNCOA** and **CNCOAM** were amorphous compounds (Figure S4b). For example, DSC thermogram of derivative **CNCOA** is displayed in Fig. 2c. When the sample of **CNCOA** was heated during the first scan, no peaks due to melting and crystallisation appeared. During the first and the second heating scans glass transition (T$_g$) at 92 °C was observed (Fig. 2c). The similar behaviour was observed for compounds **CN4T, CNCF3, CNCOA** and **CNCOAM** which showed T$_g$ values in the range from 84 to 109 °C (Table 2). The highest T$_g$ value of 109 °C was obtained for compound **CNCOAM** suggesting the highest morphological stability of its layers in electronic devices under Joule heating.
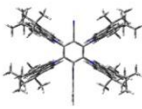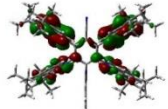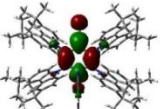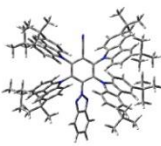
3

106
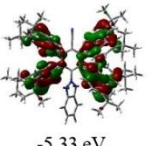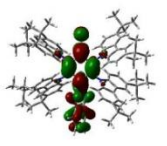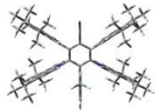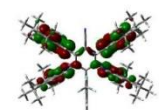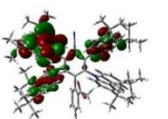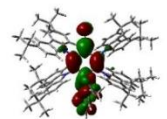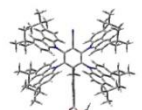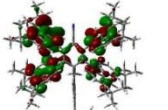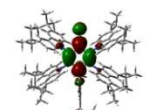
Optimized structure	HOMO	LUMO	ΔE_ST	Dihedral angle
CNCN	−5.25 eV	−2.06 eV	0.09 eV	90°
CN4T	−5.33 eV	−2.31 eV	0.01 eV	67°
CNCF3	−5.28 eV	−2.01 eV	0.07 eV	90°
CNCOA	−5.25 eV	−1.95 eV	0.06 eV	82°
CNCOAM	−5.35 eV	−2.05 eV	0.02 eV	90°

Fig. 1. HOMO and LUMO of **CNCN, CN4T, CNCF3, CNCOA** and **CNCOAM** calculated at B3LYP/6-31G (d,p) level.

2.4. Photophysical properties

The similar absorption spectra were recorded of the solutions of the compounds in toluene, THF solutions and neat films displaying practically the same ground-state energy levels in media of the different polarity (Fig. 3a). Taking into account the absorption spectrum of di-*tert*-butylcarbazole and literature data for carbazole-based compounds (Figure S5) [15,19,20], the absorption bands observed in the range of ca. 300–350 nm are ascribed to n-π* transitions of electron donating units of compounds **CNCN, CN4T, CNCF3, CNCOA** and **CNCOAM**. The bands observed in the high-energy region of absorption spectra at ca. 275–300 nm are related to overlapping of π -π* transitions of di-*tert*-butylcarbazole moiety and electron accepting units (Figure S5). The low-energy absorption bands observed at ca. 365–475 nm for compound **CN4T** and at ca.365–450 nm for the other compounds are of intramolecular charge transfer (CT) character. In contrast to the CT of previously published multi-carbazole derivatives containing the same acceptor moiety [15,20], the broad CT band with two recognized maxima (marked by arrows) were observed for the developed asymmetrical multi-carbazole based compounds (Fig. 3a). According to the DFT calculations (Figure S2), those doubled CT bands apparently resulted from transitions between di-*tert*-butylcarbazolyl groups and both the acceptor moieties. To support the mentioned claim that the doubled CT bands apparently resulted from transitions between di-*tert*-
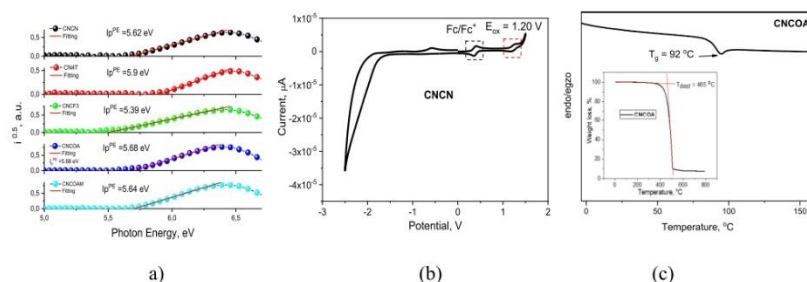
a)   b)   c)

Fig. 2. Photoelectron emission spectra of the solid films of compounds recorded in air (a), CV curve of dilute solutions of **CNCN** in dichloromethane (100 mV/s) (b) and DSC curve of **CNCOA** (c) (Inset shows TGA curve of CNCOA).

Table 1
Energy levels of **CNCN**, **CN4T**, **CNCF3**, **CNCOA**, and **CNCOAM**.

Derivative	E^{ox}_{onset} E^{ox}_{reduct} vs Fc, [eV]	IP_{CV}, [a][eV]	EA_{CV}, [b][eV]	I^{PE}_P, [c][eV]	E^{PE}_A, [d][eV]
CNCN	0.83	5.76	2.93	5.62	2.85
CN4T	0.86	5.80	3.14	5.9	3.34
CNCF3	0.85	5.79	2.96	5.39	2.66
CNCOA	0.86	5.80	2.97	5.68	2.92
CNCOAM	0.83	5.76	2.93	5.64	2.93

[a] $IP_{CV} = \left| -\left(1.4 \times 1e^{-} E^{ox}_{onset} \, vs \, Fc/V\right) - 4.6 \right| eV$ [18]; [b] $EA_{CV} = -(|IP_{CV}| - E^{opt}_g)$ (E^{opt}_g is onset oxidation potential vs the Fc/Fc$^+$; $E^{opt}_g = 1240/\lambda_{edge}$. λ_{edge} is the onset wavelength of absorption spectrum of the dilute THF solution. [c] I^{PE}_P is the ionization potential of thin solid layers estimated by photoelectron emission spectrometry. [d] E^{PE}_A is electron affinity of thin solid layers estimated by the formula $E^{PE}_A = I^{PE}_P - E_g$. The optical band-gaps (E_g) were taken from absorption spectra of the layers (Fig. 3a).

butylcarbazolyl groups and both the acceptor moieties, we compared the absorption spectra of molecules with absorption spectra of individual donor and acceptor compounds (Figure S5). The new absorption bands of compounds **CNCN**, **CN4T**, **CNCF3**, **CNCOA** and **CNCOAM**, which are absent in absorption spectra of the individual donor and acceptor compounds, are definitely related to transitions between the corresponding donor and acceptor units. The second low-intensity CT band was earlier observed for multi-carbazole derivative and attributed to the presence of excited states with enhanced delocalization, which may enhance mixing between local energy (LE) and CT states inducing high RISC rates [13]. In this work, much clearer evidence of the second CT band, thus much stronger delocalization of excited states, was observed for the studied asymmetrical compounds suggesting their high RISC rates. The red-shifted CT bands of compound **CN4T** in comparison to those of other compounds studied in this work is apparently related to the stronger accepting ability of the combination of benzonitrile and benzotriazole moieties. This combination of acceptor unit is even not appropriate for getting blue emission as it was revealed by photoluminescence (PL) measurements (Fig. 3b).

With the aim to understand whether optical excitation of the doubled CT bands equally affects emission properties of the studied compounds, PL decays at the different excitation wavelengths were recorded for compound **CNCOAM** (Fig. 3c). Practically the same profiles of PL decays at emission wavelength of 480 nm were obtained for the toluene solution of **CNCOAM**. As a result, the same excitation spectra were obtained for the prompt (recorded immediately after excitation with a delay of few nanoseconds) and delayed (time delays of > 200 ns) emission of **CNCOAM** at the wavelength of 480 nm (Figure S6a). This observation

indicates that excitation of doubled ICT bands of **CNCOAM** caused formation of the same excited CT states. As a result of emissive recombination of excited CT states, emission with unstructured PL spectra peaking at the wavelengths in the range of 457–522 nm were observed for the toluene and THF solutions as well as for neat films of **CNCN**, **CN4T**, **CNCF3**, **CNCOA** and **CNCOAM** (Fig. 3b). The strongest red shift of PL spectrum of highly polar THF solution with respect of low-polarity toluene solution was observed for compound **CN4T**. Meanwhile, PL spectra of the solutions of other compounds studied were practically independent on the different solvent polarity of toluene and THF despite the CT character of their first singlet excited state. To investigate this observation in more details, solvatochromic effect was additionally studied and analyzed by Lippert-Mataga model recording absorption and emission spectra of the solutions of compounds **CNCN**, **CN4T**, **CNCF3**, **CNCOA** and **CNCOAM** in different solvents (Figure S7). Relatively small redshifts of 39, 51, 44, 43, and 43 nm were observed for PL spectra of the solutions of **CNCN**, **CN4T**, **CNCF3**, **CNCOA** and **CNCOAM** after replacement of low-polarity solvent cyclohexan with highly polar DMF. For example, the the solutions of the previously published multi-carbazole-based TADF emitter with one accepting moiety 9,9',9'',9'''-(6-(4,6-diphenyl-1,3,5-triazine-2-yl)benzene-1,2,3,4,5-pentayl) pentakis(9H-carbazole was characterized by ca. twice higher red shift of PL spectra of 96 nm after replacement of cyclohexan by DMF [7]. The studied compounds **CNCN**, **CN4T**, **CNCF3**, **CNCOA** and **CNCOAM** were characterized by relatively small slopes of their Lippert-Mataga dependences of 8691, 6962, 8490, 8620, 9111 cm^{-1}, respectively (Figure S7b). This observation may be explained by weak CT in these compounds possibly with not pure CT or LE emission nature. On the other hand, we proposed hypothesis on "stucked" moieties without freedom of change of dihedral angels and/or without freedom of the formation of different conformers exhibiting relatively weak solvatochromic effects in comparison to those of other similar multi-carbazole-based TADF emitters [7,9,21,22]. The "stuck" can be partly attributed to the non-covalent intramolecular interactions (e.g. C–H⋯F, O, N hydrogen bonding). However, the effect of non-covalent intramolecular interactions on emission properties of the studied compounds was not very strong since no big differences between UV–vis and PL spectra of toluene solutions recorded before and after six hours of ultrasonic treatments were observed (Fig. 3d,e). Nevertheless, compounds **CN4T**, **CNCF3**, **CNCOA** showed higher PL intensity before the ultrasonic treatment of the solutions. Thus intramolecular interactions (e.g. between *tert*-butyl groups and F, O, N-containing moieties) slightly affect their TADF properties. In case of compound **CN4T**, not only PL intensity but also PL peak wavelength slightly shifted from 504 to 499 nm after ultrasonic treatment of the solution.

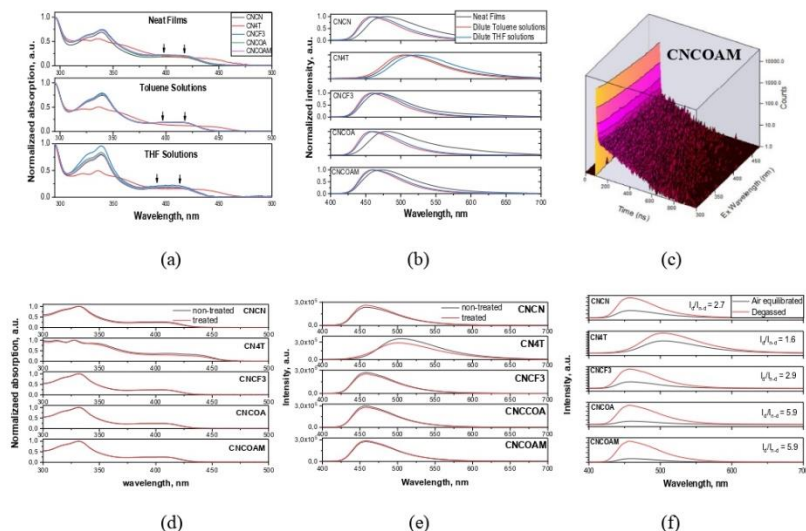PL intensity of toluene solutions of all five compounds strongly

5

108

(a)   (b)   (c)

(d)   (e)   (f)

Fig. 3. UV–vis (a) and photoluminescence (b) spectra of toluene or THF solutions and neat films of the studied compounds. PL decays at the emission wavelength of 480 nm recorded at different excitation wavelengths for toluene solution of **CNCOAM** (c). UV–vis (d) and PL (e) spectra of toluene solutions before and after ultrasonic treatments (d,e) and PL spectra (f) of toluene solutions before and after deoxygenation.

Table 2
Photophysical and thermal properties of the synthesized compounds.

Parameters	Sample	CNCN	CN4T	CNCF3	CNCOA	CNCOAM
T_g, [°C] [b]	Powder	89	103	84	92	109
T_d^{onset} [°C] [c]		452	363	457	465	449
λ_{max}^{abs}, nm	Neat film	295/ 339/-	293/ 336/-	296/341/-	294/339/-	297/ 340/-
λ_{max}^{PL}, nm		480	513	470	483	472
FWHM, nm		88	91	75	91	82
PLQY(%)	Toluene[a]/THF/neat/film of compound(10 wt%):mCP	77/32/34/50	82/53/17/26	49/32/21/39	48/33/22/37	55/34/26/44
ΔEST[eV]	THF at 77 K	0.11	0.05	0.10	0.13	0.14
ΔE_{S1T1}, eV	Film of compound doped in mCPat 77 K	0.0167	0.025	0.0241	0.015	0.021
E_{S1}, eV		2.8	2.607	2.804	2.819	2.813
E_{T1}, eV		2.783	2.582	2.779	2.804	2.792
$k_{RISC} \times 10^6$, s^{-1}	Toluene	0.18	2.32	0.05	0.11	0.07
	Film of compound(10 wt%):mCP	0.18	2.32	0.047	0.11	0.072

[a] – Deoxygenated toluene [b] T_g - glass-transition temperature taken from 2nd heating scan, [c] T_d^{onset} is the temperature of onset of weight loss (20 °C/min, nitrogen atmosphere).

increased when the solutions were deoxygenated by purging with inert gas during 10 min (Fig. 3f). High PLQY values were recorded for deoxygenated toluene solutions of the studied compounds by absolute photoluminescence quantum yield (PLQY) measurements using an integrated sphere (Table 2). This emission enhancement is related to the emissive harvesting of triplet excitons when they are not quenched by triplet oxygen. This assumption is in very good agreement with the results of PL decay measurements of toluene solutions under air and after deoxygenation demonstrating increase of the ratio of long-lived components after removal of oxygen (Figure S8). In total emission of deoxygenated toluene solutions, the highest percentage (ratio) of long-lived component (τ_2) of 56% was obtained for compound **CN4T** (Fig. 4a).

Taking the results of analysis of PL decays (Table S1), the radiation

transition rates of the doped films of the compounds were calculated using the formula presented in the supplementary information. Displaying effect of acceptor asymmetry, the studied compounds demonstrated very different rates of reverse intersystem crossing (k_{RISC}) in a wide range from 0.047×10^6 to 2.32×10^6 s^{-1} (Table 2). Very similar PL spectra were obtained for prompt and delayed emissions (Fig. 4b, S8 b-d). Both of them originate from recombination of the same excited states, thus the lowest singlet CT states.

In contrast to the toluene solutions, the contributions of delayed emission components (τ_2, τ_3) were increased for the films of the compounds (10 wt%) doped in 1,3-bis(N-carbazolyl)benzene (mCP) (Figure S9). The contribution of long-lived components increased in **CN4T** > **CNCN** > **CNCOA** > **CNCOAM** > **CNCF3** (Table S1). (Fig. 4c).

6

(a)   (b)   (c)

(d)   (e)   (f)
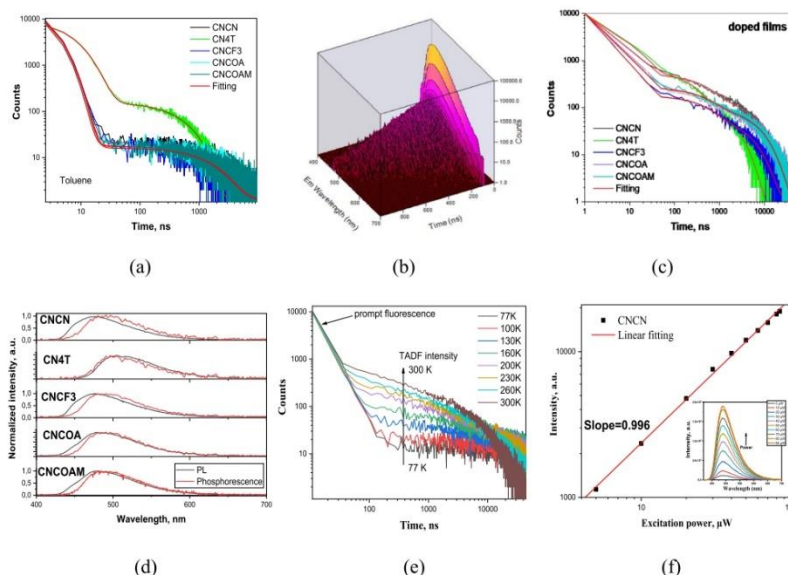
Fig. 4. PL decays of the solutions of compounds in toluene (374 nm) (a), PL spectra recorded at different delays after excitation (b), PL decays of the neat films (c), fluorescence and phosphorescence spectra of the THF solutions recorded at 77 K (d), PL decay curves of the film of **CNCN** doped in mCP recorded at different temperatures (e), intensity of delayed emission versus excitation power for the film of **CNCN** doped in mCP (inset shows delayed emission spectra recorded at the different excitation power) (f).

The same row is obtained for singlet–triplet splitting recorded for compounds in solutions and solid state (Fig. 4d, S10, Table 2). Phosphorescence spectra of the solutions of compounds **CNCN**, **CN4T**, **CNCF3**, **CNCOA** and **CNCOAM** can be attributed to recombination of their CT triplet excited states. They are red-shifted with respect to the phosphorescence spectra of the individual donor and acceptor compounds (Figure S5c).

To determine the nature of delayed emission, PL spectra (Figure S11) and PL decays (4e, Figure S12) of the films of the compounds doped in mCP were recorded under inert atmosphere at the different temperatures. In addition, PL measurements at different excitation were performed for the same samples (Figure S13). The linear fitting with the slope close to unity of the plots of PL intensity versus excitation density excluded contribution of triplet–triplet annihilation mechanism to delayed fluorescence (Fig. 4f, S14) [23]. Thus, TADF is mechanism of delayed fluorescence. This conclusion is additionally supported by temperature dependences of PL spectra, PL intensities and PL decays. Intensity of long-lived emission constantly grew up with increasing temperature from 77 to 300 K proving the TADF nature of emission. Indeed, intensity of long-lived emission is constantly growing up with increasing temperature from 77 to 300 K proving the TADF nature of emission (Fig. 4e, S8). Closely situated spectra of the films of the compounds doped in mCP recorded at different temperatures indicate close energies of fluorescence and phosphorescence of the studied compounds, thus the small singlet–triplet splitting (Figure S10).

To investigate effect of aggregation on emission of the compounds, PL spectra of their dispersions in the THF-water mixtures with various water fractions were recorded (Figure S15, S16). Such measurements allow to test emission properties of the developed compounds in solution and solid-state under the same conditions (the same concentration of oxygen, the same temperature, etc.). Due to the increasing polarity of the solvent mixture with the addition of water and its strong effect on CT states, PL intensities of the dispersions of the studied emitters in THF-water mixtures decreased with increasing water fractions up to ca. 40%. The further increase of water fractions leads to aggregate formations due to the poor solubility of the compounds in water. The longer low-energy tails (marked by arrows) of absorption spectra of THF-water(90%) mixtures in comparison to those of the corresponding THF solutions additionally prove formation of aggregates (Figure S16 b). In the solid state (when aggregates are formed) even higher PL intensities were observed than those of the corresponding THF solutions under the same conditions. This observation demonstrates that compounds **CNCN**, **CN4T**, **CNCF3**, **CNCOA** and **CNCOAM** are characterized by aggregation induced emission enhancement. Relatively high PLQY values were obtained for the neat films of the compounds (Table 2). High PLQY values were observed for the films of the compounds doped in mCP. It should be noted that these PLQYs were measured under air conditions without a precise selection of excitation wavelengths (Figure S17, S18). The results of PLQY measurements demonstrate that compounds **CNCN** and **CNCOAM** exhibiting the highest PLQY values in the solid state are the most promising as OLED emitters.

7

110

2.5. Fabrication and characterization of OLEDs

Electroluminescence (EL) properties of the compounds were investigated using different device structures based on non-doped and doped emitting layers. The structures of OLEDs were as follows: ITO/MoO$_3$ (1 nm)/ NPB (30 nm)/ mCP (4 nm) / light emitting layer (20 nm) / TSPO1 (8 nm)/TPBi (40 nm)/LiF(0.5 nm):Al(100 nm) where light emitting layer was of **CNCN, CN4T, CNCF3, CNCOA** or **CNCOAM** for the non-doped devices n1, n2, n3, n4, and n5 and **CNCN**(10 wt%):mCP, **CN4T** (10 wt%):mCP, **CNCF3**(10 wt%):mCP, **CNCOA**(10 wt%):mCP or **CNCOAM**(10 wt%):mCP for the doped devices d1, d2, d3, d4, and d5, respectively. Molybdenum trioxide (MoO$_3$) was used for the deposition of hole injection layer, N,N′-di (1-naphthyl)-N,N′-diphenyl-(1,1′-biphenyl)-4,4′-diamine (NPB) for hole transporting layer, mCP for exciton blocking layer, diphenyl-4-triphenylsilylphenyl-phosphine oxide (TSPO1) for hole/exciton blocking layer, 2,2′,2″-(1,3,5-benzine-triyl)-tris(1-phenyl-1-H-benzimidazole) (TPBi) for electron transporting layer, and lithium fluoride (LiF) for electron injection layer. The functional layers of the fabricated devices were chosen for providing efficient charge injection, charge transport, charge recombination and exciton recombination within light-emitting layers taking into account the HOMO/LUMO of all functional layers. The corresponding HOMO/LUMO are given in equilibrium energy diagram of the studied non-doped n1-5 and doped d1-5 OLEDs (Fig. 5a,b). In addition, the selection of exciton-blocking layers of mCP and TSPO1 was performed taking into account their lowest triplet levels (T$_1$) to be sure that the triplets of the exciton-blocking layers are higher than triplets of the developed blue TADF emitters (Fig. 5c). Major electroluminescent characteristics of OLEDs n1-5 and d1-5 are given in Fig. 6. The electroluminescence parameters are summarized in Table 3.

The similar unstructured broad EL spectra were observed at different applied voltages for n1-5 devices proving that recombination of electron-hole pairs occurred within the light-emitting layers (Fig. 6a). The EL spectra were very similar to the corresponding PL spectra of neat films of the studied compounds (Fig. 3b). The different excitation sources (optical and electrical ones) caused the slight differences between PL and EL spectra of the studied compounds. In addition to the most red-shifted emission spectrum and lower triplet energy of compound **CN4T** relative to those of other compounds studied (Fig. 5c, 3b), additional high-energy band (shoulder) was observed for device d2. Its intensity increased with increasing applied voltages. Most probably, this observation cannot be attributed to energy leakage from light-emitting layer to the exciton/charge-blocking mCP and TSPO1 layers due to their high triplet energies and high barriers for holes and electrons (Fig. 5). The high-energy band observed under electrical excitation can apparently be attributed to the intrinsic emission of **CN4T**. To understand this result in more detail, the following analyses and

measurements were performed. It is known, that some moieties can react under external forces resulting in the formation of new materials. For example, imidazole ring in the presence of oxygen under UV-irradiation is subjected the ring-opening reaction which results in the formation of new materials [24,25]. Similarly, photochemical degradation and photo-oxidation of benzotriazole based compounds was previously detected [26,27]. Such chemical instability of benzotriazole moieties may be the reason of the high-energy shoulder in CN4T based OLEDs as well as much lower T$_d^{onset}$ (363 °C) of **CN4T** and much lower maximum EQE (2% for n2) values in comparison to the corresponding values estimated for the other compounds (Table 2, 3). To check this hypothesis, PL spectra were repeatable recorded of dopant-free spin-coated films of **CNCN, CN4T, CNCF3, CNCOA** and **CNCOAM** during constant UV treatment (Figure S19). The high-energy shoulder in PL spectra of UV treated film of **CN4T** was well observed proving photochemical instability of the compound. Intensity of this shoulder increased with increasing time of UV treatment. Similarly, the high-energy shoulder appeared in EL spectra of **CN4T**-based devices under electrical excitation. These observation suggests limited utilization of benzotriazole moiety in design of optoelectronic functional materials despite superior TADF properties of benzotriazole-based compounds (Table 2). The other compounds studied did not show any new emission bands (Figure S19). All the non-doped devices showed EL spectra in sky-blue region. They peaked at 474–490 nm. The wavelengths of EL intensity maxima arranged in the odder n1 > n2 > n5 > n4 > n3.

For the doped devices d1-5, EL spectra similar to those of the non-doped ones were observed (Figure S20). The **CN4T**-based device also showed two EL bands. Apparently, due to the polarity sensitive CT emission of the studied compounds and due to the low polarity of the host mCP (dielectric constant of ε = 2.84)[28], blue-shifts were observed for EL spectra of devices d1-5 in comparison to the corresponding spectra of non-doped devices n1-5. As a result, the doped OLEDs showed blue El. The International Commission on Illumination (CIE1931) colour coordinates (x, y) of devices n1-5 and d1-5 can be found in Table 3. The CIE 1931 chromaticity diagrams are shown in Fig. 6b. The CIE$_x$ values observed for non-doped devices range from 0.173 to 0.232 while the values estimated for the doped ones are between 0.184 and 0.225. At the same time, the devices containing a neat emissive layer were characterized by CIE$_y$ values between 0.265 and 0.432 whereas these values for the doped devices ranged from 0.234 to 0.391. The deep-blue electroluminescence with colour coordinates having lower CIE$_x$ and CIE$_y$ values, were obtained for the optimized devices based on the emitter **CNCN** or **CNCOAM** with 3,3′-di(9H-carbazol-9-yl)-1,1′-biphenyl (mCBP) as the host as it will be discussed below (Fig. 6b).

Relatively low as for blue OLEDs turn-on voltages observed for all the devices n1-5 and d1-5 devices indicate efficient injection from electrodes and transport to the emissive layer of charge carriers. The doping
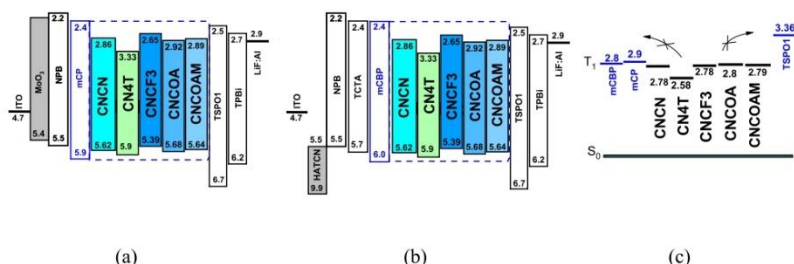

(a)   (b)   (c)

Fig. 5. Equilibrium energy diagram of the non-optimized n1-5, d1-5 (a) and optimized o1a-c, o5a-c (b) devices. Jablonski energy diagram with schematic presentation of triplet levels (T$_1$) for the system exciton-blocking layer/light-emitting layer (c).

8
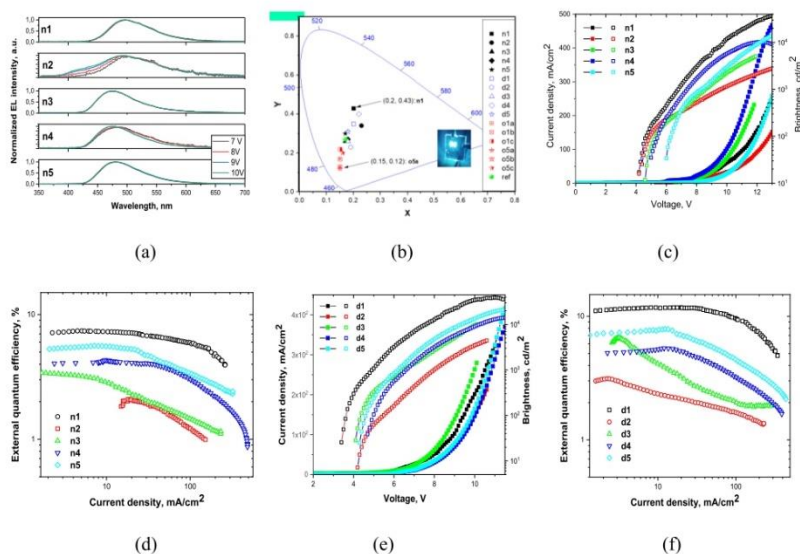
(a) (b) (c)

(d) (e) (f)

Fig. 6. EL spectra (a) at different voltages, CIE1931 coordinates (b), current density and brightness versus voltage curves (c, e) and external quantum efficiencies versus current density (d,f) for non-doped (c, d) and doped (e, f) OLEDs.

Table 3
Parameters of OLEDs.

Device	Light emitting layer	V_{on},[a]V	Maxbrightness,[b]cd/m^2	CE$_{max}$,[c]cd/A	EQE$_{max}$,[d] %	λ,[e]nm	CIE[f]
Non doped OLEDs: ITO/MoO3/NPB/mCP/ Light emitting layer/TSPO1/TPBi/LiF:Al							
n1	CNCN	4.1	36,000	19.4	7.3	495	(0.2, 0.43)
n2	CN4T	4.2	2800	3.8	2	490	(0.23, 0.34)
n3	CNCF3	4.6	5050	6	3.4	474	(0.17, 0.26)
n4	CNCOA	5	8243	7.8	4.3	476	(0.18, 0.27)
n5	CNCOAM	6	16,988	12.1	5.6	480	(0.17, 0.30)
Doped OLEDs: ITO/MoO3/NPB/mCP/ Light emitting layer /TSPO1/TPBi/LiF:Al							
d1	CNCN(20 wt%):mCP	3.4	39,260	28	11.8	485	(0.2, 0.35)
d2	CN4T(20 wt%):mCP	4.2	4415	4.8	3.1	470	(0.19, 0.23)
d3	CNCF3(20 wt%):mCP	4.1	10,144	12.9	6.6	471	(0.18, 0.26)
d4	CNCOA(20 wt%):mCP	4.6	14,176	12.2	5.6	495	(0.22, 0.4)
d5	CNCOAM(20 wt%):mCP	4.3	21,110	17.5	7.9	481	(0.18, 0.31)
Optimized structure ITO/HAT-CN/NPB/TCTA/mCBP/ Light emitting layer /TPBi/LiF:Al							
o1a	CNCN(10 wt%):mCBP	3.9	11,831	28.3	15.1	466	(0.15, 0.17)
o1b	CNCN(20 wt%):mCBP	4	17,456	39.3	18.3	468	(0.15, 0.17)
o1c	CNCN(30 wt%):mCBP	3.9	19,516	27.4	12.4	476	(0.15, 0.22)
o5a	CNCOAM(10 wt%):mCBP	3.8	5453	22.7	11.6	457	(0.15, 0.12)
o5b	CNCOAM(20 wt%):mCBP	3.9	19,551	24.8	14.1	457	(0.15, 0.13)
o5c	CNCOAM(30 wt%):mCBP	4.3	17,115	20.3	10.3	463	(0.16, 0.20)
ref	PFBP-2b(10 wt%):mCBP	3.8	13,420	22.8	11.5	480	(0.17, 0.27)

[a]Turn-on voltage at a luminance of 10 cd m^{-2}, [b] Maximum brightness, [c] Maximum current efficiency, [d] Maximum external quantum efficiency, [e] Wavelength of the peak of EL spectrum at 6 V, [f] Commission Internationale de l'Eclairage (CIE) 1931 color coordinates.

allowed to slightly decrease turn-on voltages of devices d1-5 in comparison to turn-on voltages of the corresponding non-doped devices n1-5. This observation can most probably be attributed to the improved charge-transporting properties of light-emitting layers containing ambipolar host mCP with relatively high hole and electron mobilities of 4×10^{-4} cm^{2}V^{-1}s^{-1} and 2.8×10^{-4} cm^{2}V^{-1}s^{-1} at respectively the electric

field of ca. 2.5×10^5 Vcm^{-1} [29].

At external voltage of 10 V, the highest brightness exceeding 10000 cd/m^2 and the lowest brightness exceeding only 1000 cd/m^2 were obtained for devices n1 and n2, respectively (Fig. 6c, Table 3). Similarly, the highest maximum EQE of 7.3% and the lowest maximum EQE of 2% were observed for devices n1 and n2, respectively (Fig. 6d, Table 3). The

9

similar trend in brightness and maximum EQEs were observed for the doped devices d1-5 (Fig. 6d, Table 3). EQEs of the fabricated OLEDs decreased in orders n1 > n5 > n3 ~ n4 > n2 and d1 > d5 > d3 ~ d4 > d2. Since all the emitters used exhibited TADF, the EQEs of devices n1-5 were mainly related to PLQYs of light-emitting layers (except CN4T-based one) which decreased in the same order (Table 2). Taking the PLQY values of deoxygenated toluene solutions of CNCN, CN4T, CNCF3, CNCOA and CNCOAM of 77, 82, 49, 48, 55% maximum theoretical EQEs were calculated by the formula EQE = $\eta_{rec} \times \eta_{ex} \times \eta_{PLQY} \times \eta_{out}$ [30] where charge curriers recombination probability (η_{rec}) and exciton generation probability (η_{ex}) are equal to unity and assuming outcoupling efficiency (η_{out}) of 0.3 as maximum for glass substrates. They were found to be of 23.1, 24.6, 14.7, 14.4, and 16.5% respectively. These maximum theoretical EQEs may be even higher taking into account aggregation induced emission enhancement properties of the studied compounds. Unfortunately, we cannot prove this prediction since we do not have access to equipment for recording PLQYs of solid-samples in oxygen free conditions. Nevertheless, the order of the theoretical maximum EQEs of CN4T > CNCN > CNCOAM ~ CNCF3 ~ CNCOA is practically the same as the orders n1 > n5 > n3 ~ n4 > n2 and d1 > d5 > d3 ~ d4 > d2 observed for experimental maximum EQEs of the fabricated devices, except CN4T based devices n2 and d2 (Table 3). Unfortunately, compound CN4T did not demonstrate good stability under electrical excitation and CN4T can not be suggested for optoelectronic application despite its superior spin-flip rate as it was discussed above.

Devices d1 and d5 exhibited maximum EQEs of 11.8 and 7.9% respectively with relatively low roll-off efficiencies showing practical potential of the developed emitters CNCN or CNCOAM. These device efficiencies can be further improved if appropriate optimization of device structure and concentration of emitters in the light-emitting layers is performed. To confirm this prediction using, additional optimization of the structures devices based on emitters CNCN and CNCOAM was carried out involving the layer of 1,4,5,8,9,11-hexaazatriphenylenehexacarbonitrile (HAT-CN) as hole-injecting layer, the layer of tris(4-carbazoyl-9-ylphenyl)amine (TCTA) as additional hole transporting layer for the reduction of energy barrier between NPB and electron-blocking mCBP layer. With the aim of optimization of concentration of emitters in the host OLEDs with emitting layers containing the different amounts of emitters CNCN or CNCOAM in mCBP were fabricated. Devices with light-emitting layers of CNCN(10, 20 or 30 wt%):mCBP were named as o1a, o1b or o1c respectively. OLEDs with light-emitting layers of CNCOAM(10, 20 or 30 wt%):mCBP were named as o5a, o5b, o5c The updated device structures were ITO/HAT-CN(5 nm)/NPB(40 nm)/TCTA (10 nm)/mCBP(10 nm)/ light-emitting layer/ TPBi (30 nm)/LiF(0.5 nm)/Al. In order to compare the output parameters of the optimized devices o1a-c and o5a-c devices with those of previously reported highly efficient OLEDs based on the known sky-blue TADF emitters, a reference

device (ref.) based on the light-emitting layer of 10,10′-(perfluoro-[1,1′-biphenyl]-4,4′-diyl)bis(2,7-di-*tert*-butyl-9,9-dimethyl-9,10-dihydro-acridine) (PFBP-2b) (10%) doped in mCBP was fabricated in the same conditions [31].

Devices o1a-c and o5a-c showed EL spectra with similar shapes under different voltages but blue-shifted in comparison to the EL spectra of the corresponding devices d1 and d5 with light-emitting layers CNCN(20 wt %):mCP or CNCOAM(20 wt%):mCP (Fig. 7a). Such shifts of EL spectra of the devices are apparently related to the lower dielectric constant of mCBP in comparison to those of previously used hosts, i.e., mCP, TPBi. As a result, blue or even deep-blue electroluminescence was observed for devices o1a-c and o5a-c. For example, CIE coordinates of (0.15, 0.12) were observed for device o5a (Fig. 6b, Table 3). Slightly increased turn-on voltages of devices o1a-c and o5a-c were obtained in comparison to the corresponding values of devices d1 and d5 (Fig. 7b, Table 3). The differences in turn-on voltages can be attributed either to increased photon energy of blue shifted EL spectra of devices o1a-c and o5a-c, to slightly higher total thicknesses of the devices or to the increased number of organic/organic interfaces of the optimized devices relative to that of OLEDs d1 and d5. In addition, lower maximum brightness was observed for o1a-c and o5a-c than for the corresponding devices d1 and d5 (Fig. 7b, Table 3). This observation can be explained by lower sensitivity of human eyes to blue than for sky-blue emission. However low maximum brightness does not affect device efficiency as it will be shown below.

As it was expected, device optimization allowed not only to improve colour quality of blue electroluminescence of CNCN or CNCOAM based OLEDs but also allowed to achieve higher maximum EQEs of 18.3 and 14.1% for devices o1b and o5b, respectively (Fig. 7c, Table 3). These results can apparently be attributed to the improved charge balance within light-emitting layer due to the improved hole and electron mobilities of host mCBP in comparison to those of mCP [32]. Notably, EQEs of devices o1b and o5b devices were higher than corresponding EQE (11.5%) of the reference device. The maximum EQEs (up to 18.3%) of OLEDs o1b and o5b prove high potential of the developed blue TADF emitters CNCN or CNCOAM and well illustrates potential of the strategy of acceptor asymmetry for the design of TADF emitters.

3. Conclusions

Motivated to investigate whether spin-flip efficiency of blue TADF multicarbazol-based emitters can be improved by exploitation of acceptor asymmetry, we synthesized and studied five tetra-*tert*-butyl-carbazolyl-substituted benzonitriles containing additional acceptor moieties with the different accepting abilities. All the synthesized compounds were characterized by TADF with photoluminescence quantum yields of their deoxygenated toluene solutions ranging from 55 to 82%. The weak influence of non-covalent intramolecular interactions
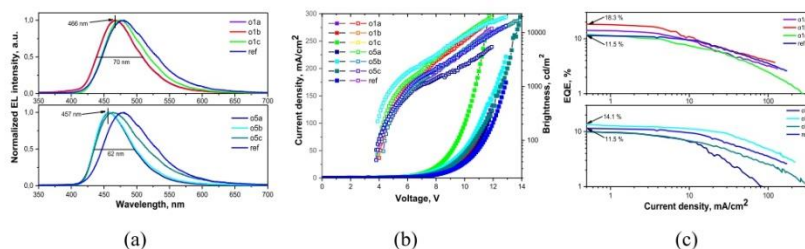

Fig. 7. EL spectra (a), current density and brightness versus voltage curves (b), and external quantum efficiencies versus current density (c) for the devices o1a-c, o5a-c and ref.

on emission properties of the studied compounds in toluene solutions was detected by spectroscopic study in combination with ultrasonic treatment. Different TADF properties, thus different spin-flip abilities with RISC rates ranging from 0.047×10^6 to 2.32×10^6 s^{-1} were observed for the synthesized tetra-*tert*-butyl-carbazolyl-substituted benzonitriles. Their different combination of acceptors with the different electron withdrawing ability allowed to tune emission colours. CIE coordinates of (0.15, 0.12) were estimated for electroluminescence of doped OLEDs. Despite the similar molecular structures of the compounds, OLEDs fabricated using them as emitters demonstrated very different external quantum efficiencies. Their values ranged from 2 to 7.3% for non-doped devices and from 3.1 to 11.7% for the doped ones, demonstrating effect of the spin-flip tuning by acceptor asymmetry. After simple optimization of the devices, the best emitters allowed to achieve external quantum efficiencies of 14.1 and 18.3% for blue TADF OLEDs.

Declaration of Competing Interest

The authors declare that they have no known competing financial interests or personal relationships that could have appeared to influence the work reported in this paper.

Acknowledgments

Appendix A. Supplementary data

Supplementary data to this article can be found online at https://doi.org/10.1016/j.cej.2021.130236.

References

[1] C.W. Tang, S.A. VanSlyke, Organic electroluminescent diodes, Appl. Phys. Lett. 51 (12) (1987) 913–915, https://doi.org/10.1063/1.98799.

[2] S.R. Forrest, The path to ubiquitous and low-cost organic electronic appliances on plastic, Nature. 428 (6986) (2004) 911–918, https://doi.org/10.1038/nature02498.

[3] T.B. Fleetham, L. Huang, K. Klimes, J. Brooks, J. Li, Tetradentate Pt(II) Complexes with 6-Membered Chelate Rings: A New Route for Stable and Efficient Blue Organic Light Emitting Diodes, Chem. Mater. 28 (10) (2016) 3276–3282, https://doi.org/10.1021/acs.chemmater.5b0495710.1021/acs.chemmater.5b04957.s001.

[4] Z. Chen, L. Wang, S. Su, X. Zheng, N. Zhu, C.-L. Ho, S. Chen, W.-Y. Wong, Cyclometalated Iridium(III) Carbene Phosphors for Highly Efficient Blue Organic Light-Emitting Diodes, ACS Appl. Mater. Interfaces. 9 (46) (2017) 40497–40502, https://doi.org/10.1021/acsami.7b0917210.1021/acsami.7b09172.s001.

[5] J.-H. Lee, C.-H. Chen, P.-H. Lee, H.-Y. Lin, M.-K. Leung, T.-L. Chiu, C.-F. Lin, Blue organic light-emitting diodes: Current status, challenges, and future outlook, J. Mater. Chem. C. 7 (20) (2019) 5874–5888, https://doi.org/10.1039/C9TC00204A.

[6] S. Scholz, D. Kondakov, § Bjö Rn Lü, K. Leo, Degradation Mechanisms and Reactions in Organic Light-Emitting Devices, (2015). https://doi.org/10.1021/cr400704v.

[7] L.-S. Cui, A.J. Gillett, S.-F. Zhang, H. Ye, Y. Liu, X.-H. Chen, Z.-S. Lin, E.W. Evans, W.K. Myers, T.K. Ronson, H. Nakanotani, S. Reineke, J.-L. Bredas, C. Adachi, R. H. Friend, Fast spin-flip enables efficient and stable organic electroluminescence from charge-transfer states, Nat. Photonics. 14 (10) (2020) 636–642, https://doi.org/10.1038/s41566-020-0668-z.

[8] F.B. Dias, T.J. Penfold, A.P. Monkman, Photophysics of thermally activated delayed fluorescence molecules, Methods Appl. Fluoresc. 5 (1) (2017) 012001, https://doi.org/10.1088/2050-6120/aa537e.

[9] H. Noda, X.-K. Chen, H. Nakanotani, T. Hosokai, M. Miyajima, N. Notsuka, Y. Kashima, J.-L. Brédas, C. Adachi, Critical role of intermediate electronic states for spin-flip processes in charge-transfer-type organic molecules with multiple donors and acceptors, Nat. Mater. 18 (10) (2019) 1084–1090.

[10] M. Wang, T. Chatterjee, C.J. Foster, T. Wu, C.-L. Yi, H, K.-T. Wong, B. Hu, Exploring mechanisms for generating spin-orbital coupling through donor–acceptor design to realize spin flipping in thermally activated delayed fluorescence,

[11] J. Mater. Chem. C. 8 (10) (2020) 3395–3401, https://doi.org/10.1039/C9TC06078B.

[11] A. Endo, K. Sato, K. Yoshimura, T. Kai, A. Kawada, H. Miyazaki, C. Adachi, Efficient up-conversion of triplet excitons into a singlet state and its application for organic light emitting diodes, Appl. Phys. Lett. 98 (8) (2011) 083302, https://doi.org/10.1063/1.3558906.

[12] H. Uoyama, K. Goushi, K. Shizu, H. Nomura, C. Adachi, Highly efficient organic light-emitting diodes from delayed fluorescence, Nature. 492 (7428) (2012) 234–238, https://doi.org/10.1038/nature11687.

[13] D. Zhang, X. Song, A.J. Gillett, B.H. Drummond, S.T.E. Jones, G. Li, H. He, M. Cai, D. Credgington, L. Duan, Efficient and Stable Deep-Blue Fluorescent Organic Light-Emitting Diodes Employing a Sensitizer with Fast Triplet Upconversion, Adv. Mater. 32 (19) (2020) 1908355, https://doi.org/10.1002/adma.v32.1910.1002/adma.201908355.

[14] G. Kreiza, D. Banevičius, J. Jovaišaitė, K. Maleckaitė, D. Gudeika, D. Volyniuk, J. V. Grazulevicius, S. Juršėnas, K. Kazlauskas, Suppression of benzophenone-induced triplet quenching for enhanced TADF performance, J. Mater. Chem. C. 7 (37) (2019) 11522–11531, https://doi.org/10.1039/C9TC02408E.

[15] X. Zheng, R. Huang, C. Zhong, G. Xie, W. Ning, M. Huang, F. Ni, F.B. Dias, C. Yang, Achieving 21% External Quantum Efficiency for Nondoped Solution-Processed Sky-Blue Thermally Activated Delayed Fluorescence OLEDs by Means of Multi-(Donor/Acceptor) Emitter with Through-Space/-Bond Charge Transfer, Adv. Sci. 7 (7) (2020) 1902087, https://doi.org/10.1002/advs.v7.710.1002/advs.201902087.

[16] W. Yuan, H. Yang, C. Duan, X. Cao, J. Zhang, H. Xu, N. Sun, Y. Tao, W. Huang, Molecular Configuration Fixation with C–H···F Hydrogen Bonding for Thermally Activated Delayed Fluorescence Acceleration, Chem. 6 (8) (2020) 1998–2008, https://doi.org/10.1016/j.chempr.2020.04.021.

[17] J. Zhao, T. Song, S. Zhu, L. Xu, Solvent controlled regioselective reaction of 1,2,3-benzotriazole (BtH) with pentafluorobenzene derivatives, Tetrahedron. 67 (5) (2011) 910–914, https://doi.org/10.1016/j.tet.2010.12.016.

[18] B. Dandrade, S. Datta, S. Forrest, P. Djurovich, E. Polikarpov, M. Thompson, Relationship between the ionization and oxidation potentials of molecular organic semiconductors, Org. Electron. 6 (1) (2005) 11–20, https://doi.org/10.1016/j.orgel.2005.01.002.

[19] Y.-H. Chen, C.-H. Chen, C.-M. Chang, B.-A. Fan, D.-G. Chen, J.-H. Lee, T.-L. Chiu, P.-T. Chou, M.-K. Leung, Control of p-p stacking in carbazole-benzimidazoh1,2-fiphenanthridines: the design of electron-transporting bipolar hosts for phosphorescent organic light-emitting diodes †, J. Mater. Chem. C. 8 (2020) 3571, https://doi.org/10.1039/c9tc06550d.

[20] J. Jayakumar, T.-L. Wu, M.-J. Huang, P.-Y. Huang, T.-Y. Chou, H.-W. Lin, C-H. Cheng, Pyridine-Carbonitrile-Carbazole-Based Delayed Fluorescence Materials with Highly Congested Structures and Excellent OLED Performance, ACS Appl. Mater. Interfaces. 11 (23) (2019) 21042–21048, https://doi.org/10.1021/acsami.9b04664.

[21] P. Arsenyan, B. Vigante, K. Leitonas, D. Volyniuk, V. Andruleviciene, L. Skhirtladze, S. Belyakov, V. Grazulevicius, Dual versus normal TADF of pyridines ornamented with multiple donor moieties and their performance in OLEDs †, (2021). https://doi.org/10.1039/d0tc05745b.

[22] B. Igante, K. Leitonas, D. Volyniuk, V. Andruleviciene, J. Simokaitiene, A. Ivanova, J Audriusb, J. V Grazulevicius, P. Rsenyan, Synthesis of Linear and V-ShapedC arbazolyl-Substituted Pyridine-3,5-dicarbonitriles Exhibiting EfficientB ipolarC harge Transport and E-Type Fluorescence, (n.d.). https://doi.org/10.1021/chem.201805323.

[23] X. Qiao, D. Ma, Nonlinear optoelectronic processes in organic optoelectronic devices: Triplet-triplet annihilation and singlet fission, Mater. Sci. Eng. R Reports. 139 (2020) 100519, https://doi.org/10.1016/j.mser.2019.100519.

[24] Y. Yu, R. Zhao, C. Zhou, X. Sun, S. Wang, Y.u. Gao, W. Li, P. Lu, B. Yang, C. Zhang, Highly efficient luminescent benzoylimino derivative and fluorescent probe from a photochemical reaction of imidazole as an oxygen sensor, Chem. Commun. 55 (7) (2019) 977–980, https://doi.org/10.1039/C8CC08558G.

[25] J. Liu, J. Chen, Y. Dong, Y. Yu, S. Zhang, J. Wang, Q. Song, W. Li, C. Zhang, The origin of the unusual red-shifted aggregation-state emission of triphenylamine-imidazole molecules: Excimers or a photochemical reaction? Mater. Chem. Front. 4 (5) (2020) 1411–1420, https://doi.org/10.1039/C9QM00737G.

[26] L.J. Hem, T. Hartnik, R. Roseth, G.D. Breedveld, Photochemical Degradation of Benzotriazole, J. Environ. Sci. Heal. Part A 38 (3) (2003) 471–481, https://doi.org/10.1081/ESE-120016907.

[27] H.S. Munro, J. Banks, A. Recca, F.A. Bottino, A. Pollicino, A preliminary investigation of the surface photo-oxidation of copolymers of styrene and 2-(2-hydroxy-3-vinyl-5-methylphenyl)-benzotriazole, Polym. Degrad. Stab. 15 (2) (1986) 161–172, https://doi.org/10.1016/0141-3910(86)90070-4.

[28] E. Skuodis, O. Bezvikonnyi, A. Tomkeviciene, D. Volyniuk, V. Mimaite, A. Lazauskas, A. Bucinskas, R. Keruckiene, G. Sini, J.V. Grazulevicius, Aggregation, thermal annealing, and hosting effect on performances of an acridan-based TADF emitter, Org. Electron. 63 (2018) 29–40, https://doi.org/10.1016/j.orgel.2018.09.002.

[29] T. Tsuboi, S.-W. Liu, M.-F. Wu, C.-T. Chen, Spectroscopic and electrical characteristics of highly efficient tetraphenylsilane-carbazole organic compound as host material for blue organic light emitting diodes, Org. Electron. 10 (7) (2009) 1372–1377, https://doi.org/10.1016/j.orgel.2009.07.020.

114

[30] T. Tsutsui, Progress in electroluminescent devices using molecular thin films, MRS Bull. 22 (6) (1997) 39–45, https://doi.org/10.1557/S0883769400033613.

[31] I. Hladka, D. Volyniuk, O. Bezvikonnyi, V. Kinzhybalo, T.J. Bednarchuk, Y. Danyliv, R. Lytvyn, A. Lazauskas, J.V. Grazulevicius, Polymorphism of derivatives of tert-butyl substituted acridan and perfluorobiphenyl as sky-blue OLED emitters exhibiting aggregation induced thermally activated delayed fluorescence †, J. Mater. Chem. C. 6 (48) (2018) 13179–13189, https://doi.org/10.1039/C8TC04867C.

[32] P. Wei, S. Zhao, Z. Xu, D. Song, B. Qiao, P. Wang, J. Yang, Improved carrier injection and balance in solution-processed blue phosphorescent organic light emitting diodes based on mixed host system and their transient electroluminescence, Synth. Met. 252 (2019) 15–20, https://doi.org/10.1016/j.synthmet.2019.04.003.

115

Ornamenting of Blue Thermally Activated Delayed Fluorescence Emitters by Anchor Groups for the Minimization of Solid-State Solvation and Conformation Disorder Corollaries in Non-Doped and Doped Organic Light-Emitting Diodes

Malek Mahmoudi, Dalius Gudeika, Stepan Kutsiy, Jurate Simokaitiene, Rita Butkute, Levani Skhirtladze, Kai Lin Woon, Dmytro Volyniuk,* and Juozas Vidas Grazulevicius*

Cite This: https://doi.org/10.1021/acsami.2c12475   Read Online

ACCESS | Metrics & More | Article Recommendations | Supporting Information

ABSTRACT: Motivated to minimize the effects of solid-state solvation and conformation disorder on emission properties of donor–acceptor-type emitters, we developed five new asymmetric multiple donor–acceptor type derivatives of *tert*-butyl carbazole and trifluoromethyl benzene exploiting different electron-accepting anchoring groups. Using this design strategy, for a compound containing four di-*tert*-butyl carbazole units as donors as well as 5-methyl pyrimidine and trifluoromethyl acceptor moieties, small singlet-triplet splitting of *ca.* 0.03 eV, reverse intersystem crossing rate of 1×10^6 s^{-1}, and high photoluminescence quantum yield of neat film of *ca.* 75% was achieved. This compound was also characterized by the high value of hole and electron mobilities of 8.9×10^{-4} and 5.8×10^{-4} cm^2 V^{-1} s^{-1} at an electric field of 4.7×10^5 V/cm, showing relatively good hole/electron balance, respectively. Due to the lowest conformational disorder and solid-state solvation effects, this compound demonstrated very similar emission properties (emission colors) in non-doped and differently doped organic light-emitting diodes (OLEDs). The lowest conformational disorder was observed for the compound with the additional accepting moiety inducing steric hindrance, limiting donor–acceptor dihedral rotational freedom. It can be exploited in the multi-donor–acceptor approach, increasing the efficiency. Using an emitter exhibiting the minimized solid-state solvation and conformation disorder effects, the sky blue OLED with the emitting layer of this compound dispersed in host 1,3-bis(N-carbazolyl)benzene displayed an emission peak at 477 nm, high brightness over 39 000 cd/m^2, and external quantum efficiency up to 15.9% along with a maximum current efficiency of 42.6 cd/A and a maximum power efficiency of 24.1 lm/W.

KEYWORDS: *donor, acceptor, trifluoromethyl group, tert-butyl carbazole, blue TADF, organic light-emitting diodes*

1. INTRODUCTION

Organic light-emitting diodes (OLEDs) are promising devices for display and lighting applications thanks to their potentially long operational lifetime and low power consumption.[1,2] Recently, OLEDs with external quantum efficiencies (EQEs) exceeding 30% have been reported utilizing luminophores with thermally activated delayed fluorescence (TADF).[3,4] Utilization of TADF materials in OLEDs as the efficient approach to harvest non-emissive triplet excitons without usage of any complicated metal–organic frameworks, requiring relatively inexpensive starting reagents for the synthesis and being sufficiently stable can considerably boost the efficiency of devices, reduce power consumption, and reduce environmental problems in comparison with common prompt fluorescence (PF)-based OLEDs or in comparison with phosphorescent OLEDs.[5] TADF materials now are considered as the third generation of OLED emitters which allow us to reach internal quantum efficiencies of the

devices of 100% without involving noble-metal complexes and incorporation of triplet excitons in radiation which induce the elongated emission lifetimes.[6] However, regardless of all the efforts dedicated, blue OLEDs remain bottlenecks for the wider application of OLEDs.[7] To prevent these bottlenecks, the phenomenon of TADF has been studied extensively by the researchers whose interest is related to OLEDs.[8,9] It received much attention in academic and industrial communities

ACS Publications   A
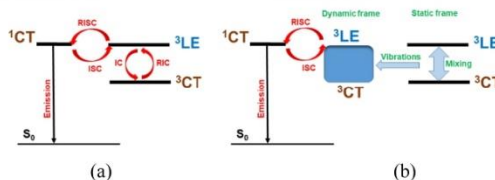
Figure 1. Schematic static (a) and dynamic (b) diagrams of excited states energies of TADF compounds.[27−30] S_0 is the ground state, ISC is intersystem crossing, IC is internal conversion, and RIC is reverse internal conversion.

involved in the development of efficient and stable blue OLEDs.[10,11]

Multiple donor−acceptor-type carbazole derivatives as blue TADF emitters showed great potential for the improvement of efficiency and stability of sky-blue OLEDs.[12] The state-of-art performance (device life-time T90 of *ca.* 600 h at brightness of 1000 cd×m^{-2} and maximum EQE of 29.3%) of sky-blue TADF OLEDs with electroluminescence (EL) spectrum peaking at 486 nm was observed using 9,9′,9″,9‴,9⁗-[6-(4,6-diphenyl-1,3,5-triazine-2-yl)benzene-1,2,3,4,5-pentayl]pentakis(9*H*-carbazole) as blue TADF emitter with extremely fast spin-flipping characterized by reverse intersystem crossing (RISC) rate of 1.5×10^7 s^{-1}.[13] Exploiting strong electron-withdrawing inductive effects of the trifluoromethyl group, in our previous work, we developed asymmetric multi-carbazole-based emitters by utilizing two different types of electron-withdrawing moieties which helped to improve their TADF properties and to achieve efficient blue emission.[14] These and other examples prove that efficient triplet exciton utilization is possible using multi-channel RISC of multi-donor−acceptor molecules as well as obtaining small singlet-triplet energy splitting (ΔE_{ST}) resulting from through space and bond charge transfer effects of the molecules.[15] It could be expected that the alternating arrangement of donor and acceptor units may lead to the coexistence of through-bond charge transfer (TBCT) and through-space charge transfer (TSCT) effects, resulting in a small ΔE_{ST} and high photoluminescence quantum yield (PLQY). On the other hand, the multi-(donor/acceptor) structures of the designed compounds promotes spin-vibronic mixing among the multiple excited states, which is indispensable to the efficient multi-channel RISC process.[16] The carbazole unit is commonly used as electron donor in the design of functional materials for OLEDs.[17] Carbazole derivatives show good amorphous film-forming features, high triplet energy, hole-transporting ability, low redox potential, and good thermal stability.[17] The *tert*-butyl group has been widely used in the design of fluorophores.[5] The attachment of tert-butyl groups to the carbazole moiety allowed us to reduce the concentration-quenching effect and increase solid-state PLQY and stability of the compounds.[18,19] Using this approach, derivatives of carbazole and benzonitrile as blue TADF emitters were prepared.[9] OLEDs based on these emitters showed improved device lifetimes and maximum EQE exceeding 21%.[9] Variety of conjugated electron-accepting groups such cyanobenzene, triazine, oxadiazole, diphenyl sulfoxide, and so forth were used in the design of TADF emitters.[20,21] However, TADF emitters containing strong electron-deficient trifluoromethyl group have been rarely reported.[22,23]

Molecular design of TADF compounds is performed in such a way, that their lowest excited singlet and triplet states lie very close energetically due to the spatial separation of molecular orbitals of donating and accepting moieties.[24] This can lead to the thermally activated upconversion from the latter to the former state through RISC which is actually the inverse transition processes of phosphorescence.[25] The first demonstration of exploitation of RISC phenomenon in OLEDs was reported by Adachi et al.[8,26] The emission process of TADF compounds is controlled by intramolecular charge transfer (CT) transitions via triplet excitons.[8] Hence, to meet the requirements of CT and small ΔE_{ST} values at the same time, the combination of electron-donating and electron-withdrawing moieties through a twisted structure is necessary for the rational molecular design of TADF compounds.[5]

It should be noted that the TADF mechanism is not as simple as it is briefly disclosed above. To better investigate/explain/understand the TADF mechanism, different excited state−energy diagrams were proposed including the "dynamic" one (Figure 1).[27,28] The main components of those diagrams are not only singlet ^{1}CT and triplet ^{3}CT states of TADF molecules but also a local excited singlet (^{1}LE) and triplet (^{3}LE) states of electron-donating and/or electron-accepting species of the molecules (Figure 1).

According to the abovementioned diagrams, RISC/TADF efficiency is to the great extent predominated by energy differences between ^{3}CT−^{3}LE and ^{1}CT−^{3}LE (Figure 1). Highly efficient blue TADF can be achieved at equability ^{1}CT = ^{3}LE = ^{3}CT when there are no energy barriers for RISC. Such equability can be achieved by molecular engineering (e.g., by smart molecular design[31]) or physical approaches (e.g., by an appropriate host selection[32]). Notably, ^{1}CT and ^{3}CT states are very sensitive to media polarity and are different in different surrounding conditions (solvents, hosts different concentrations, conformations, polymorphs, etc.).[33] Meanwhile, ^{1}LE and ^{3}LE states are unchangeable under different environments and depend mainly on the chemical structures. As a result, it is easy to lose the "perfect" equability ^{1}CT = ^{3}LE = ^{3}CT for the most efficient TADF materials especially if the CT-type compounds are characterized by very strong solid-state solvation effects and/or conformation disorder.[34,35] In this work, we aimed to minimize the effects of solid-state solvation and conformation disorder on emission properties of TADF emitters exploiting multi-donor−acceptor molecular engineering.

With this fundamental concern, in this work, we designed and synthesized a series of highly efficient blue TADF emitters based on four 3,6-di-*tert*-butylcarbazole moieties as donors and two electron acceptors. The general electron acceptor for all the synthesized compounds was the trifluoromethyl phenyl group. Our aim in this work was mostly related to the study of the effect of an additional acceptor moiety attached through the para

117

position of the trifluorotoluene moiety on the properties of the emitters. A compound containing four di-*tert*-butyl carbazole units as donors as well as 5-methyl pyrimidine and trifluoromethyl acceptor moieties demonstrated the similar photoluminescence (PL) and electroluminescent (EL) spectra in the layers of non-doped and doped compound and in OLEDs. Thus, the effects of solid-state solvation and conformation disorder of this compound on its TADF properties were considerably decreased which is not typical for TADF compounds.[36]

2. EXPERIMENTAL SECTION

2.1. Materials. 1-Bromo-2,3,5,6-tetrafluoro-4-(trifluoromethyl)-benzene, pyrimidine-5-boronic acid, pyrimidine-2-boronic acid, 2-methyl-4-cyanophenylboronic acid, 2-pyridineboronic acid, and cesium carbonate (Cs$_2$CO$_3$) were purchased from Sigma-Aldrich. 3,6-Di-*tert*-butyl-9*H*-carbazole (**tCz**) was synthesized according to the previously reported procedure.[16]

2.1.1. General Procedure for Pd-Catalyzed Suzuki–Miyaura Cross-Coupling Reactions of 1-Bromo-2,3,5,6-tetrafluoro-4-(trifluoromethyl)benzene with Aryl Boronic Acids. The compounds of 1-bromo-2,3,5,6-tetrafluoro-4-(trifluoromethyl)benzene (1 equiv), aryl boronic acids (1.5 equiv.), and K$_2$CO$_3$ (2 M) were dissolved in toluene and stirred at room temperature, to which Pd(PPh$_3$)$_4$ (10 mol %) was added under nitrogen atmosphere protection. Then, the reaction mixture was refluxed at 90 °C for 16 h under a nitrogen atmosphere. After the mixture was cooled down, water was added to the resulting solution and the mixture was extracted with dichloromethane three times. The organic phase was dried over anhydrous magnesium sulfate and concentrated in vacuum. The dry crude products were used for the further reactions without purification.

5-[2,3,5,6-Tetrafluoro-4-(trifluoromethyl)phenyl]pyrimidine (CF1). Light yellow solid, yield (0.75 g, 76%). MS (APCI$^+$, 20 V), *m/z*: 297 ([M + H]$^+$).

2-[2,3,5,6-Tetrafluoro-4-(trifluoromethyl)phenyl]pyrimidine (CF2). Light yellow solid, yield (0.61 g, 61%). MS (APCI$^+$, 20 V), *m/z*: 297 ([M + H]$^+$).

2′,3′,5′,6′-Tetrafluoro-2-methyl-4′-(trifluoromethyl)-[1,1′-biphen-yl]-4-carbonitrile (CF3). Light yellow solid, yield (0.81 g, 73%). MS (APCI$^+$, 20 V), *m/z*: 334 ([M + H]$^+$).

2-[2,3,5,6-Tetrafluoro-4-(trifluoromethyl)phenyl]pyridine (CF4). Light yellow solid, yield (0.68 g, 69%). MS (APCI$^+$, 20 V), *m/z*: 296 ([M + H]$^+$).

2.1.2. General Procedure for Pd-Free Reaction of 1,2,4,5-Tetrafluoro-3-(trifluoromethyl)benzene with 3,6-Di-tert-butyl-9H-carbazole. 9,9′,9″,9‴-[3-(Pyrimidin-5-yl)-6-(trifluoromethyl)-benzene-1,2,4,5-tetrayl]tetrakis(3,6-di-*tert*-butyl-9*H*-carbazole) (CN1). To a solution of 3,6-di-*tert*-butyl-9*H*-carbazole (1.27. g, 4.55 mmol) in dimethylformamide (DMF) (10 ml) under an argon atmosphere was added Cs$_2$CO$_3$ (1.32 g, 4.05 mmol) at 80 °C, and the mixture was stirred for 5 min. 5-[2,3,5,6-Tetrafluoro-4-(trifluoromethyl)phenyl]pyrimidine (**CF1**) (0.3 g, 1.01 mmol) was added, and the mixture was then stirred for 24 h at 120 °C. When the reaction was completed, it was quenched with water. The crude product was extracted with ethylacetate, excess solvent was removed under reduced pressure. The crude product was purified by column chromatography using ethylacetate/*n*-hexane (1:7) as an eluent to give compound **CN1** as a light yellow solid. Yield: 0.56 g, 42%. ^{1}H NMR (400 MHz, CDCl$_3$, *δ*, ppm): 8.29 (d, *J* = 8.6 Hz, 2H), 7.60 (d, *J* = 1.7 Hz, 3H), 7.47 (d, *J* = 1.7 Hz, 3H), 7.28 (d, *J* = 8.6 Hz, 3H), 7.22–7.18 (m, 3H), 7.15 (dd, *J*$_1$ = 8.6 Hz, *J*$_2$ = 1.7 Hz, 4H), 7.07–6.99 (m, 7H), 6.80 (d, *J* = 8.5 Hz, 3H), 1.38 (s, 36H), 1.32 (s, 36H). ^{13}C NMR (101 MHz, CDCl$_3$, *δ*, ppm): 157.7, 154.6, 143.0, 139.6, 139.4, 139.0, 138.0, 129.0, 128.2, 127.8, 125.3, 123.8, 123.3, 122.6, 116.5, 115.5, 109.9, 109.1, 34.4, 31.8. MS (APCI$^+$, 20 V), *m/z*: 1334 ([M + H]$^+$). Elemental analysis calcd (%) for C$_{91}$H$_{99}$F$_3$N$_6$: C, 81.94; H, 7.48; F, 4.27; N, 6.30. Found: C, 81.99; H, 7.52; N, 6.34.

9,9′,9″,9‴-[3-(Pyrimidin-2-yl)-6-(trifluoromethyl)benzene-1,2,4,5-tetrayl]tetrakis(3,6-di-*tert*-butyl-9*H*-carbazole) (CN2) was synthesized using the same procedure as **CN1** but using CF2 (0.3 g, 1.01 mmol) to replace CF1. The crude product was purified by column chromatography using ethylacetate/*n*-hexane (1:6) as an eluent to give compound **CN2** as a light yellow solid. Yield: 0.79 g, 59%. ^{1}H NMR (400 MHz, CDCl$_3$, *δ*, ppm): 7.90 (d, *J* = 4.9 Hz, 2H), 7.58 (d, *J* = 1.6 Hz, 3H), 7.41 (d, *J* = 1.6 Hz, 3H), 7.31–7.28 (m, 3H), 7.22–7.18 (m, 3H), 7.14–7.10 (m, 7H), 7.05–7.00 (m, 6H), 1.40 (s, 36H), 1.34 (s, 36H). ^{13}C NMR (101 MHz, CDCl$_3$, *δ*, ppm): 155.7, 149.2, 142.4, 142.1, 140.8, 140.8, 140.8, 129.0, 128.2, 125.3, 123.5, 123.1, 122.5, 122.3, 115.2, 115.4, 110.8, 109.9, 34.4, 31.9. MS (APCI$^+$, 20 V), *m/z*: 1334 ([M + H]$^+$). Elemental analysis calcd (%) for C$_{91}$H$_{99}$F$_3$N$_6$: C, 81.94; H, 7.48; F, 4.27; N, 6.30. Found: C, 81.97; H, 7.43; N, 6.33.

9,9′,9″,9‴-[3-Bromo-6-(trifluoromethyl)benzene-1,2,4,5-tetrayl]-tetrakis(3,6-di-*tert*-butyl-9*H*-carbazole) (CN3) was synthesized using the same procedure as **CN1** but using 1-bromo-2,3,5,6-tetrafluoro-4-(trifluoromethyl)benzene (0.3 g, 1.01 mmol). The crude product was purified by column chromatography using ethylacetate/*n*-hexane (1:8) as an eluent to give compound **CN3** as a light yellow solid. Yield: 0.83 g, 62%. ^{1}H NMR (400 MHz, CDCl$_3$, *δ*, ppm): 7.62 (d, *J* = 1.8 Hz, 6H), 7.60 (d, *J* = 1.8 Hz, 2H), 7.14 (dd, *J*$_1$ = 8.6 Hz, *J*$_2$ = 1.8 Hz, 2H), 7.12 (d, *J* = 1.8 Hz, 4H), 7.11–7.08 (m, 3H), 7.08–7.01 (m, 5H), 6.90 (d, *J* = 8.6 Hz, 2H), 1.40 (s, 36H), 1.37 (s, 36H). ^{13}C NMR (101 MHz, CDCl$_3$, *δ*, ppm): 143.0, 139.1, 138.2, 137.1, 123.9, 123.2, 122.6, 122.4, 115.4, 109.7, 109.0, 34.5, 32.8. MS (APCI$^+$, 20 V), *m/z*: 1334 ([M + H]$^+$). Elemental analysis calcd (%) for C$_{87}$H$_{96}$BrF$_3$N$_4$: C, 78.29; H, 7.25; Br, 5.99; F, 4.27; N, 4.20. Found: C, 78.33; H, 7.30; N, 4.24.

2′,3′,5′,6′-Tetrakis(3,6-di-*tert*-butyl-9*H*-carbazol-9-yl)-2-methyl-4′-(trifluoromethyl)-[1,1′-biphenyl]-4-carbonitrile (CN4) was synthesized using the same procedure as **CN1** but using CF1 was replaced by **CF3** (0.3 g, 0.90 mmol). The crude product was purified by column chromatography using ethylacetate/*n*-hexane (1:7) as an eluent to give compound **CN4** as a light yellow solid. Yield: 0.62 g, 51%. ^{1}H NMR (400 MHz, CDCl$_3$, *δ*, ppm): 7.68 (d, *J* = 1.6 Hz, 2H), 7.63–7.55 (m, 3H), 7.51 (dd, *J*$_1$ = 5.9 Hz, *J*$_2$ = 1.6 Hz, 3H), 7.44 (dd, *J*$_1$ = 7.3 Hz, *J*$_2$ = 5.9 Hz, 3H), 7.36 (t, *J* = 5.9 Hz, 2H), 7.21 (d, *J* = 7.3 Hz, 2H), 7.13–7.02 (m, 2H), 6.78–6.64 (m, 5H), 6.58–6.44 (m, 5H), 2.12 (s, 3H), 1.45 (s, 36H), 1.26 (s, 36H). ^{13}C NMR (101 MHz, CDCl$_3$, *δ*, ppm): 143.2, 142.7, 139.2, 138.5, 137.3, 132.5, 129.9, 128.4, 127.1, 123.7, 123.4, 123.2, 122.5, 121.8, 115.6, 115.1, 110.3, 109.4, 34.3, 31.9, 21.3. MS (APCI$^+$, 20 V), *m/z*: 1372 ([M + H]$^+$). Elemental analysis calcd (%) for C$_{95}$H$_{102}$F$_3$N$_5$: C, 83.23; H, 7.50; F, 4.16; N, 5.11. Found: C, 83.27; H, 7.54; N, 5.17.

9,9′,9″,9‴-[3-(Pyridin-2-yl)-6-(trifluoromethyl)benzene-1,2,4,5-tetrayl]tetrakis(3,6-di-*tert*-butyl-9*H*-carbazole) (CN5) was synthesized using the same procedure as **CN1** but using CF4 (0.3 g, 1.02 mmol). The crude product was purified by column chromatography using ethylacetate/*n*-hexane (1:9) as an eluent to give compound **CN5** as a light yellow solid. Yield: 0.93 g, 69% ^{1}H NMR (400 MHz, CDCl$_3$, *δ*, ppm): 7.74 (d, *J* = 4.2 Hz, 1H), 7.59 (d, *J* = 1.6 Hz, 4H), 7.42 (d, *J* = 1.6 Hz, 4H), 7.14 (dd, *J*$_1$ = 4.2 Hz, *J*$_2$ = 1.6 Hz, 4H), 7.10–6.92 (m, 13H), 6.77–6.71 (m, 1H), 6.43–6.34 (m, 1H), 1.39 (s, 36H), 1.33 (s, 36H). ^{13}C NMR (101 MHz, CDCl$_3$, *δ*, ppm): 148.2, 142.5, 142.2, 139.6, 138.7, 138.2, 134.7, 123.6, 123.1, 122.7, 122.5, 122.3, 122.1, 115.2, 114.7, 110.2, 110.1, 34.4, 31.9. MS (APCI$^+$, 20 V), *m/z*: 1333 ([M + H]$^+$). Elemental analysis calcd (%) for C$_{92}$H$_{100}$F$_3$N$_5$: C, 82.91; H, 7.56; F, 4.28; N, 5.25. Found: C, 82.88; H, 7.54; N, 5.21.

3. RESULTS AND DISCUSSION

3.1. Synthesis and Characterization. Compounds CN1−CN5 were prepared by catalyst-free aromatic nucleophilic substitution reactions of bromo-2,3,5,6-tetrafluoro-4-(trifluoromethyl)benzene, 5-[2,3,5,6-Tetrafluoro-4-(trifluoromethyl)phenyl]pyrimidine (CF1), 2-[2,3,5,6-tetra-fluoro-4-(trifluoromethyl)phenyl]pyrimidine (CF2), 2′,3′,5′,6′-tetrafluoro-2-methyl-4′-(trifluoromethyl)-[1,1′-bi-phenyl]-4-carbonitrile (CF3), and 2-[2,3,5,6-tetrafluoro-4-(trifluoromethyl)phenyl]pyridine (CF4) with 3,6-di-*tert*-butyl-9*H*-carbazole (Scheme 1, see also Supporting Information). 3,6-

118

Scheme 1. Synthesis of CN1−CN5[a]
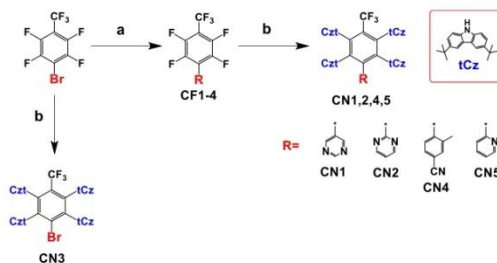
[a]Reagents and conditions: (a) aryl boronic acids (pyrimidine-5-boronic acid, pyrimidine-2-boronic acid, 2-methyl-4-cyanophenylboronic acid, 2-pyridineboronic acid), K₂CO₃, Pd(PPh₃), toluene, 90 °C, 16 h; (b) Cs₂CO₃, DMF, 120 °C, 24 h

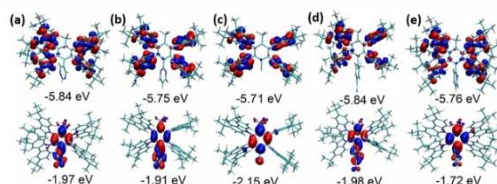**Figure 2.** HOMO (top) and LUMO (bottom) along with their energy levels of (a) **CN1**, (b) **CN2**, (c) **CN3**, (d) **CN4**, and (e) **CN5**.

Di-*tert*-butyl-9*H*-carbazole was prepared according to the procedure reported in the literature.[16] Intermediate compounds **CF1-4** were synthesized by Pd-catalyzed Suzuki cross-coupling reactions of 1-bromo-2,3,5,6-tetrafluoro-4-(trifluoromethyl)-benzene with aryl boronic acids, that is, pyrimidine-5-boronic acid, pyrimidine-2-boronic acid, 2-methyl-4-cyanophenylboronic acid, and 2-pyridineboronic acid. All the compounds were obtained with relative good yields. The target derivatives were fully characterized by ¹H NMR, ¹³C NMR spectroscopies, elemental analysis, and mass spectrometry. Synthetic procedures and characterization data for **CN1−CN5** can be found in the Supporting Information.

3.2. Frontier Orbitals. Density functional theory (DFT) using range-separated hybrid functional LC-*ω*PBEh was used to obtain the ground state molecular geometry at the def2-svp basis set. *ω* was tuned using the golden ratio algorithm under the polarizable continuum model (PCM) with a dielectric constant of 2.38 corresponding to toluene and a solvent radius of 3.48 Å. The optimum *ω* was determined to be of 0.0144 for **CN1−CN5**. Their optimized structures are shown in Figure 2. The **CN1−CN5** exhibited large dihedral angles of 72.7, 71.6, 72.2, 71.7, and 69.6° between 3,6-di-*tert*-butyl-9H-carbazoles which are located next to trifluoromethyl and the acceptor moieties, respectively. The dihedral angles between donor moieties close to **R** and the acceptors are of 51.8, 69.2, 69.2, 73.6, and 70.3°, respectively. The smaller dihedral angle in **CN1** is due to steric hindrance from the proximity of the hydrogen atoms at 5-[4-(trifluoromethyl)phenyl]pyrimidine. The shortest distance between the hydrogen atom at 4, 6 positions to the next nearest hydrogen atom in the donor is of 2.98 Å for **CN1**, while in **CN2**, the smallest distance between the nitrogen atoms to the

hydrogen atom in the donor is of 3.85 Å. This results in the re-position of the donors next to sterically hindered acceptor moiety in **CN1**. Cyanobenzene, pyrimidine, and pyridine as **R** in Scheme 1 are additional electron acceptor moieties. Their dihedral angles with (trifluoromethyl)benzene moieties are of 64.8, 58.6, 68.9, and 70.5° for **CN1**, **CN2**, **CN4**, and **CN5**, respectively. The large dihedral angle should disrupt the conjugation. However, in this case, it behaves similar to a single acceptor with least unoccupied molecular orbital (LUMO) extending into the trifluoromethyl groups due to hyper-conjugation (Figure 2). **CN3** has the deepest LUMO compared with the other compounds studied, indicating that Br is the strongest electron accepting substituent compared with cyanobenzene, pyrimidine, and pyridine. As expected, pyridine is the weakest electron acceptor among the groups as it has only one nitrogen atom and hence **CN5** has the shallowest LUMO level. The highest occupied molecular orbital (HOMO) levels are approximately the same for **CN1** to **CN5** with a variation between −5.71 and −5.84 eV as the HOMO level is dominated by the 3,6-di-*tert*-butyl-9H-carbazole moiety.

Vertical excited states were obtained using time-dependent-DFT/LC-*ω*PBEh//def2-svp at optimal *ω* under the same PCM model. The singlet and triplet transitions for **CN1−CN5** exhibited the charge-transfer character dominated by HOMO to LUMO transition. An excited state wavefunction is represented as the linear combination of the single-determinant configurations with associated coefficients. The coefficients are of 0.986, 0.986, 0.840, 0.972, and 0.992 for singlet transition from HOMO to LUMO in **CN1−CN5**, respectively. For **CN3**, singlet transitions are also contributed by HOMO → LUMO+1 with the associated coefficient of 0.503. The vertical excitation

D

119
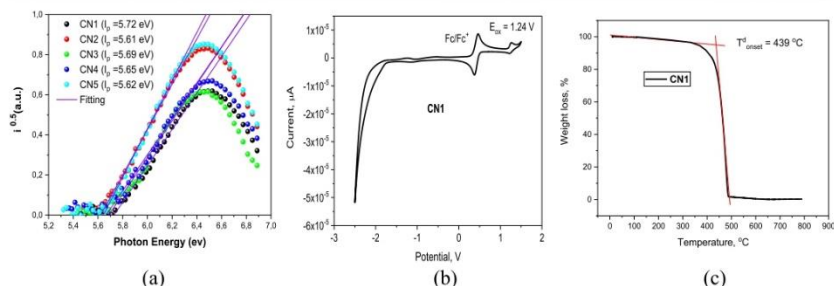
Figure 3. Photoelectron emission spectra of solid films of the compounds recorded in air (a), CV curve of dilute solutions of **CN1** in dichloromethane (100 mV/s) (b) and TGA curve of **CN1** (c).

Table 1. Oxidation Potential versus the Fc/Fc⁺, Ionization Potentials, Electron Affinities, and Optical Bad Gaps of CN1−CN5

derivative	$E_{onsetox}$ vs Fc,[a] V	IP_{CV},[a] eV	E_g^b, eV	EA_{CV},[c] eV	IP_{PE},[d] eV	E_g^e, eV	EA_{PE}^f, eV
CN1	0.83	5.76	2.9	2.86	5.72	2.87	2.85
CN2	0.78	5.69	2.93	2.74	5.61	2.98	2.63
CN3	0.82	5.75	2.95	2.8	5.69	2.97	2.72
CN4	0.78	5.69	2.93	2.76	5.65	2.97	2.68
CN5	0.75	5.65	2.99	2.66	5.62	2.96	2.66

[a]Estimated by CV of solutions in CH_2Cl_2.[38] [b]Taken from the absorption spectra of the dilute THF solutions. [c]$EA_{CV} = IP_{CV} - E_g$ [d]Estimated by photoelectron emission spectrometry of solid films. [e]Taken from the absorption onset of solid films. [f]$EA_{PE} = IP_{PE} - E_g$.

Table 2. Photophysical and Thermal Properties of CN1−CN5

| Parameters	Sample / equation	CN1	CN2	CN3	CN4	CN5
T_d^{onset} [°C][a]		439	441	433	449	462
λ^{abs}_{max}, nm	Neat film	278/287/ 316/328	278/288/ 317/329	279/287/ 318/330	277/288/ 317/330	278/288/ 318/330
λ^{Pl}_{max}, nm		482	508	482	490	480
FWHM, nm		86	104	126	94	106
E_S, eV	Neat film at 77 K	2.92	2.77	3.04	3.04	2.91
E_T, eV		2.89	2.72	3.00	3.0	2.87
ΔE_{ST}, eV		0.03	0.05	0.04	0.04	0.04
E_S, eV	THF at 77 K	2.83	2.81	2.9	2.97	2.88
E_T, eV		2.82	2.78	2.83	2.92	2.84
ΔE_{ST}, eV		0.01	0.03	0.07	0.05	0.04
PLQY(%)	Toluene/neat films[b]	44/76	12/51	8/4	17/27	13/49
η_{PF}[b]	$\eta_{PF} = PLQY * PF(\%)/100(\%)$	0.24	0.16	0.02	0.13	0.07
η_{DF}[b]	$\eta_{DF} = PLQY * DF(\%)/100(\%)$	0.52	0.35	0.02	0.14	0.42
τ_{PF}, ns (%) [b]	from PL decay fitting by I=A+B1exp(-t/τ_{PF})+B2exp(-t/τ_{DF})	9(31)	13(32)	23(57)	23(48)	21(15)
τ_{DF}, μs (%) [b]		2.4 (69)	1.5 (68)	0.8 (43)	1.8 (52)	2.9 (85)
k_{PF}, s⁻¹ [b]	$k_{PF} = \dfrac{\eta_{PF}}{\tau_{PF}}$	2.6×10^7	1.2×10^7	9.9×10^5	5.7×10^6	3.4×10^6
k_{ISC}, s⁻¹ [b]	$k_{ISC} = \dfrac{\eta_{DF}}{\eta_{PF} + \eta_{DF}} k_{PF}$	1.8×10^7	8×10^5	4.2×10^3	2.9×10^6	2.9×10^6
k_{DF}, s⁻¹ [b]	$k_{DF} = \dfrac{\eta_{DF}}{\tau_{DF}}$	2.1×10^5	2×10^5	2.1×10^4	7.6×10^4	1.4×10^5
k_{RISC}, s⁻¹ [b]	$k_{RISC} = \dfrac{\eta_{DF}}{\eta_{PF}} \cdot \dfrac{k_{PF} \cdot k_{DF}}{k_{ISC}}$	7×10^5	8×10^5	3.7×10^4	1.6×10^5	1×10^6
k_{RISC}, s⁻¹	Deoxygenated toluene	8×10^5	5×10^5	6.7×10^4	9.3×10^4	5.5×10^6
E_A^{ISC}, meV	from fitting by	22	6.8	3.9	15.4	5.1
E_A^{RISC}, meV	k=A×exp(−E_a/k_BT)	30	22.5	26.2	25.9	24.8
ΔE_{ST}, meV	calculated	8	16	22	15	20

[a]T_d^{onset} is the temperature of onset of weight loss (20 °C/min, nitrogen atmosphere). [b]Neat films.

energies for **CN1−CN5** are of 2.83, 2.84, 2.91, 2.91, and 2.98 eV with singlet and triplet gaps of 0.03, 0.04, 0.04, 0.06, and 0.08 eV which are very small.

3.3. Electrochemical and Thermal Properties. The ionization potential (IP_{CV}) and electron affinity (EA_{CV}) values of **CN1−CN5** were estimated by cyclic voltammetry (CV)

E

120
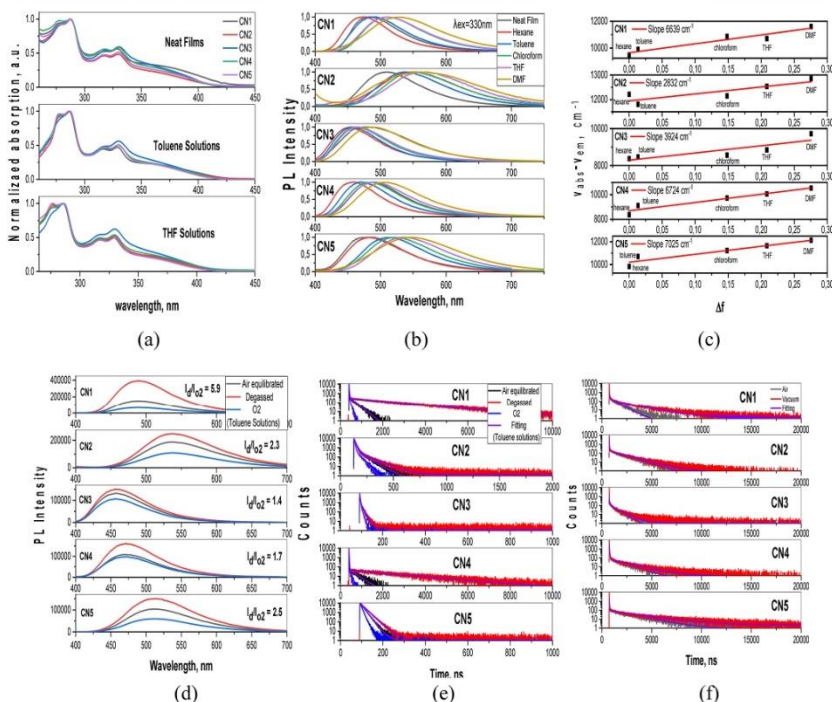
Figure 4. UV−vis (a) and PL (b) spectra of dilute solutions (concentration of 10^{-5} M) and films of compounds **CN1−CN5**, Lippert−Mataga plot of the compounds ($\Delta\nu = \nu_{abs} - \nu_{em}$ is Stokes shift and Δf is orientation polarizability of solvents). (c) PL spectra (d) and PL decay curves (e,f) of air-equilibrated, degassed, and oxygenated toluene solution of compounds (d,e) and films (f) of compounds **CN1−CN5** under air and vacuum. Excitation wavelength λ_{ex} = 330 nm.

measurements. As shown in Figures 3 and S2, the similar quasi-reversible oxidations were observed for the compounds corresponding to the oxidation of the di-*tert*-butyl carbazolyl moiety in the anodic scans. The onset oxidation potentials were found to be of 1.24 V for **CN1**, 1.31 V for **CN2**, 1.27 V for **CN3**, 1.20 V for **CN4**, and 1.23 V for **CN5**. Taking the results of the onset potentials versus the Fc/Fc$^+$ of the oxidation curves, the IP$_{CV}$ values were calculated to be in an extremely close range of 5.65−5.76 eV. This small variation is consistent with the DFT calculation. EA$_{CV}$ values were determined according to the equation EA$_{CV}$ = −(|IP$_{CV}$| − E_g) using the optical band gap energies taken from absorption spectra of the compounds. Photoelectron emission spectroscopy was employed to investigate the ionization energy (IP$_{PE}$) of the solid samples of the compounds (Figure 3a and Table 1). The IP$_{PE}$ values were obtained from the intersection points of the linearly extrapolated low binding energy sides of the spectra with the horizontal axis.[37] The IP$_{PE}$ values of the studied compounds were found to be in the close range of 5.61 to 5.72 eV.

The temperatures of thermal transitions of compounds **CN1**, **CN2**, **CN3**, **CN4**, and **CN5** were measured by thermogravimetric analysis (TGA) and differential scanning calorimetry. The data obtained are given in Table 2. During the TGA experiments, **CN1−CN5** compounds exhibited complete weight losses, indicating sublimation. Their temperatures of the onsets of weight loss ranged from 433 to 462 °C (Supporting Information, see Figure S1). All the derivatives (**CN1−CN5**) did not show evident signals of glass transitions or meltings within the entire range from −40 to 425 °C.

3.4. Photophysical Properties. UV−vis absorption and PL spectra of the dilute solutions and neat films of the compounds are presented in Figure 4a,b. The selected spectral data are summarized in Table 2. The similar absorption profiles were recorded for the toluene and THF solutions as well as neat films of the compounds. All the synthesized emitters showed broad absorption bands in the range of 340−425 nm, which apparently originate from intramolecular charge transfer transition between *tert*-butyl carbazole donors and trifluoromethyl phenyl and/or

additional acceptor. In addition, all the synthesized compounds demonstrated absorption band in the high-energy region, that is, in the range of 276−287 nm attributed to the overlapping of $\pi-\pi^*$ transitions of electron-withdrawing and -donating units and the absorption bands observed in the range of 316−330 nm which can be ascribed to $n-\pi^*$ transitions of di-*tert*-butylcarbazole moieties of compounds **CN1−CN5**.[39] Non-structured PL spectra of neat films of compounds **CN1−CN5** were observed with the peaks at 482, 508, 482, 490, and 480 nm, respectively (Figure 4b). In order to investigate the solvatochromic behavior of the compounds, PL spectra of the solutions in five different solvents were recorded. Such measurements allow us to obtain information on the emission nature of the compounds. CT emission of TADF compounds is highly sensitive to solvent polarity.[24] Featureless emission spectra with a single broad band of the conventional TADF emitters must is red-shifted and broadened with the increase in solvent polarity due to the CT character of the first singlet excited state.[40,41] No obvious shifts of absorption spectra, but considerable red shifts of the fluorescence spectra on going from non-polar hexane (dielectric constant $\varepsilon = 1.88$, $\Delta f = 0.0001$) to highly polar DMF ($\varepsilon = 36.7$, $\Delta f = 0.2755$) were observed. This observation indicates that the dipole moment changes were contributed by the excited states. The largest Stokes shift between steady state absorption and fluorescence spectra in the series was observed for **CN5** (Figure 4b). PL spectra of this compound with the maxima at 488 and 550 nm were recorded for the solutions in low-polarity hexane and highly polar DMF. Thus, the shift of 68 nm was recorded. Smaller red shifts of 50, 14, 30, and 50 were observed for PL spectra of the solutions of **CN1−CN4**. The plot of Stokes shift $[\Delta(\nu)]$ versus orientation polarizability (Δf) described by the Lippert−Mataga equation is displayed in Figure 4c.[42] The linear dependence with a slope of 7025 cm^{-1} was obtained using linear fitting of the Lippert−Mataga plot showing the difference of dipole moments (μ) of **CN5** in the ground and excited states. However, in general, the studied compounds were characterized by relatively small slopes of their Lippert−Mataga dependences. This observation can be explained by the weak CT character of PL of these compounds probably with not pure CT or LE emission nature. It should be noted that conventional TADF emitters are characterized by much higher slopes of their Lippert−Mataga dependences than 10 000 cm^{-1}.[43,44] This result additionally indicates that the emission of compounds **CN1−CN5** is less sensitive to media polarity in comparison to that of conventional TADF emitters.

Using the integrate sphere, PLQY values of the solutions of the synthesized compounds in toluene and of the solid samples under ambient and oxygen-free conditions were measured. The data are summarized in Table 2. The solid-state PLQY of compound **CN1** in oxygen-free conditions exceeded 75%, which is excellent value for OLED applications. The PLQY values of the degassed solutions of **CN1−CN5** in toluene were found to be of 44, 12.4, 7.5, 16.7, and 13.4%, respectively. These results indicate the phenomenon of aggregation-induced emission enhancement (AIEE). To support the statement concerning AIEE, we provided PL measurements for the dispersions of compounds **CN1−CN5** in the mixtures of THF and water (see "AIEE" section in the Supporting Information). Figure 4d shows PL spectra of air-equilibrated, degassed, and oxygenated toluene solutions of the compounds. The significant drop-off of intensities of the emission measured for oxygenated toluene solutions compared to those observed after deoxygenation with argon is obvious for all compounds. The oxygen sensitivity and

emission enhancement after deoxygenation reveal the involvement of triplet states in emission. The PL intensity of the deoxygenated toluene solution of **CN1** was found to be by *ca.* 6 times higher than that of the oxygenated toluene solution (Figure 4d). We also conducted the PL decay measurements of the toluene solutions of the compounds at room temperature. As it is shown in Figure 4e, delayed emission of oxygenated toluene solutions of the compounds was effectively quenched by oxygen and could no longer be detected. Unlike oxygenated samples, degassed solutions of all the emitters exhibited double exponential decays containing both PF and delayed fluorescence (DF) components. The lifetimes of DF and PF (τ_{DF} and τ_{PF}) estimated for air-equilibrated and degassed toluene solutions were obtained by fitting the transients with double exponential decay profiles (Figure 4e, Tables S1 and S4). The significant longer fluorescence lifetimes were found for the toluene solution of compounds **CN1** and **CN4**. They showed longer lifetimes of delayed components in comparison with other compounds. The PL decay curve of degassed solution of **CN1** displays a prompt emission with the lifetime (τ_{PF}) of 15 ns together with delayed emission with the lifetime (τ_{DF}) of 2.1 μs. The percentage of PF is 19.9% and that of DF is 80.1%. After exposition of the solution to air, the delayed component became negligible ($\tau_{DF} = 56$ ns), demonstrating that the delayed emission of **CN1** increased from the triplet states. The determined lifetimes as well as PLQYs and DF/PF intensity ratios were further used to calculate the RISC rate (k_{RISC}) according to the previously reported method assuming that non-radiative decay occurs mainly from the triplet states.[45,46] The recorded k_{RISC} values of the studied compounds were found to be in the range from 6.7×10^4 to 5.5×10^6 s^{-1}. Compounds **CN1** and **CN5** exhibited blue TADF with fast spin-flip and very high RISC rates of 8×10^5 and 5.5×10^6 s^{-1}, respectively. The fast RISC process results in the reduction of the possibility of the degradation mechanisms in which triplet excitons are involved. The main degradation pathway of TADF OLEDs occurs owing to the instability of the TADF emitters and unwanted photophysical parameters such as a small RISC rate (k_{RISC}) and a long DF lifetime (τ_d).[47,48] Steady-state fluorescence spectra and PL decay curves of the films of compounds **CN1−CN5** recorded at room temperature are shown in Figures 4f and S3. The data are collected in Table S2. Upon removing air, the PL intensities increased, while shapes of the spectra remained unchanged. This observation is another proof of the contribution of triplet states in whole PL spectra of the compounds. Figure S3 shows PL spectra of the films of **CN1−CN5** recorded in air and in vacuum. The highest increase of emission intensity after evacuation was recorded for the solid layer of compound **CN1** ($I_{vacuum}/I_{air} = 1.6$). PL decay curves of the neat films recorded under air and in vacuum were biexponential, manifesting the combination of PF and DF components. PL decay curves of all the compounds showed an increase in the delayed component under the vacuum condition (Figure 4f). Taking into account that no phosphorescence was observed at room temperature (only at low temperatures) and the PL spectra of the delayed and prompt emissions were similar, the delayed component can mostly be assigned to the TADF mechanism. It is noteworthy that the DF lifetime of the neat film of **CN3** under vacuum is as short as 0.77 μs and there is very small difference between the contribution of DF in PL decay curves recorded under air and in vacuum conditions [τ_{DF} under air = 0.61 μs (42%), τ_{DF} under vacuum = 0.77 μs (43%)]. Taking into account that **CN3** was the only compound which had a bromine atom instead of additional conjugated acceptor, this

G

122
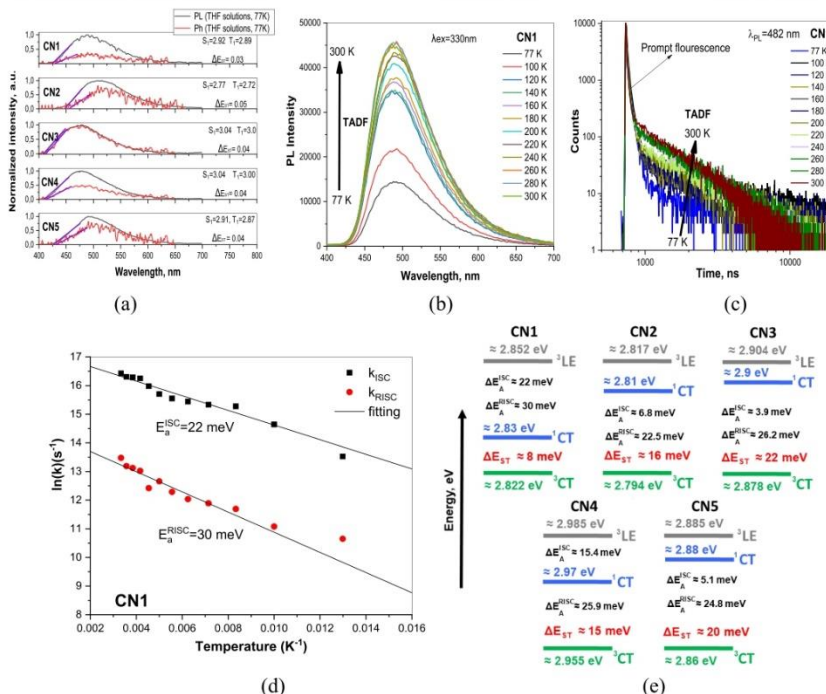
Figure 5. Fluorescence and phosphorescence spectra of the THF solutions of **CN1** recorded at 77 K (a), PL spectra (b), PL decay curves (c), temperature dependences of k_{ISC} and k_{RISC} (d) for the film of **CN1**, and energy diagram (e) of compounds **CN1–CN5**.

observation can prove the considerable impact of additional conjugated acceptor moieties on delayed emission properties. Meanwhile, the results of PL decay measurements of neat films of other compounds under air and vacuum demonstrated increase of the shares of long-lived components after removal of oxygen. For example, high share delayed emission with a lifetime (τ_d) of 2.9 μs was recorded for **CN5** neat film under vacuum. The contribution of DF in the PL decay curves of this compound increased from 65.3 to 85.16% after evacuation (Figure 4d and Table S2). The calculations were also performed to determine the rate constants and efficiencies of the key photophysical transitions of the films of **CN1–CN5** (Table 2). At 300K, the rates of intersystem crossing (k_{ISC}) ranged between 4.2×10^5 and $1.8 \times 10^7 s^{-1}$. The rates of RISC (k_{RISC}) ranged between 3.7×10^4 and $1 \times 10^6 s^{-1}$ which are favorable for the highly efficient up-conversion process of TADF.

Using the temperature dependences of rate constants k_{ISC} and k_{RISC} (Figures 5d and S13, see also "Temperature dependent steady state and time resoled PL measurements" section in the Supporting Information), the ISC and RISC activation energies (E_A^{ISC} and E_A^{RISC}) were calculated from the slopes of the plots

(Table 2). The Arrhenius dependence $k = A \times \exp(-E_a/k_B T)$ was used for the fitting in which E_a is the activation energy, k_B is the Boltzmann constant, and A is the frequency factor involving the spin–orbit coupling constant.[49] The close E_A^{RISC} values ranging from 22.5 to 30 meV were obtained for **CN1–CN5**. Meanwhile, the values of E_A^{ISC} were found to be quite different. The highest E_A^{ISC} of 22 eV was obtained for compound **CN1**. As a result, the smallest ΔE_{ST} of 8 meV was obtained for this compound as it is depicted in the energy diagram (Figure 5e). The smallest E_A^{ISC} of 3.9 eV and the highest ΔE_{ST} of 20 meV were obtained for compound **CN3** suggesting its relatively poor TADF properties. The similar trends of experimental and calculated ΔE_{ST} values were obtained for **CN1–CN5** (Table 2). The presented energy diagram was constructed according to the procedure described in ref 34. ^{1}CT levels were experimentally estimated. Taking into account that the intersystem and RISC are uphill processes in case of **CN1–CN5**, the ^{3}LE, ^{3}CT, and ΔE_{ST} energies were calculated by the questions ^{3}LE $= ^1$CT $+ E_A^{ISC}$, ^{3}CT $= ^3$LE $- E_A^{RISC}$, and $\Delta E_{ST} = ^1$CT-^{3}CT using the corresponding activation energies. The different energy maps of

H

123

(a)

(b)

(c)

(d)

(e)

(f)
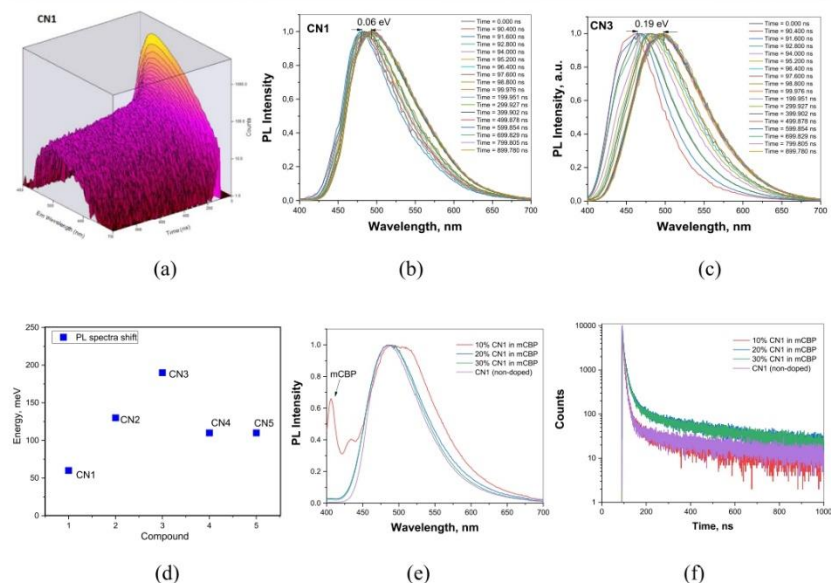
Figure 6. TRES data in 3D (a) and 2D (b,c) plots, the relative PL spectral shifts for the studied compounds (d), PL spectra (e), and PL decays (f) of the films of neat **CN1** and doped in the mCBP host.

[1]CT, [3]LE, and [3]CT of **CN1−CN5** are mainly responsible for their different TADF efficiencies.

To further investigate the photophysical properties of compounds **CN1−CN5**, PL and phosphorescence spectra of their THF solutions (10^{-5} M) were recorded at 77 K (Figure 5a). From the onsets of PL and phosphorescence spectra of the solutions of the emitters in THF, the ΔE_{ST} values of **CN1−CN5** were estimated to be 0.03, 0.05, 0.04, 0.04, and 0.04 eV. This observation confirms that in this type of multi-(donor/acceptor) molecules frontier orbitals can be separated which bring about small ΔE_{ST} (Table 2).

To gain more insights into the DF, temperature-dependent steady-state and time-resolved emission measurements were performed for neat film of compound **CN1**. Figure 5b shows PL spectra of the films of **CN1** recorded at the different temperatures. The intensity of DF increased with the increase of the temperature between 77 and 300 K. This observation confirms thermal activation of the delayed emission. As shown in Figure 5c, PL decay curves of the film of recorded at the different temperatures exhibit two clear components of PF in the nanosecond scale and DF in the microsecond region. The share of long-lived (DF) component was obviously temperature dependent on the temperature. The ratio of the delayed to prompt components slowly grew when the temperature was increased, demonstrating the occurrence of a thermally activated process. Following the temperature increase, the ratio of DF showed significant enhancement trend up to 51% at 300 K,

proving the distinct TADF properties of **CN1** (Figure 5b). The small singlet-triplet splitting, very high PLQY, and fast RISC rate (k_{RISC}) of **CN1** suggest that is a good candidate as a highly efficient TADF emitter for OLED.

We also investigated the conformer formation and hosting effects for **CN1−CN5** on their emission properties (Figure 6). First, time-resolved emission spectra (TRES) were recorded for vacuum-deposited neat films (Figures 6a−c and S4). According to TRES data in 3D (combination of all the spectra recorded in the time range of up to 1 μs) or in 2D (selected spectra recorded at the different delays after excitation), there are shifts of PL spectra which can be attributed to the different conformational disorders of **CN1−CN5**.[34] The lowest conformational disorder was observed for compound **CN1** for which the lowest shift of PL spectra of 0.06 eV was observed (Figure 6d). The highest conformational disorder was obtained for compound **CN3** containing no additional accepting moiety. This observation well supports the selection of multi-donor−acceptor molecular engineering for the minimization of effects of solid-state solvation and conformation disorder on emission properties of TADF emitters. The similar PL spectra and PL decays were also recorded for the films of neat **CN1** and doped in the mCBP host (Figure 6e,f). Due to the low effect of conformation disorder, the similar EL spectra were also obtained for non-doped and doped devices as it will be discussed in the section "Fabrication and Characterization of OLEDs". The high **CN3** conformational disorder indicated that the presence of additional accepting

I

moiety increases steric hindrance between the additional accepting moiety with the donor reducing the freedom of torsional disorder between the donor and acceptor. The lower conformational disorder of **CN1** compared to that of **CN2** provided the further clue of the role of steric hindrance in the reduction of conformational disorder. In **CN1**, the hydrogen atoms at 4,6 positions gave rise to the steric repulsive forces against further dihedral distortion. In **CN2**, the hydrogen atoms at 4,6 positions are situated further from the donor moiety. This resulted in reduced steric hindrance.

3.5. Charge Transporting Properties. Investigation of charge-transporting properties of potential functional materials for OLED applications is vitally important because holes and electrons have to recombine within light-emitting layers of OLEDs.[50] In the ideal case, non-doped light-emitting layers of OLEDs are characterized by bipolar/ambipolar charge-transporting properties with well-balanced hole and electron mobilities. Otherwise, the appropriate host has to be selected.[51] Therefore, to estimate the applicability of compounds **CN1**−**CN5** as emitters in OLEDs, their charge-transporting properties were studied by the time of flight (TOF) method. The samples with the structure indium tin oxide (ITO)/thick vacuum-deposited layer/Al were fabricated. Having TOF current transients in linear scales (Figure 7, inset), transit time (t_{tr})
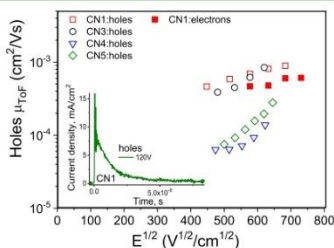
Figure 7. Hole (open symbols) and electron (filled symbols) mobilities of the vacuum-deposited films of **CN1**−**CN5** as the function of electric field plotted according to the Poole−Frenkel charge mobility dependence $[\mu = \mu_0 \times \exp(\beta \times E^{1/2})$.[53] Inset shows the TOF signal in linear scales for holes in the film of **CN1** recorded at 120 V.

could not be accurately estimated due to the dispersive charge transport. However, for compounds **CN1** and **CN3**-5, t_{tr} were well observed in TOF current transients in log−log scales under applied positive voltages to the ITO side, indicating the hole transport (Figure S5). Charge transport in **CN2** was not detected by the TOF experiment apparently because of strong charge recombination. From TOF current transients recorded under the negative voltages, t_{tr} values were obtained only for compound **CN1** additionally, indicating its electron-transporting property (Figure S5). Thus, both p-type (hole) and n-type (electron) transport was confirmed for **CN1** by the TOF measurements. Hole and electron mobilities were calculated at the different electric fields using t_{tr} values from the corresponding TOF current transients (Figures 7 and S5). **CN1** was characterized by the highest value of hole mobility of 8.9×10^{-4} cm^2 V^{-1} s^{-1} at electric field of 4.7×10^5 V/cm. Its electron mobility of 5.8×10^{-4} cm^2 V^{-1} s^{-1} was not much lower than hole mobility at the same electric field showing relatively

good hole/electron balance and suitability for the application in non-doped OLEDs. The values of hole/electron mobilities of **CN1** were among the highest as for TADF emitters.[52]

Compound **CN3** demonstrated similar hole-transporting properties to those of **CN1**. Meanwhile, electron transport was not detected for **CN3**. Apparently the CF$_3$ group is not strong enough acceptor to induce the electron-transporting ability for **CN3**. Compounds **CN4** and **CN5** were characterized by lower hole mobilities of 1.4×10^{-4} and 2×10^{-4} cm^2 V^{-1} s^{-1}, respectively, at an electric field of 3.9×10^5 V/cm apparently because the different HOMO−HOMO overlappings caused by molecular packing properties (Figure 7). As a result, the best EL performances can be expected for **CN1**.

3.6. Fabrication and Characterization of OLEDs. Owing to high PLQY values of neat films (exceeding 0.75) and high RISC rates up to 1×10^6 s^{-1}, the studied compounds can be regarded as promising blue TADF emitters for OLEDs. EL properties of the compounds were investigated using different device structures based on non-doped and doped emitters in device structures ITO/HAT-CN/NPB/TCTA/mCBP/**CNs**/TPBi/LiF:Al for non-doped and ITO/HAT-CN/NPB/TCTA/mCBP/mCBP: **CNs**/TPBi/LiF:Al for doped devices. The device structures, energy diagram, and chemical structures of organic materials are shown in Figure 8a,b. In this architecture, hexaazatriphenylene hexacarbonitrile (HAT-CN) was functionalized as a hole injection material, N,N'-di (1-naphthyl)-N,N'-diphenyl-(1,1'-biphenyl)-4,4'-diamine (NPB) as a hole-transporting material, tris(4-carbazoyl-9-ylphenyl)amine (TCTA) as an electron-blocking material, 3,3'-di(9H-carbazol-9-yl)-1,1'-biphenyl (mCBP) as a host and exciton blocking compound, 2,2',2''-(1,3,5-benzine-triyl)-tris(1-phenyl-1-H-benzimidazole) (TPBi) as an electron-transporting material, and the layer of lithium fluoride (LiF) as an electron injection layer. Vacuum-deposited doped layers were fabricated by employing 10 wt % doping concentration of **CN1**−**CN5** emitters in the mCBP host. mCBP was selected as the host material because of its high singlet (3.6 eV) and triplet (2.9 eV) energies.[54] mCBP is often combined with high band gap, blue-light emitters in the emissive layer of OLEDs.[54] To evaluate the EL performance of **CN1** more precisely and with the aim of additional optimization of device structure OLEDs with the different concentrations of emitter (10, 20 to 30 wt %) in the host were fabricated. The device characteristics such as current density−voltage−luminance (J−V−L) characteristics, EQE versus current density curves as well as the EL spectra and CIE color coordinates are presented in Figures 8, 9, S7, and S8. The key parameters are summarized in Table 3. Figure 8c,d shows the EL spectra and emission color coordinates of OLEDs containing the layers of non-doped and doped **CN1**−**CN5**. All the fabricated devices exhibited unstructured bright blue emission with EL peaks (λ_{EL}) at 473−497 nm and EL spectra similar to PL spectra in the neat films. Due to the low polarity of the host mCBP and due to the polarity-sensitive CT emission of the synthesized compounds, blue shifts were recorded for the EL spectra of the doped devices d1−d5 compared to the corresponding spectra of non-doped devices n1−n5. In order to evaluate the device stability, EL spectra were recorded at the different voltages. Very stable EL spectra were observed under the different driving voltages (Figure 8c,d). The stable EL spectra indicate the absence of effects of conformation disorder which could be present under the different driving voltages. The CIE coordinates of fabricated devices were also rather stable under various driving voltages. The CIE$_x$ color coordinates of the fabricated devices were
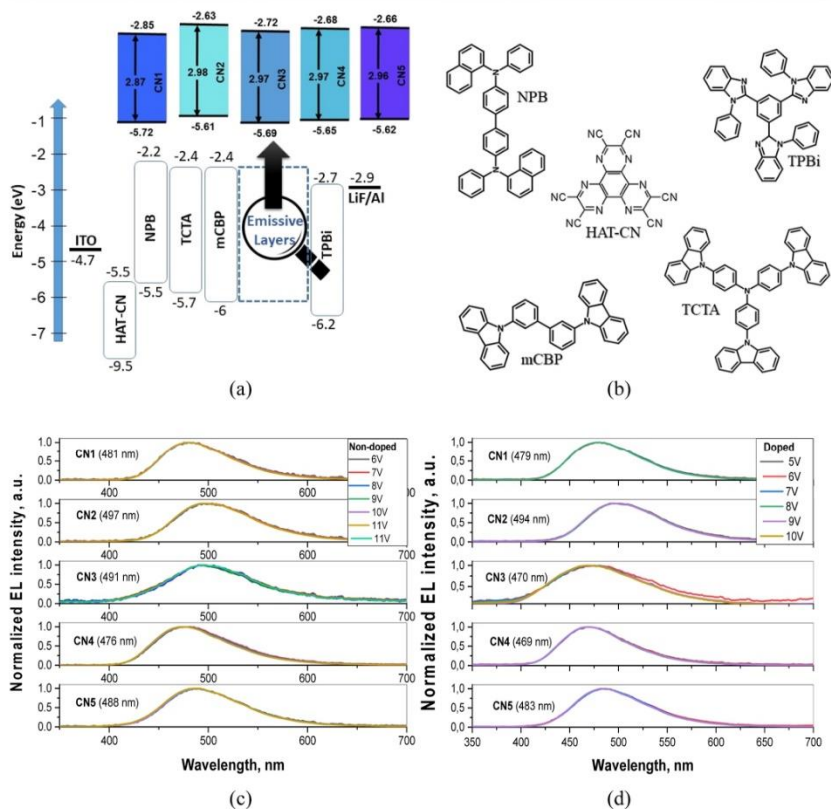
Figure 8. Visualized device structure with indication of energy levels of all functional layers (a) the molecular structures of the compounds used in the devices (b), EL spectra of non-doped (c), and doped devices (d) recorded at different voltages.

measured to be in the range of 0.16−0.21 and CIE_y color coordinates were in the range of 0.19−0.4 (Figure 9c and Table 3). Figure 9a,b and Table 3 indicate that relatively low turn-on voltages were observed for both fabricated non-doped and doped devices. This observation confirms efficient injection from electrodes and transport of charge carriers to the emissive layers. Doped devices d1−d5 were characterized by lower turn-on voltages than non-doped ones (n1−n5). This observation can most probably be assigned to good charge-transporting properties of light-emitting layers containing ambipolar host mCBP with relatively high hole and electron mobilities. The turn-on voltages (V_{on}) from 5.2 to 7.9 V were observed for non-doped devices, while for the doped OLEDs, these values were considerably lower (4.1−5 V).

Non-doped device n1 based on compound **CN1** showed sky-blue EL peaking at 481 nm with Commission Internationale de L'Eclairage (CIE) coordinates of (0.16, 0.27), maximum brightness (B_{max}) of 19 735 cd/m², maximum current efficiency (CE_{max}) of 20.5 cd/A, maximum power efficiency (PE_{max}) of 12.4 lm/W, and EQE_{max} of 8.4%. The optimal doping concentrations of compound **CN1** in mCBP was determined to be 20 wt %. The optimized device d1b with EL peak at 477 nm showed high maximum EQE, current efficiency (CE), and brightness of 15.9%, 42.6 cd/A, and 39 226 cd/m², respectively (Figure S6 and Table 3). With the increased concentration of the emitter in the host of 30 wt %, device d1c showed slightly lower efficiency than d1a and d1b. This decrease of efficiency is apparently related to the concentration quenching and exciton annihilation effects governed by strong intermolecular inter-
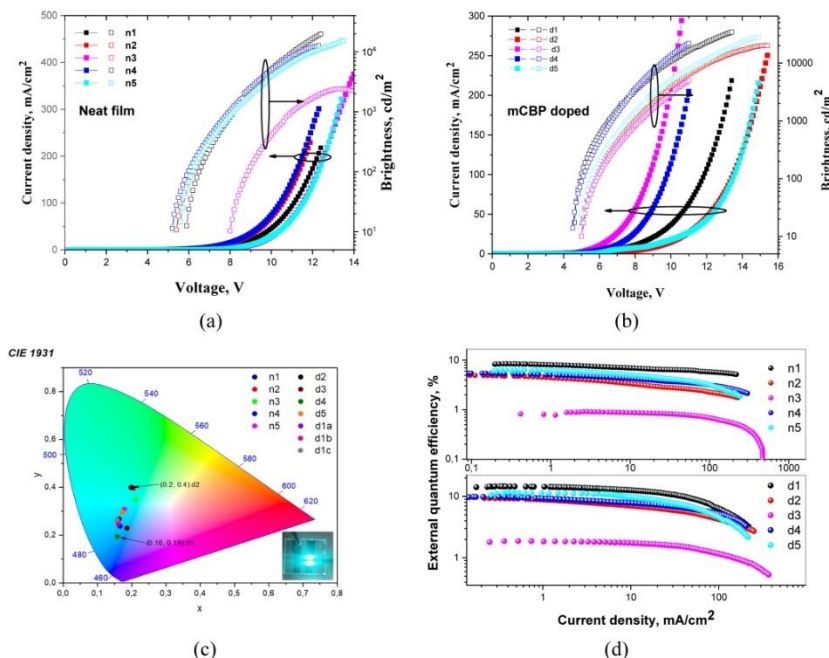
126

Figure 9. Current density and brightness vs voltage curves (a,b), CIE1931 coordinates (c), and EQE vs current density (d) of the fabricated OLEDs.

Table 3. Parameters of OLEDs

Device	Light emitting layer	V_{on},[a] V	Max brightness,[b] cd/m^2	CE_{max}[c] cd/A	EQE_{max},[d] %	λ_s[e] nm	CIE[f]
			OLED structures: ITO/HAT-CN/NPB/TCTA/mCBP/ Light emitting layer /TPBi/LiF:Al				
n1	**CN1**	5.8	19735	20.5	8.4	481	(0.16, 0.27)
n2	**CN2**	5.4	10496	10.8	4.9	497	(0.20, 0.40)
n3	**CN3**	7.9	2387	2.5	0.9	491	(0.21, 0.35)
n4	**CN4**	5.2	12634	11.5	5.5	476	(0.17, 0.24)
n5	**CN5**	5.5	15975	14.6	6.3	488	(0.18, 0.31)
d1a	mCBP: **CN1**(10wt.%)	4.6	34500	37.7	14.6	473	(0.16, 0.24)
d1b	mCBP: **CN1**(20wt.%)	4.1	39226	42.6	15.9	477	(0.16, 0.25)
d1c	mCBP: **CN1**(30wt.%)	4.9	30928	33.9	12.8	479	(0.16, 0.26)
d2	mCBP: **CN2**(10wt.%)	4.9	20154	24	9.4	494	(0.20, 0.40)
d3	mCBP: **CN3**(10wt.%)	5	4958	4.3	1.9	470	(0.19, 0.23)
d4	mCBP: **CN4**(10wt.%)	4.5	21963	26.5	9.8	469	(0.16, 0.19)
d5	mCBP: **CN5**(10wt.%)	4.8	28129	30	11.7	483	(0.17, 0.30)

[a]Turn-on voltage at a luminance of 10 cd m^{-2}. [b]Maximum brightness. [c]Maximum current efficiency. [d]Maximum EQE. [e]Wavelength of the peak of EL spectrum at 6V. [f]Commission Internationale de l'Eclairage (CIE) 1931 color coordinates.

actions.[55] This device exhibited maximum EQE of 12.8%, maximum current efficiency of 33.9 cd/A, and brightness of 30 928 cd/m^2 with slightly red-shifted EL peak (at 479 nm) as compared to the devices d1a and d1b with lower concentration

of emitter in the host. Because the relatively low triplet levels of mCBP (2.9 eV) and TPBi (2.74 eV), the studied OLEDs did not show high EQE values (Table 3).[56] Considering high triplet levels (2.72–3.0 eV) of the developed emitters **CN1**–**CN5**

L

127

(Table 2), further optimization of our device structures should be related to the replacement of used host mCBP and electron-transporting layer TPBi by appropriate materials with high triplet levels (at least on 0.2 eV higher triplet levels than that of **CN1−CN5**). To demonstrate how much the experimental EQE values are lower than the corresponding theoretical EQEs, we performed the additional analysis according to the formula $\eta_{ext} = \gamma \times \Phi_{PL} \times \chi \times \eta_{out}$,[57] where γ corresponds to the charge-balance factor, Φ_{PL} is the PL quantum efficiency, χ is the efficiency of exciton production, and η_{out} corresponds to the outcoupling efficiency. The theoretical analysis of EQE values was carried out taking γ and χ as 1 which are typical values for TADF compounds. η_{out} is typically in the range from 0.2 to 0.3 for glass-based substrates. For the devices based on emitters **CN1**, **CN2**, **CN3**, **CN4**, and **CN5**, the theoretical η_{ext} values are expected in the ranges of 15.2−22.8, 10.2−15.3, 0.8−1.2, 5.4−8.1, and 9.8−14.7%, respectively. This statement is in very good agreement with the increased EQE value up to 15.9% for the optimized device d1b when concentration of emitter **CN1** of 20 wt % was used (Table 3). When novel functional layers and host materials are available,[56] optimization of EL performance of the developed compounds are expected.

Finally, it should be noted that the similarity of EL performances of non-doped and doped OLEDs especially those based on emitter **CN1** well proved the proposed concept of minimization of effects of solid-state solvation and conformation disorder on emission properties of TADF emitters. To additionally support our molecular design strategy, we compared maxima of EL spectra of non-doped (λ_{nd}) and doped (λ_d) OLEDs based on the emitters designed using the multiple donor−acceptor strategy (this work) and on some other multi-carbazole-based emitters (Table S5). It should be noted that compound CN1 showed state-of-art performance with respect to the solid-state solvation and conformation disorder (the lowest difference between the wavelengths of maxima of EL spectra of non-doped and doped OLEDs of 4 nm was observed).

4. CONCLUSIONS

High-performance TADF materials were designed using the multiple donor−acceptor strategy. Highly efficient blue TADF emitters based on four 3,6-di-*tert*-butylcarbazole moieties as donors and two electron acceptors, one of which was trifluorotoluene unit were obtained. The effect of the additional acceptor moiety attached through para position of trifluorotoluene unit on the properties of the emitters was studied. The co-existence of through-space and TBCT ensured very small singlet-triplet energy gaps of 8−22 meV. The highly twisted structure of the multiple donor−acceptor-type derivatives 3,6-di-*tert*-butylcarbazole and trifluorotoluene lead to high PLQYs (up to 76% in solid state) and to the additional channels of RISC. The nearly identical first singlet and triplet excited-state configurations were observed for the synthesized derivative of 3,6-di-*tert*-butylcarbazole and trifluorotoluene with the additional pyrimidine acceptor moiety (**CN1**). The singlet-triplet energy gap of this compound was lower than 0.03 eV due to the multiple RISC channels through either electronic or vibrational couplings. **CN1** exhibited a high RISC rate constant of *ca.* 7 × 10^5 s^{-1}. The fabricated sky-blue TADF non-doped and doped OLEDs based on **CN1** exhibited high maximum EQE values of 8.4 and 15.9%, maximum brightness values of 19 735 and 39 226 cd/m², and maximum current efficiencies of 42.6 and 20.5 cd/A, respectively. The multi-donor−acceptor concept is appropriate

for the further development of organic emitters with the absence of effects of solid-state solvation and conformation disorder on TADF emission properties.

■ ASSOCIATED CONTENT

Ⓢ Supporting Information

The Supporting Information is available free of charge at https://pubs.acs.org/doi/10.1021/acsami.2c12475.

> "Instrumental" section; additional data and descriptions on thermal, electrochemical, photophysical, electrooptical, EL, and theoretical investigations of the studied compounds; molecular structures of multi-carbazole-based emitters and a comparison of their EL spectra in doped and non-doped devices; PL decay curve fitting parameters; rate constants of deoxygenated toluene solutions of compounds; PL spectra; and optimized molecular structure data for **CN1−5** compounds (PDF)

■ AUTHOR INFORMATION

Corresponding Authors

Dmytro Volyniuk − *Department of Polymer Chemistry and Technology, Kaunas University of Technology, Kaunas LT-50254, Lithuania;* ◉ orcid.org/0000-0003-3526-2679; Email: dmytro.volyniuk@ktu.lt

Juozas Vidas Grazulevicius − *Department of Polymer Chemistry and Technology, Kaunas University of Technology, Kaunas LT-50254, Lithuania;* ◉ orcid.org/0000-0002-4408-9727; Email: juozas.grazulevicius@ktu.lt

Authors

Malek Mahmoudi − *Department of Polymer Chemistry and Technology, Kaunas University of Technology, Kaunas LT-50254, Lithuania;* ◉ orcid.org/0000-0002-9580-6220

Dalius Gudeika − *Department of Polymer Chemistry and Technology, Kaunas University of Technology, Kaunas LT-50254, Lithuania*

Stepan Kutsiy − *Department of Electronic Devices, Lviv Polytechnic National University, Lviv 79013, Ukraine*

Jurate Simokaitiene − *Department of Polymer Chemistry and Technology, Kaunas University of Technology, Kaunas LT-50254, Lithuania*

Rita Butkute − *Department of Polymer Chemistry and Technology, Kaunas University of Technology, Kaunas LT-50254, Lithuania*

Levani Skhirtladze − *Department of Polymer Chemistry and Technology, Kaunas University of Technology, Kaunas LT-50254, Lithuania*

Kai Lin Woon − *Low Dimensional Material Research Centre, Department of Physics, University Malaya, Kuala Lumpur 50603, Malaysia;* ◉ orcid.org/0000-0002-2037-8313

Complete contact information is available at:
https://pubs.acs.org/10.1021/acsami.2c12475

Notes

The authors declare no competing financial interest.

128

■ REFERENCES

(1) Tang, C. W.; VanSlyke, S. A. Organic Electroluminescent Diodes. *Appl. Phys. Lett.* **1987**, *51*, 913−915.

(2) Baldo, S. R.; O'Brien, D. F.; Thompson, M. E.; Forrest, S. R. Excitonic Singlet-Triplet Ratio in a Semiconducting Organic Thin Film. *Phys. Rev. B: Condens. Matter Mater. Phys.* **1999**, *60*, 14422−14428.

(3) Lin, T. A.; Chatterjee, T.; Tsai, W. L.; Lee, W. K.; Wu, M. J.; Jiao, M.; Pan, K. C.; Yi, C. L.; Chung, C. L.; Wong, K. T.; Wu, C. C. Sky-Blue Organic Light Emitting Diode with 37% External Quantum Efficiency Using Thermally Activated Delayed Fluorescence from Spiroacridine-Triazine Hybrid. *Adv. Mater.* **2016**, *28*, 6976−6983.

(4) Wu, T. L.; Huang, M. J.; Lin, C. C.; Huang, P. Y.; Chou, T. Y.; Chen-Cheng, R. W.; Lin, H. W.; Liu, R. S.; Cheng, C. H. Diboron Compound-Based Organic Light-Emitting Diodes with High Efficiency and Reduced Efficiency Roll-Off. *Nat. Photonics* **2018**, *12*, 235−240.

(5) Yin, X.; He, Y.; Wang, X.; Wu, Z.; Pang, E.; Xu, J.; Wang, J. Recent Advances in Thermally Activated Delayed Fluorescent Polymer-Molecular Designing Strategies. *Front. Chem.* **2020**, *8*, 725.

(6) Kumar, M.; Ribeiro, M.; Pereira, L. New Generation of High Efficient OLED Using Thermally Activated Delayed Fluorescent Materials. *Light-Emitting Diode - an Outlook on the Empirical Features and its Recent Technological Advancements*; InTech, 2018.

(7) Schmidbauer, S.; Hohenleutner, A.; König, B. Chemical Degradation in Organic Light-Emitting Devices: Mechanisms and Implications for the Design of New Materials. *Adv. Mater.* **2013**, *25*, 2114−2129.

(8) Uoyama, H.; Goushi, K.; Shizu, K.; Nomura, H.; Adachi, C. Highly Efficient Organic Light-Emitting Diodes from Delayed Fluorescence. *Nature* **2012**, *492*, 234−238.

(9) Zhang, D.; Cai, M.; Zhang, Y.; Zhang, D.; Duan, L. Sterically Shielded Blue Thermally Activated Delayed Fluorescence Emitters with Improved Efficiency and Stability. *Mater. Horizons* **2016**, *3*, 145−151.

(10) Kim, J. U.; Park, I. S.; Chan, C. Y.; Tanaka, M.; Tsuchiya, Y.; Nakanotani, H.; Adachi, C. Nanosecond-Time-Scale Delayed Fluorescence Molecule for Deep-Blue OLEDs with Small Efficiency Rolloff. *Nat. Commun.* **2020**, *11*, 1−8.

(11) Volyniuk, D.; Cherpak, V.; Stakhira, P.; Minaev, B.; Baryshnikov, G.; Chapran, M.; Tomkeviciene, A.; Keruckas, J.; Grazulevicius, J. V. Highly Efficient Blue Organic Light-Emitting Diodes Based on Intermolecular Triplet-Singlet Energy Transfer. *J. Phys. Chem. C* **2013**, *117*, 22538−22544.

(12) Yuan, W.; Yang, H.; Duan, C.; Cao, X.; Zhang, J.; Xu, H.; Sun, N.; Tao, Y.; Huang, W. Molecular Configuration Fixation with C-H···F Hydrogen Bonding for Thermally Activated Delayed Fluorescence Acceleration. *Chem* **2020**, *6*, 1998−2008.

(13) Cui, L. S.; Gillett, A. J.; Zhang, S. F.; Ye, H.; Liu, Y.; Chen, X. K.; Lin, Z. S.; Evans, E. W.; Myers, W. K.; Ronson, T. K.; Nakanotani, H.; Reineke, S.; Bredas, J. L.; Adachi, C.; Friend, R. H. Fast Spin-Flip Enables Efficient and Stable Organic Electroluminescence from Charge-Transfer States. *Nat. Photonics* **2020**, *14*, 636−642.

(14) Mahmoudi, M.; Gudeika, D.; Volyniuk, D.; Leitonas, K.; Butkute, R.; Danyliv, I.; Grazulevicius, J. V. Tuning of Spin-Flip Efficiency of Blue Multicarbazolyl-Substituted Benzonitriles by Exploitation of the Different Additional Electron Accepting Moieties. *Chem. Eng. J.* **2021**, *423*, 130236.

(15) Zheng, X.; Huang, R.; Zhong, C.; Xie, G.; Ning, W.; Huang, M.; Ni, F.; Dias, F. B.; Yang, C. Achieving 21% External Quantum Efficiency for Nondoped Solution-Processed Sky-Blue Thermally Activated Delayed Fluorescence OLEDs by Means of Multi-(Donor/Acceptor) Emitter with Through-Space/-Bond Charge Transfer. *Adv. Sci.* **2020**, *7*, 1902087.

(16) Liu, Y.; Nishiura, M.; Wang, Y.; Hou, Z. π-Conjugated Aromatic Enynes as a Single-Emitting Component for White Electroluminescence. *J. Am. Chem. Soc.* **2006**, *128*, 5592.

(17) Albrecht, K.; Matsuoka, K.; Fujita, K.; Yamamoto, K. Carbazole Dendrimers as Solution-Processable Thermally Activated Delayed-Fluorescence Materials. *Angew. Chem., Int. Ed.* **2015**, *54*, 5677−5682.

(18) Chen, C. H.; Tang, C. W.; Shi, J.; Klubek, K. P. Recent Developments in the Synthesis of Red Dopants for Alq3 Hosted Electroluminescence. *Thin Solid Films* **2000**, *363*, 327−331.

(19) Wu, Y. S.; Liu, T. H.; Chen, H. H.; Chen, C. H. A New Yellow Fluorescent Dopant for High-Efficiency Organic Light-Emitting Devices. *Thin Solid Films* **2006**, *496*, 626−630.

(20) Wong, M. Y.; Zysman-Colman, E. Purely Organic Thermally Activated Delayed Fluorescence Materials for Organic Light-Emitting Diodes. *Adv. Mater.* **2017**, *29*, 1605444.

(21) Ding, D.; Wang, Z.; Li, C.; Zhang, J.; Duan, C.; Wei, Y.; Xu, H. Highly Efficient and Color-Stable Thermally Activated Delayed Fluorescence White Light-Emitting Diodes Featured with Single-Doped Single Emissive Layers. *Adv. Mater.* **2020**, *32*, 1906950.

(22) Yang, C.-H.; Mauro, M.; Polo, F.; Watanabe, S.; Muenster, I.; Fröhlich, R.; De Cola, L. Deep-Blue-Emitting Heteroleptic Iridium(III) Complexes Suited for Highly Efficient Phosphorescent OLEDs. *Chem. Mater.* **2012**, *24*, 3684−3695.

(23) Nasiri, S.; Thiyagarajan, M. D.; Balijapalli, U.; Mahmoudi, M.; Volyniuk, D.; Simokaitiene, J.; Pathak, M.; Iyer, S. K.; Grazulevicius, J. V. Electroluminescence of Iridium(III) Complexes Containing F or CF3 Substituents. *Synth. Met.* **2021**, *273*, 116673.

(24) Dias, F. B.; Penfold, T. J.; Monkman, A. P. Photophysics of Thermally Activated Delayed Fluorescence Molecules. *Methods Appl. Fluoresc.* **2017**, *5*, 012001.

(25) Penfold, T. J. On Predicting the Excited-State Properties of Thermally Activated Delayed Fluorescence Emitters. *J. Phys. Chem. C* **2015**, *119*, 13535−13544.

(26) Zhang, Q.; Li, B.; Huang, S.; Nomura, H.; Tanaka, H.; Adachi, C. Efficient Blue Organic Light-Emitting Diodes Employing Thermally Activated Delayed Fluorescence. *Nat. Photonics* **2014**, *8*, 326−332.

(27) Noda, H.; Chen, X.-K.; Nakanotani, H.; Hosokai, T.; Miyajima, M.; Notsuka, N.; Kashima, Y.; Brédas, J.-L.; Adachi, C. Critical Role of Intermediate Electronic States for Spin-Flip Processes in Charge-Transfer-Type Organic Molecules with Multiple Donors and Acceptors. *Nat. Mater.* **2019**, *18*, 1084.

(28) Andruleviciene, V.; Leitonas, K.; Volyniuk, D.; Sini, G.; Grazulevicius, J. V.; Getautis, V. TADF versus TTA Emission Mechanisms in Acridan and Carbazole-Substituted Dibenzo[a,c]-Phenazines: Towards Triplet Harvesting Emitters and Hosts. *Chem. Eng. J.* **2021**, *417*, 127902.

(29) Etherington, M. K.; Franchello, F.; Gibson, J.; Northey, T.; Santos, J.; Ward, J. S.; Higginbotham, H. F.; Data, P.; Kurowska, A.; Dos Santos, P.; Graves, D.; Batsanov, D. R.; Dias, A. S.; Bryce, F. B.; Penfold, M. R.; Monkman, T. J.; Monkman, A. P. Regio- and conformational isomerization critical to design of efficient thermally-activated delayed fluorescence emitters. Regio-and Conformational Isomerization Critical to Design of Efficient Thermally-Activated Delayed Fluorescence Emitters. **2017**. *8*, 14987. DOI: DOI: 10.1038/ncomms14987.

(30) Dias, F. B.; Santos, J.; Graves, D. R.; Data, P.; Nobuyasu, R. S.; Fox, M. A.; Batsanov, A. S.; Palmeira, T.; Berberan-Santos, M. N.; Bryce, M. R.; Monkman, A. P. The Role of Local Triplet Excited States and D-A Relative Orientation in Thermally Activated Delayed Fluorescence: Photophysics and Devices. *Adv. Sci.* **2016**, *3*, 1600080.

(31) Wada, Y.; Nakagawa, H.; Matsumoto, S.; Wakisaka, Y.; Kaji, H. Organic Light Emitters Exhibiting Very Fast Reverse Intersystem Crossing. *Nat. Photonics* **2020**, *14*, 643−649.

(32) Etherington, M. K.; Gibson, J.; Higginbotham, H. F.; Penfold, T. J.; Monkman, A. P. Revealing the spin-vibronic coupling mechanism of thermally activated delayed fluorescence. *Nat. Commun.* **2016**, *7*, 1−7.

(33) Han, C.; Zhang, J.; Ma, P.; Yang, W.; Xu, H. Host Engineering Based on Multiple Phosphorylation for Efficient Blue and White TADF Organic Light-Emitting Diodes. *Chem. Eng. J.* **2021**, *405*, 126986.

(34) Serevičius, T.; Skaisgiris, R.; Fiodorova, I.; Kreiza, G.; Banevičius, D.; Kazlauskas, K.; Tumkevičius, S.; Juršėnas, S. Single-Exponential Solid-State Delayed Fluorescence Decay in TADF Compounds with

Minimized Conformational Disorder. *J. Mater. Chem. C* **2021**, *9*, 836−841.

(35) Serevičius, T.; Skaisgiris, R.; Dodonova, J.; Kazlauskas, K.; Juršėnas, S.; Tumkevičius, S. Minimization of solid-state conformational disorder in donor-acceptor TADF compounds. *Phys. Chem. Chem. Phys.* **2019**, *22*, 265−272.

(36) Data, P.; Okazaki, M.; Minakata, S.; Takeda, Y. Thermally Activated Delayed Fluorescence vs. Room Temperature Phosphorescence by Conformation Control of Organic Single Molecules. *J. Mater. Chem. C* **2019**, *7*, 6616−6621.

(37) Schober, M. *Charge Transport in Organic Light-Emitting Diodes Experiments & Simulations*; Technische Univ. Dresden, 2012.

(38) Dandrade, B. W.; Datta, S.; Forrest, S. R.; Djurovich, P.; Polikarpov, E.; Thompson, M. E. Relationship between the Ionization and Oxidation Potentials of Molecular Organic Semiconductors. *Org. Electron.* **2005**, *6*, 11−20.

(39) Jayakumar, J.; Wu, T. L.; Huang, M. J.; Huang, P. Y.; Chou, T. Y.; Lin, H. W.; Cheng, C. H. Pyridine-Carbonitrile-Carbazole-Based Delayed Fluorescence Materials with Highly Congested Structures and Excellent OLED Performance. *ACS Appl. Mater. Interfaces* **2019**, *11*, 21042−21048.

(40) Gudeika, D.; Bezvikonnyi, O.; Volyniuk, D.; Skuodis, E.; Lee, P. H.; Chen, C.H.; Ding, W. C.; Lee, J. H.; Chiu, T. L.; Grazulevicius, J. V. Oxygen sensing and OLED applications of di-tert-butyl-dimethylacridinyl disubstituted oxygafluorene exhibiting long-lived deep-blue delayed fluorescence. *J. Mater. Chem. C* **2020**, *8*, 9632−9638.

(41) Divac, V. M.; Šakić, D.; Weitner, T.; Gabričević, M. Solvent Effects on the Absorption and Fluorescence Spectra of Zaleplon: Determination of Ground and Excited State Dipole Moments. *Spectrochim. Acta, Part A* **2019**, *212*, 356−362.

(42) Noboru, M.; Kaifu, Y.; Koizumi, M. Solvent Effects upon Fluorescence Spectra 465 Solvent Effects upon Fluorescence Spectra and the Dipolemoments of Excited Molecules. *Bull. Chem. Soc. Jpn.* **1956**, *29*, 465.

(43) Chen, D. G.; Lin, T. C.; Chen, C. L.; Chen, Y. T.; Chen, Y. A.; Lee, G. H.; Chou, P. T.; Liao, C. W.; Chiu, P. C.; Chang, C. H.; Lien, Y. J.; Chi, Y. Optically Triggered Planarization of Boryl-Substituted Phenoxazine: Another Horizon of TADF Molecules and High-Performance OLEDs. *ACS Appl. Mater. Interfaces* **2018**, *10*, 12886−12896.

(44) Grybauskaite-Kaminskiene, G.; Volyniuk, D.; Mimaite, V.; Bezvikonnyi, O.; Bucinskas, A.; Bagdziunas, G.; Grazulevicius, J. V. Aggregation-Enhanced Emission and Thermally Activated Delayed Fluorescence of Derivatives of 9-Phenyl-9H -Carbazole: Effects of Methoxy and tert -Butyl Substituents. *Chem.—Eur. J.* **2018**, *24*, 9581−9591.

(45) Kreiza, G.; Banevičius, D.; Jovaišaitė, J.; Maleckaitė, K.; Gudeika, D.; Volyniuk, D.; Gražulevičius, J. V.; Juršėnas, S.; Kazlauskas, K. Suppression of Benzophenone-Induced Triplet Quenching for Enhanced TADF Performance. *J. Mater. Chem. C* **2019**, *7*, 11522−11531.

(46) Goushi, K.; Yoshida, K.; Sato, K.; Adachi, C. Organic Light-Emitting Diodes Employing Efficient Reverse Intersystem Crossing for Triplet-to-Singlet State Conversion. *Nat. Photonics* **2012**, *6*, 253−258.

(47) Jeon, S. K.; Lee, H. L.; Yook, K. S.; Lee, J. Y. Recent Progress of the Lifetime of Organic Light-Emitting Diodes Based on Thermally Activated Delayed Fluorescent Material. *Adv. Mater.* **2019**, *31*, 1803524.

(48) Kim, M.; Jeon, S. K.; Hwang, S.-H.; Lee, J. Y. Stable Blue Thermally Activated Delayed Fluorescent Organic Light-Emitting Diodes with Three Times Longer Lifetime than Phosphorescent Organic Light-Emitting Diodes. *Adv. Mater.* **2015**, *27*, 2515−2520.

(49) Nikolaenko, A. E.; Cass, M.; Bourcet, F.; Mohamad, D.; Roberts, M. Thermally Activated Delayed Fluorescence in Polymers: A New Route toward Highly Efficient Solution Processable OLEDs. *Adv. Mater.* **2015**, *27*, 7236−7240.

(50) Kang, S.; Huh, J. S.; Kim, J. J.; Park, J. Highly Efficient Deep-Blue Fluorescence OLEDs with Excellent Charge Balance Based on

Phenanthro[9,10-d]Oxazole-Anthracene Derivatives. *J. Mater. Chem. C* **2020**, *8*, 11168−11176.

(51) Lee, S.; Koo, H.; Kwon, O.; Jae Park, Y.; Choi, H.; Lee, K.; Ahn, B.; Min Park, Y. The Role of Charge Balance and Excited State Levels on Device Performance of Exciplex-Based Phosphorescent Organic Light Emitting Diodes. *Sci. Rep.* **2017**, *7*, 1−9.

(52) Lee, H.; Kim, K. J.; Moon, Y. J.; Kim, Y. K.; Kim, T. Analysis of Interrelationship between Efficiency and Charge Transport Properties of Green TADF Organic Light-Emitting Diodes with Mixed Host by Impedance Spectroscopy. *Org. Electron.* **2020**, *84*, 105816.

(53) Pautmeier, L.; Richert, R.; Bässler, H. Poole-Frenkel Behavior of Charge Transport in Organic Solids with off-Diagonal Disorder Studied by Monte Carlo Simulation. *Synth. Met.* **1990**, *37*, 271−281.

(54) Ihn, S.-G.; Lee, N.; Jeon, S. O.; Sim, M.; Kang, H.; Jung, Y.; Huh, D. H.; Son, Y. M.; Lee, S. Y.; Numata, M.; Miyazaki, H.; Gómez-Bombarelli, R.; Aguilera-Iparraguirre, J.; Hirzel, T.; Aspuru-Guzik, A.; Kim, S.; Lee, S. An Alternative Host Material for Long-Lifespan Blue Organic Light-Emitting Diodes Using Thermally Activated Delayed Fluorescence. *Adv. Sci.* **2017**, *4*, 1600502.

(55) Godumala, M.; Choi, S.; Cho, M. J.; Choi, D. H. Recent Breakthroughs in Thermally Activated Delayed Fluorescence Organic Light Emitting Diodes Containing Non-Doped Emitting Layers. *J. Mater. Chem. C* **2019**, *7*, 2172−2198.

(56) Janai, M. A. B.; Woon, K. L.; Chan, C. S. Design of Efficient Blue Phosphorescent Bottom Emitting Light Emitting Diodes by Machine Learning Approach. *Org. Electron.* **2018**, *63*, 257−266.

(57) Tsutsui, T. Progress in Electroluminescent Devices Using Molecular Thin Films. *MRS Bull.* **1997**, *22*, 39−45.

130

9. ACKNOWLEDGMENTS